



**HAL**  
open science

**Study of the mechanism of complex coacervation  
between beta-lactoglobulin and the major fractions of  
acacia gum - comparaison with the unfractionnated  
acacia gum**

Suzanna Akil

► **To cite this version:**

Suzanna Akil. Study of the mechanism of complex coacervation between beta-lactoglobulin and the major fractions of acacia gum - comparaison with the unfractionnated acacia gum. Food and Nutrition. Institut National Polytechnique de Lorraine, 2007. English. NNT : 2007INPL020N . tel-01752840

**HAL Id: tel-01752840**

**<https://hal.univ-lorraine.fr/tel-01752840>**

Submitted on 29 Mar 2018

**HAL** is a multi-disciplinary open access archive for the deposit and dissemination of scientific research documents, whether they are published or not. The documents may come from teaching and research institutions in France or abroad, or from public or private research centers.

L'archive ouverte pluridisciplinaire **HAL**, est destinée au dépôt et à la diffusion de documents scientifiques de niveau recherche, publiés ou non, émanant des établissements d'enseignement et de recherche français ou étrangers, des laboratoires publics ou privés.



## AVERTISSEMENT

Ce document est le fruit d'un long travail approuvé par le jury de soutenance et mis à disposition de l'ensemble de la communauté universitaire élargie.

Il est soumis à la propriété intellectuelle de l'auteur. Ceci implique une obligation de citation et de référencement lors de l'utilisation de ce document.

D'autre part, toute contrefaçon, plagiat, reproduction illicite encourt une poursuite pénale.

Contact : [ddoc-theses-contact@univ-lorraine.fr](mailto:ddoc-theses-contact@univ-lorraine.fr)

## LIENS

Code de la Propriété Intellectuelle. articles L 122. 4

Code de la Propriété Intellectuelle. articles L 335.2- L 335.10

[http://www.cfcopies.com/V2/leg/leg\\_droi.php](http://www.cfcopies.com/V2/leg/leg_droi.php)

<http://www.culture.gouv.fr/culture/infos-pratiques/droits/protection.htm>

**THESE**

**pour obtenir le grade de  
Docteur de l'Institut National Polytechnique de Lorraine**

Discipline : Chimie-Physique

Spécialité: Procédés Biotechnologiques et Alimentaires

par

Suzanna AKIL

**Etude du mécanisme de coacervation complexe  
entre les fractions principales de la gomme  
d'Acacia et la  $\beta$ -lactoglobuline - Comparaison avec  
la gomme d'Acacia non fractionnée**

soutenue publiquement le 19 Avril 2007

**JURY**

Président : Saïd BOUHALLAB, Directeur de recherches à l'INRA-Rennes

Rapporteur : Luc PICTON, Maître de conférences à l'Université de Rouen

Rapporteur : Frank BOURY, Professeur à l'INSERM de Angers

Examineur : Denis RENARD, Chargé de recherches à l'INRA-Nantes

Examineur : Christian SANCHEZ, Professeur à l'ENSAIA-INPL-Vandoeuvre



*À mes parents*

*À Safi*

*Dieu*

*Fais moi profiter de ce que tu m'as fait connaître*

*Et fais moi connaître ce qui m'est utile*

*Imam Ali (ع)*



## **Abstract**

The complex coacervation mechanism, an associative phase separation mainly induced by electrostatic interactions, between  $\beta$ -lactoglobulin (BLG, animal protein) and Acacia gum (AG, vegetal polysaccharide) was studied in this work. The most significant difficulty to understand complex coacervation between BLG and AG at the molecular level is the molecular weight polydispersity of AG. From there, the main motivation of this research was to better understand and control the interactions between BLG and the major molecular fractions of AG, FI (~88% of AG) and FII (~10% of AG) using isothermal titration calorimetry, static and dynamic light scattering, electrophoretic mobility, Granulo-Polarimetry and optical microscopy. Higher energy of interaction, lower stoichiometry of association and then favorable complexation were shown between BLG and FII in relation with higher accessibility and density of charges for FII. The major results of this study reveal then different roles of AG fractions in complex coacervation with BLG.

**Keywords:**  $\beta$ -lactoglobulin, Acacia gum, interaction, phase, separation, complexation, coacervation, polydispersity, fractions, thermodynamics, stoichiometry, association, light, scattering.

## **Résumé**

La coacervation complexe, une séparation de phase associative principalement induite par des interactions électrostatiques, entre la  $\beta$ -lactoglobuline (BLG, protéine animale) et la gomme d'Acacia (AG, polysaccharide végétal) a été étudiée dans ce travail. La plus grande difficulté pour comprendre la coacervation complexe au niveau moléculaire entre BLG et AG révèle être la polymolécularité élevée d'AG. A partir de là, la motivation principale de cette thèse était de comprendre et contrôler les interactions entre la BLG et les fractions moléculaires d'AG, FI (~88% d'AG) et FII (~10% d'AG) en utilisant la titration calorimétrique isotherme, la diffusion statique et dynamique de lumière, la mobilité électrophorétique, la Granulo-Polarimétrie et la microscopie optique. Une énergie d'interaction plus forte, une stoechiométrie d'association plus faible et ainsi une complexation favorable ont été montrées entre la BLG et FII en relation avec l'accessibilité et la densité de charges plus élevées de FII. Les résultats majeurs de cette étude ont ainsi montré des rôles différents des fractions de l'AG dans la coacervation complexe avec la BLG.

**Mots clés:**  $\beta$ -lactoglobuline, gomme d'Acacia, interaction, séparation, phase, complexation, coacervation, polymolécularité, fractions, thermodynamique, stoechiométrie, association, lumière, diffusion.



## **Récapitulatif français de la thèse**

La stabilité des dispersions colloïdales est d'une grande importance dans un certain nombre de secteurs tels que les produits pharmaceutiques, la céramique, les peintures et les pigments. Les mélanges colloïdaux présentent une étonnante diversité d'équilibre de phases en fonction de l'équilibre délicat entre les forces inter-particulaires attractives et répulsives. Le contrôle de ces interactions est nécessaire dans les applications technologiques. La théorie DLVO qui considère les interactions colloïdales (interactions électrostatiques et de van der Waals) en milieu polaire a été décrite dans cette thèse. Globalement d'autres types d'interaction qui régissent également la stabilité colloïdale ont été évoqués (par exemple, les interactions stériques et hydrophobes). La thermodynamique des solutions macromoléculaires a été décrite par le biais de la théorie de Flory-Huggins et miscibilité polymère-polymère. Les principaux mécanismes de séparation de phase qui se produisent dans des mélanges macromoléculaires, la floculation, et la séparation de phase ségrégative et associative ont été étudiés. L'accent a été mis sur la coacervation complexe, un processus de séparation phase associative liquide-liquide, car elle correspond au mécanisme de démixtion qui se déroule dans notre système biopolymérique. Puis nous nous sommes concentrés sur la coacervation complexe entre la  $\beta$ -lactoglobuline et la gomme d'Acacia, la protéine et le polysaccharide d'intérêt pour cette thèse.

Avant d'aborder les caractéristiques de ce mélange, on a présumé le cas des mélanges de biopolymères. Ainsi, les interactions de biopolymères provoquant la formation de complexes ont été largement étudiées dans les systèmes biologiques aussi bien que dans un certain nombre de processus technologiques. Dans le cas des systèmes biologiques tels que protéine-ADN, complexes d'enzyme/substrat et protéine-polysaccharide, il est difficile d'élucider entièrement le mécanisme d'interactions intermoléculaires. Par exemple, nombreuses sont les études du comportement structural des systèmes protéine-polysaccharide. Néanmoins, il y a toujours un manque d'information sur tous les types d'interactions ayant lieu entre les biopolymères, la cinétique et la dynamique du mécanisme de séparation de phase.

$\beta$ -lactoglobuline (BLG) / gomme d'Acacia (AG) est un système protéine-polysaccharide intensivement utilisé dans une variété d'applications (microencapsulation, lait écrémé, cosmétiques, etc.) grâce à la compatibilité thermodynamique des deux biopolymères, résultant en une coacervation complexe. Ce processus se définit comme étant une séparation de phase

associative dans les systèmes colloïdaux. Généralement, la coacervation complexe est principalement provoquée par des interactions électrostatiques entre des biopolymères de charges opposées. Mais d'autres interactions peuvent contribuer à la formation des complexes (par exemple van der Waals, liaisons hydrogène, interactions hydrophobes).

Les deux types de séparation de phase se présentant généralement dans les mélanges de biopolymères sont illustrés dans Fig.1.

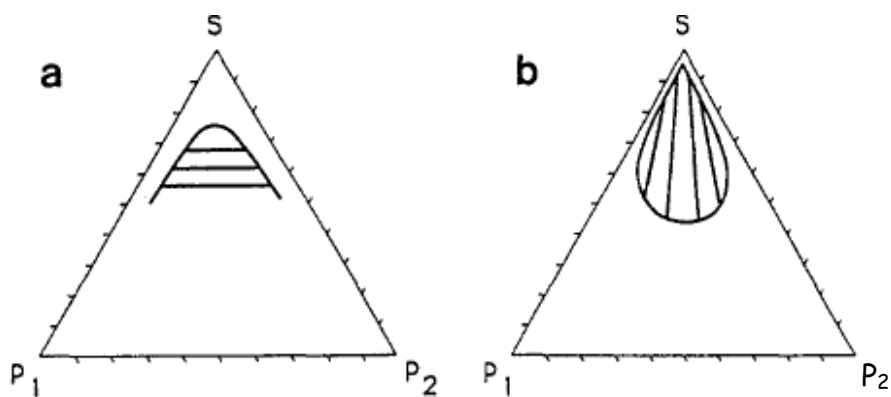


**Fig.1.** Schéma du diagramme de phase de la séparation ségrégative (a) et (b) associative de phase dans un mélange de polymères (ou biopolymères) solutions. S et P désignent solvant et polymère. Adapté de (Bungenberg de Jong and Kruyt, 1949a).

Dans cette thèse, nous mettons l'accent sur ce type de séparation de phase. Nous décrivons ensuite d'une façon détaillée la thermodynamique de ce phénomène.

En se fondant sur la théorie de description de la miscibilité polymère-polymère, une valeur négative de  $A_2$  (deuxième coefficient virial) indique les interactions thermodynamiquement favorables entre macromolécules en solution, qui est une attraction mutuelle. De telles interactions peuvent conduire à une diminution du potentiel chimique de polymères et, par conséquent, à une diminution de l'énergie totale de l'ensemble du système. L'inverse est vrai pour une valeur positive de  $A_2$ . C'est ainsi que les interactions polymère-polymère thermodynamiquement favorables sont à la base de l'auto-association (agrégation) de polymère.

La compatibilité thermodynamique ou séparation de phase associative dans un mélange de polymères indique que deux macromolécules ont tendance à se présenter dans la même phase concentrée. Ce mécanisme est défini par coacervation complexe qui est une séparation de

phase liquide / liquide. Le terme "coacervation" a été présenté par Bungenberg de Jong et Kruyt et découle du latin "acervus", qui signifie l'agrégation (un tas), et le préfixe "collaboration", qui signifie en même temps "Coacervation" et signifie l'union des particules colloïdales. La coacervation de deux colloïdes de charges opposées est dénoté coacervation complexe. D'autre part, la coacervation d'un seul polymère est dénoté coacervation simple.

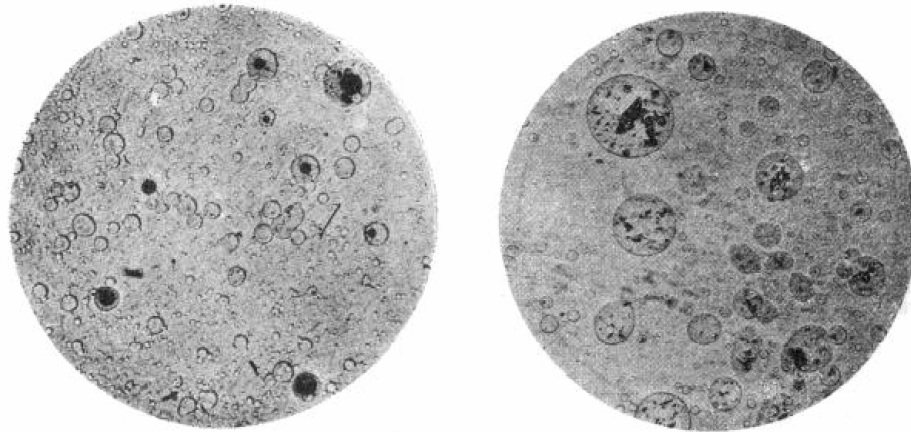


**Fig.2.** Micrographies de gouttelettes de coacervats complexes avec des particules de carbone encapsulés. (a): tetrahydro-naphtalene droplets encapsulé avec de l'encre. (b): Magnification approximative de 75 x. Figures prises de F. Weinbreck (PhD).

La complexation (ou la coacervation complexe) est une caractéristique intrinsèque de l'interaction entre deux biopolymères chargés différemment, ce qui peut résulter d'effets entropiques et enthalpiques. En outre, les interactions électrostatiques jouent un rôle majeur dans la complexation / coacervation. Mais la complexation trouve son origine dans de nombreuses forces d'interaction telles que les liaisons d'hydrogène, les interactions hydrophobes et de van der Waals. Par exemple, la neutralité de la complexation des polysaccharides avec d'autres biopolymères résulte des interactions par liaisons hydrogène. Les complexes formés peuvent être solubles ou insolubles. Le grand nombre de complexes "insolubles" va se concentrer en gouttelettes de coacervats liquides, que pour la suite elles vont s'unir et se séparer de la phase aqueuse pour former une couche de coacervats (Fig.3).

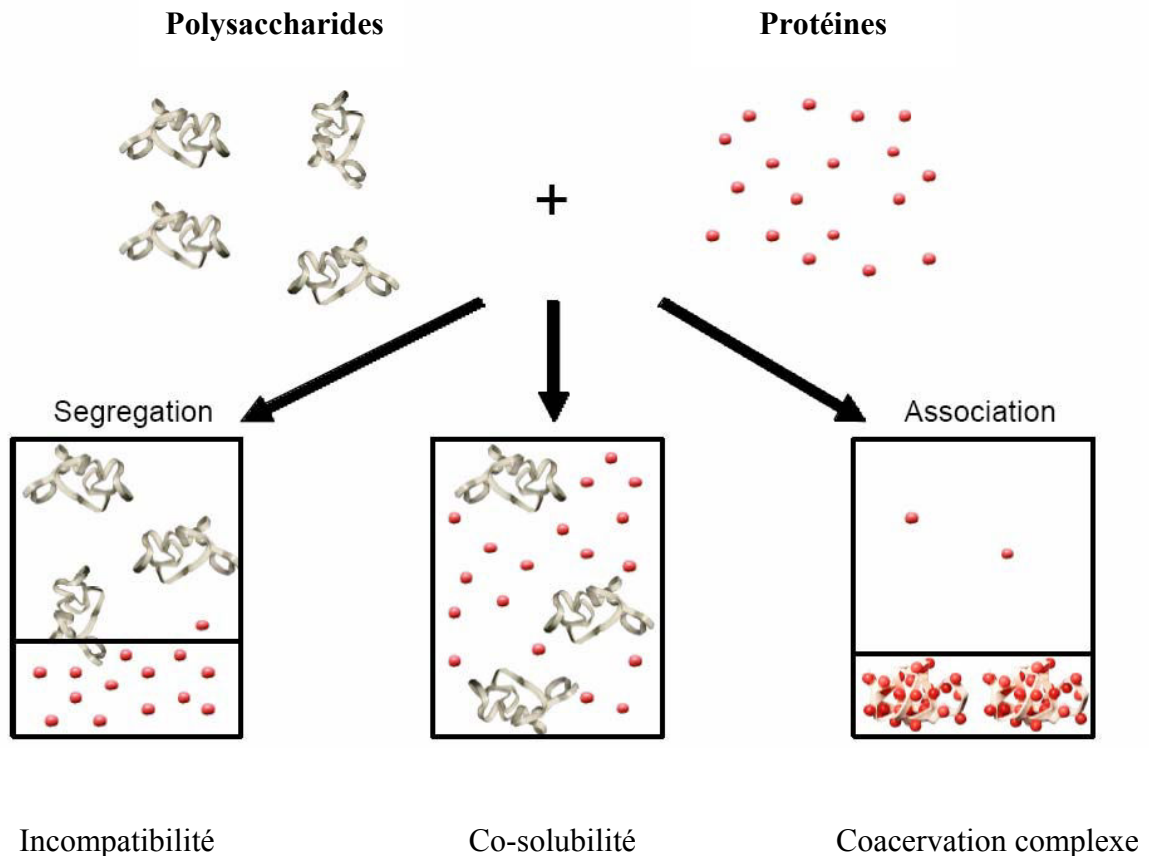


**Fig.3.** Grandes tendances dans le comportement des mélanges protéines / polysaccharides. Adapté de Weinbreck (PhD).

Nous nous concentrons ici sur le fondement théorique des modèles expliquant le mécanisme de coacervation complexe. Ce dernier processus ayant lieu entre des protéines et des polysaccharides de charges opposés a été découvert par Tiebackx en 1911. En mélangeant de la gélatine et de la gomme arabique (GA) dans une solution d'acide acétique, il a vu de l'opalescence ou des précipitations. La coacervation complexe dans le système gomme arabique - gélatine a été largement étudiée pour la première fois par Bungenberg de Jong et Kruy.

Le premier modèle théorique de coacervation complexe a été développé par Voorn et Overbeek et fondé sur la grande quantité de données obtenues par Bungenberg de Jong et al. (1929). Ils ont considéré que la coacervation de la gélatine et de la GA est une compétition entre des forces électrostatiques attractives qui ont tendance à s'accumuler les polyions et des effets entropiques qui tendent à les disperser.

Des modèles théoriques successifs ont été élaborés par les collègues Veis, Nakajima et Sato et Tainaka.

Veis et Aranyi ont mis au point un modèle global de la phase diluée, qui a suggéré que la coacervation complexe a lieu en deux étapes. D'abord, l'interaction électrostatique des polyélectrolytes globalement chargés pour former des agrégats neutres de faible entropie configurationnelle, et ensuite réorganisation de ces agrégats pour former des coacervats. L'appariement d'agrégats d'ions formés dans la première étape présents dans les deux phases de coacervats et la phase diluée. La Coacervation est favorisée par le gain en entropie configurationnelle quand les agrégats (dans les complexes solubles) vont se réorganiser en coacervats.

Les théories Voorn-Overbeek et Veis-Aranyi se limitent à faible densité.

Tainaka a développé un troisième modèle de la Veis et Aranyi modèle, qui a estimé que la coacervation est favorisée par les forces attractives entre agrégats. Selon ce modèle, les agrégats formés sont neutres et éventuellement présents dans les deux phases, mais sans appariement d'ions spécifiques. De cette théorie, il convient de noter qu'une certaine gamme de densité et de longueur de la chaîne polyélectrolytes vont permettre à la coacervation de se produire. Si la densité est trop élevée et la longueur de la chaîne est trop longue, les deux polyélectrolytes formeront un précipité en raison de la longue portée des forces attractives entre les agrégats interagissant. D'autre part, pour une trop faible densité et trop courte longueur de chaîne, la solution diluée est stabilisé à courte portée par les forces de répulsion, et la coacervation n'aura pas lieu. La Tainaka théorie s'applique à la fois à haute et basse densité. Mais, il ne fournit pas une explication complète du processus de coacervation, tels que la suppression de la coacervation à faible force ionique.

De nombreuses différences existent entre ces trois modèles dans les rôles de l'interaction électrostatique, l'entropie, et l'ampleur de l'interaction solvant - soluté. Aucune de ces théories ne peut décrire tous les cas de la coacervation complexe. Cependant, ces théories de fournir une explication raisonnable pour un grand nombre de systèmes.

## **Coacervation Complexe entre la $\beta$ -lactoglobuline et la gomme d'Acacia :**

### **Caractéristiques de la $\beta$ -lactoglobuline :**

La  $\beta$ -lactoglobuline (BLG) est la principale protéine du lactosérum du lait de vache. Il s'agit d'une protéine globulaire qui est reconnue pour ses propriétés fonctionnelles telles que gélifiantes, moussantes, hydratantes et émulsifiantes dans les aliments formulés. Cependant, la fonction biologique de  $\beta$ -lg est encore inconnue. Dans sa forme native, BLG a une structure globulaire, qui se caractérise par un poids moléculaire de 18400 g/mole et composée de 10-12% d'hélice- $\alpha$  et de  $\sim$  50% de feuillets- $\beta$ . BLG peut exister dans un certain nombre d'états structuraux en fonction du pH. La multimérisation de la BLG est électrostatique et associe facilement à basse force ionique et à un pH proche de son, pI, qui est d'environ 5,2. Dans les conditions physiologiques, BLG existe sous la forme dimérique mais sa structure présente un grand degré de diversité en fonction des conditions environnementales telles que la concentration de protéines, la force ionique et la température. En dessous du pH 3, elle se dissocie en monomères. Elle existe en équilibre monomère/dimère à pH 3, et dans un mélange de monomère, dimère et oligomère entre pH 6 et 3,5 avec la présence de plus grands agrégats. Un grand nombre d'études a signalé l'asymétrie des distributions de charges (hétérogénéité de charges), des protéines ainsi que pour BLG. Ces distributions locales sont fortement influencées par l'état de charges de certains acides aminés.

### **Particularités de la gomme d'Acacia :**

Comme plusieurs polysaccharides, la gomme d'Acacia (AG) est un hydrocolloïde qui est souvent utilisé pour renforcer la stabilité dans un liquide alimentaire telles que les dispersions de boissons gazeuses, mais surtout pour stabiliser les émulsions huile dans l'eau et de produire également des huiles d'arômes dispersées et des microcapsules. Il s'agit d'un hétéropolysaccharide chargé négativement de poids moléculaire élevé et ayant une structure complexe, hétérogène (polymolécularité,  $M_w / M_n$  de  $\sim$  2,3) et mal connue. Une grande variété de techniques comme la chromatographie d'interaction hydrophobe (HIC), Chromatographie d'exclusion stérique (SEC), la spectroscopie UV-Visible, Dichroïsme Circulaire (CD), et Viscosimètre a permis de caractériser ses propriétés physiques et biochimiques. En ce qui concerne la structure chimique de la gomme d'Acacia, la plupart des

études ont mis en évidence par fractionnement chromatographique la présence de trois composantes principales dans AG différentes dans le rapport protéine/sucre: une fraction de arabinogalactane-peptide (~ 88% en poids de l'ensemble de la gomme), une arabinogalactane-protéine (10-12% en poids de l'ensemble de la gomme), et glycoprotéines (~ 2% en poids de l'ensemble de la gomme). En revanche, peu d'informations sont actuellement disponibles sur la conformation moléculaire des fractions de AG. La gomme d'Acacia totale, l'arbinogalactane-peptide et l'arabinogalactane-protéine seront respectivement désignés ci-après par TAG, FI et FII. Le terme AG sera utilisée pour définir l'ensemble de ces molécules et correspond à la fois à la gomme totale et ses fractions moléculaires à la fois.

### **Mélanges de $\beta$ -lactoglobuline et gomme d'Acacia :**

En solution aqueuse et dans des conditions particulières de pH et force ionique, les interactions attractives entre BLG et AG vont entraîner la coacervation complexe.

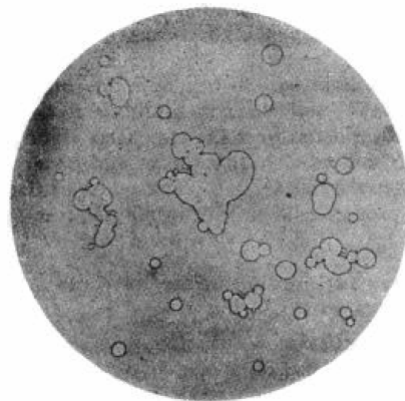


**Fig.4.** Image microscopique de coacervation complexe de l'albumine sérique bovine et AG (120x). Photo Reproduite à partir de [Bungenberg de Jong et Kruyt, 1929].

Les premières études de la cinétique de coacervation complexe sont apparues sur le système composé de  $\beta$ -lactoglobulin et gomme d'Acacia en utilisant la spectroscopie, la diffusion d'ondes (DWS) et la microscopie confocale à balayage au laser (CSLM). Les schémas en DWS étaient difficiles à interpréter en raison de la coalescence et de la sédimentation des gouttelettes de coacervats ayant eu lieu en même temps. Un grand intérêt et de nombreuses études ont été menées sur la cinétique de la coacervation complexe du système  $\beta$ -lactoglobulin / Acacia gomme / eau en raison de son implication dans de nombreux procédés alimentaires. L'utilisation de la diffusion statique de la lumière aux petits angles (SALS) n'a

pas permis de conclure sur la survenance des phénomènes de décomposition spinodale (SD) ou nucléation et croissance (NG). C'est parce que le mélange des deux biopolymères au pH et Pr:Pol, où un taux maximal d'interactions électrostatiques a eu lieu, a induit une séparation de phase instantanée. Une approche intéressante consiste à acidifier in situ des mélanges par glucono-delta-lactone (GDL) dans le but de ralentir le taux de démixion. Ainsi, le pH peut être diminué lentement d'une valeur à laquelle ne se déroule pas d'interaction à une valeur à laquelle la séparation de phase se produit. Récemment, Sanchez et al. (2006) ont cherché à mieux comprendre le mécanisme du coacervation complexe dans le système BLG / AG. Les auteurs ont suggéré que la coacervation complexe entre BLG et AG suit un mécanisme de Nucléation et de Croissance.

De nombreuses études ont porté sur le contrôle des paramètres gérant la séparation de phase (telles que la densité de charges, le pH, la force ionique, le ratio polymère, la concentration en polymère et la température). La variation de la force ionique et du pH dans le système gélatine / AG a mis en évidence que la coacervation était une conséquence de interactions électrostatique. Le pH joue un rôle clé dans la force de l'interaction électrostatique, puisque c'est elle qui détermine la densité de la protéine. La présence de sel peut supprimer la coacervation, selon la nature et la concentration de sel. Le ratio de mélange est aussi un paramètre essentiel, car pour un mélange de polymères il existe un ratio optimal correspondant à un montant électrique équivalent de chaque polymère. Le mécanisme de coacervation dépend aussi de la concentration de polymère, au-dessus d'une concentration critique une suppression de la coacervation survient. Le rôle de la température sur la coacervation n'est guère abordé, il a été tout d'abord étudié par Bungenberg de Jong (1949). La Veis et Aranyi théorie était fondée sur un cas particulier de la coacervation durant la réduction de la température entre deux gélatines de charges opposées, une augmentation du paramètre de Flory - Huggins pendant la diminution de la température a été présentée. Weinbreck et al. (2003) a montré un léger effet de la température sur le  $pH_{\phi}$ .

Malgré le grand nombre d'études sur les interactions protéines - polysaccharides, le mécanisme de séparation de phase n'est pas complètement élucidé. Le grand nombre de travaux sur des systèmes polymère-polymère et protéine-polymère et sur un nombre limité de systèmes protéine-polysaccharide n'a pas abouti à une bonne description des transitions structurales ayant lieu pendant la complexation / coacervation. Ces travaux ont défini coacervation complexe induite par le pH comme un processus en deux étapes. Deux pH de



transitions structurales,  $pH_c$  (pH critique, correspond au déclenchement de l'interaction) et  $pH_\phi$  (le pH de séparation de phase), ont été identifiés. Les complexes solubles sont formés au  $pH_c$ . Au-dessous de  $pH_\phi$ , la survenance d'une séparation de phase visuelle est détectée. Les complexes solubles sont formés à un pH au-dessus du point isoélectrique (pI) de la protéine, c'est-à-dire à un pH où la protéine est globalement chargée négativement, comme le polyélectrolyte. Un modèle a été proposé afin de préciser si les pH de transitions et les complexes solubles de protéines et de polysaccharides formés pour les biopolymères sont comme pour les systèmes de polymères synthétiques. L'étude prédit que la complexation ait lieu au-dessus du pI de la protéine en raison de la présence (au hasard) d'une certaine hétérogénéité de charges (patches) à la surface des protéines. Récemment, Mekhloufi et al. ont déterminé plus de pH de transitions structurales au cours de la coacervation complexe induite par le pH de BLG et AG, en utilisant des méthodes expérimentales complémentaires. Ces transitions ont été identifiés comme correspondant à (i) la formation de complexes solubles (ii) les changements de conformation de la protéine induite par la complexation (iii) la agrégation des complexes (iv) L'initiation de la séparation de phase (v) la séparation de phase et (vi) la première parution de coacervats.

La première étude de la thermodynamique du système BLG / AG a été effectuée par Schmitt et al. (2006) en utilisant la Titration Calorimétrique Isotherme (ITC). Il a été montré que la coacervation complexe entre BLG et AG est essentiellement un processus exothermique. Les auteurs ont ajustés les courbes de titrage par un modèle d'une seule série de sites de liaison afin de déterminer les paramètres thermodynamiques de l'interaction, ce qui reflète la présence de sites similaires et indépendants.

## **Objectifs de la thèse :**

Comme on a déjà évoqué ci-dessus, le grand nombre d'études n'a pas pleinement élucidé la cinétique et la dynamique de la complexation et de la séparation de phase dans le mélange BLG / TAG. Les principales raisons de ce manque d'informations est le poids moléculaire élevé et la polymolécularité de la TAG et des contributions non connues de ses fractions moléculaires dans le mécanisme de complexation / coacervation.

A partir de là, l'objectif principal de cette thèse est de comprendre le rôle de la polymolécularité moléculaire de la TAG sur la coacervation complexe afin d'obtenir un aperçu plus quantitatif de ce mécanisme. Notre démarche a été d'étudier la séparation de phase entre chaque fraction moléculaire de TAG et BLG. On a essayé de comparer les résultats des trois systèmes différents (BLG / TAG, BLG / FI et BLG / FII) afin de préciser le rôle spécifique de chaque moléculaire fraction dans le processus de coacervation complexe.

Dans un premier temps, les interactions entre les deux grandes fractions de TAG et BLG ont été étudiées afin de mieux comprendre le rôle et la contribution de chaque molécule dans les interactions. Pour cela, nous avons tenté de déterminer l'énergie d'interaction, la stoechiométrie et la constante d'association dans tous les systèmes. Il a été indiqué ci-dessus que la thermodynamique de miscibilité biopolymère-biopolymère dépend de nombreux facteurs, tels que le pH, le ratio biopolymère, la concentration en biopolymère et la température. À partir de là, l'impact de ces paramètres sur les paramètres thermodynamiques et la nature des interactions ont été étudiés.

Une faible acidification par Glucono- $\delta$ -Lactone a été réalisée afin de déterminer la nature du mécanisme de séparation de phase des mélanges, les transitions structurales et la morphologie des interfaces dans des systèmes séparés. Le suivi du diamètre hydrodynamique, de la mobilité électrophorétique et de l'intensité de lumière diffusée, à un rapport massique du mélange Pr:Pol (2:1) où une forte interaction existe entre les deux biopolymères, nous a permis d'atteindre ces objectifs.

Comme une force d'interaction élevée peut masquer le rôle des propriétés intrinsèques des macromolécules, les mêmes paramètres étudiés au cours de l'acidification des mélanges, au

rapport de mélange 2:1, ont ensuite été mesurés à différents rapports massiques du mélange et différentes valeurs de concentration totales en biopolymères. Le but était de mettre en évidence les effets de la structure moléculaire et des propriétés des fractions moléculaires de la TAG (par exemple le poids moléculaire, le nombre et la densité de charges et le rayon de gyration) dans la complexation / coacervation avec BLG.

## Aperçu de la thèse :

Cette thèse est composée de quatre chapitres. Le premier chapitre correspond à une étude théorique de la dynamique des interactions dans les systèmes colloïdaux. Dans les autres chapitres, des études expérimentales du mécanisme de séparation de phase des systèmes BLG / AG ont été faites.

Dans le chapitre I, une étude bibliographique décrit tout d'abord l'ensemble des types d'interactions qui contrôlent la stabilité dans les systèmes polymériques et biopolymériques. Les mécanismes de démixion qui se produisent dans les solutions macromoléculaires ont été décrits. Une étude particulière a été réservée à la dynamique du système BLG / TAG. Les objectifs de cette thèse ont été décrits dans ce chapitre.

Dans le chapitre II, les interactions entre BLG et AG ont été étudiées. Le but de ce chapitre est d'obtenir une meilleure compréhension de la coacervation complexe au niveau moléculaire basée sur une étude thermodynamique utilisant un modèle de titrage micro-calorimétrique, (par Titration Calorimétrique Isotherme). Les effets de différents paramètres physico-chimiques (par exemple concentration en biopolymères, pH et température) sur les caractéristiques thermodynamiques ont été étudiés. Une modélisation des courbes d'interaction a été faite et une détermination des paramètres thermodynamiques des interactions est discutée.

Le chapitre III porte sur coacervation complexe induite par le pH lors d'une acidification lente in situ des mélanges BLG / AG par GDL. Dans ce chapitre, nous avons cherché à mettre en évidence les comportements des différentes moléculaires de TAG dans la complexation / coacervation en utilisant la diffusion de la lumière statique et dynamique (SALS et DLS) et les mesures de la mobilité électrophorétique ( $\mu_E$ ). La taille, la charge des complexes, le pH des transitions structurales, la nature du mécanisme de séparation de phase et la compacité des particules ont été étudiées.

Le chapitre IV donne une vue plus générale sur le mécanisme de complexation / coacervation entre BLG et AG. Dans ce chapitre, l'objectif principal était de mieux évaluer le rôle structural de l'AG qui a été mis en évidence dans les chapitres II et III. Dans ce contexte, nous

avons modifié les paramètres définis dans le chapitre II et qui peuvent modifier le mécanisme de séparation de phase, en particulier le rapport de mélange et la concentration totale en biopolymères. Ainsi, le même type d'expériences que dans le chapitre III, mais pour différents ratios de mélange, a été fait en utilisant SALS, DLS et les mesures de  $\mu_E$ . L'influence de la quantité totale de biopolymères a été étudiée dans le but d'obtenir une vision plus approfondie de la structure en utilisant la Granulo-Polarimétrie et la microscopie optique. Les grandes lignes de cette thèse qui résument toutes ces études expérimentales sont décrites ci-dessous. Ainsi les résultats récoltés dans les trois derniers chapitres peuvent être récapitulés par les points suivants.

## **Caractérisation thermodynamique des interactions entre la $\beta$ -lactoglobuline et les fractions moléculaires majoritaires de la gomme d'Acacia**

Dans le chapitre II, les propriétés thermodynamiques du système BLG/AG ont été étudiées par titration calorimétrique isotherme (ITC). La force d'interaction a été contrôlée en changeant les conditions environnementales telles que le pH, la concentration initiale en AG et la température afin d'élucider la nature des interactions et le mécanisme de formation des complexes. Les mesures consistent à titrer une dispersion de la gomme d'acacia totale (TAG) ou une de ses deux fractions moléculaires principales (FI ou FII) dans une dispersion de BLG à température constante.

Fig.5 montre le flux thermique par rapport au temps et courbes isothermes correspondantes découlant de l'injection d'aliqotes de TAG (BLG / TAG), FI (BLG / FI) ou FII (BLG / FII) dans une dispersion BLG dispersion. Aussi, un mélange de dispersions de FI et FII a été fait en vue de reconstituer la gomme d'acacia totale, et qu'il est de même titré dans BLG (BLG / FI + mélange FII).

Pour toutes les courbes, une séquence de pics exothermiques relativement intenses et d'énergie libérée constante a été initialement observée. L'énergie constante peut indiquer que les sites de liaison occupés à chaque injection sont similaires et induisent la même chaleur libérée. Les résultats révèlent une plus grande gamme ( $\mu\text{cal}$ ) de l'échange thermique par rapport aux résultats des témoins BLG et TAG. Avec l'avancement du procédé de titrage, l'énergie de liaison libérée a diminué progressivement, puis elle est inversée. La forte intensité des pics exothermique peut être attribuée à l'interaction de BLG aux molécules de l'AG. Une deuxième séquence de pics endothermiques faibles ( $\Delta H$  positive). L'énergie libre est une fois de plus inversée et une dernière séquence de faibles pics exothermiques atteint la chaleur de dilution de TAG en l'absence de BLG (témoin), et tend à un état de stabilité thermodynamique vers la fin des injections. Dans tous les cas, les courbes de titrage ont révélé trois points d'inflexion. Le premier point (P1) a été observé à la diminution de l'énergie libérée, le deuxième point (P2) est apparu à l'opposition de la chaleur de réaction produite de l'exothermique en endothermique et la dernier (P3) est survenu au début de la courbe de stabilisation.

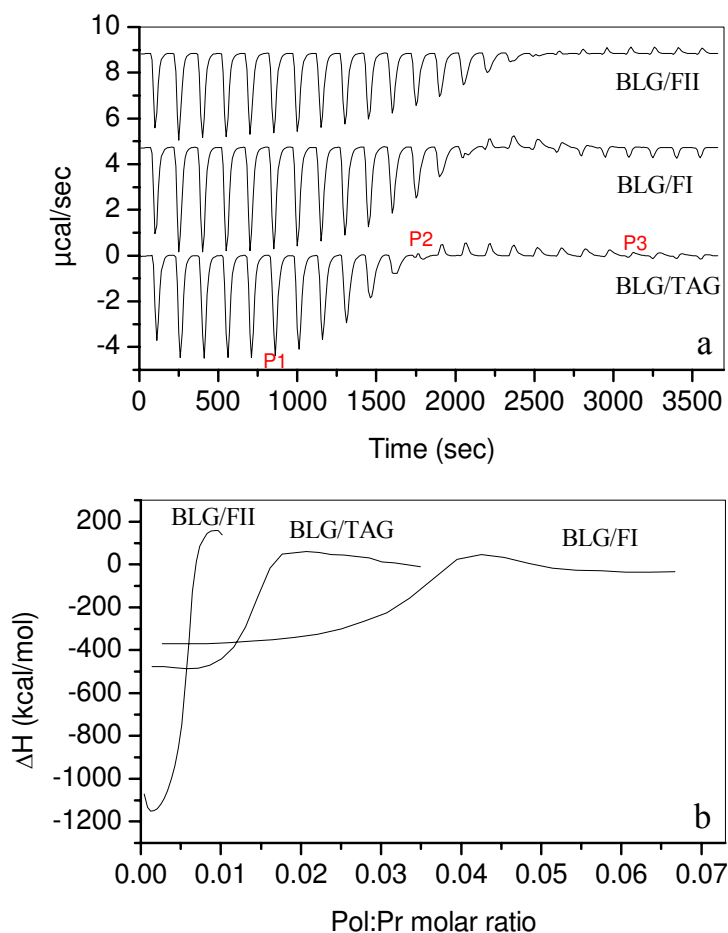


**Fig.5.** (a) Thermogramme correspondant à la titrage d'une dispersion aqueuse de la gomme d'Acacia totale (1.8 wt %) ou de la fraction arabinogalactane-peptide (FI) (1.8 wt %) ou de la fraction arabinogalactan-protéine (FII) (1.8 wt %) dans une dispersion aqueuse de  $\beta$ -lactoglobuline (0.6 wt %) à pH 4.2 et 25 °C. (b) Isotherme d'interaction correspondant à la l'expérience de titrage précédente. P1, P2 et P3 correspondent aux trois points de transition observés dans les isothermes d'interaction. Les expériences ont été faites en double.

Les expériences montrent que la complexation est principalement induite par des variations d'enthalpie dues à la contribution majeure de l'étape exothermique de la courbe de titrage. De Kruif et al. (2001) ont indiqué que la diminution de l'énergie libre de Gibbs pendant coacervation complexe s'accompagne de modifications de l'enthalpie ou de l'entropie ou des deux. Un rejet de contre-ions, suite à l'interaction entre les polymères de charges opposés, augmente l'entropie de mélange qui peut devenir la force motrice pour la phase de séparation, selon le type du polymère. Par conséquent, la diminution de l'énergie libérée (P1) peut être attribuée à la compensation de l'enthalpie par les différents effets entropiques. Parmi ces

contributions, il y a les changements de structures des biopolymères, la libération de contre-ions et de molécules d'eau à proximité des sites de liaison.

Afin de mieux définir les caractéristiques des courbes d'interaction entre BLG et les fractions moléculaires de l'AG, l'influence des conditions telles que le pH de la solution, la température et la concentration en biopolymères est nécessaire de comprendre les facteurs influant sur la nature et la force des interactions protéines-polysaccharides. Les effets de ces trois paramètres sur les aspects de la thermodynamique d'interaction des systèmes BLG/TAG, BLG/FI et BLG/FII ont été étudiés.

Une augmentation de la **concentration** AG a conduit à une diminution continue du nombre des premiers pics exothermiques, et à une augmentation du nombre des pics endothermiques. Ainsi, un décalage des points de transitions structurales vers les valeurs les plus faibles de temps a été observé. Ce résultat révèle une saturation plus rapide des sites de liaison due à l'augmentation du nombre de molécules d'AG à chaque injection.

Concernant l'effet du **pH** :

À toutes les valeurs de pH, deux grandes séries de pics sont apparues: une grande séquence de pics exothermiques intenses et une deuxième séquence de pics exothermique-endothermique relativement faibles. Depuis le début du titrage jusqu'à la sixième injection, la séquence exothermique présentait une intensité constante des pics à un pH de 4,2. Toutefois, à partir de la troisième injection, l'intensité a nettement diminué, aux autres valeurs de pH. Ainsi, une augmentation du nombre de pics endothermiques contre les pics exothermiques a été observée avec l'augmentation du pH. Il faut noter que cette diminution de l'intensité révèle plus remarquable à un pH de 4,5. Des changements dans la force des interactions ont été également observés. L'enthalpie des interactions électrostatiques ( $\Delta H_{\text{exo}}$ ) a diminué avec l'augmentation du pH et possédait une valeur maximale à un pH de 4,2. L'augmentation du pH a conduit à la réorientation de toutes les transitions structurales vers des valeurs faibles de temps, en accord avec une complexation à plus faible stœchiométrie d'association. Les densités de charges de BLG et AG diminuent avec l'augmentation du pH, ce qui conduit à rapport de charge de Pr:Pol initial plus faible. Par conséquent, la saturation des sites de liaison de BLG se produit à un nombre de molécules plus faible de TAG c'est-à-dire à une stœchiométrie inférieure de l'association.



Des effets semblables de la **température** ont été observés dans tous les systèmes. Le chauffage des dispersions de BLG et de TAG et à un pH de 4,2 a induit une nette diminution de l'intensité des pics exothermiques. En conséquence, une diminution apparente de l'enthalpie libérée, en accord avec une diminution de la force de l'interaction entre BLG et AG. En parallèle, les pics endothermiques ont disparu à la température de 4 °C et avec l'augmentation de la température au-delà de 35 °C. La disparition de la deuxième étape endothermique des courbes d'interaction peut être due à la diminution de la force d'interaction, en relation avec une complexation moins étendue.

Les changements de la capacité calorifique ( $\Delta C_p$ ,  $\Delta H = \int_0^T \Delta C_p \cdot dT$ ) qui est un paramètre clé thermique permettant la détermination de tous les paramètres thermodynamiques ont été étudiés. Pour ce faire, il a été déterminé dans le but de mieux comprendre l'influence de la température sur la thermodynamique des interactions.

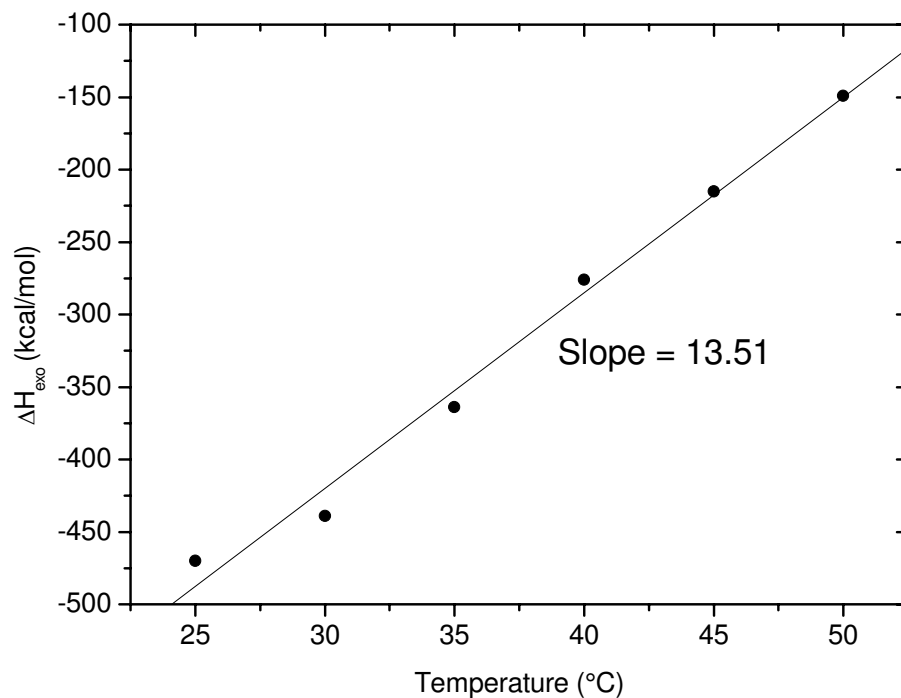


**Fig.6.** Evolution de la  $\Delta H_{\text{exo}}$  avec la température au cours du titrage d'une dispersion aqueuse de gomme Acacia totale (1,8% en poids) dans une dispersion aqueuse de  $\beta$ -lactoglobuline (0,6% en poids) à un pH de 4,2. La ligne correspond à un ajustement linéaire des données. Chaque expérience a été faite en double.

Fig.6 montre une diminution linéaire de  $|\Delta H_{\text{exo}}|$  avec l'augmentation de la température. Un  $\Delta C_p$  de  $13,51 \text{ kcal.mol}^{-1}.\text{°C}^{-1}$  a été déterminée. Cette haute valeur positive de  $\Delta C_p$  complexes indique que la formation est accompagnée de la disparition des groupes hydrophiles, exposés aux solvants avec l'augmentation de la température. Cette fonctionnalité peut indiquer une rupture des liens avec de l'hydrogène de chauffage et de négliger le rôle des interactions hydrophobes.

En résumé, dans ce chapitre, Une comparaison entre les comportements des fractions moléculaires de l'AG dans la complexation avec la BLG a été effectuée. En général, les trois systèmes étudiés ont montré des courbes de titrage semblables, formées généralement d'une séquence de forts pics exothermiques et d'une séquence de faibles pics endothermiques. Cependant, FII a montré un comportement thermodynamique différent par rapport à FI. Ainsi, FII a mené à une cinétique de complexation plus rapide (stoechiométrie d'interaction inférieure) et à une énergie d'interactions plus forte (des valeurs plus élevées de l'enthalpie d'interaction) avec la BLG. Dans tous les systèmes, les interactions électrostatiques ont principalement induit la complexation en raison de la dominance de la contribution exothermique dans toutes les courbes de titrage. Mais un rôle des interactions par liaisons hydrogène a été montré. Quatre ratios de charge de transitions structurales ont été déterminés dans tous les mélanges et correspondent à:  $r_{\text{agg}}$ , ratio d'agrégation des complexes;  $r_{\text{isto}}$ , ratio de l'initiation de la stœchiométrie;  $r_{\text{eq}}$ , ratio d'équilibre enthalpie/entropie et  $r_{\text{sat}}$ , ratio de saturation des sites d'interaction. Tous ces ratios sont plus faibles pour le mélange de BLG/FII en raison des interactions favorisées par les possibles plus grandes densité et accessibilité de charges de FII. Les propriétés thermodynamiques des systèmes et la force d'interaction dépendaient fortement des facteurs physicochimiques du milieu (pH, concentration initiale en AG et température). Une augmentation de tous les paramètres a conduit à un décalage des courbes de titrage vers les faibles valeurs de temps et ensuite à une complexation plus rapide. L'énergie d'interaction des trois systèmes a été maximale au pH de 4.2. Les mesures d'ITC à différentes températures ont prouvé que le complexation/coacervation dans le système de BLG/AG peut résulter d'un ensemble de forces d'interactions (électrostatiques, hydrogènes, van der Waals) qui sont fonction de la structure de l'AG et des conditions du milieu.

## **Influence de la polymolécularité de la gomme de d'Acacia sur la coacervation complexe avec la $\beta$ -lactoglobuline**

Le travail présenté dans le chapitre III a été consacré à l'étude de l'effet de la polymolécularité de la TAG sur la coacervation complexe induite par le pH avec la BLG au ratio Pr:Pol massique de 2:1. L'acidification lente par la glucono-delta-lactone de trois dispersions mélangées, BLG/TAG, BLG/FI et BLG/FII, a été effectuée afin de suivre *in situ* les transitions structurales pendant l'interaction en utilisant la diffusion statique et dynamique de la lumière (SALS et DLS) et les mesures de mobilité électrophorétique ( $\mu_E$ ).

L'évolution du diamètre hydrodynamique ( $d$ ) des particules en fonction du pH dans tous les systèmes a été mesurée par DLS. Les résultats ont montré que FI conduit à la formation de particules de plus grande taille, à l'exception des valeurs de pH les plus élevées. Il est complexé avec moins de charge positive de BLG (c'est-à-dire à des valeurs de pH plus élevées) par rapport à FII.

Les mesures de Mobilité électrophorétique ( $\mu_E$ ) ont été utilisées pour donner des informations sur la charge totale de surface de BLG, TAG, FI, FII et des complexes de BLG/TAG, BLG/FI et BLG/FII. Ce dernier système montre une valeur absolue inférieure de  $\mu_E$  par rapport aux dispersions de BLG/TAG et BLG/ FI quel que soit le pH. Cette caractéristique semble indiquer que FII induit une complexation / coacervation favorable avec BLG (Fig.7). L'explication peut être la composition chimique et les caractéristiques structurales de FII qui permettent une plus forte interaction à BLG, c'est-à-dire dans des conditions de pH où la densité de charge de BLG est inférieure.

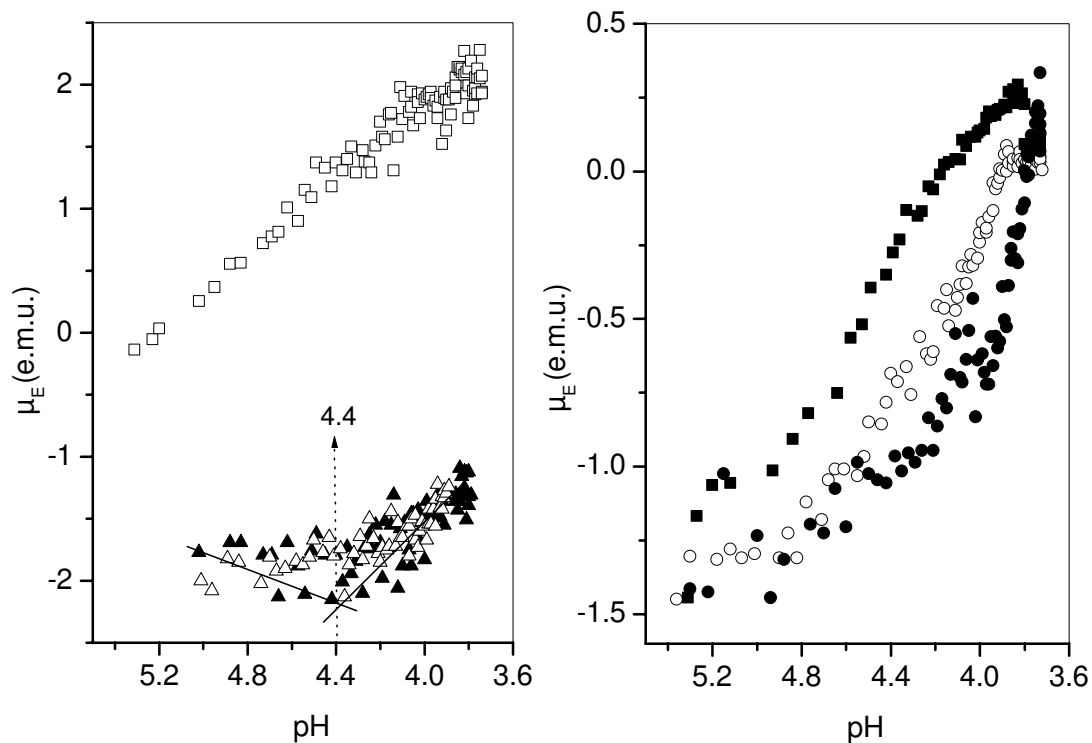


**Fig.7.** Evolution de la mobilité électrophorétique ( $\mu_E$ ) (e.m.u.) en fonction du pH à une concentration totale en biopolymères de 0.1wt% et à un ratio massique Pr:Pol de 2:1 pour les dispersions mélangées  $\beta$ -lactoglobuline (BLG)/gomme d'Acacia (TAG) ou Arabinogalactane-peptide (FI) ou Arabinogalactan-protéine (FII) et pour les dispersions stockées de  $\beta$ -lactoglobulin (BLG) ou gomme d'Acacia (AG). (●) BLG/TAG, (○) BLG/FI, (■) BLG/FII, (□) BLG, (▲) TAG et (Δ) FII. La ligne pointillée sert de guide pour les yeux. Chaque expérience a été faite en double.

Les mesures SALS ont permis de conclure sur les points suivants :

La séparation de phase dans les mélanges est conduite par un mécanisme de nucléation et croissance (NG). Six pH de transitions structurales ont été déterminés dans les trois mélanges:  $pH_{sc}$ , pH de formation des complexes solubles;  $pH_{ca}$ , pH d'agrégation des complexes;  $pH_{ps}$ , pH de séparation phase;  $pH_{coa}$ , pH de coacervation et  $pH_{neut}$ , pH de neutralisation des charges. De plus faibles valeurs de pH ont été déterminées pour le mélange BLG/FII par rapport à BLG/FI au dessous de  $pH_{ps}$ , en relation avec une complexation/coacervation favorisée. Ce résultat montre que la première phase de complexation a eu lieu aux mêmes pH de transitions dans tous les mélanges avant le déclenchement de la séparation de phase. Concernant les caractéristiques structurales des mélanges, l'interface entre les phases séparées était plus hétérogène dans BLG/FII à la dernière étape de la séparation de phase que dans BLG/FI. Aussi, de plus petits coacervats ont été formés dans ce mélange en comparaison avec BLG/FI.

## **Contrôle de la force des interactions entre la $\beta$ -lactoglobuline et la gomme d'Acacia moléculaire fractions**

Le chapitre IV fournit une vue plus générale du mécanisme de coacervation complexe du système BLG/AG en se basant sur la variation de la force d'interactions en changeant le ratio massique de mélange (Pr:Pol) et la concentration totale en biopolymères (Cp). Ainsi, des mesures de SALS, DLS,  $\mu_E$ , Granulo-Polarimétrie et microscopie optique ont été faites à différents Pr:Pol et Cp.

### **Rôle du rapport de charge Pr:Ps**

Un aperçu de la structure des complexes et des coacervates peut être obtenu à partir des mesures de DLS et de  $\mu_E$ . L'évolution du diamètre (d) des particules en fonction du pH pour les dispersions mélangées des BLG/TAG, BLG/FI et BLG/FII à différents Pr:Pol massiques est étudiée. Avec l'augmentation du Pr: Pol, les courbes de (d) sont déplacées vers les pH élevés, en accord avec la complexation à faible densité de charge positive de BLG. Cela est dû à l'augmentation du nombre de charges positives de BLG dans les dispersions.

À tous les ratios Pr:Pol (sauf le 4:1 pour les dispersions de BLG/FI), il y a eu la baisse de la valeur absolue de  $\mu_E$  en fonction du pH dans tous les mélanges, indiquant la formation de complexes. La diminution progressive de  $\mu_E$  peut être attribuée à l'augmentation du nombre de charges positives de BLG dans les dispersions. En outre, l'augmentation du rapport de mélange conduit à un plus grand nombre de particules chargées positivement au-dessous du pH d'électroneutralité (zéro  $\mu_E$ ). Cette fonctionnalité peut indiquer la formation de systèmes plus stables avec l'augmentation du rapport de mélange Pr:Pol.

Pour tous les mélanges, le maximum de l'intensité diffusée du mélange BLG/FII était inférieur à celui de BLG/TAG et BLG/FI à l'exception du ratio Pr:Pol de 40:1. Cette fonctionnalité peut indiquer la diminution du nombre de particules dans le mélange BLG/FII.

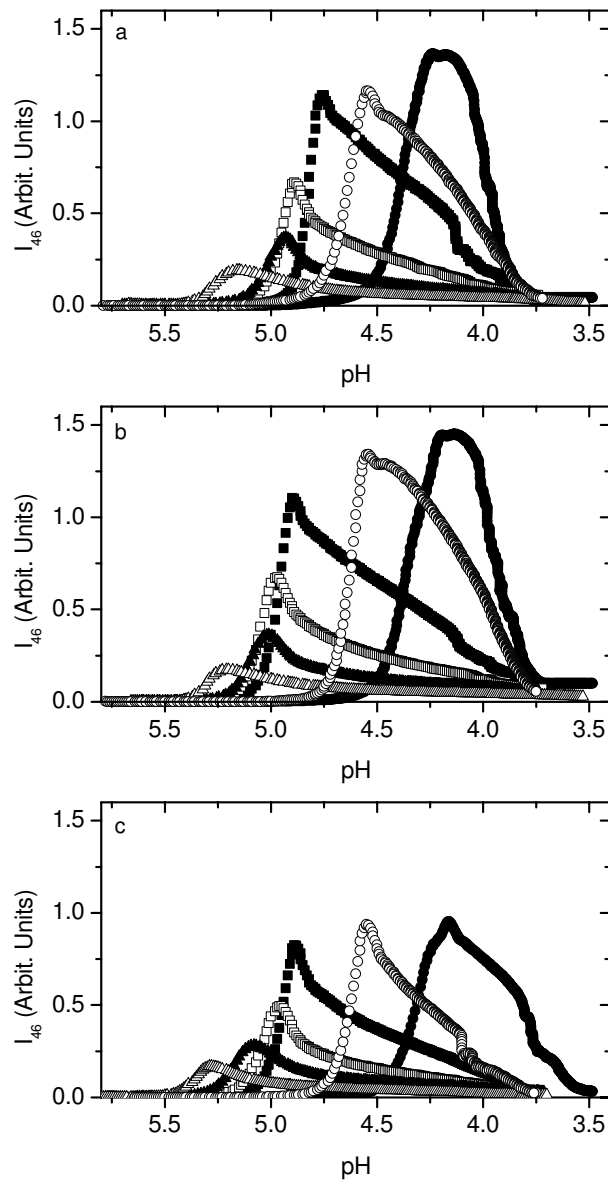


**Fig.8.** Evolution de l'intensité de lumière diffuse  $I_{46}$  (Unités Arbitraires) à un angle de diffusion de  $46^\circ$  en fonction du pH pour les dispersions mélangées de BLG/TAG (a), BLG/FI (b) et BLG/FII (c) à une concentration totale en biopolymères de 0.1 wt % et différents ratios massiques Pr:Pol. (●) 2:1, (○) 3:1, (■) 4:1, (□) 8:1, (▲) 16:1 et (Δ) 40:1. Chaque expérience a été faite en double.

Vraisemblablement, les systèmes ont montré différentes structures des particules avec le changement du rapport de mélange. C'est ainsi que, nous suggérons que le rôle des molécules et des caractéristiques structurales de l'AG sur la structure des complexes peut être mis en évidence par une diminution de la force d'interaction dans les mélanges en se basant sur une modification du rapport de mélange.

### Rôle de la concentration totale en biopolymères

La méthode de Granulo-polarimétrie est un outil pour l'étude quantitative des médias aléatoires. Elle permet de caractériser la densité du système en mesurant la longueur de transport ( $l^*$ ) dans différentes conditions externes (par exemple le cisaillement).  $l^*$ , qui est le libre parcours moyen de la lumière dans un milieu, correspond à l'unique paramètre nécessaire pour quantifier la dispersion de la lumière. Par conséquent, le présent appareil peut être d'un grand intérêt pour obtenir plus d'informations sur la structure des particules.

Fig. 9 montre l'évolution la longueur de transport au cours de la structuration des mélanges étudiés induite par le pH. En ce qui concerne la forme des courbes, tous les mélanges présentent la même évolution de  $l^*$  en fonction du pH. Ainsi, un minimum a été atteint entre deux gammes opposées de pH.

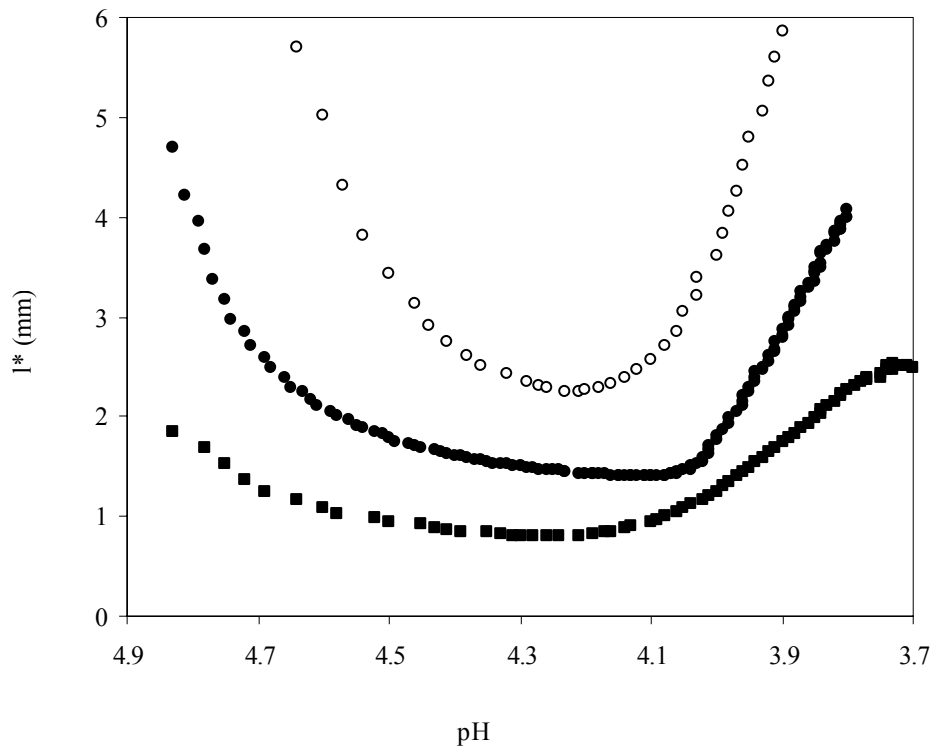


**Fig.9.** Evolution de la longueur de transport de la lumière ( $l^*$ ) (mm) en fonction du pH pour des dispersions mélangées de  $\beta$ -lactoglobuline (BLG)/ gomme d'Acacia (TAG) ou Arabinogalactane-peptide (FI) ou Arabinogalactane-protéine (FII) à une concentration totale en biopolymères de 4wt% et un ratio massique Pr: Pol de 2:1. (●) BLG / TAG, (○) BLG / FI, (■) BLG / FII. Chaque expérience a été faite en double.

Dans la première série,  $l^*$  a diminué en passant de pH 4,8 à pH ~ 4,12, 4,21 et 4,24 dans les mélanges BLG/TAG, BLG/FI et BLG/FII, indiquant l'augmentation de la turbidité dans les dispersions. À ces pH,  $l^*$  a atteint les valeurs minimales de 1,4 ; 2,3 et 0,8 mm. Une

augmentation de  $I^*$  semblait alors un bon moyen d'observer la baisse de la turbidité. Le minimum de  $I^*$  correspond à un maximum de la turbidité dans les dispersions.

Généralement, une diminution de  $I^*$  peut être due à une augmentation de la fraction volumique et / ou une diminution de la taille des objets diffusants dans le milieu. Les résultats de SALS ont montré que la séparation de phase suit le mécanisme de nucléation et croissance avec un point de transition au pH de  $\sim 4,2$ . Par la suite, le minimum de  $I^*$  peut être attribuée à la force d'interaction maximale ( $pH_{\text{mis}}$ ) entre les biopolymères en question. L'augmentation de  $I^*$  au-dessous du  $pH_{\text{mis}}$  peut être due à une diminution du nombre de particules. Pour un même niveau de pH, le système BLG/FII présente des valeurs plus faibles de  $I^*$  en comparaison avec le mélange BLG/FI, en accord avec une turbidité plus élevée en raison des interactions plus fortes entre FII et BLG, comme le montre le chapitre II.

Le transport de polarisation de la lumière a été étudié afin de mesurer la taille des particules indépendamment de la fraction volumique. La mesure de taille a été obtenue à partir de l'amplitude des effets de la polarisation linéaire. Une inversion de taille a été faite par les simulations de Monte Carlo correspondant à un indice de 1,2 m. A partir de l'amplitude de polarisation, une moyenne de la taille des objets a été déduite.

Fig.10 montre l'évolution de la taille des particules en fonction du pH dans tous les systèmes. Deux phases d'évolution opposées peuvent être observées dans tous les systèmes. Tout d'abord,  $d$  diminue jusqu'à un minimum de  $\sim 598$  nm à un pH de 4,23 dans le mélange BLG/FI. La diminution de la taille dans les dispersions de BLG/FI peut être attribuée à la dissociation des particules et / ou de l'augmentation de la fraction volumique d'objets.



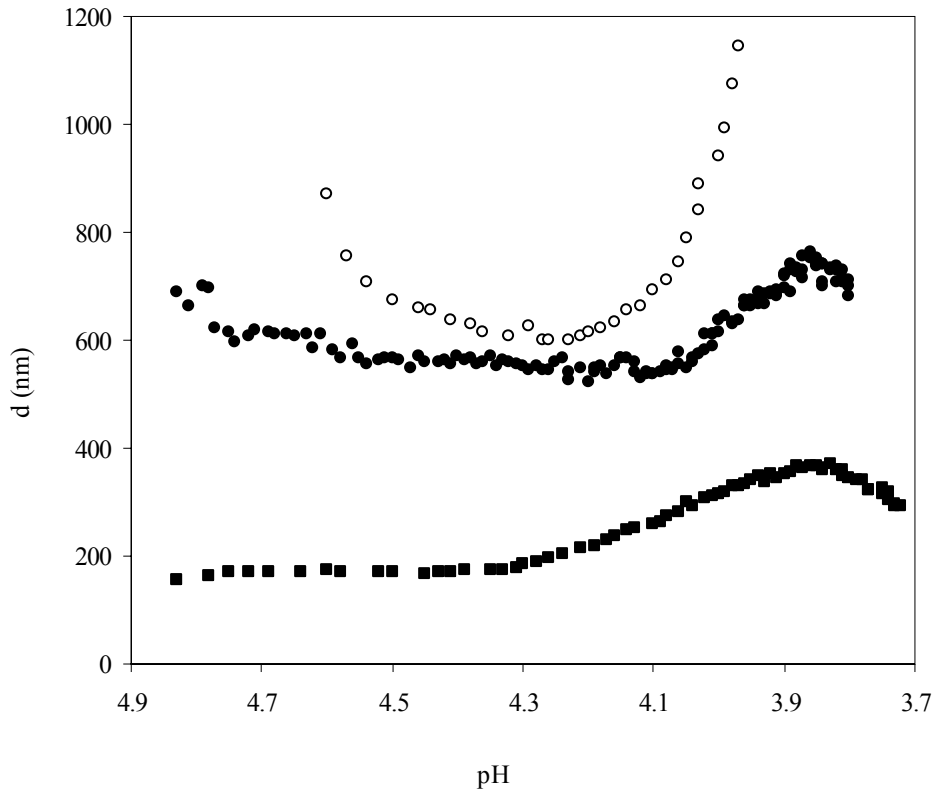


**Fig.10.** Evolution du diamètre des particules  $d$  (nm) en fonction du pH pour des dispersions mélangées de  $\beta$ -lactoglobuline (BLG)/gomme d'Acacia (TAG) ou Arabinogalactane-peptide (FI) ou Arabinogalactane-protéine (FII) à une concentration totale en biopolymères de 4wt% et à un ratio massique Pr: Pol de 2:1. (●) BLG / TAG, (○) BLG / FI, (■) BLG / FII. Chaque expérience a été faite en double.

D'un autre côté, une évolution relativement constante de la taille est parue dans les mélanges BLG/TAG et BLG/FII jusqu'à pH 4,12 ( $\sim 539$  nm) et de 4,35 ( $\sim 172$  nm), respectivement. Dans la deuxième phase, la taille augmente dans tous les mélanges. Il semble que les particules BLG/TAG ont une taille intermédiaire entre celles des autres systèmes. Quel que soit le pH, la plus petite taille des particules est observée dans le système BLG/FII par rapport au mélange BLG/FI en accord avec les résultats DLS. De là, il est important de noter que BLG/FI et BLG/FII présentent de différentes tendances de l'évolution de  $d$  à une valeur élevée de concentration ( $C_p$ ). Les mélanges BLG/TAG et BLG/FII ont montré des formes de courbes similaires. Ainsi, les résultats ont montré de différentes valeurs de taille dans les trois systèmes à haute concentration totale en biopolymères. Il faut noter que la force d'interaction élevée dans la dispersion BLG/FII par rapport à BLG/FI peut masquer le rôle de ses

propriétés structurales et conduire ensuite à une évolution constante de la taille durant la première gamme de pH (4.8-4.35) pendant l'acidification.

Connaissant la taille et les propriétés optiques ( $m = 1,2$ ), l'utilisation de la théorie de Mie (décrite dans le chapitre IV) permet de calculer la fraction de volume ( $\phi$ ) des objets diffusants. Les données brutes dans la Fig11 montrent que la courbe ( $\phi$  vs pH) possède la même cinétique par rapport à  $l^*$  dans tous les systèmes.

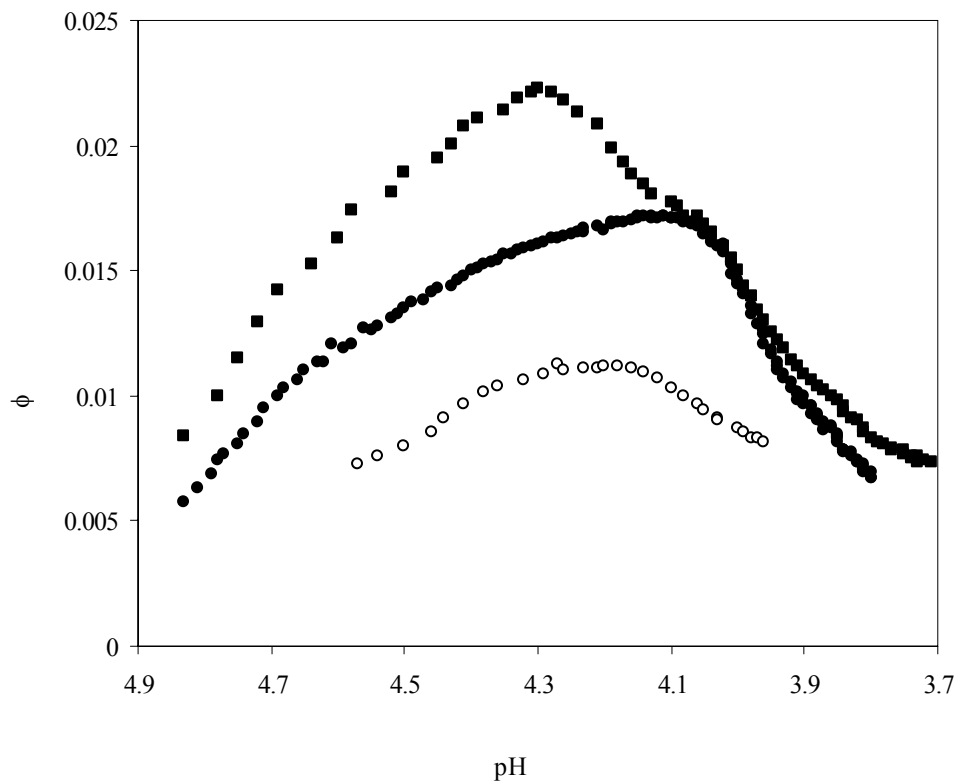


**Fig.11.** Evolution de la fraction de photons dispersés ( $\phi$ ) en fonction du pH pour des dispersions mélangées de  $\beta$ -lactoglobuline (BLG)/gomme d'Acacia (TAG) ou Arabinogalactane-peptide (FI) ou Arabinogalactane-protéine (FII) à une concentration totale en biopolymères de 4wt% et à un ratio massique Pr: Pol de 2:1. (●) BLG / TAG, (○) BLG / FI, (■) BLG / FII. Chaque expérience a été faite en double.

Un maximum de  $\phi$  est parvenu à un pH de 4,13, 4,21 et 4,31 dans les mélanges BLG/TAG, BLG/ FI et BLG/FII. Entre pH 4,8 et ces valeurs de pH, la fraction volumique augmente révélant une augmentation du nombre de particules (Fig.11). En dessous de ces pH, la concentration des objets diminue, ce qui correspond à une diminution du nombre de particules en raison de leur croissance et de coalescence. Le système BLG/FII révèle les valeurs les plus

élevées de  $\phi$  quel que soit le pH, ce qui indique la présence d'un nombre plus élevé de particules en dispersion.

Dans le chapitre II, il a été suggéré que la fraction volumique peut rester constante ou diminuer, au-dessus du  $\text{pH}_{\text{mis}}$ , au cours de l'acidification. Cependant, les résultats actuels obtenus dans un milieu concentré montrent une augmentation de la fraction volumique depuis le début de l'acidification jusqu'à  $\text{pH}_{\text{mis}}$ . En outre, la taille des particules est restée constante dans les systèmes BLG/TAG et BLG/FII au-dessus du  $\text{pH}_{\text{mis}}$ . Par conséquent, nous suggérons que certaines particules disparaissent et d'autres apparaissent simultanément lors de la complexation. Ainsi, une dissociation des particules se pose au cours de la phase de nucléation du mécanisme de coacervation complexe.

Pour résumer sur l'étude par Granulo-polarimétrie, les mélanges BLG/FI et BLG/FII révèlent des comportements différents au cours de la complexation / coacervation avec BLG induite par le pH en milieu concentré. Le système BLG/FI présentait des valeurs supérieures de  $l^*$  et inférieures de la fraction volumique, en relation avec une plus grande taille et de plus faible nombre de particules, en comparaison avec le mélange BLG/FII. Bien que la plus grande taille de FII ( $R_G$  supérieur), en théorie conduirait à l'augmentation de la taille des particules, l'inverse a été observé. Comme un excès de charges négatives est présent dans BLG/FII, nous suggérons que les interactions stériques et électrostatiques répulsives pouvant exister entre les complexes neutralisés de BLG/FII et ne favorisent pas ainsi la coalescence des complexes par rapport à BLG/FI. La répulsion stérique peut résulter de l'augmentation du nombre de particules présentes dans les dispersions de BLG/FII comme le montre les résultats de la fraction volumique.

Pour obtenir de plus amples renseignements sur l'évolution de la taille des dispersions, la **microscopie optique** a été utilisée en parallèle avec les mesures de Granulo-polarimétrie pour suivre les variations microstructurales induites par le pH dans un milieu concentré. Nous montrons les résultats du mélange BLG/TAG (Fig.12). Deux phases de l'évolution de la taille avec le pH sont apparues. Depuis le début de l'acidification jusqu'au  $\text{pH} \sim 4,14$ , une augmentation progressive du nombre d'entités structurales a été observée avec une taille constante. À un pH de  $\sim 4,14$ , un nombre maximum de particules a été observé. Au-dessous du  $\text{pH} \sim 4,14$ , les particules ont grandi en taille, mais leur nombre est réduit. Cette caractéristique peut être attribuée à la coalescence des coacervats ou maturation d'Ostwald, et probablement

aussi à la sédimentation des particules les plus grandes. La tendance d'évolution de  $d$  est en accord avec l'évolution de la taille obtenue par les mesures de SALS et Granulo-polarimétrie. On peut déduire que la coacervation est survenue dans la gamme de 4.25-3.9 de pH, puisque des gouttelettes sphériques de 2  $\mu\text{m}$  de diamètre ont été détectés dans cet intervalle.

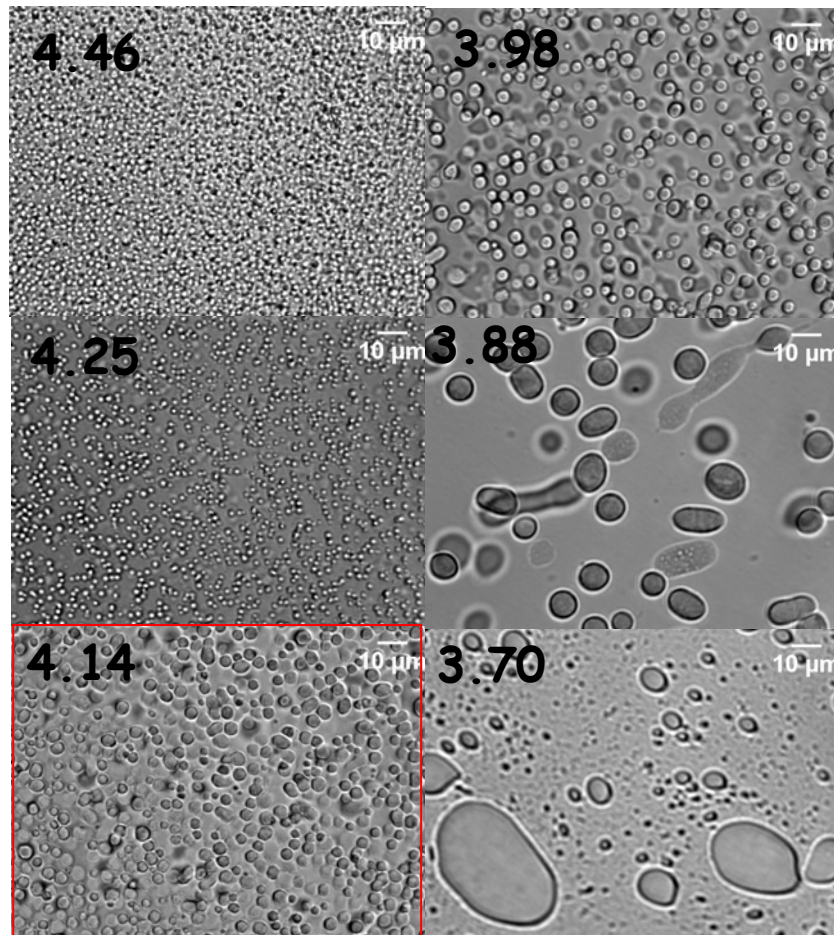


**Fig.12.** Micrographes d'Epi-fluorescence prises au cours de la coacervation complexe induite par le pH pour les dispersions mélangées de BLG/TAG à une concentration totale en biopolymères de 4wt% et à un ratio massique de Pr:Pol de 2:1. La barre représente 10  $\mu\text{m}$ . Le contraste et la luminosité des micrographes ont été traités par le ImageJ freeware (version beta 1.36).

Nous montrons dans la Fig.13 les micrographes des trois mélanges aux pH de 4,25 et de 3,88 pour mettre en évidence l'ampleur des différences entre les systèmes. Il a été observé des structures plus petites dans les mélanges de BLG/FII par rapport à BLG/FI à chacune des valeurs de pH. Le système BLG/TAG révèle des particules de tailles intermédiaires entre ceux des mélanges de BLG/FI et BLG/FII.

Il faut noter que la Granulo-polarimétrie a montré une taille maximale de  $\sim 1,18 \mu\text{m}$  dans le système BLG/FI ; alors que dans les Micrographes optiques, la taille des particules atteint une valeur moyenne de  $4,5 \mu\text{m}$  à un pH de 3,7. Cette différence de taille entre les deux techniques peut être attribuée au fait que la Granulo-polarimétrie permet de déterminer une taille moyenne et en se basant une approximation dans la méthode de calcul.

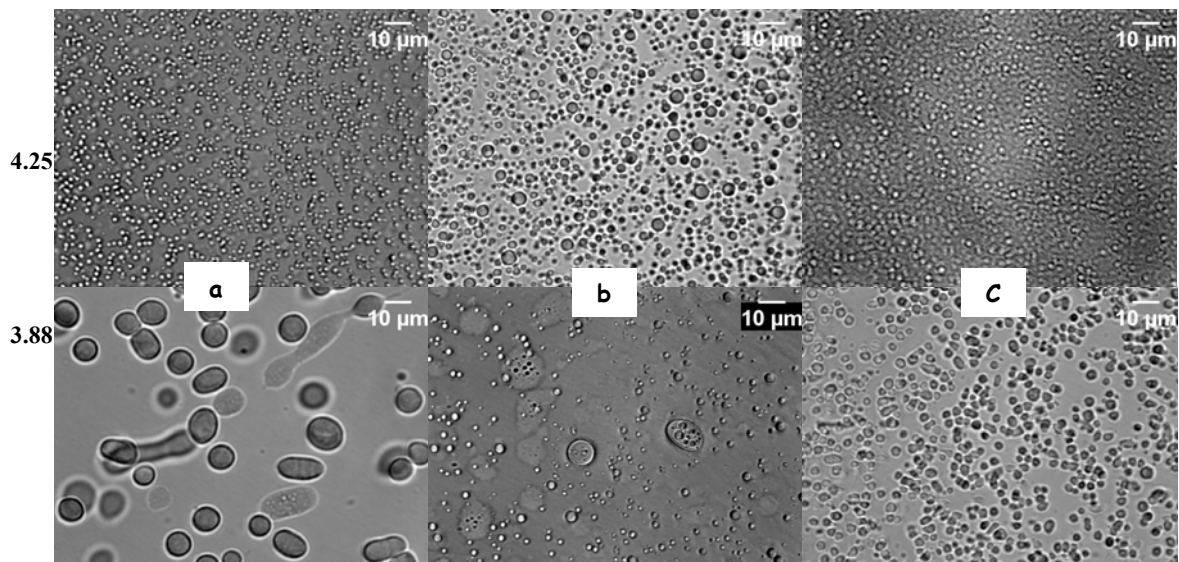


**Fig.13.** Micrographes d'Epi-fluorescence aux pH de 4,25 et de 3,88 ( $\pm 0,02$ ) pour les dispersions mélangées de BLG/TAG à une concentration totale en biopolymères de 4wt% et à un ratio massique de Pr: Pol de 2:1. (A) BLG / TAG, (b) BLG / FI et (c) BLG / FII. La barre représente 10  $\mu\text{m}$ . Le contraste et la luminosité des micrographes ont été traités par le ImageJ freeware (version beta 1.36).

La Granulo-polarimétrie et de la microscopie optique ont montré des résultats similaires des pH de transitions structurales dans un milieu concentré par rapport à ceux obtenus en milieu dilué dans les chapitres précédents. Ainsi, une augmentation de la concentration totale en biopolymères (40 fois) n'a modifié ni le comportement des phases de ni la cinétique de la séparation de phase. Ce résultat est en accord avec Mattison et al. (1995) qui indiquait que  $\text{pH}_c$  et  $\text{pH}_\phi$  restent constants avec l'augmentation de  $C_p$ . La principale raison est que l'équilibre de charges entre BLG et AG n'est pas modifié par l'augmentation  $C_p$ . Les changements des microstructures au cours de la séparation de phase induite par le pH du mélange BLG/TAG à  $C_p$  de 0.1wt% ont été étudiés par Mekhloufi et al. (2005). La première détection de structures était à un pH de 4,20. Cependant, dans nos micrographes il a été possible d'observer de petites fluctuations de la lumière sur l'écran de contrôle à un pH de

4,90, ce qui indique un avancement dans l'occurrence de la séparation de phase dans nos systèmes par rapport à ces auteurs. Une raison possible est la purification de nos biopolymères qui éliminent la projection d'ions et d'accélérer ensuite les interactions.

L'évolution du nombre et la taille des particules durant l'acidification, en milieux dilué et concentré, est en bon accord avec le mécanisme de nucléation et croissance discuté dans le chapitre III, qui indique que le mécanisme de séparation de phase n'est pas modifié avec l'augmentation de Cp. Ensuite, ce mécanisme dans les systèmes BLG/AG est indépendant de la concentration totale en biopolymères, mais cela dépend du pH, du rapport de mélange et des propriétés intrinsèques des macromolécules. Cependant, des structures de plus grand nombre et de plus grande taille ont été formées à haute Cp à toutes les valeurs de pH. Ceci est dû à l'augmentation du nombre de molécules de BLG et AG à haute Cp. Nous notons que la grande force d'interaction à haute Cp a permis de révéler les différences entre les systèmes. Toutefois, l'interaction forte à faible rapport de mélange a permis d'observer les comportements de ces trois systèmes

Pour résumer quant à l'effet de polymolécularité de la TAG : FI et FII ont montré des cinétiques différentes au cours de la complexation / coacervation avec BLG. Les différents comportements observés dans les mélanges sont dus à des différences dans les caractéristiques structurales et moléculaires (densité de charge, poids moléculaire, l rayon de giration, nombre de charges) des fractions de l'AG. En général, les polymères à haut poids moléculaire ont une forte tendance à induire la séparation de phase en raison de leur volume d'exclusion élevé et des effets stériques. Ceci est dû à la restriction de la marge de liberté qui réduit l'entropie du mélange et permet plus facilement la séparation de phase. En effet, lorsque la masse moléculaire et la flexibilité (durée de persistance de FII est de  $\sim 3$  nm, Sanchez et al., Résultats non publiés) d'une molécule augmente, le nombre de sites capables d'interagir avec une autre molécule augmente, en accord avec un taux de maturation plus rapide de la séparation de phase dans le mélange BLG/FII.

Il faut noter que la Granulo-polarimétrie et la densité optique n'ont pas permis de montrer des différences importantes entre les différents mélanges malgré les propriétés intrinsèques des molécules de l'AG. Cela pourrait être dû à la force des interactions électrostatiques à un Pr:Pol massique de 2:1, ce qui peut masquer les contributions moléculaires et structurales des fractions de la TAG. De là, l'étude des effets du rapport de mélange Pr:Pol et de la

concentration totale en biopolymères (dans un large intervalle) sur la complexation /coacervation entre BLG et les fractions moléculaires de l'AG pourrait être une autre approche pour mieux élucider leurs comportements structuraux.

En résumé, quel que soit le ratio, des plus petits complexes ont été présents dans le mélange BLG/FII par rapport à BLG/FI. Ceci pourrait être dû aux répulsions stériques et électrostatiques entre les particules de BLG/FII. Les mesures de SALS et DLS (à faible  $C_p$ ) ont montré qu'en augmentant le ratio Pr:Pol on favorise la complexation et/ou la séparation de phase à plus faible densité de charge de la BLG. La DLS a montré une augmentation de la taille des particules dans le mélange de BLG/FII aux ratios de mélange supérieurs à 2:1. Cette augmentation pourrait être due à la diminution de la force d'interaction en diminuant le ratio, ce qui révèle le rôle des propriétés structurales de FII tel que son plus grand rayon de giration qui devrait conduire à la formation de plus gros complexes. De plus, la morphologie des interfaces séparées devenait de moins en moins hétérogène, surtout pour les mélanges BLG/FII. Ceci a été évalué par la détermination d'exposants  $\gamma$ , des profils de diffusion  $I(q) \sim q^{-\gamma}$ , plus élevés des courbes de diffusion, qui ont atteint la valeur de Porod de 4 indiquant la formation d'une interface lisse. Aux deux valeurs les plus élevées du ratio de Pr:Pol (16:1 et 40:1), des particules moins compactes et une interface moins homogène ont été formées dans le mélange BLG/FI en comparaison avec BLG/FII. Ceci montre mieux l'effet de la structure de l'AG avec la diminution de la force d'interaction (augmentation du ratio). La variation de la concentration totale en biopolymères ( $C_p$ ) des mélanges n'a pas affecté la dynamique (mécanisme) et la cinétique (points de transitions structurales) de la coacervation complexe dans tous les mélanges. Le mécanisme de séparation de phase était toujours une nucléation et croissance. Les pH de transitions structurales restaient constants avec l'augmentation de  $C_p$ . Néanmoins, à  $C_p$  élevée, les coacervats formés sont plus grands et aussi plus nombreux. La Granulo-Polarimétrie et microscopie optique ont montré la présence de plus grosses particules dans le mélange BLG/FI avec l'augmentation de  $C_p$ , en comparaison avec BLG/FII.

Concernant l'effet de la polymolécularité de la TAG sur la coacervation complexe avec BLG, ces résultats peuvent être récapitulés de la façon suivante ; les deux fractions moléculaires principales de la TAG agissent différemment avec la BLG pendant la coacervation complexe dans les mêmes conditions expérimentales. Mais la somme de leurs comportements

correspond à celui de la gomme totale. En effet, FII induit une coacervation complexe plus favorisée et une énergie d'interaction plus importante avec la BLG, en comparaison avec FII. Une raison possible est que les propriétés structurales de cette fraction moléculaire (tel que poids moléculaire, nombre de charges et rayon de giration plus grands) favorisent la complexation avec la BLG.

Il est important de noter que les mélanges ont été préparés aux mêmes ratios massiques et non pas aux mêmes ratios de charge. Pour cela, les travaux futurs devraient étudier les trois systèmes préparés à des ratios de charge pour évaluer les différents comportements des molécules de la TAG. Malgré la difficulté pour attribuer un modèle thermodynamique d'interaction au système BLG/AG à partir des résultats ITC, cette méthode s'est avérée fructueuse pour étudier la thermodynamique de la coacervation complexe mais aussi pour mieux comprendre l'effet de la polymolécularité de la TAG. L'influence de certains paramètres comme la force ionique est envisageable pour mettre en évidence les différents types d'interactions, comme l'ITC a prouvé que la coacervation complexe du système BLG/AG n'est pas seulement le résultat des interactions électrostatiques. Il s'avère aussi nécessaire de faire des mesures de taille des particules à différents ratios de charges pour les trois systèmes afin de mieux comprendre les résultats DLS obtenus et les différences de structures entre les mélanges.

Dans le cadre de certaines études, l'utilisation d'une fraction moléculaire de la TAG au lieu d'une autre peut être suggérée pour aboutir à certaines propriétés du mécanisme de séparation de phase (force d'interaction, vitesse de maturation des particules) ou des structures obtenues (taille, forme). Par exemple, FII peut être employée pour favoriser une plus forte énergie d'interaction, une séparation de phase plus rapide et des coacervats de plus petites tailles à forte énergie d'interaction. Dans une expérience qui exige une faible polymolécularité ou pureté du matériel (comme l'ITC), les fractions moléculaires de la TAG peuvent la remplacer. Il est également important de noter que notre approche « l'effet de la polymolécularité de la TAG », qui reflète son impact structural sur les interactions avec la BLG, peut être aussi une bonne approche pour mieux comprendre la structure complexe de la TAG.



## **List of publications**

This thesis is based on the following publications:

Akil S., Renard D. and Sanchez C. (2006). Influence of Acacia gum molecular polydispersity on the complex coacervation with  $\beta$ -lactoglobulin, *Journal of Colloid and Interface Science* (submitted).

Akil S., Renard D. and Sanchez C. (2006). Complexation/ coacervation transition: control of the strength of interactions between  $\beta$ -lactoglobulin and Acacia gum molecular fractions, *Biomacromolecules* (submitted).

Akil S., Renard D. and Sanchez C. (2006). Thermodynamic characterization of interactions between  $\beta$ -lactoglobulin and major molecular fractions of Acacia gum (in preparation).

Akil S., Renard D. and Sanchez C. (2006). Study of complex coacervation between  $\beta$ -lactoglobulin and molecular fractions of Acacia gum by small angle static light scattering, *Proc. 4th International Symposium on Food Rheology and Structure (ISFRS)*, CD.

Dillet J., Baravian C., Sanchez C. et Akil S. (2006). Caractérisation des suspensions concentrées par Granulo-Polarimétrie, *Proc. Groupe de Recherches en Francophonie (GRF)*, CD.

Akil S., Renard D. et Sanchez C. (2004). Etude des interactions dans les mélanges de protéines et de polysaccharides, *Proc. Séminaire annuel de l'Ecole Doctorale de Nancy*, CD.

## **Conferences and Meetings**

Dillet J., Baravian C., Sanchez C. and Akil S. (2006). Caractérisation des suspensions concentrées par Granulo-Polarimétrie, Groupe de Recherches en Francophonie (GRF), 18-20 October, Cherbourg, France.

Akil S., Sanchez C. and Renard D. (2006). Complex coacervation between  $\beta$ -lactoglobulin and molecular fractions of Acacia gum: thermodynamic insights. European Colloid and Interface Society (ECIS), 16-22 September, Budapest, Hungary.

Akil S., Renard D. et Sanchez C. (2006) Interactions dans les complexes macromoléculaires et supramoléculaires des dispersions de  $\beta$ -lactoglobuline et gomme d'Acacia, Cinquième Conférence Internationale sur la Science des Matériaux (CSM5), 17-19 May, Beyrouth, Liban.

Akil S., Renard D. and Sanchez C. (2006). Study of complex coacervation between  $\beta$ -lactoglobulin and molecular fractions of Acacia gum by small angle static light scattering, 4th International Symposium on Food Rheology and Structure (ISFRS), 23-27 February, Zurich, Swizerland.

Akil S., Renard D. et Sanchez C. (2004). Etude des interactions dans les mélanges de protéines et de polysaccharides, Séminaire Annuel de l'Ecole Doctorale de Nancy, 25-28 January, Nancy, France.



# Table of contents

<b>Chapter I</b>	<b><i>Interactions and dynamics in colloidal systems</i></b>	<b>1</b>
<b>I.1.</b>	<b>Introduction</b>	<b>3</b>
<b>I.2.</b>	<b>Theoretical description of interaction forces</b>	<b>5</b>
I.2.1.	DLVO interactions	5
I.2.1.1.	Electrostatic interactions	5
I.2.1.2.	Van der Waals interactions	9
I.2.2.	Non DLVO interactions	10
I.2.2.1.	The hydration or solvation effect	11
I.2.2.2.	Hydrophobic interactions	12
<b>I.3.</b>	<b>Interactions in macromolecular solutions</b>	<b>14</b>
I.3.1.	Thermodynamics of polymer-polymer miscibility	14
I.3.1.1.	The Flory-Huggins theory	14
I.3.1.2.	Dynamics of phase separation	19
I.3.2.	Main demixing mechanisms in mixed macromolecular solutions	21
I.3.2.1.	Depletion flocculation	21
I.3.2.2.	Thermodynamic incompatibility: segregative phase separation	22
I.3.2.3.	Thermodynamic compatibility: associative phase separation	24
<b>I.4.</b>	<b>Complex coacervation between <math>\beta</math>-lactoglobulin and Acacia gum</b>	<b>27</b>
I.4.1.	Characteristics of $\beta$ -lactoglobulin	27
I.4.2.	Particularity of Acacia gum	27
I.4.3.	Mixtures of $\beta$ -lactoglobulin and Acacia gum	28
<b>I.5.</b>	<b>Objectives of the thesis</b>	<b>31</b>
<b>I.6.</b>	<b>Outline of the thesis</b>	<b>32</b>
<b>I.7.</b>	<b>References</b>	<b>34</b>
<b>Chapter II</b>	<b><i>Thermodynamic characterization of interactions between <math>\beta</math>-lactoglobulin and major molecular fractions of Acacia gum</i></b>	<b>41</b>
<b>II.1.</b>	<b>Introduction</b>	<b>42</b>
<b>II.2.</b>	<b>Experimental Section</b>	<b>45</b>
II.2.1.	Materials	45
II.2.2.	Preparation of $\beta$ -Lactoglobulin (BLG) and Acacia gum (AG) stock dispersions	46
II.2.3.	Isothermal Titration Calorimetry	46
II.2.4.	Optical density	47
<b>II.3.</b>	<b>Results and Discussion</b>	<b>48</b>
II.3.1.	Thermodynamic characteristics of BLG/AG interactions	48
II.3.2.	Ratio-induced structural transitions during complexation between BLG and AG	53
II.3.3.	Thermodynamic contribution of individual molecular fraction of TAG in interactions with BLG	55
II.3.4.	Parameters influencing the thermodynamic characteristics of the different BLG/AG systems	58
II.3.4.1.	Initial concentration of AG	59
II.3.4.2.	pH	60
II.3.4.3.	Temperature	64
<b>II.4.</b>	<b>Conclusions</b>	<b>69</b>
<b>II.5.</b>	<b>References</b>	<b>71</b>

**Chapter III Influence of Acacia gum molecular polydispersity on the complex coacervation with  $\beta$ -lactoglobulin ..... 75**

<b>III.1. Introduction.....</b>	<b>77</b>
<b>III.2. Experimental section .....</b>	<b>79</b>
III.2.1. Materials.....	79
III.2.2. Samples preparation .....	80
III.2.2.1. Stock solutions of $\beta$ -lactoglobulin (BLG) and Acacia Gum (AG) .....	80
III.2.2.2. Mixed dispersions.....	80
III.2.3. Dynamic light scattering.....	81
III.2.4. Electrophoretic mobility measurements ( $\mu_E$ ).....	81
III.2.5. Small Angle Static Light Scattering (SALS).....	82
<b>III.3. Results and Discussion.....</b>	<b>83</b>
III.3.1. Dynamic light scattering (DLS) .....	83
III.3.2. Electrophoretic mobility ( $\mu_E$ ) .....	85
III.3.3. Small angle static light scattering (SALS).....	88
<b>III.4. Conclusions.....</b>	<b>101</b>
<b>III.5. References.....</b>	<b>102</b>

**Chapter IV Control of the strength of interactions between  $\beta$ -lactoglobulin and Acacia gum molecular fractions ..... 105**

<b>IV.1. Introduction.....</b>	<b>107</b>
<b>IV.2. Experimental section .....</b>	<b>109</b>
IV.2.1. Materials.....	109
IV.2.2. Preparation of $\beta$ -Lactoglobulin (BLG), Acacia gum (AG) stock dispersions and BLG/AG mixed dispersions.....	109
IV.2.3. Dynamic light scattering.....	110
IV.2.4. Electrophoretic mobility measurements ( $\mu_E$ ).....	111
IV.2.5. Small Angle Static Light Scattering (SALS).....	111
IV.2.6. Granulo-Polarimetry.....	112
IV.2.7. Epi-fluorescence Microscopy .....	113
<b>IV.3. Results and Discussion.....</b>	<b>114</b>
IV.3.1. Effect of the Pr:Pol ratio on complexation/coacervation mechanism.....	114
IV.3.1.1. Dynamic light scattering .....	114
IV.3.1.2. Electrophoretic mobility .....	117
IV.3.1.3. Small angle static light scattering .....	119
IV.3.2. Effect of the total biopolymer concentration (Cp).....	127
IV.3.2.1. Granulo-Polarimetry .....	127
IV.3.2.2. Optical microscopy .....	131
<b>IV.4. Conclusions.....</b>	<b>135</b>
<b>IV.5. References.....</b>	<b>137</b>

**Summary..... 139**

**Acknowledgments..... 144**

**Curriculum Vitae..... 145**

## List of abbreviations

AG	Acacia gum
BLG	beta-lactoglobulin
C <sub>p</sub>	total biopolymer concentration
C <sub>p</sub>	calorific capacity
d	particle diameter
DLS	dynamic light scattering
GDL	glucono- $\delta$ -lactone
FI	first molecular fraction of Acacia gum (arabinogalactan-peptide)
FII	second molecular fraction of Acacia gum (arabinogalactan-protein)
ITC	isothermal titration calorimetry
TAG	total Acacia gum
I <sub>46</sub>	scattered light intensity at scattering angle of 46°
K	association constant
l*	transport mean free path of a photon
LS	light scattering
N	stoichiometry
NG	nucleation and growth
O.D.	optical density
pH <sub>mis</sub>	pH of maximum of interaction strength
pH <sub>coa</sub>	pH of coacervation
pH <sub>sc</sub>	pH at which soluble complexes are formed
pH <sub>ps</sub>	pH of phase separation
pI	isoelectric pH
Pr:Pol	protein-to-polysaccharide ratio
R <sub>G</sub>	radius of gyration
R <sub>h</sub>	hydrodynamic radius
r <sub>coa</sub>	ratio of coacervation
r <sub>ps</sub>	ratio of phase separation
r <sub>sat</sub>	ratio of saturation
SALS	small angle light scattering
SD	spinodal decomposition
$\Delta G$	free binding enthalpy
$\Delta H$	binding enthalpy
$\Delta H_{obs}$	binding enthalpy observed
$\Delta H_{endo}$	endothermic binding enthalpy
$\Delta H_{exo}$	exothermic binding enthalpy
$\Delta H_{rea}$	binding enthalpy of reaction
$\Delta S$	binding entropy
$\gamma$	exponent of the scattering profiles $I(q) \sim q^{-\gamma}$
$\mu_E$	electrophoretic mobility
$\tau$	turbidity
$\phi$	scatterer volume fraction

## List of tables

Tab. II.1. Number of negative charges and molecular parameters of TAG and its two major molecular fractions FI and FII. Adapted from Renard <i>et al.</i> (2006).....	46
Tab. II.2. Binding parameters of interaction between $\beta$ -lactoglobulin and Acacia gum molecular fractions obtained from the titration of an aqueous dispersion of AG (1.8 wt %) into an aqueous dispersion of $\beta$ -lactoglobulin (0.6 wt %) at 25 °C and pH 4.2. N: stoichiometry, K: binding constant, $\Delta H_{\text{exo}}$ : binding enthalpy, $\Delta S_{\text{exo}}$ : binding entropy and $\Delta G_{\text{exo}}$ : free Gibbs energy of binding. exo: exothermic peaks. Parameters were calculated for the first exothermic stage in the titration curves.....	53
Tab. II.3. Number of charges in BLG, TAG, FI and FII dispersions at different pH values, determined by titration measurements (Renard <i>et al.</i> , 2006) or calculated (Cannan <i>et al.</i> , 1941).....	53
Tab. II.4. Binding parameters of interaction between $\beta$ -lactoglobulin and Acacia gum molecular fractions obtained from the titration of an aqueous dispersion of AG (1.8 wt %) into an aqueous dispersion of $\beta$ -lactoglobulin (0.6 wt %) at 25 °C. N: stoichiometry, K: binding constant, $\Delta H_{\text{exo}}$ : binding enthalpy, $\Delta S_{\text{exo}}$ : binding entropy and $\Delta G_{\text{exo}}$ : free Gibbs energy of binding. exo: exothermic peaks. Parameters were calculated for the first exothermic stage in the titration curves.....	62
Tab. III.1. Characteristic pH of structural transitions in BLG/TAG, BLG/FI and BLG/FII mixed dispersions at a total biopolymer concentration of 0.1wt% and a protein:polysaccharide (Pr:Pol) weight ratio of 2:1, determined by different parameters derived from light scattering and electrophoretic mobility measurements. Each value is the average of three independent experiments.....	99
Tab. IV.1. Size of particles, $d$ ( $\mu\text{m}$ ), determined at both the pH of phase separation ( $\text{pH}_{\text{ps}}$ ) and pH of neutralization ( $\text{pH}_{\text{neut}}$ ) (where $\mu_E$ is zero e.m.u.) as a function of the Pr:Pol mixing weight ratio. $r_{\text{neut}}$ : the Pr:Pol charge ratio of neutralization determined at $\mu_E$ is zero e.m.u. ....	116
Tab. IV.2. Size of particles, $d$ ( $\mu\text{m}$ ), determined at the pH of complex coacervation ( $\text{pH}_{\text{coa}}$ ) as a function of the Pr:Pol mixing weight ratio.....	119
Tab. IV.3. Calculated Pr:Pol charge ratios for BLG/TAG, BLG/FI and BLG/FII mixed dispersions at pH 4.2.	121

## List of figures

- Fig. I.1. Illustrations of colloidal stabilization by steric and electrostatic interactions. Adapted from SpecialChem website: [www.SpecialChem.com](http://www.SpecialChem.com). ..... 4
- Fig. I.2. Schematic view of the components of a charge-stabilized colloidal dispersion. Ionizable surface groups dissociate in solution, leaving charges bound to the spheres' surfaces and counterions in solution. These counterions are augmented by other simple ions already in solution. Electrostatic interactions among all of these species result in an effective interaction between the spheres.  $k^{-1}$  is the screening length that describes how the simple ions' correlations with the macroions fall off with distance due to screening of the electric field.  $h$ : distance between two spheres. .... 6
- Fig. I.3. The Gouy-Chapman-Stern-Grahame electric double layer model (a) charge distribution (b) potential distribution. Figure taken from (Jolivet 1994) ..... 7
- Fig. I.4. The triple layer model. IHP: Inner Helmholtz plane, OHP: Outer Helmholtz plane. Adapted from (Jolivet, 1994) <sup>31</sup>. ..... 8
- Fig. I.5. Schematic view of the Electrical Double Layer (EDL)..... 8
- Fig. I.6. Calculated energy profiles as a function of the distance between particle surfaces taking into account DLVO interactions. (a) Conditions in which surfaces repel strongly while colloidal particles remain stable. (b) Conditions for which surfaces come into a stable equilibrium at the secondary minimum (if it is deep enough); colloids then coagulate reversibly. (c) The interaction curve approaches the pure van der Waals curve; colloids coagulate irreversibly. Conditions used to compute the curves: Particle diameter = 1  $\mu\text{m}$  : Hamaker constant =  $1.5 \times 10^{-13}$  ergs : Salt (NaCl) concentration = 0.001 M (curve a), 0.03 M (curves b-c): Particle surface potential = 35 mV (curve a), 35/30/25mV (curves b) and 10 mV (curve c). Taken from (Stoll and Buffle 1995) ..... 11
- Fig. I.7. Two dimensional lattice model of a mixture of polymer chains. Units of equal size corresponding to monomers of the two polymers occupy the lattice sites. Taken from Van der Haegen *et al.* (1989) ..... 15
- Fig. I.8. a) Dependence of the Gibbs free energy of mixing  $\Delta G_{\text{mix}}$  on the composition  $\phi$  at constant temperature. At the two inflection points (A and B) in the graph, the second derivative  $\partial^2 \phi \Delta G_{\text{mix}}$  vanishes. The inflection points define the spinodal. b) The two phase region is enclosed by the binodal. In the region under the spinodal the mixture is unstable while between the curves the blend is metastable (nucleation and growth of phase separated domains). Above the critical temperature  $T_c$  the blend is stable in the mixed phase. A temperature quench from the one-phase to the two-phase region induces phase separation. c) Variables used in the description of the mixing process of two polymers A and B. Adapted from Van der Haegen *et al.* (1989) <sup>55</sup>..... 18
- Fig. I.9. Schematic view of the theoretical phase diagram for a binary polymeric system. Adapted from Horst *et al.* ..... 20
- Fig. I.10. Schematic view of the phase separation by the nucleation and growth, and spinodal decomposition phenomena. Taken from Olabisi *et al.* <sup>50</sup> and Kwei *et al.* (1978) ..... 20
- Fig. I.11. Schematic view of the mechanism of depletion interaction. Adapted from Lin *et al.* (2001). ..... 22
- Fig. I.12. Schematic phase diagram of segregative (a) and associative (b) phase separation in mixed polymer (or biopolymer) solutions. S denotes solvent and P polymer. Adapted from (Bungenberg de Jong and Kruyt, 1949a) <sup>20</sup>. ..... 23



- Fig. II.1. Microcalorimetric titration thermogram for the dilution of total Acacia gum (1.8 wt %) into water (...) and (—) water into  $\beta$ -lactoglobulin (0.6 wt %), at pH 4.2 and 25 °C. Each experiment was made in triplicate..... 49
- Fig. II.2. Thermograms corresponding to the titration of water into an aqueous dispersion  $\beta$ -lactoglobulin (0.6 wt %) at pH 4.2 and at different temperatures. Each experiment was made in duplicate..... 50
- Fig. II.3. (a) Thermogram corresponding to the titration of an aqueous dispersion of total Acacia gum (1.8 wt %) or arabinogalactan-peptide fraction (FI) (1.8 wt %) or arabinogalactan-protein fraction (FII) (1.8 wt %) into an aqueous dispersion of  $\beta$ -lactoglobulin (0.6 wt %) at pH 4.2 and 25 °C. (b) Binding isotherm corresponding to the previous titration experiment. P1, P2 and P3 correspond to three transition points observed in binding isotherms. The experiments were made in duplicate. .... 51
- Fig. II.4. Binding isotherm derived from the titration of an aqueous dispersion of Acacia gum into an aqueous dispersion of  $\beta$ -lactoglobulin (0.6 wt %) at pH 4.2 and 25 °C. (●) titration of total Acacia gum (1.8 wt %) into  $\beta$ -lactoglobulin, (○) titration of FI fraction (1.8 wt %) into  $\beta$ -lactoglobulin and (■) titration of FII fraction (1.8 wt %) into  $\beta$ -lactoglobulin. Dotted line is guide for eyes. Each experiment was made in triplicate..... 54
- Fig. II.5. Evolution of the Optical Density (O.D.) as a function of Pr:Pol charge ratio during the titration of an aqueous dispersion of Acacia gum (1.8 wt %) into an aqueous dispersion of  $\beta$ -lactoglobulin (0.6 wt %) at pH 4.2 and 25 °C. (●) titration of total Acacia gum (1.8 wt %) into  $\beta$ -lactoglobulin, (○) titration of FI fraction (1.8 wt %) into  $\beta$ -lactoglobulin and (■) titration of FII fraction (1.8 wt %) into  $\beta$ -lactoglobulin. Dotted line is guide for eyes. Each experiment was made in triplicate. .... 57
- Fig. II.6. (a) Thermograms corresponding to the titration of an aqueous dispersion of Acacia gum into an aqueous dispersion of  $\beta$ -lactoglobulin (0.6 wt %) at different concentrations for Acacia gum at pH 4.2 and 25 °C. (b) Binding isotherm corresponding to the previous titration experiments. (●) 1.8 wt %, (○) 2.4 wt %, (■) 3 wt % and (□) 6 wt %. Dotted line is guide for eyes. Each experiment was made in duplicate. .... 59
- Fig. II.7. (a) Thermograms corresponding to the titration of an aqueous dispersion of Acacia gum (1.8 wt %) into an aqueous dispersion of  $\beta$ -lactoglobulin (0.6 wt %) at 25 °C and different pH. (b) Binding isotherm corresponding to the previous titration experiments. (●) pH 3.8, (○) pH 4.2 and (■) pH 4.5. Dotted line is guide for eyes. Each experiment was made in duplicate. .... 61
- Fig. II.8. Evolution of the Optical Density (O.D.) at 633 nm as a function of pH for the Pr /Pol mixed dispersions at 0.1 wt % total biopolymer concentration and Pr:Pol weight ratio of 2:1. (●) BLG/TAG, (○) BLG/FI, (■) BLG/FII. Each curve is the average of three independent experiments. .... 63
- Fig. II.9. Thermograms corresponding to the titration of an aqueous dispersion of Acacia gum (1.8 wt %) into an aqueous dispersion of  $\beta$ -lactoglobulin (0.6 wt %) at pH 4.2 and different temperatures. (a) titration of total Acacia gum (1.8 wt %) into  $\beta$ -lactoglobulin, (b) titration of FI fraction (1.8 wt %) into  $\beta$ -lactoglobulin. Each experiment was made in duplicate..... 64
- Fig. II.10. (a) Thermograms corresponding to the titration of an aqueous dispersion of Acacia gum (1.8 wt %) into an aqueous dispersion of  $\beta$ -lactoglobulin (0.6 wt %) at pH 4.2 and different temperatures. (b) Binding isotherm corresponding to the previous titration experiments. (●) 25°C, (○) 30 °C, (■) 35 °C, (□) 40 °C, (▲) 45 °C and (Δ) 50 °C. Dotted line is guide for eyes. Each experiment was made in duplicate. .... 66
- Fig. II.11. Evolution of the ratio of complex aggregation ( $r_{agg}$ ) as a function of temperature during the titration of an aqueous dispersion of total Acacia gum (1.8 wt %) into an aqueous dispersion of  $\beta$ -lactoglobulin (0.6 wt %) at pH 4.2 and different temperatures. Dotted line is guide for eyes. Each experiment was made in duplicate. .... 67

- Fig. II.12. Evolution of  $\Delta H_{\text{exo}}$  with temperature during the titration of an aqueous dispersion of total Acacia gum (1.8 wt %) into an aqueous dispersion of  $\beta$ -lactoglobulin (0.6 wt %) at pH 4.2. Line corresponds to a linear fit of data. Each experiment was made in duplicate. .... 68
- Fig. III.1. Evolution of the diameter of particles as a function of pH for  $\beta$ -lactoglobulin (BLG) / Acacia Gum (TAG) or Arabinogalactan-peptide (FI) or Arabinogalactan-protein (FII) mixed dispersions at 0.1wt% total biopolymer concentration and Pr:Pol weight ratio of 2:1. (●) BLG/TAG, (○) BLG/FI, (■) BLG/FII. Each experiment was made in triplicate. Inset: a zoomed region of the same curve. .... 84
- Fig. III.2. Evolution of the particles diameter (d) (nm) as a function of pH for Acacia Gum (TAG) or Arabinogalactan-peptide (FI) or Arabinogalactan-protein (FII) stock dispersions at 0.1wt% total biopolymer concentration and Pr:Pol weight ratio of 2:1. (●) TAG, (○) FI, (■) FII. Each experiment was made in duplicate. .... 85
- Fig. III.3. Evolution of the electrophoretic mobility ( $\mu_E$ ) (e.m.u.) as a function of pH at 0.1wt% total biopolymer concentration and Pr:Pol weight ratio of 2:1 for  $\beta$ -lactoglobulin (BLG) / Acacia Gum (TAG) or Arabinogalactan-peptide (FI) or Arabinogalactan-protein (FII) mixed dispersions and for  $\beta$ -lactoglobulin (BLG) or Acacia Gum (AG) stock dispersions. (●) BLG/TAG, (○) BLG/FI, (■) BLG/FII, (□) BLG, (▲) TAG and (Δ) FII. Dotted line is guide for the eye. Each experiment was made in duplicate. .... 86
- Fig. III.4. Evolution of the charge-to-molecular weight ratio ( $C/M_w$ ) with pH for TAG, FI and FII stock dispersions. (●) TAG, (○) FI, (■) FII. The charge values of all biopolymers were determined by titration measurements (Renard *et al.*, 2006). .... 88
- Fig. III.5. Evolution of the scattered light intensity at a scattering angle of  $46^\circ$  ( $I_{46}$ ) (arbitrary units) as a function of pH for  $\beta$ -lactoglobulin (BLG) / Acacia Gum (TAG) or Arabinogalactan-peptide (FI) or Arabinogalactan-protein (FII) mixed dispersions at 0.1wt% total biopolymer concentration. (●) BLG/TAG 2:1 weight ratio, (○) BLG/(FI+FII) 2:1, (■) BLG/FI 2.3:1, (□) BLG/FII 17:1. Each experiment was made in triplicate. .... 89
- Fig. III.6. Evolution of the scattered light intensity at a scattering angle of  $46^\circ$  ( $I_{46}$ ) (arbitrary units) as a function of pH for  $\beta$ -lactoglobulin (BLG) / Acacia Gum (TAG) or Arabinogalactan-peptide (FI) or Arabinogalactan-protein (FII) mixed dispersions at 0.1wt% total biopolymer concentration and protein:polysaccharide (Pr:Pol) weight ratio of 2:1 (a) and 40:1 (b). (●) BLG/TAG, (○) BLG/FI, (■) BLG/FII. Each experiment was made in triplicate. .... 90
- Fig. III.7. Evolution of the derivative of the scattered light intensity at  $46^\circ$  scattering angle  $dI_{46}/dt$  (arbitrary units) as a function of pH for  $\beta$ -lactoglobulin (BLG) / Acacia Gum (TAG) or Arabinogalactan-peptide (FI) or Arabinogalactan-protein (FII) mixed dispersions at 0.1wt% total biopolymer concentration and Pr:Pol weight ratio of 2:1. (●) BLG/TAG, (○) BLG/FI, (■) BLG/FII. Each curve is the average of three independent experiments. .... 92
- Fig. III.8. Scattering profiles  $I(q)$  (arbitrary units) as a function of  $q$  ( $\mu\text{m}^{-1}$ ) recorded during slow acidification of BLG/TAG mixed dispersion at 0.1wt% total biopolymer concentration and Pr:Pol weight ratio of 2:1 in a pH range where a correlation peak does not appear. (●) pH 5.4, (○) pH 5.2, (■) pH 5.0, (□) pH 4.8, (▲) pH 4.6 and (Δ) pH 4.5. Each experiment was made in triplicate. .... 93
- Fig. III.9. Scattering profiles  $I(q)$  (arbitrary units) as a function of  $q$  ( $\mu\text{m}^{-1}$ ) recorded during slow acidification of BLG/TAG mixed dispersion at 0.1wt% total biopolymer concentration and Pr:Pol weight ratio of 2:1 in a pH range where a correlation peak appeared. (●) pH 4.33, (○) pH 4.25, (■) pH 4.2, (□) pH 4.18, (▲) pH 4.12, (Δ) pH 4.10, (◆) pH 4.04, (◇) pH 4.00 and (-) pH 3.95. Continuous lines correspond to weighted curve fits with three or fourth-order polynomial function. Dot line highlights the shift of the scattering maximum towards smaller  $q$  values. Each experiment was made in triplicate. .... 94
- Fig. III.10. Evolution of the maximum wave vector  $q_{\text{max}}$  ( $\mu\text{m}^{-1}$ ) as a function of pH for  $\beta$ -lactoglobulin (BLG) / Acacia Gum (TAG) or Arabinogalactan-peptide (FI) or Arabinogalactan-protein (FII) mixed dispersions at

- 0.1wt% total biopolymer concentration and Pr:Pol weight ratio of 2:1. (●) BLG/TAG, (○) BLG/FI, (■) BLG/FII. Each experiment was made in triplicate. .... 95
- Fig. III.11. Evolution of the maximum wave vector  $q_{\max}$  ( $\mu\text{m}^{-1}$ ) as a function of time for  $\beta$ -lactoglobulin (BLG) / Acacia Gum (TAG) or Arabinogalactan-peptide (FI) or Arabinogalactan-protein (FII) mixed dispersions at 0.1wt% total biopolymer concentration and Pr:Pol weight ratio of 2:1. (●) BLG/TAG, (○) BLG/FI, (■) BLG/FII. Continuous lines correspond to weighted curve fits using a power law function. Each experiment was made in triplicate. .... 96
- Fig. III.12. Evolution of the exponent  $\gamma$  obtained from the scattering profiles  $I(q) \sim q^{-\gamma}$  ( $3.546 < q < 10.414 \mu\text{m}^{-1}$ ) of the  $\beta$ -lactoglobulin (BLG) / Acacia Gum (TAG) or Arabinogalactan-peptide (FI) or Arabinogalactan-protein (FII) mixed dispersions at 0.1wt% total biopolymer concentration and Pr:Pol weight ratio of 2:1. (●) BLG/TAG, (○) BLG/FI, (■) BLG/FII. Each experiment was made in triplicate. .... 97
- Fig. IV.1. Evolution of the particle diameter  $d$  ( $\mu\text{m}$ ) as a function of pH for the BLG/TAG (a), BLG/FI (b) and BLG/FII (c) mixed dispersions at 0.1 wt % total biopolymer concentration and different Pr:Pol weight ratios. (●) 2:1, (○) 4:1, (■) 8:1 and (□) 16:1. Each experiment was made in duplicate. .... 115
- Fig. IV.2. Evolution of the particle diameter  $d$  ( $\mu\text{m}$ ) as a function of pH for the BLG stock dispersion at 0.066, 0.08 and 0.088 wt % total biopolymer concentration and BLG to water ratio of (●) 2:1, (○) 4:1 and (■) 8:1, respectively. Each experiment was made in duplicate. .... 116
- Fig. IV.3. Evolution of the electrophoretic mobility  $\mu_E$  (e.m.u.) as a function of pH for the BLG/TAG (a), BLG/FI (b) and BLG/FII (c) mixed dispersions at 0.1 wt % total biopolymer concentration and different Pr:Pol weight ratios. (●) 2:1, (○) 4:1, (■) 8:1 and (□) 16:1. Each experiment was made in duplicate. .... 118
- Fig. IV.4. Evolution of the scattered light intensity  $I_{46}$  (Arbitrary Units) at  $46^\circ$  scattering angle as a function of pH for the BLG/TAG (a), BLG/FI (b) and BLG/FII (c) mixed dispersions at 0.1 wt % total biopolymer concentration and different Pr:Pol weight ratio. (●) 2:1, (○) 3:1, (■) 4:1, (□) 8:1, (▲) 16:1 and (△) 40:1. Each experiment was made in duplicate. .... 120
- Fig. IV.5. Evolution of the turbidity  $\tau$  ( $\text{cm}^{-1}$ ) as a function of pH for mixed dispersions at 0.1 wt % total biopolymer concentration and Pr:Pol weight ratio of 2:1 (a) and 16:1 (b). (●) BLG/TAG, (○) BLG/FI and (■) BLG/FII. Each experiment was made in duplicate. .... 122
- Fig. IV.6. Scattering profiles  $I(q)$  (arbitrary units) as a function of  $q$  ( $\mu\text{m}^{-1}$ ) recorded during slow acidification of BLG/TAG mixed dispersions at 0.1wt% total biopolymer concentration and Pr:Pol weight ratio of 16:1 in a pH range where a correlation peak appeared. (●) pH 4.94, (○) pH 4.83, (■) pH 4.73, (□) pH 4.65, (▲) pH 4.51, (△) pH 4.40, (◆) pH 4.29 and (◇) pH 4.20. Continuous lines correspond to weighted curve fits with three or fourth-order polynomial function. Dot line highlights the shift of the scattering maximum towards smaller  $q$  values. Each experiment was made in triplicate. .... 123
- Fig. IV.7. Evolution of the maximum wave vector  $q_{\max}$  ( $\mu\text{m}^{-1}$ ) as a function of time for the BLG/TAG mixed dispersions at 0.1 wt % total biopolymer concentration and two Pr:Pol weight ratios. (●) 2:1, (○) 16:1. Each experiment was made in duplicate. .... 124
- Fig. IV.8. Evolution of the slope value  $\gamma$  of  $\log I$  vs  $\log q$  ( $3.546 < q < 10.414 \mu\text{m}^{-1}$ ) with pH for BLG/AG mixed dispersions at 0.1 wt % total biopolymer concentration and different Pr:Pol weight ratios. (●) BLG/TAG, (○) BLG/FI and (■) BLG/FII. Dotted lines are guide for eyes. Each experiment was made in duplicate. 125
- Fig. IV.9. Evolution of the slope value  $\gamma$  as a function of Pr:Pol weight ratio at pH 3.8. (●) BLG/TAG, (○) BLG/FI and (■) BLG/FII. Each experiment was made in duplicate. .... 126
- Fig. IV.10. Evolution of the transport length ( $l^*$ ) (mm) as a function of pH for  $\beta$ -lactoglobulin (BLG) / Acacia Gum (TAG) or Arabinogalactan-peptide (FI) or Arabinogalactan-protein (FII) mixed dispersions at 4wt%

total biopolymer concentration and Pr:Pol weight ratio of 2:1. (●) BLG/TAG, (○) BLG/FI, (■) BLG/FII. Each experiment was made in duplicate..... 128

Fig. IV.11. Evolution of the diameter of scatterers particles  $d$  (nm) as a function of pH for  $\beta$ -lactoglobulin (BLG) / Acacia Gum (TAG) or Arabinogalactan-peptide (FI) or Arabinogalactan-protein (FII) mixed dispersions at 4wt% total biopolymer concentration and Pr:Pol weight ratio of 2:1. (●) BLG/TAG, (○) BLG/FI, (■) BLG/FII. Each experiment was made in duplicate..... 129

Fig. IV.12. Evolution of the fraction of photons internally scattered ( $\phi_i$ ) as a function of pH for  $\beta$ -lactoglobulin (BLG) / Acacia Gum (TAG) or Arabinogalactan-peptide (FI) or Arabinogalactan-protein (FII) mixed dispersions at 4wt% total biopolymer concentration and Pr:Pol weight ratio of 2:1. (●) BLG/TAG, (○) BLG/FI, (■) BLG/FII. Each experiment was made in duplicate. .... 130

Fig. IV.13. Epi-fluorescence micrographs taken during the pH-induced complex coacervation for the BLG/TAG mixed dispersions at 4wt% total biopolymer concentration and Pr:Pol weight ratio of 2:1. Bar represents 10 $\mu$ m. Contrast and brightness of micrograph were treated by the ImageJ freeware (version Beta 1.36, Wayne Rasband)..... 132

Fig. IV.14. Epi-fluorescence micrographs at pH 4.25 and 3.88 ( $\pm 0.02$ ) for the BLG/AG mixed dispersions at 4wt% total biopolymer concentration and Pr:Pol weight ratio of 2:1. (a) BLG/TAG, (b) BLG/FI and (c) BLG/FII. Bar represents 10 $\mu$ m. Contrast and brightness of micrograph were treated by the ImageJ freeware (version Beta 1.36, Wayne Rasband)..... 133

## *Chapter I*

# **Interactions and dynamics in colloidal systems**

### **Abstract**

This chapter consists of an introduction into the interactions and resulting demixing mechanisms in colloidal mixtures. The colloidal stability of dispersion is of great importance in a number of industries such as pharmaceutical, ceramic, paints and pigments. Colloidal mixtures exhibit a surprisingly diverse range of equilibrium phases depending on the delicate balance between attractive and repulsive inter-particle forces. The control of these interactions is required in technological applications. The DLVO theory that considers colloidal interactions (electrostatic and van der Waals interactions) in polar media has been described. Overall other types of interaction that also govern colloidal stability were reported (e.g. steric interactions, hydrophobic interactions). The thermodynamics of macromolecular solutions was described by means of the Flory-Huggins theory and polymer-polymer miscibility. The main mechanisms of phase separation occurring in macromolecular mixtures, the depletion flocculation, and the segregative and associative phase separation were investigated. Emphasis was put on complex coacervation process, a liquid-liquid associative phase separation, since it corresponds to the demixing mechanism that takes place in our biopolymeric system. We focused then on the complex coacervation between  $\beta$ -lactoglobulin and Acacia gum, the protein and polysaccharide of interest in this thesis. At the end of this chapter, the objectives of the thesis and its outline were given.



## I.1. Introduction

Colloidal materials appear in a wide range of natural phenomena and fundamental problems in soft matter physics. Colloids are ubiquitous in industry (food, paints, ceramics, cosmetics, etc). They are used to control flow (glass), optical characteristics (photonic devices, sensors), texture (food products), stability (pharmaceutical compounds) and other physical characteristics<sup>1,2,3,4,5,6,7,8,9</sup>. The physical properties of these microstructured materials are regulated by the complex interactions between colloidal particles. Colloidal interactions have been largely investigated and have frequently been used as model systems to address fundamental issues in condensed matter physics such as liquid ordering and crystallization<sup>10,11,12,13,14,15</sup>.

Colloidal stability and aggregation are governed by the balance between attractive and repulsive inter-particle forces such as van der Waals attraction, double-layer repulsion and steric interaction (see Fig. I.1). In polar media, colloidal interactions have been described at a fundamental level such as in the well know theory due to Deryaguin and Landau and Verwey and Overbeek (DLVO theory)<sup>16</sup>. This theory combines van der Waals attraction between particles and repulsion due to overlap of the surrounding ions. Colloids can also be sterically stabilized by chemically or physically attached polymers to the particle surface. In a good solvent, colloids repel each other when overlap of their polymer layers forces the polymers into unfavorable conformations<sup>17</sup>. The stability characteristics can be also modified by the addition of soluble, non-adsorbing polymer into the colloidal dispersion. Understanding and controlling these interactions are essential to efficient process design and the functionality of end products. Colloidal mixtures exhibit a surprisingly diverse range of equilibrium phases depending on the size, shape, and concentration of dispersion compounds<sup>18</sup>.

Food is a classical example of naturally colloid and complex soft condensed matter. Thus, a basic understanding of the interactions and different non-equilibrium situations encountered in food systems has become important for improving product quality as well as for designing novel food materials<sup>17</sup>. For example, the union of natural colloids (protein and polysaccharide) arises in a wide number of food products and can lead to a demixing mechanism (complex coacervation)<sup>19,20</sup>.

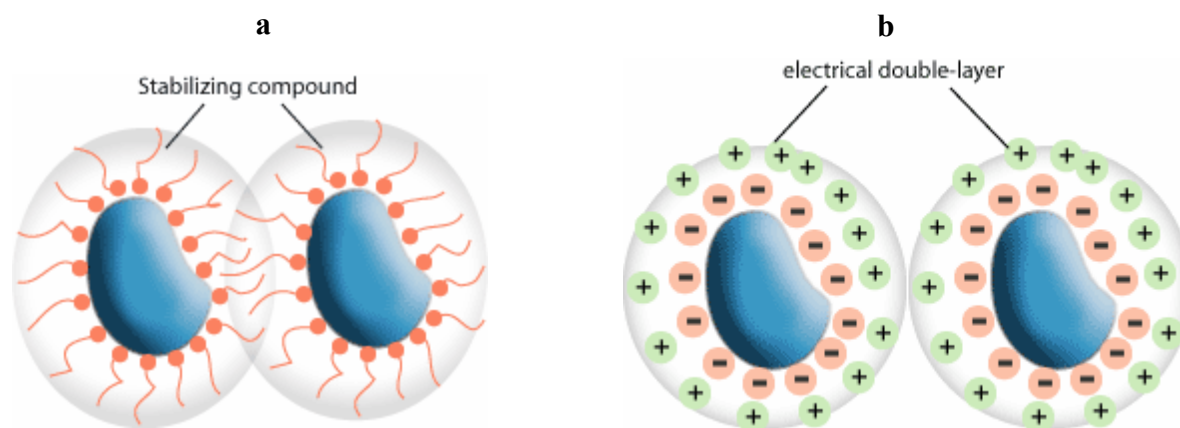


**Fig. 1.1.** Illustrations of colloidal stabilization by steric and electrostatic interactions. Adapted from SpecialChem website: [www.SpecialChem.com](http://www.SpecialChem.com).

This chapter touches the well-established theory of electrostatic stabilization in colloidal dispersions. We also describe all interaction forces that control the thermodynamics of colloidal dispersions. We then discuss instability mechanisms resulting from attractive interactions among oppositely-charged macromolecules and introduce the case of our system. Finally, we address our approach in order to better explain the dynamics of complex coacervation taking place in our biopolymeric system.



## **I.2. Theoretical description of interaction forces**

### **I.2.1. DLVO interactions**

Colloids of a given type (e.g., clouds, ink, milk, polysaccharides) may aggregate together (homoaggregation) or with colloids of other types (heteroaggregation). The homocoagulation of compact particles is generally quantified by the Smoluchowski equations and DLVO theory<sup>21,22,23</sup>. In this theory, the van der Waals attraction is combined with the double-layer repulsion and an energy–distance curve can be established to describe the conditions of stability/instability. According to DLVO theory, the interaction energy between two compact, spherical colloids results essentially from (i) their surface charge, this defines the electrical field around each particle, and (ii) the attractive van der Waals forces between them. The electrical and van der Waals forces define an energy barrier which, if overcome by the kinetic energy of the particles moving in water, will lead to aggregation and an unstable dispersion.

For submicron colloids, this kinetic energy results mainly from Brownian motion and little from hydrodynamic or gravitational forces<sup>24,25</sup> whereas for larger particles or aggregates, hydrodynamic processes such as differential sedimentation and fluid shear can provide the necessary energy for aggregation<sup>26,27</sup>.

The DLVO is a mean-field theory that describes the fluctuations in simple ions distributions. The theory neglects correlations between the counterions and as a consequence there is an attractive force component lacking in it. The attractive component turns out to be the dominating when the ion–ion interaction is strong<sup>28</sup>.

#### **I.2.1.1. Electrostatic interactions**

The electrostatic interactions will be described in details as compared to the other interaction forces due to its major contribution in the present study. The electrostatic coupling among charged colloidal particles results from a hierarchy of many-body interactions. In general, charged colloidal particles interact not only with each other, but also with a sea of surrounding ions, some with the same charge called coions, and others with opposite charge called counterions, as shown schematically in Fig. I.2. The electric surface charge of an entity in solution can develop in many ways. For example, particles may have an intrinsic charge while for other surfaces, the ionization/dissociation of surface functional groups or the

adsorption of ions may lead to the charging of surfaces. The sign and magnitude of the charge are frequently affected by the pH and ionic strength of the medium.

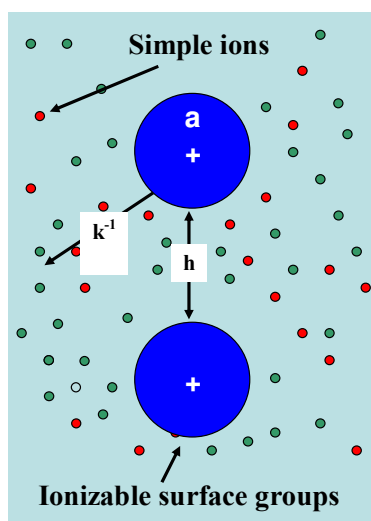


**Fig. I.2.** Schematic view of the components of a charge-stabilized colloidal dispersion. Ionizable surface groups dissociate in solution, leaving charges bound to the spheres' surfaces and counterions in solution. These counterions are augmented by other simple ions already in solution. Electrostatic interactions among all of these species result in an effective interaction between the spheres.  $k^{-1}$  is the screening length that describes how the simple ions' correlations with the macroions fall off with distance due to screening of the electric field.  $h$ : distance between two spheres.

In a liquid, the distribution of ions between the surface of the particles and the surrounding solution is generally not homogenous because of the nature of the particles. The charges on the particles are counterbalanced by an equivalent number of counterions in the aqueous solution. The charged particle and the electrostatically attracted counterions form the electric double layer (see Fig. I.5).

The electric double layer (EDL) is a central concept in the understanding of the static and dynamical properties of charged colloidal systems. The early works of Gouy, Debye, and Hückel introduced the notion in order to describe the microions distribution close to a charged colloidal surface <sup>29</sup>. The EDL width determines the electric interaction range between macromolecules and therefore controls their static phase behavior. On the other hand, at the dynamical level the EDL is at the origin of numerous electrokinetic effects (e.g. electrophoresis, electro-osmosis, streaming current or potential, etc.) <sup>30</sup>. The extension of the EDL is typically on the order of a few nanometers.

The earliest model of the EDL is generally attributed to Helmholtz (1879) who treated the double layer mathematically based on a physical model in which a single layer of ions was adsorbed at the surface. In the later (1910-1913) Gouy and Chapman model, the surface potential decreases exponentially due to the adsorption of counter-ions.

The Gouy-Chapman-Grahame-Stern (GCGS) (Fig. I.3.a) model combines the Helmholtz single adsorbed layer with the Gouy-Chapman diffuse layer. Usually, the GCGS model is widely used to describe the EDL. This model consists of two layers: Stern layer (SL) and diffuse layer (DL). The SL is the region next to the surface, and ions in the SL are bound near the surface due to non-Coulombic and Coulombic interactions. The DL is the region next to the SL and ions in the DL can move freely in any direction.

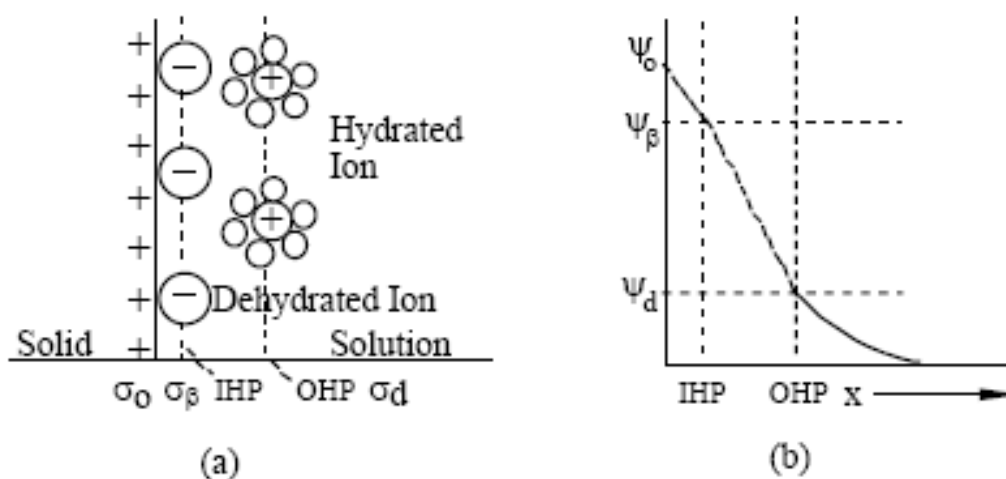


**Fig. I.3.** The Gouy-Chapman-Stern-Grahame electric double layer model (a) charge distribution (b) potential distribution. Figure taken from (Jolivet 1994)<sup>31</sup>.

The Stern layer is further subdivided into a layer of dehydrated ions (Inner Helmholtz Plane, IHP) and a layer of hydrated ions (Outer Helmholtz Plane, OHP) (see Fig. I.4). The solid/liquid interface can be therefore visualized in terms of three layers of charge. The first is due to the surface layer of the solid surface itself, the second is formed at the inner Helmholtz plane and the final compact layer of counter charge where the ions are only weakly attached to the solid surface is the diffuse layer. The different layers of the EDL are illustrated in Fig. I.5.

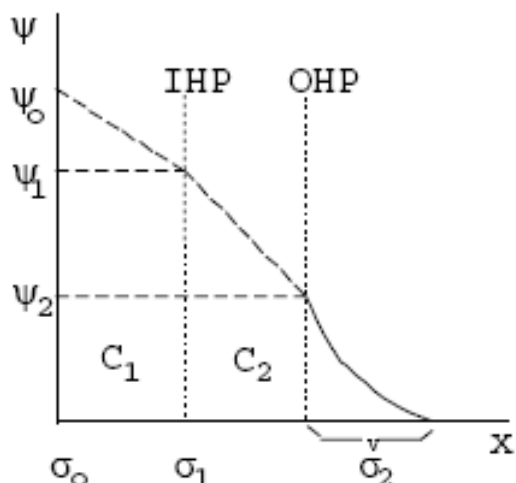


**Fig. I.4.** The triple layer model. IHP: Inner Helmholtz plane, OHP: Outer Helmholtz plane. Adapted from (Jolivet, 1994)<sup>31</sup>.

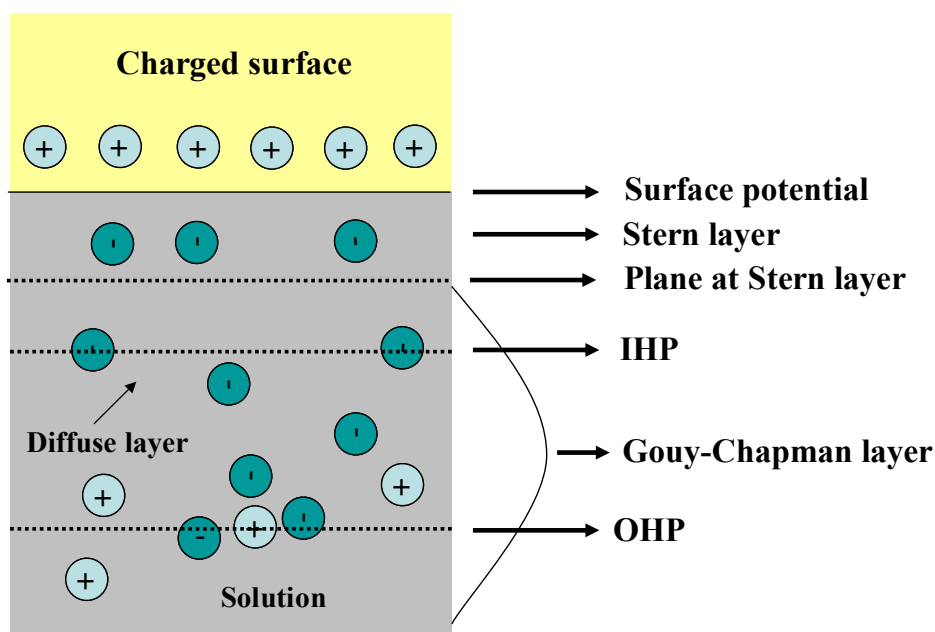


**Fig. I.5.** Schematic view of the Electrical Double Layer (EDL).

Among the important approximations incorporated into this model are: (i) ions are effectively point charges, (ii) the only significant interactions are Coulombic, (iii) electric permittivity is constant throughout the double layer, (iv) the solvent is uniform at the atomic scale, (v) ions in the Stern layer are considered to have lost their hydration water, (vi) ions in diffuse layer retain their hydration water.

### I.2.1.2. Van der Waals interactions

For two surfaces separated by a small distance, electric and magnetic polarizations produce an electromagnetic field that fluctuates within the medium<sup>32</sup> and can be responsible for colloidal aggregation. The potential energy of this van der Waals interaction is a function of the separation distance,  $r$ , between dipoles (see Fig. I.2). van der Waals forces are always present and always attractive between particles of the same nature.

Two theoretical ways allow the evaluation of the attractive interaction: the microscopic and the macroscopic approach. The first approach is the classical or microscopic approach and is due mainly to Hamaker<sup>33</sup> and it is based on the assumption of additivity of London pair interaction energy. This predicts the van der Waals attraction with an accuracy of 80%–90%. The macroscopic approach, that eliminates the additivity assumption of Hamaker approach has been suggested by Lifschitz<sup>34</sup>. It gives a more accurate evaluation of the van der Waals attraction and it is based on the correlation between electric fluctuations of two macroscopic phases. However, this approach requires quantification of the dielectric dispersion data, which are available for only a limited number of systems. For this reason, most results on the van der Waals attraction are based on the microscopic approach that is described below.

For a one-component system, individual atoms or molecules attract each other at short distances due to van der Waals forces. The latter may be considered to consist of three contributions: dipole–dipole (Keesom), dipole–induced dipole (Debye) and London dispersion interactions. For not too large separation distances between atoms or molecules, the attractive energy  $G_a$  is short range in nature and it is inversely proportional to the sixth power of the interatomic distance  $r$ :

$$G_a = -\frac{\beta_{11}}{r^6} \quad \text{Eq. I.1}$$

where  $\beta_{11}$  is a constant referring to identical atoms or molecules.

In the microscopic approach, the net interaction between two entities can be obtained by summing all interactions. However, while this approach can be easily applied to various geometries, the assumption of complete additivity is imperfect since it always over-estimates the interactions. In the following this approach will be examined in greater detail. Hamaker replaced the summation of all particle interactions by a double integral, in order to obtain an

expression that he was able to divide into a purely geometrical part and a constant,  $A$ , known as the Hamaker constant. This constant is related to the properties of the particles and the medium. Assuming two spheres of radius  $a_1$  and  $a_2$ , with surfaces separated by a distance,  $h$ , the energy of attractive interaction is given by:

$$V_A = -\frac{A_{12}}{6} \left[ \frac{2a_1 a_2}{h^2 + 2a_1 h + 2a_2 h} + \frac{2a_1 a_2}{h^2 + 2a_1 h + 2a_2 h + 4a_1 a_2} + \ln \left( \frac{h^2 + 2a_1 h + 2a_2 h}{h^2 + 2a_1 h + 2a_2 h + 4a_1 a_2} \right) \right]$$

**Eq. I.2**

For small separation distances, the above equation can be reduced to:

$$V_A = -\frac{A_{12}}{6h} \frac{a_1 a_2}{(a_1 + a_2)} \quad \text{Eq. I.3}$$

and if the spheres are identical with radii,  $a_1$  :

$$V_A = -\frac{A_{11} a_1}{12h} \quad \text{Eq. I.4}$$

These expressions show that the energy of interaction is inversely proportional to the separation distance (see Fig. I.6). Therefore,  $V_A$  is always predominant at small separation distances, and for still shorter distances (1-2 nm) the interaction energy falls drastically, causing the total energy to approach minus infinity. Typical values of  $A$  are of the order of one  $kT$  ( $3.7 \times 10^{-20}$  J for water)<sup>32,35</sup>.

## **I.2.2. Non DLVO interactions**

Non DLVO forces such as steric interactions, hydration pressures, hydrogen bonding and hydrophobic effects, although rarely considered in quantitative attempts to model colloidal interactions, are recognized as important forces contributing to the aggregation of colloids<sup>36</sup>. For example, in aqueous systems, it is now clear that non DLVO hydration effects are possible due to the reorganization of surface bound water upon approach of the colloidal particle. Furthermore, hydrophobic surfaces have a greater tendency to aggregate than

predicted by DLVO theory alone due to the migration of water from the solid- water interface to the bulk solution.

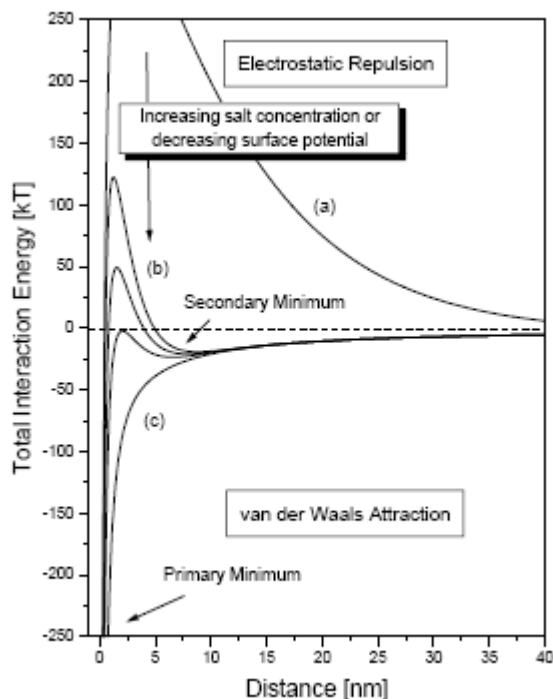


**Fig. 1.6.** Calculated energy profiles as a function of the distance between particle surfaces taking into account DLVO interactions. (a) Conditions in which surfaces repel strongly while colloidal particles remain stable. (b) Conditions for which surfaces come into a stable equilibrium at the secondary minimum (if it is deep enough); colloids then coagulate reversibly. (c) The interaction curve approaches the pure van der Waals curve; colloids coagulate irreversibly. Conditions used to compute the curves: Particle diameter =  $1\ \mu\text{m}$  : Hamaker constant =  $1.5 \times 10^{-13}$  ergs : Salt (NaCl) concentration = 0.001 M (curve a), 0.03 M (curves b-c): Particle surface potential = 35 mV (curve a), 35/30/25mV (curves b) and 10 mV (curve c). Taken from (Stoll and Buffle 1995) <sup>37</sup>.

### I.2.2.1. The hydration or solvation effect

Short-range deviations from the DLVO theory are attributed to solvation/hydration or structural forces. Many experimental studies have termed this interaction a “hydration pressure” or “solvation pressure” because the repulsion results from the partial ordering or polarization of water or solvent molecules by the hydrophilic bilayer surface <sup>38,39,40</sup>.

At very short distances (1-2 nm) the structure of the liquid confined between two surfaces does not follow a continuum theory any longer. The overlap between the solvent layers on the surfaces results in changes in liquid density (oscillations), causing oscillating structural forces <sup>41</sup>. The properties of the water molecules close to the surface of the particles can be very different from those in the solution. Frequently a monolayer of water is chemically adsorbed

on the surface of particles (e.g. lipid membranes, proteins, metal oxides, clays). Such colloid-water interactions can retard the aggregation of colloidal systems, due to additional repulsive interaction that is distinct from the repulsion of the electric double layer. This repulsion comes from the reorganization of the surface hydration layers (several nm) so that the contact between the particles cannot take place. This induces an increase of the free energy of the system, unfavorable for colloid interactions. This hydration force is relatively important compared with the repulsion due to the electric double layer. It has an effect on colloidal stability, particularly for high ionic strengths and for small particles.

Short range repulsive interactions between electroneutral lipid bilayers were first measured 30 years ago <sup>42</sup>. Similar interactions have been observed in systems such as DNA and polysaccharides indicating an ubiquitous nature of these forces <sup>43</sup>. Israelachvili <sup>41</sup> has described the importance of several non-DLVO forces (solvation, structural, hydration, steric, and fluctuation) in the interaction of surfaces separated by liquid. For example, in milk fat globules (MFG), steric repulsion caused by interpenetration and/or compression of hydrophilic chains that extend from the MFG surface has been implicated <sup>44</sup>.

The origin of the hydration force remains the subject of intense study, both in experiment and theory. Unfortunately, there are no theoretical models allowing to calculate the magnitude and range of the hydration pressure. For example, the magnitude of this pressure in lipid bilayers has been shown to be proportional to the square of the dipole potential measured in monolayers in equilibrium with liposomes, suggesting that the “hydration” pressure results, at least in part, from the polarization of interbilayer water by electric fields arising from the lipid and water dipoles <sup>42,43</sup>.

### **I.2.2.2. Hydrophobic interactions**

Longer-range attractive deviations to the DLVO theory are attributed to hydrophobic forces between hydrophobic surfaces, as well as steric and fluctuation forces between diffuse interfaces, when polymer chains are present at the surface <sup>45</sup>.

The low affinity between hydrophobic particles and water may be due to the absence of ionic or polar groups and sites for hydrogen bonds. The properties of the water molecules in contact with the surfaces are thus different from those in the solution. Indeed, hydrogen bonds among



water molecules structure ordinary water. The presence of a hydrophobic surface can restrict the natural tendency of water to structure by imposing a barrier, which prevents the organization of aggregates in a direction. If the interstice between particles is narrow, the limitation is important and there is an increase in the free energy of the water compared to that of the solution. In other words, there is an attraction of hydrophobic surfaces due to the migration of water molecules from the interstice to the solution, where the possibilities of creating hydrogen bonds are not restricted.

Accurate measurement of interaction forces between different surfaces is important for a variety of natural phenomena and industrial processes<sup>46,47</sup>. From there, hydrophobic force is among the most important nonspecific interactions in biological systems and plays a central role in many surface phenomena. Hydrophobic interactions have been largely investigated to describe a variety of biochemical processes such as the conformational changes of biopolymers, the substrate/enzyme binding, and the association of subunits to form a multisubunit enzyme<sup>48</sup>. Also, they are relevant in formation of detergent micelles, protein-amphiphile complexes, and biological membranes<sup>49</sup>.

Although a number of studies were carried out over the past 20 years, the nature of the hydrophobic force is still unclear. Moreover, no single theory can account for all observed experimental behavior even the experimental data on similar systems is often contradictory. The magnitude and the range of the force are dependent not only on the hydrophobic surface but also on the method of surface preparation.

## **I.3. Interactions in macromolecular solutions**

### **I.3.1. Thermodynamics of polymer-polymer miscibility**

When a solution of polymer A is added to a solution of polymer B, the main characteristic of the blend will be the thermodynamic compatibility or incompatibility of the components. Thus, two different events might occur: the two solutions will mix or the solutions will not mix and the system separates into two phases. Complete miscibility or stability in a mixture of two polymers requires that the change in Gibbs energy upon mixing ( $\Delta G_{\text{mix}}$ ) must be lower than zero<sup>50</sup>. However, phase separation take place in the case of  $\Delta G_{\text{mix}} > 0$ .

The thermodynamic properties of a macromolecular blend, giving rise to miscibility or phase separation, depends on many factors, of which the most important are the chemical structure of the polymers, their molecular mass, temperature (T) and blend composition  $\phi$ . For example, heating or cooling the sample shifts the blend from the mixed state to a completely demixed one. Therefore, a critical temperature and a critical composition define the boundary between the mixed state and the demixed state. The phase diagram of a polymer-polymer system is a representation of the critical volume fraction of one component (for example  $\phi_A$ ) as a function of T (see Fig. I.8).

#### **I.3.1.1. The Flory-Huggins theory**

Flory and Huggins<sup>51</sup> developed independently a general theory that provides a basic understanding of the occurrence of different types of phases as a function of temperature and molecular weights. Their mean-field theory, mainly concerned with the positional or combinatorial entropy of mixing of the blend components, proved to be very useful in describing the coexistence curve of a blend.

The Flory-Huggins theory<sup>51,52,53,54</sup> describes a mean field lattice model in which the distribution of molecules on a lattice is calculated. The theoretical model assumes a mixture of  $n_A$  polymer chains of type A, each consisting of  $N_A$  segments and  $n_B$  polymer chains of type B with  $N_B$  segments. Each of the  $N_i$  segments of identical size  $v$ , occupy only one site on a lattice consisting of a total number of  $N$  sites. This simple situation is depicted in Fig. I.7.

The assumptions that are made in this model are i) each lattice site is occupied by either a polymer segment or a solvent molecule, ii) the polymers are flexible and iii) the nearest-neighbor pair interactions are dominating in the lattice.

The Flory–Huggins theory considers the change in the so-called “Gibbs free energy of mixing” given by:

$$\Delta G_{\text{mix}} = G_{\text{A+B}} - (G_{\text{A}} + G_{\text{B}}) \quad \text{Eq. I.5}$$

where  $G_{\text{A+B}}$ ,  $G_{\text{A}}$  and  $G_{\text{B}}$  denote the Gibbs free energies for the mixture (A+B) and for the free compounds A and B, respectively. From the first and second law of thermodynamics an alternative expression for  $\Delta G_{\text{mix}}$  is derived:

$$\Delta G_{\text{mix}} = \Delta H - T \cdot \Delta S \quad \text{Eq. I.6}$$

where  $\Delta H$  and  $T \cdot \Delta S$  are the enthalpic and entropic contributions to the Gibbs free energy of mixing, respectively.

The ratio between enthalpy and entropy of a mixture is strongly dependent on the polymer concentration. At low polymer concentration, an increase of the polymer chain mobility leads to an entropic gain. Then, a compensation of the enthalpic contribution take place and a homogeneous system is obtained. At high concentration, a low endothermic change in system becomes sufficient to induce phase separation. Thus, the free energy of mixture  $\Delta G_{\text{mix}}$  can be positive in such case.

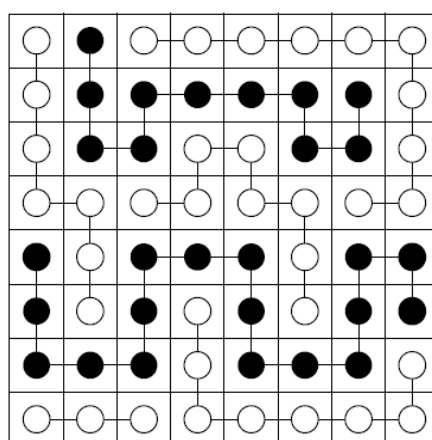


**Fig. I.7.** Two dimensional lattice model of a mixture of polymer chains. Units of equal size corresponding to monomers of the two polymers occupy the lattice sites. Taken from Van der Haegen *et al.* (1989)<sup>55</sup>.

The second term in  $\Delta G_{\text{mix}}$  represents the increase in the translational entropy associated with the motion of the center of mass of all the molecules. In the pure state, the configurational space available to the center of mass of a molecule of type  $i$  is  $V_i$  and the associated entropy for its translational degrees of freedom is  $k_B \ln V_i$ . In the mixture, a larger volume  $V$  is accessible to mixed chains compared to  $V/2$  for the chains in the phase separated phase (Fig. I.8.c).

The associated entropy increase is  $k_B \ln(V_i/V) = k_B \ln \phi_i$ , where  $\phi_i$  is the volume fraction of component  $i$ . Specifically, for the two components A and B,  $\phi_A$  and  $\phi_B$  are given by:

$$\phi_A = \frac{V_A}{V} = \frac{n_A}{n_A + n_B}$$

$$\phi_B = \frac{V_B}{V} = \frac{n_B}{n_A + n_B}$$

where  $V_A = n_A \cdot v$  and  $V_B = n_B \cdot v$ .

Considering the total number of conformations available for the system:

$$\Omega = \frac{(n_A + n_B)!}{n_A! n_B!} \quad \text{Eq. I.7}$$

The change in the entropy of mixing is computed using the Boltzmann relation  $S = k_B \ln \Omega$ :

$$\frac{\Delta S}{n k_B} = -\frac{\phi_A}{N_A} \ln \phi_A + \frac{\phi_B}{N_B} \ln \phi_B \quad \text{Eq. I.8}$$

The factor  $1/N_i$  shows the strong influence of the length of the macromolecules on the mixing behavior of a polymer blend. With increasing molecular mass of the components, the miscibility of the two polymers decreases. Therefore, small molecules are better miscible than polymers.

On the other hand, the first term in  $\Delta G_{\text{mix}}$  can favor or inhibit the mixing depending on the monomer–monomer pair interaction. Flory and Huggins assumed that this energy stems from purely enthalpic nearest–neighbor interactions. Because the reference chain is in contact with a large number of other chains, the interactions are effectively integrated over the different monomer–monomer interactions. Therefore, the chain can be considered in a mean–field

created by the surrounding polymers chains. For simple van der Waals interactions, the attraction between equal monomers is stronger compared to unlike pairs. This selectivity implies that  $\Delta H > 0$  opposes mixing. The change in enthalpy is given by:

$$\Delta H = nk_B T \phi_A \phi_B \quad \text{Eq. I.9}$$

where  $n = n_A + n_B$  is the total number of monomers.

Using Eq. I.8 and Eq. I.9 together with the expression of the Gibbs free energy of mixing (Eq. I.5), the so-called Flory–Huggins relation for polymer mixtures and solutions is obtained:

$$\Delta G_{\text{mix}} \Big|_{\text{site}} = -nK_B T \left\{ \frac{\phi_A}{N_A} \ln \phi_A + \frac{\phi_B}{N_B} \ln \phi_B + \chi(\phi_A, \phi_B, T) \phi_A \phi_B \right\} \quad \text{Eq. I.10}$$

where  $\chi$  is the so-called pair interaction parameter or 'Flory–Huggins parameter'. It determines in an empirical manner the change in the local free energy per reference unit. It is dimensionless and is the decisive factor that determines whether the blend stays in the mixed state or it phase separates. In a binary system, the Flory-Huggins parameter  $\chi$  allows to characterize the solvent-solvent ( $\chi_{11}$ ), segment-segment ( $\chi_{22}$ ) and solvent-segment ( $\chi_{12}$ ) interactions. Thus, the nature of interactions, whether repulsive or attractive, between two polymers can be monitored by the sign of the interaction parameter  $\chi$  of the Flory-Huggins theory.

The last equation (Eq.I.10) can be used to interpret the bimodal shape of spinodal<sup>(1)</sup> and cloud point curves (CPC) of polymer blends and to theoretically predict the coexistence curve of a binary mixture, for which the temperature is an important factor affecting the polymers miscibility. This curve is a temperature vs. composition diagram given by the locus of points that separate the two phase region from the one phase region. Therefore, it defines the equilibrium composition of the coexisting phases. The points on the coexistence curve (see Fig. I.8) where the two phases become identical are the critical points, while the temperature at which the phase boundary between the two phases disappears is called the critical

<sup>(1)</sup> The spinodal curve defines the limit of metastability. For a polymer blend, it is the locus of points where the second composition derivative  $\partial^2 \phi \Delta G_{\text{mix}}$  of the free energy vanishes.

temperature.

In a binary mixture, this temperature defines the extremum of the coexistence curve. If the extremum is a maximum it is called the upper critical solution temperature (UCST) and if it is a minimum it is called the lower critical solution temperature (LCST)<sup>56</sup>.

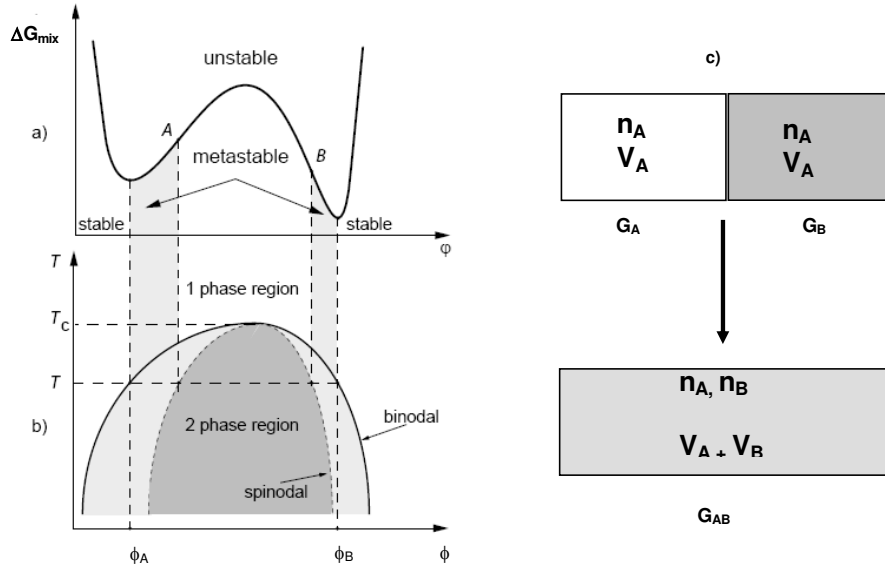


**Fig. I.8. a)** Dependence of the Gibbs free energy of mixing  $\Delta G_{\text{mix}}$  on the composition  $\phi$  at constant temperature. At the two inflection points (A and B) in the graph, the second derivative  $\partial^2 \Delta G_{\text{mix}} / \partial \phi^2$  vanishes. The inflection points define the spinodal. **b)** The two phase region is enclosed by the binodal. In the region under the spinodal the mixture is unstable while between the curves the blend is metastable (nucleation and growth of phase separated domains). Above the critical temperature  $T_c$  the blend is stable in the mixed phase. A temperature quench from the one-phase to the two-phase region induces phase separation. **c)** Variables used in the description of the mixing process of two polymers A and B. Adapted from Van der Haegen *et al.* (1989)<sup>55</sup>.

On the basis of the equilibrium criteria, stability limits and criticality, the coexistence curve (binodal), spinodal line and critical point can be predicted using Eq.I.11:

- Binodal

$$\frac{\Delta G_{\text{mix}}(\phi_A) - \Delta G_{\text{mix}}(\phi_B)}{\phi_A - \phi_B} = \frac{\partial \Delta G_{\text{mix}}}{\partial \phi} \Big|_{\phi_A} = \frac{\partial \Delta G_{\text{mix}}}{\partial \phi} \Big|_{\phi_B} \quad \text{Eq. I.11}$$

- Spinodal

$$\frac{\partial^2 \Delta G_{\text{mix}}}{\partial \phi^2} = 0 \quad \text{Eq. I.12}$$

- Critical point

$$\frac{\partial^3 \Delta G_{\text{mix}}}{\partial \phi^3} = 0 \quad \text{Eq. I.13}$$

For a given temperature the double tangent construction expressed by the binodal equation in Eq. I.11 gives the volume fractions  $\phi_A$  and  $\phi_B$  of the two coexisting phases (Fig. I.8.b). The homogeneous mixture is stable outside the coexistence curve, metastable between binodal and spinodal lines (the nucleation and growth region) and unstable inside the spinodal line.

### I.3.1.2. Dynamics of phase separation

In general, Nucleation and Growth (NG) or Spinodal Decomposition (SD) describe the dynamics of phase separation<sup>57</sup>. Nucleation theory predicts that small droplets of a minority phase develop over time in a homogeneous mixture that has been brought into the metastable region of the phase diagram (Fig. I.9). Droplet growth proceeds by diffusion of material from the supersaturated continuum. However, once the composition of the supernatant reaches equilibrium, further increases in droplet size occur by droplet coalescence or Ostwald ripening. In the metastable state, homogeneous mixtures must overcome a free energy barrier in order to nucleate a new phase.

When a binary mixture is quenched from the miscible region into the thermodynamically immiscible (unstable) state in the phase diagram, phase separation occurs via mechanism of spinodal decomposition. This process was first described theoretically by Cahn<sup>58</sup>. Generally, in the early stage, phase separation is controlled by concentration fluctuation and the decrease of bulk energy. At the later stage, phase separation is controlled by diffusion and convection, and the decrease of surface energy. It is established that the domain size  $R(t)$  satisfies a scaling law,  $R(t) \sim t^\alpha$ , during phase separation, where  $\alpha$  is the growth exponent<sup>60</sup>.

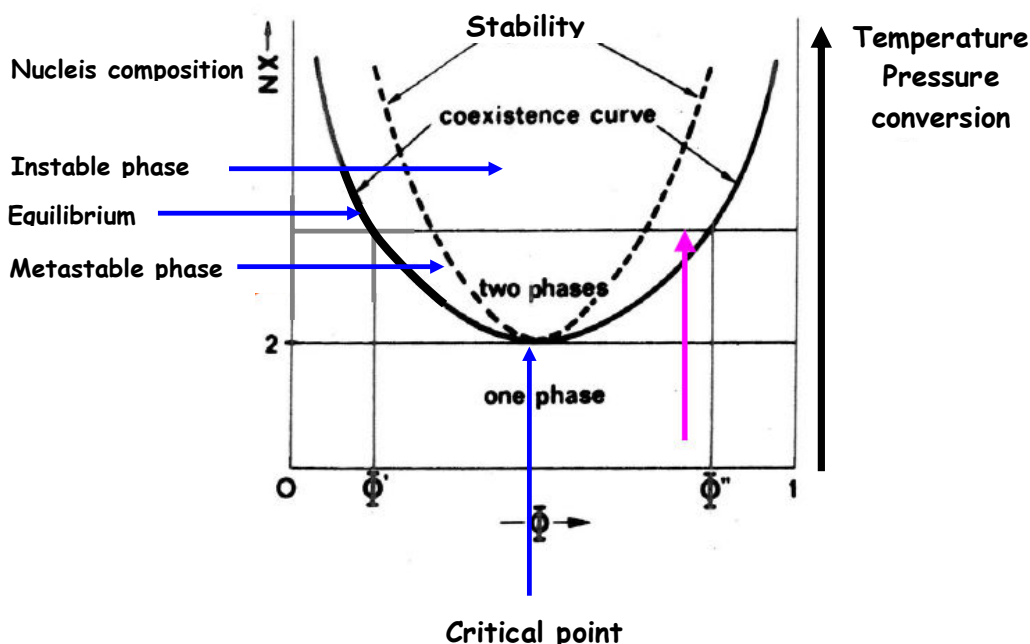


**Fig. I.9.** Schematic view of the theoretical phase diagram for a binary polymeric system. Adapted from Horst *et al.*<sup>59</sup>.

Spinodal decomposition may result in a disordered bicontinuous two-phase structure, as contrasted in Fig. I.10. Almost immediately after the bicontinuous pattern begins to form, interfacial tension drives the system to reduce its surface area by increasing the size of droplets. In both nucleation and growth and spinodal decomposition cases, the driving force behind coarsening is the minimization of the interfacial tension through a reduction in interfacial area.

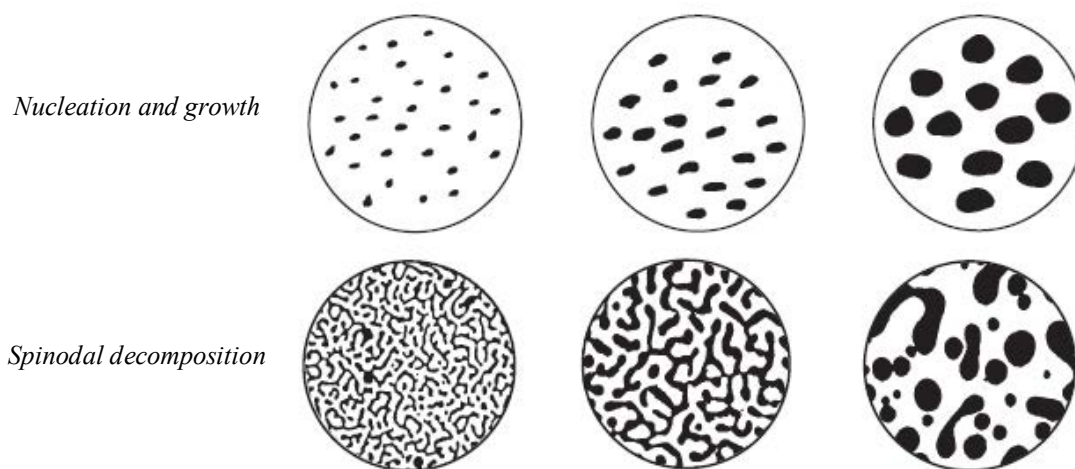


**Fig. I.10.** Schematic view of the phase separation by the nucleation and growth, and spinodal decomposition phenomena. Taken from Olabisi *et al.*<sup>50</sup> and Kwei *et al.* (1978)<sup>60</sup>.



### I.3.2. Main demixing mechanisms in mixed macromolecular solutions

Polymer solutions can show segregative or associative phase separation. In the absence of attractive interaction, a segregative phase separation can occur. In case of a moderate interaction, a complete miscibility may be obtained. In case of a strong attractive interaction, associative phase separation may occur, giving one phase rich in polymer and one phase highly polymer depleted.

The molecular parameters that control the polymer self-association or segregation are primarily the weight average molecular weight ( $M_w$ ), the radius of gyration ( $R_G$ ) or the hydrodynamic radius ( $R_h$ ) and the second virial coefficient,  $A_2$ , which is the second coefficient in the expansion of the chemical potentials of both solvent and polymer on a polymer concentration<sup>61,62,63</sup>. The sign and the magnitude of the second virial coefficient provide the information on the deviation of a macromolecular solution from the ideal state and reflect the nature and the intensity of the intermolecular pair interactions (polymer-polymer and polymer-solvent) in solutions.

#### I.3.2.1. Depletion flocculation

The depletion model gives the thermodynamic explanation for the phase separation of colloids and polymers in a solution on the basis of excluded volume<sup>64</sup>. This is produced on the addition of “free”, non-adsorbing polymer to a dispersion<sup>65</sup>. The system can be pictured as in Fig. I.11. The free polymer cannot approach the particle surface by a distance  $\Delta$  (that is approximately equal to twice the radius of gyration of the polymer,  $2R_G$ ). The exclusion of the polymer due to depletion or loss of configurational entropy results in attractive force, which is proportional to the osmotic pressure of the polymer in the bulk solution, between the particles. This attractive force results in particle dispersion instability referred to as depletion flocculation. The first quantitative analysis of this process was carried out by Asukara and Osawa<sup>66</sup>, who derived the following expression for the depletion free energy of attraction:

$$G_{\text{dep}} = -\frac{3}{2} \phi_2 \cdot \frac{R}{\Delta} \cdot x^2 \quad \text{Eq. I.14}$$

with  $0 < x < 2$  and it is given by:

$$x = \frac{\Delta - \frac{h}{2}}{\Delta} \quad \text{Eq. I.15}$$

where  $\Delta$  is the distance between polymer and colloidal surface particle,  $h$  is the distance between particles and  $\phi_2$  is the volume concentration of the free polymer:

$$\phi_2 = \frac{\frac{4}{3}\pi\Delta^3 N^2}{V} \quad \text{Eq. I.16}$$

where  $N^2$  is the total number of coils and  $V$  is the volume of solution.

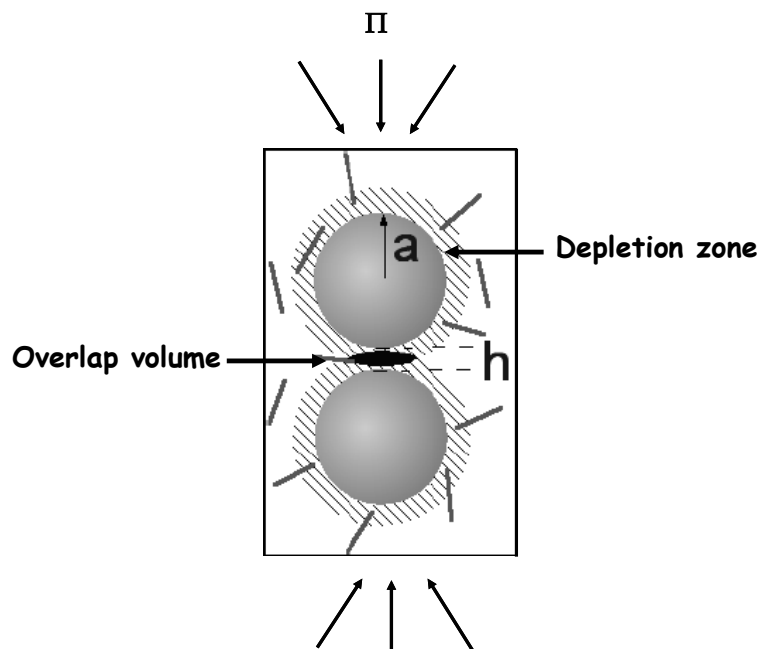


**Fig. I.11.** Schematic view of the mechanism of depletion interaction. Adapted from Lin *et al.* (2001)<sup>67</sup>.  $\Pi$ : osmotic pressure.

Fig. I.11 shows the model that is also used to describe the phase separation for systems in which polymers are larger than colloidal particles<sup>68,69</sup>.

### I.3.2.2. Thermodynamic incompatibility: segregative phase separation

As assessed above, the phase behavior of a binary blend is reflected in its phase diagram (Fig. I.12.a). In totally miscible binary blends, the phase diagram is a continuous 1-phase region

(Fig. I.8). In polymer blends that segregate, the composition of the phases depends on the spinodal and the temperature. The binodal being the border between the 1- and 2-phase regions. When segregation occurs at a definite temperature, the equilibrium composition of the segregated phases,  $\phi_A$  and  $\phi_B$ , is defined by the binodal<sup>50,70</sup>. It must be noticed that the temperature-dependence of phase behavior is established for polymer blends and it is not well investigated for biopolymeric systems.

The segregative phase separation phenomenon is the general main consequence of the thermodynamically unfavorable interactions between polymers with high concentrations, which mainly arise from the excluded volume effects and the electrostatic repulsions between the like charged polymers. The difference in the thermodynamic affinities of the polymers for an aqueous medium is the second most important parameter that determines the water partitioning between the coexisting phases<sup>71</sup>. It is well established that the segregative phase separation is often due to changes in the solvent-polymer affinity.

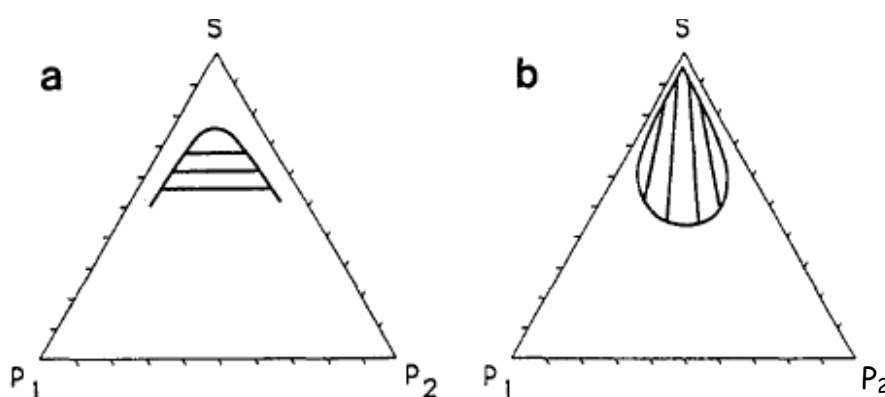


**Fig. I.12.** Schematic phase diagram of segregative (a) and associative (b) phase separation in mixed polymer (or biopolymer) solutions. S denotes solvent and P polymer. Adapted from (Bungenberg de Jong and Kruyt, 1949a)<sup>20</sup>.

The phenomenon of thermodynamic incompatibility of biopolymers is already known since 1896, when Beijerinck discovered the demixing of gelatine and soluble starch dispersions<sup>72</sup>. If the biopolymers are incompatible, i.e. they repel each other, thermodynamic phase separation occurs. During the past century, the incompatibility of biopolymers has been the subject of many studies which resulted in a large quantity of experimental data<sup>73,74</sup>. These data mainly give a qualitative description of the phase separating conditions. The chemical

structure of the polymers, pH, ionic strength and temperature are important parameters for the phase separation.

The number of qualitative and quantitative descriptions of biopolymer phase separation is relatively scarce. This is due to the fact that most biopolymers are polydisperse in their molar mass and often have the tendency to form a gel already at a low concentration or at moderate temperatures<sup>75,76,77,78,79</sup>. The formation of a gel arrests the phase separation. Gelation also increases the apparent molar mass of the gelling polymer, which in turn speeds up the phase separation<sup>80</sup>. Apart from the experimental data of the phase behavior, theoretical models describing the phase behavior of polymers have been developed<sup>81,82,83,84</sup>. However, it is not clear to what extent these theories are valid for the phase separation of mixtures of biopolymer solutions.

### **I.3.2.3. Thermodynamic compatibility: associative phase separation**

We focus on this type of phase separation because it is the demixing mechanism that takes place in our macromolecular mixture. We describe then in details the thermodynamics of this phenomenon. Fig. I.12.b shows a typical phase diagram of complex coacervation.

Based on the theoretical description of polymer-polymer miscibility, a negative value of  $A_2$  (second virial coefficient) indicates the thermodynamically favorable interactions between macromolecules in solution that is a mutual attraction. Such interactions lead to a decrease in the polymer chemical potential and, consequently, to a decrease in the free energy of the system as a whole. The opposite is true for a positive value of  $A_2$ . The polymer-polymer thermodynamically favorable interactions form the basis of the polymer self-association (aggregation)<sup>85</sup>.

Thermodynamic compatibility or associative phase separation in a polymer blend indicates that two macromolecules tend to assemble in the same concentrated phase<sup>86,87</sup>. This mechanism is defined by complex coacervation which is a liquid/liquid phase separation<sup>88</sup>. The term “coacervation” was introduced by Bungenberg de Jong and Kruyt<sup>19</sup> and derives from Latin “acervus”, which means aggregation (a heap), and the prefix “co”, which means together. “Coacervation” signifies the union of the colloidal particles. The coacervation of

two oppositely charged colloids is denoted complex coacervation. On the other hand, the coacervation of a single polymer is denoted simple coacervation.

The complexation (or the complex coacervation) is an intrinsic feature of interaction between two oppositely charged biopolymers, which can result from entropic and enthalpic effects<sup>89,90,91,92</sup>. Besides, electrostatic interactions play a major role in complexation/coacervation. But the complexation has its origin in many interaction forces such the hydrogen bonding, hydrophobic interactions and van der Waals<sup>93,94,95,96,97</sup>. For example, the complexation of neutral polysaccharides with other biopolymers results from the hydrogen bonding<sup>98</sup>. The complexes formed can be either soluble or “insoluble”. The great number of “insoluble” complexes concentrate in liquid coacervate droplets, that further coalesce and phase separate to form a separate coacervate layer<sup>99</sup>.

Let us focus here on the theoretical background of models explaining the complex coacervation mechanism. Complex coacervation between oppositely charged proteins and polysaccharides was discovered by Tiebackx in 1911. By mixing gelatin and gum arabic (GA) in an acetic acid solution, he observed opalescence or precipitation. Complex coacervation on the system gum Arabic-gelatin was extensively investigated for the first time by Bungenberg de Jong and Kruyt (1929)<sup>19</sup>.

The first theoretical model of complex coacervation was developed by Overbeek and Voorn based on the large amount of data obtained by Bungenberg de Jong *et al.* (1929). They considered the spontaneous coacervation of gelatin and GA as a competition between the electrostatic attractive forces which tend to accumulate charged polyions and entropy effects which tend to disperse them<sup>100</sup>. Subsequent theoretical models were developed by Veis and coworkers, Nakajima and Sato and Tainaka<sup>101,102,103,104,105,106</sup>.

Veis and Aranyi developed a dilute phase aggregate model, which suggested that complex coacervation occurred in two steps. First, unlike charged polyelectrolytes aggregate by electrostatic interaction to form neutral aggregates of low configurational entropy, and then these aggregates rearrange to form coacervate. The ion pairing aggregates formed in the first step are present in both coacervate phase and equilibrium dilute phase. Coacervation is driven by the gain in configurational entropy when aggregates (soluble complexes) rearrange into a randomly distributed coacervation phase.

The Voorn-Overbeek theory and Veis and Aranyi theory are restricted to low charge density systems.

Tainaka developed a third model from the Veis and Aranyi model, which considered that coacervation is driven by attractive forces among aggregates. According to this model, the aggregates formed are possibly neutral and present in both phases, but without specific ion pairing. From this theory, it must be noted that a certain range of either the charge density and chain length of polyelectrolytes allow coacervation to occur. If the charge density is too high or the chain length is too long, the two polyelectrolytes will co-precipitate because of the aggregates interact through strong long range attractive forces. On the other hand, for too low charge density and too short chain length, the dilute solution is stabilized by short-range repulsive forces, and coacervation will not take place. The Tainaka theory is applicable to both high and low charge density systems. But, it does not provide a full explanation of coacervation process, such as suppression of coacervation at low ionic strength.

Many differences exist between these three models in the roles of electrostatic interaction, entropy, and the magnitude of solvent-solute interaction. None of these theories can describe all cases of complex coacervation. However, these theories provide a reasonable explanation for a large number of systems.

## **I.4. Complex coacervation between $\beta$ -lactoglobulin and Acacia gum**

### **I.4.1. Characteristics of $\beta$ -lactoglobulin**

$\beta$ -lactoglobulin (BLG) is the major protein of the bovine milk whey. It is a globular protein that is recognized for its gelling, foaming, hydrating and emulsifying functional properties in formulated foods<sup>107,108</sup>. However, the biological function of  $\beta$ -lg is still unknown<sup>109</sup>. In the native form, BLG has a globular structure, characterized by a molecular weight of 18400 g/mol and it contains  $\sim$  50% of  $\beta$ -sheets and 10-12% of  $\alpha$ -helix<sup>110,111</sup>. BLG can exist in a number of pH-depending structural states<sup>112</sup>. Multimerization of BLG is electrostatic and associates readily at low ionic strength at pH close to its  $pI$ , that is about 5.2<sup>113</sup>. At physiological conditions, BLG exists in dimeric form but its structure exhibits a large degree of diversity as a function of environmental conditions such as protein concentration, ionic strength and temperature<sup>114</sup>. Below pH 3, it dissociates into monomers. It exists in a monomer-dimer equilibrium at pH 3, and in a mixture of monomer, dimer and oligomer between pH 6 and 3.5 with the presence of larger aggregates<sup>115,116</sup>. A wide number of studies reported the asymmetry of charge distributions (charge heterogeneity) in proteins as well as for BLG. These local distributions are strongly influenced by the charge state of particular amino acids<sup>117</sup>.

### **I.4.2. Particularity of Acacia gum**

Like several polysaccharides, Acacia gum is a hydrocolloid that is often used to enhance stability in fluid food dispersions such soft drinks, but especially to stabilize oil-in-water emulsions and to produce dispersed flavor oils and microcapsules<sup>118,119</sup>. It is a high molecular weight negatively charged heteropolysaccharide with a complex, heterogeneous (polydispersity,  $M_w/M_n$ , of  $\sim$  2.3)<sup>140</sup> and poorly known structure<sup>120,121,122</sup>. A wide variety of techniques as Hydrophobic Interaction Chromatography (HIC), Steric Exclusion Chromatography (SEC), UV-Visible spectroscopy, Circular Dichroism (CD), and Viscosimetry allowed to characterize its biochemical and physical properties<sup>123,124,125</sup>. Regarding the chemical structure of Acacia gum, most existing studies have highlighted by

chromatographic fractionation the presence of three major components differing in the protein to sugar ratio: an arabinogalactan-peptide fraction (~ 88 wt % of whole gum), an arabinogalactan-protein (10-12 wt % of whole gum), and glycoproteins (~ 2 wt % of whole gum)<sup>126,127,128,129</sup>. On the other hand, little information is currently available about the conformation of AG molecular fractions<sup>130,131,132,133,134</sup>. The total Acacia gum, arbinogalactan-peptide and arabinogalactan-protein fractions will be respectively described hereafter as TAG, FI and FII. The term of AG will be used to define all these molecules meaning that it corresponds to both the whole gum and molecular fraction.

### **I.4.3. Mixtures of $\beta$ -lactoglobulin and Acacia gum**

In aqueous solution at peculiar pH and ionic strength conditions, attractive interactions between BLG and AG lead to complex coacervation. First kinetic studies of complex coacervation appeared on the system composed of  $\beta$ -lactoglobulin and Acacia gum (AG) using diffusing wave spectroscopy (DWS) and confocal scanning laser microscopy (CSLM)<sup>135</sup>. The DWS patterns were difficult to interpret because coalescence and sedimentation of the coacervate droplets occurred at the same time. Further kinetic studies and great interest were carried out in complex coacervation of  $\beta$ -lactoglobulin/Acacia gum/water system because of its implication in many food processes<sup>3,57,61,62,63,135,136,140</sup>. Using Small Angle Static Light Scattering (SALS), it was not possible to conclude on the occurrence of spinodal decomposition or nucleation and growth phenomena. This is because mixing the two biopolymers at pH and Pr:Pol ratio where maximum electrostatic interactions took place, induced an instantaneous phase separation<sup>136</sup>. An interesting approach is to acidify mixtures in situ using glucono-delta-lactone (GDL) in order to slow down the demixing rate. Thus, the pH can be decreased slowly from a value at which no interaction takes place to a value at which phase separation occurs<sup>137</sup>. Recently, Sanchez *et al.* (2006) get a better understand about the mechanism of complex coacervation in BLG/AG system. The authors suggested that complex coacervation between BLG and AG follows a Nucleation and Growth mechanism.

Many studies were related to parameters controlling phase separation (such as charge density, pH, ionic strength, polymer ratio, polymer concentration and temperature)<sup>3,19,20,57,61,62</sup>. The variation of ionic strength and pH in gelatin/AG system highlighted that the coacervation was



a consequence of electrostatic interactions<sup>20</sup>. The pH plays a key role in the strength of electrostatic interaction, since it determines the charge density of the protein. The presence of salt can suppress the coacervation, depending on the nature and the concentration of the salt<sup>20,62</sup>. The mixing ratio is also a critical parameter, since an optimum mixing polymer ratio exists which corresponds to an electrically equivalent amount of each polymer<sup>14,91</sup>. The coacervation mechanism depends also on the polymer concentration, since above a critical concentration self suppression of the coacervation occurs<sup>3</sup>. The role of temperature on the coacervation was hardly addressed; it was firstly studied by Bungenberg de Jong (1949). The Veis and Aranyi theory was based on a particular case of coacervation upon the reduction of temperature between two oppositely charged gelatins, an increase of the Flory-Huggins parameter on temperature reduction was shown. Weinbreck *et al.* (2003) showed a slight effect of temperature on  $pH_{\phi}$ .

Despite the wide number of studies about protein-polysaccharide interactions, the mechanism of phase separation is not fully elucidated. Furthermore, all analyses of phase separation on a great number of polymer-polymer and protein-polymer systems, and on a more limited number of protein-polysaccharide systems, revealed incomplete description of the phase-delimited structural transitions<sup>15,61,62</sup>. Phase behavior for interactions between oppositely charged polyelectrolytes has been predicted by several theoretical investigations<sup>138, 7,12,13</sup>. These works defined the pH-induced complex coacervation as a two-step process. Two specific pH of structural transitions,  $pH_c$  (critical pH, corresponds to the initiation of interaction) and  $pH_{\phi}$  (pH of phase separation), were identified. Soluble complexes were formed at  $pH_c$ . Below  $pH_{\phi}$ , the occurrence of a visual phase separation is detected. Soluble complexes were formed at pH values above the isoelectric point ( $pI$ ) of the protein, i.e. at a pH where the protein is negatively charged overall, like the polyelectrolyte. A model was proposed to clarify whether pH-transitions and soluble protein-polysaccharide complexes are formed for biopolymers just as for synthetic systems. The study predicted the complexation above the protein  $pI$ , due to the presence of (randomly) charged patches on the surface of the proteins<sup>139</sup>. Recently, Mekhloufi *et al.*<sup>140</sup> determined more structural transitions during pH-induced complex coacervation of BLG and AG, using complementary experimental methods. These transitions were identified as corresponding to (i) formation of soluble complexes (ii) conformational change of the protein induced by complexation (iii) complex aggregation (iv) initiation of phase separation (v) phase separation and (vi) first appearance of coacervates.

The first thermodynamic study of BLG/AG system was done by Schmitt *et al.* (2006) using Isothermal Titration Calorimetry. It was shown that complex coacervation between BLG and AG is mainly an exothermic process. The authors fitted the titration curves by a one set of binding sites model in order to determine the thermodynamic parameters of interaction, which reflects the presence of similar and independent binding sites.

## I.5. Objectives of the thesis

As investigated above, the wide number of studies has not fully elucidated the kinetics and dynamics of complexation and phase separation in BLG/TAG mixture. The main reasons for this lack of information is the high molecular weight polydispersity of TAG and the un-known contributions of its molecular fractions in the complexation/coacervation mechanism<sup>141</sup>. From there, the main objective of this thesis was to understand the role of TAG molecular polydispersity on the complex coacervation in order to obtain more quantitative insights into this mechanism. Our approach was to investigate phase separation between each major molecular fraction of TAG and BLG. An attempt was made to compare the results of the three different systems (BLG/TAG, BLG/PI and BLG/PII) in order to clarify the specific role of each molecular fraction in the complex coacervation process.

In a first step, the interactions between the two major fractions of TAG and BLG were investigated in order to better understand the role and contribution of each molecule in the interactions. For this, we tried to determine the energy of interactions, stoichiometry of association and binding constant in all systems. It was shown above that thermodynamics of biopolymer-biopolymer miscibility depends on many factors, such as pH, biopolymer ratio, biopolymer concentration and temperature. From there, the impact of these parameters on the thermodynamic parameters and nature of interactions was studied.

A slow acidification of mixtures by Glucono- $\delta$ -Lactone was realized in order to determine the nature of phase separation mechanism, structural transitions and morphology of phase separated interfaces in systems. The follow-up of hydrodynamic diameter, electrophoretic mobility and scattered light intensity, at a Pr:Pol mixing weight ratio (2:1) where high strength of interaction exists between biopolymers, allowed us to reach these objectives.

Since the high binding strength can mask the role of intrinsic properties of macromolecules, the same parameters studied during acidification of mixtures, at 2:1 mixing ratio, were then measured at different mixing weight ratio and total biopolymer concentration. The aim was to highlight the effects of the molecular and structural properties of AG (e.g. molecular weight, number of charges, charge density and radius of gyration) in complexation/coacervation with BLG.

## **I.6. Outline of the thesis**

This thesis consists of four chapters. The first chapter corresponds to a theoretical background of interactions and dynamics in colloidal systems. In the other chapters, experimental studies of the phase separation mechanism in BLG/AG systems were made.

In chapter I, a bibliographic study describes firstly overall types of interaction that control the stability in polymeric and biopolymeric systems. The demixing mechanisms that occur in macromolecular solutions were described. A particular study was reserved for the dynamics in BLG/TAG system. The objectives of the thesis were described in this chapter.

In chapter II, the interactions between BLG and AG were studied. The aim of this chapter was to get a better understanding of complex coacervation at the molecular level based on a thermodynamic study using a micro-calorimetric titration pattern, Isothermal Titration Calorimetry. The effects of various physico-chemical parameters (e.g. biopolymer concentration, pH and temperature) on the thermodynamic characteristics were investigated. A modeling of the binding curves and determination of the thermodynamic parameters of interactions is discussed.

Chapter III deals with the pH-induced complex coacervation in BLG/AG mixtures during a slow in situ acidification by GDL. In this chapter, we aimed to highlight the behaviors of the different AG molecular fractions in the complexation/coacervation using static and dynamic light scattering (SALS and DLS), and electrophoretic mobility ( $\mu_E$ ) measurements. The size, charge of complexes, pH of structural transitions, nature of phase separation mechanism and compacity of particles were investigated.

Chapter IV provides a more general view on the complexation/coacervation mechanism of BLG/AG system. In chapter IV, the main objective was to better evaluate the structural role of AG that was detected in chapter II and III. For that purpose, we varied the parameters defined in chapter II, which can modify the phase separation mechanism, especially the mixing ratio and total biopolymer concentration. Thus, the same type of experiments as in chapter III but for different mixing ratios, were made using SALS, DLS and  $\mu_E$

measurements. The influence of the total amount of biopolymers was investigated in order to obtain a more detailed investigation of the structure using Granulo-polarimetry and optical microscopy methods. The outline of this thesis will summarize all these experimental studies.

## I.7. References

- 
- <sup>1</sup> Zancang, S.; Mitragotri, S. *Pharmaceutical Research*, **2002**, 19, 391.
  - <sup>2</sup> Prokop, A.; Kozlov, E.; Newman, G.W.; Newman, M. *Journal of Biotechnology and Bioengineering*, **2002**, 78, 459.
  - <sup>3</sup> Cooper, C.L.; Dubin, P.L.; Kayitmazer, A. B.; Turksen, S. *Current Opinion in Colloid and Interface Sciences*, **2005**, 10, 52.
  - <sup>4</sup> Guzey, D.; McClements, D.J. *Food Hydrocolloids*, **2006**, 20, 124.
  - <sup>5</sup> Tolstoguzov, V.B. *Food Hydrocolloids*, **2001**, 17, 1.
  - <sup>6</sup> Gao, J.Y.; Dubin, P.L. *Biopolymers*, **1999**, 49, 185.
  - <sup>7</sup> Dubin, P.L.; Gao, J.; Mattison, K. *Separation and Purification Methods*, **1994**, 23, 1.
  - <sup>8</sup> Gao, J.Y.; Dubin, P.L.; Muhoberac, B.B. *Journal of Analytical Chemistry*, **1997**, 69, 2945.
  - <sup>9</sup> Hattori, T.; Hallberg, R.; Dubin, P.L. *Langmuir*, **2000**, 16, 9738.
  - <sup>10</sup> Bhat, S.; Tuinier, R.; Schurtenberger, P. *Journal of Physics: Condensed Matter*, **2006**, 18, 339.
  - <sup>11</sup> Hallberg, R.K.; Dubin, P.L. *Journal of Physical Chemistry B*, **1998**, 102, 8629.
  - <sup>12</sup> Xia, J.; Dubin, P.L. *In: Macromolecular Complexes in Chemistry and Biology*, Springer Verlag: Berlin, **1994**, pp 247.
  - <sup>13</sup> Xia, J.; Dubin P.L.; Kokufuta, E.; Havel, H.; Muhoberac, B.B. *Biopolymers*, **1999**, 50, 153.
  - <sup>14</sup> Weinbreck, F.; Nieuwenhuijse, H.; Robin, G.W.; de Kruif, C.G. *Journal of Agricultural and Food Chemistry*, **2004**, 52, 3550.
  - <sup>15</sup> Girard, M.; Sanchez, C.; Laneuville, S.I.; Turgeon, S.L.; Gauthier, S.F. *Colloids and Surfaces B: Biointerfaces*, **2004**, 35, 15.
  - <sup>16</sup> Tadros, Th. F. (ed.), *Solid/Liquid Dispersions*, Academic Press, London, **1987**.
  - <sup>17</sup> Napper, D.H. *Polymeric Stabilization of Colloidal Dispersions*, Academic Press, London, **1983**, p 621.
  - <sup>18</sup> Russel, W.B.; Saville, D.A.; Schowalter, W.R. *Cambridge Monographs on Mechanics and Applied Mathematics (Cambridge University Press, Cambridge)*, **1989**.
  - <sup>19</sup> Bungenberg de Jong, H.G.; Kruyt, H.R. *Koninklijke Nederlandse Akademie van Wetenschappen (KNAW)*, **1929**, 32, 849.
  - <sup>20</sup> Bungenberg de Jong, H.G.; Kruyt, H.R. *In Colloid Science; Kruyt H.R., Ed.; Elsevier Publishing Company: Amsterdam*, **1949a**, Vol. II, Chapter VIII, p 232.

- 
- <sup>21</sup> Elimelech, M.; O'Melia, C.R. *Langmuir*, **1990**, 6, 1153.
- <sup>22</sup> O'Melia, C.R.; Stumm, W. *New York, John Wiley and Sons*, **1985**.
- <sup>23</sup> Stumm, W. *Chemistry of the solid-water interface. New York, John Wiley and Sons*, **1992**.
- <sup>24</sup> Filella, M.; Buffle J. *Colloids and Surfaces A: Physicochemical and Engineering Aspects*, **1993**, 73, 255.
- <sup>25</sup> O'Melia, C.R. *Environnemental Science and Technology*, **1980**, 14, 1052.
- <sup>26</sup> Adachi, Y.; Matsumoto, T.; Cohen Stuart, M.A. *Colloids and Surfaces A: Physicochemical and Engineering Aspects*, **2002**, 207, 253.
- <sup>27</sup> Hunt, J.R. *Environnemental Science and Technology*, **1982**, 16, 303.
- <sup>28</sup> Guldbrand, L.; Jonsson, B.; Wennerström, H.; Linse, P. *Journal of Chemical Physics*, **1984**, 80, 2221.
- <sup>29</sup> Stone, H.; Stroock, A.; Ajdari, A. *Annual Review for Fluid Mechanics*, **2004**, 36, 381.
- <sup>30</sup> Lyklema, J. *Foundations of Colloid and Interface Science (Academic Press, San Diego)*, **1995**, Vol. II.
- <sup>31</sup> Jolivet, J.-P. *Metal oxide chemistry and synthesis. From solution to solid state. New York, John Wiley and Sons*, **1994**.
- <sup>32</sup> Hunter, R.J. *Fundamentals of Colloids Science. Oxford, Clarendon Press*, **1986**.
- <sup>33</sup> Hamaker, H.C. *Physica*, **1937**, 4, 1058.
- <sup>34</sup> Lifshitz, E.M. *Soviet Physics JETP*, **1956**, 2, 73.
- <sup>35</sup> Hiemenz, P.C.; Rajagopalan, R. *Principles of Colloid and Surface Chemistry. New York, Marcel Dekker*, **1997**.
- <sup>36</sup> Grasso, D. *Reviews in Environmental Science and Biotechnology*, **2002**, 1, 17.
- <sup>37</sup> Stoll, S.; Buffle, J. *Chimia*, **1995**, 49, 300.
- <sup>38</sup> McIntosh, T. J.; Simon, S. A. *Biochemistry*, **1986**, 25, 4058.
- <sup>39</sup> Gawrisch, K.; Ruston, D.; Zimmerberg, J.; Parsegian, V.A.; Rand, R.P.; Fuller, N. *Biophysical Journal*, **1992**, 61, 1213.
- <sup>40</sup> McIntosh, T.J.; Simon, S. A. *Annual Review of Biomolecular Structures* **1994**, 23, 27
- <sup>41</sup> Israelachvili, J.N.; McGuiggan, P.M. *Science*, **1988**, 241, 795.
- <sup>42</sup> LeNeveu, D.M.; Rand, R.P.; Parsegian, V.A. *Nature*, **1976**, 259, 601
- <sup>43</sup> Rand, R.P.; Parsegian, V.A. *Biochimica and Biophysica Acta*, **1989**, 988, 351.
- <sup>44</sup> Walstra, P. *Physical chemistry of milk fat globules. Page 128 in Developments in Dairy Chemistry. 2. P. F. Fox, ed. Applied, John Wiley and Sons, New York, NY*, **1983**.

- 
- <sup>45</sup> Froberg, J.C.; Rojas, O.J., Claesson, P.M. *International Journal of Mineral Processing*, **1999**, 56, 1.
- <sup>46</sup> Ishida, N.; Sakamoto, M.; Miyahara, M.; Higashitani, K. *Journal of Colloid and Interface Science*, **2002**. 253, 112.
- <sup>47</sup> Meyer, E.E.; Lin, Q.; Israelachvili, J.N. *Langmuir*, **2005**, 21, 256.
- <sup>48</sup> Ben-Naim, A. *Hydrophobic Interactions*; Plenum Press: New York, **1980**.
- <sup>49</sup> Tanford, C. *The Hydrophobic Effect*; Wiley: New York, **1980**.
- <sup>50</sup> Olabisi, O.; Robeson, L.; Shaw, M.T. *Polymer-Polymer Miscibility*, Academic Press: New York, **1979**.
- <sup>51</sup> Flory, P. *Cornell University Press, Ithaca, New York*, **1971**.
- <sup>52</sup> Huggins, M. *Journal of Physical Chemistry*, **1942**, 46, 685.
- <sup>53</sup> Huggins, M. *Annals of the New York Academy of Sciences*, **1942**, 82, 4.
- <sup>54</sup> Huggins, M. *Journal of American Chemical Society*, **1942**, 82, 64.
- <sup>55</sup> Van der Haegen, R.; Kleintjens, L.A. *Pure and Applied Chemistry*, **1989**, 61, 159.
- <sup>56</sup> Vrij, A. *Journal of Colloid Science*, **1964**, 19, 3503.
- <sup>57</sup> Sanchez, C.; Mekhloufi, G.; Schmitt, C.; Renard, D.; Robert, P.; Lehr, C.-M.; Lamprecht, A.; Hardy, J. *Langmuir*, **2002**, 18, 10323.
- <sup>58</sup> Cahn, J.W. *Journal of Physical Chemistry*, **1965**, 42, 93
- <sup>59</sup> Horst, R.; Wolf, B.A. *Polymeric Materials Science and Engineering*, **1994**, 71, 113.
- <sup>60</sup> Kwei, T.K.; Wang, T.T. *Phase Separation Behavior of Polymer-Polymer Mixtures, in Polymer Blends, Paul, D.R. and Newman, S. Ed., Academic Press: New York*, **1978**.
- <sup>61</sup> Schmitt, C.; Sanchez, C.; Desobry-Banon, S.; Hardy, J. *Critical Reviews in Food Science and Nutrition*, **1998**, 38, 689.
- <sup>62</sup> Schmitt, C.; Sanchez, C.; Thomas, F.; Hardy, J. *Food Hydrocolloids*. **1999**, 13, 483.
- <sup>63</sup> Sanchez, C.; Paquin, P. *In Food Proteins and Their Applications*; Damodaran, S.; Paraf, A.; Dekker Marcel; Eds.; Inc.: New York, **1997**, p 503.
- <sup>64</sup> Asakura, S; Oosawa, F. *Journal of Chemical Physics*, **1954**, 22, 1255.
- <sup>65</sup> Vrij, A. *Pure and Applied Chemistry*, **1976**, 48, 471.
- <sup>66</sup> Asukara, A.; Oosawa, F. *Journal of Polymer Science*, **1958**, 93, 183.
- <sup>67</sup> Lin, K-H; Crocker, J.C.; Zeri, A.C.; Yodh, A.G. *Physical Review Letters*, **2001**, 87, 88301.
- <sup>68</sup> van der Schoot, P. *Macromolecules*, **1998**, 31, 4635.
- <sup>69</sup> Wang, S.; van Dijk, J.A.P.P.; Odijk, T.; Smit, J.A.M. *Biomacromolecules*, **2001**, 2, 1080.
- <sup>70</sup> Saeki, S.; Kuwahara, N.; Nakata M.; Kaneko, M. *Polymer*, **1976**, 17, 685.



- 
- <sup>71</sup> Tolstoguzov, V.B. *Food Hydrocolloids*, **1997**, 11, 181.
- <sup>72</sup> Beijerinck, M.W.; *Zentralblatt für Bakteriologie; Parasitenkunde; Infektionskrankheiten Abteilung 2*, **1896**, 2, 697.
- <sup>73</sup> Grinberg, V.Y.; Tolstoguzov, V.B. *Food Hydrocolloids*, **1997**, 11, 145.
- <sup>74</sup> Tolstoguzov, V.B. *Critical Reviews in Biotechnology*, **2002**, 22, 89.
- <sup>75</sup> Durrani, C.M.; Prystupa, D.A.; Donald, A.M.; Clark, A.H. *Macromolecules*, **1993**, 26, 981.
- <sup>76</sup> Durrani, C.M.; Donald, A.M. *Macromolecules*, **1994**, 27, 110.
- <sup>77</sup> Bourriot, S. Garnier C.; Doublier, J.-L. *Food Hydrocolloids*, **1998**, 13, 43.
- <sup>78</sup> Bourriot, S.; Garnier, C.; Doublier, J.-L. *Carbohydrate Polymers*, **1999**, 40, 145.
- <sup>79</sup> Garnier, C.; Schorsch, C.; Doublier, J.-L. *Carbohydrate Polymers*, **1995**, 28, 313.
- <sup>80</sup> de Hoog, E.H.A.; Tromp, R.H. *Colloids and Surfaces A*, **2003**, 213, 221.
- <sup>81</sup> Flory, P.J. *Journal of Chemical Physics*, **1941**, 9, 660.
- <sup>82</sup> Flory, P.J. *Journal of Chemical Physics*, **1942**, 10, 51.
- <sup>83</sup> Vrij, A. *Pure and Applied Chemistry*, **1976**, 48, 471.
- <sup>84</sup> Huggins, M.L. *Journal of Physical Chemistry*, **1942**, 46, 151.
- <sup>85</sup> Tanford, C. *Physical Chemistry of Macromolecules*. New York: Wiley, **1961**.
- <sup>86</sup> de Gennes, P.G. *Journal of Physical Chemistry*, **1990**, 94, 8407.
- <sup>87</sup> Thalberg, K.; Lindman B.; Karlström, G. *Journal of Physical Chemistry*, **1991**, 95, 3370.
- <sup>88</sup> Piculell, L.; Lindman, B. *Advances in Colloid and Interface Sciences*, **1992**, 41, 149.
- <sup>89</sup> Gurov, A.N.; Nuss, P.V. *Nahrung*, **1986**, 30, 349.
- <sup>90</sup> Serov, A.N.; Antonov, Y. A.; Tolstoguzov, V.B. *Nahrung*, **1985**, 1, 19.
- <sup>91</sup> Burgess, D.J.; Carless, J. E. *Journal of Colloid and Interface Science*. **1984**, 98, 1.
- <sup>92</sup> Dickinson, E. *Food Hydrocolloids*, **2003**, 17, 25.
- <sup>93</sup> Semenova, M. ; Antipova, A. ; Belyakova, L. ; Dickinson, E.; Brown, R.; Pelan, E.; Norton, I. *Food Emulsions and Foams: Interfaces, Interactions and Stability*. Cambridge: The Royal Society of Chemistry, **1999**, 163.
- <sup>94</sup> Tolstoguzov, V.B. *In Food Proteins and their Applications*, Marcel Dekker, Inc.: New York, **1997**, pp 171.
- <sup>95</sup> Phillips, G.O.; Williams, P.A. *In Ingredient interactions, effects on food quality*; Marcel Dekker, Inc.: New York, **1995**, pp 131.
- <sup>96</sup> Imeson, A.P.; Ledward, D.A.; Mitchell, J.R. *Journal of the Science of Food and Agriculture*, **1977**, 28, 669.

- 
- <sup>97</sup> Antonov, Y.A.; Soshinsky, A.A. *International Journal of Biological Macromolecules*, **2000**, 27, 279.
- <sup>98</sup> Tolstoguzov, V.B. *In Functional Properties of Food Macromolecules, Elsevier Applied Science: London*, **1986**, p 385.
- <sup>99</sup> Thalberg, K.; Lindman B.; Karlstrbm, G. *Journal of Physical Chemistry*, **1990**, 94, 4289.
- <sup>100</sup> Overbeek, J.T. J.; Voorn, M. J. *Journal of Cellular and Comparative Physiology*, **1957**, 49 (S1) 7.
- <sup>101</sup> Veis, A; Aranyi, C. *Journal of Physical Chemistry*, **1960**, 64, 1203.
- <sup>102</sup> Veis, A. *Journal of Physical Chemistry*, **1961**, 65, 1798.
- <sup>103</sup> Veis, A. *Journal of Physical Chemistry*, **1963**, 67, 1960.
- <sup>104</sup> Veis, A. *Biopolymers*, **1967**, 5, 37.
- <sup>105</sup> Nakajima, A; Sato, H. *Biopolymers*, **1972**, 10, 1345.
- <sup>106</sup> Tainaka, K. *Journal of the Physical Society of Japan*. **1979**, 46, 1899.
- <sup>107</sup> Lefèvre, T.; Subirade, M. *Food Hydrocolloids*, **2001**, 15, 365.
- <sup>108</sup> Rutten, A.A.C.M.; Bouwman, W.G.; van der Leeden, M.C. *Colloids and Surfaces A*, **2002**, 210, 243.
- <sup>109</sup> Kontopidis, G.; Holt, C.; Sawyer, L. *Journal of Molecular Biology*, **2002**, 318, 1043.
- <sup>110</sup> Uhrínová, S.; Smith, M.H.; Jameson, G.B.; Uhrín, D.; Sawyer, L.; Barlow, P.N. *Biochemistry*, **2000**, 39, 3565.
- <sup>111</sup> Timasheff, S.N.; Mescanti, L.; Basch, J.J.; Towned, R. *Journal of Biological Chemistry*, **1966**, 241, 2496.
- <sup>112</sup> Taulier, N.; Chalikian, T.V. *Journal of Molecular Biology*, **2001**, 314, 873.
- <sup>113</sup> Casal, H.L.; Kohler, U.; Mantsch, H.H. *Biochemica and Biophysica Acta*, **1988**, 957, 11.
- <sup>114</sup> Kavanagh, G. M.; Clark, A. H.; Ross-Murphy, S. B. *International Journal of Biological Macromolecules*, **2000**, 28, 41.
- <sup>115</sup> Zhang, G.; Foegending, E.A. *Food Hydrocolloids*, **2003**, 17, 785.
- <sup>116</sup> Molinari, H.; Ragona, L.; Varani, L.; Musco, G.; Consonni, R.; Zetta, L.; Monaco, H.L. *FEBS Letters*, **1996**, 381, 237.
- <sup>117</sup> Macleod, A.; Fedio, W.M.; Ozimek, L. *Milchwissenschaft*, **1995**, 50, 666.
- <sup>118</sup> Yaseen, E.I.; Herald, T.J.; Aramouni, F.M.; Alavi, S. *Food Research International*, **2004**, 38, 111.
- <sup>119</sup> Leon de Pinto, G.; Martinez, M.; Sanabria, L. *Food Hydrocolloids*, **2001**, 15, 461.
- <sup>120</sup> Ibanoglu, E. *Journal of Food Engineering*, **2001**, 52, 273.

- 
- <sup>121</sup> Buffo, R.A.; Reineccius, G.A.; Oehlert, G.W. *Food Hydrocolloids*, **2000**, 15, 53.
- <sup>122</sup> Sanchez, C.; Renard, D.; Robert, P.; Schmitt, C.; Lefèvre, J. *Food Hydrocolloids*, **2001**, 16, 257.
- <sup>123</sup> Idris, O.H.M.; Williams, P.A.; Phillips, G.O. *Food Hydrocolloids*, **1998**, 12, 379.
- <sup>124</sup> Williams, P.A.; Phillips, G.O.; Randall, R.C. *Gums and stabilizers for the food industry 5*, Royal Society of Chemistry, **1989**, 25.
- <sup>125</sup> Picton, L.; Battaille, I.; Muller, G. *Carbohydrate Polymers*, **2000**, 42, 23.
- <sup>126</sup> Redgwell, R.J.; Schmitt, C.; Beaulieu, M.; Curti, D. *Food Hydrocolloids*, **2004**, 19, 1005.
- <sup>127</sup> Randall, R.C.; Phillips, G.O.; Williams, P.A. *Food Hydrocolloids*, **1989**, 3, 65.
- <sup>128</sup> Osman, M.E.; Menzies, A.R.; Martin, B.A.; Williams, P.A.; Phillips, G.O.; Baldwin, T.C. *Phytochemistry*, **1995**, 38, 409.
- <sup>129</sup> Fenyo, J.C.; Vandeveld, M.C. *Gums and stabilizers for the food industry 5*, Royal Society of Chemistry, **1989**, 17.
- <sup>130</sup> Al-Assaf, S.; Phillips, G.O.; Williams, P.A. *Food Hydrocolloids*, **2005**, 19, 647.
- <sup>131</sup> Al-Assaf, S.; Phillips, G.O.; Williams, P.A. *Food Hydrocolloids*, **2005**, 19, 661.
- <sup>132</sup> Hassan, E.A.; Al-Assaf, S.; Phillips, G.O.; Williams, P.A. *Food Hydrocolloids*, **2004**, 19, 669.
- <sup>133</sup> Siddig, N.E.; Osman, M.E.; Al-Assaf, S.; Phillips, G.O.; Williams, P.A. *Food Hydrocolloids*, **2005**, 19, 679.
- <sup>134</sup> Flindt, C.; Al-Assaf, S.; Phillips, G.O.; Williams, P. A. *Food Hydrocolloids*, **2005**, 19, 687.
- <sup>135</sup> Schmitt, C. ; Sanchez, C. ; Lamprecht, A. ; Renard D. ; Lehr , C.M. ; de Kruif, C.G. ; Hardy, J. *Colloids and Surfaces B: Biointerfaces*, **2001**, 20, 267.
- <sup>136</sup> Sanchez, C.; Renard, D. *International Journal of Pharmaceutics*, **2002**, 242, 319.
- <sup>137</sup> Tuinier, R.; Dhont, J. K.G.; de Kruif, C.G. *Langmuir*, **2000**, 16, 1497.
- <sup>138</sup> Kaibara, K.; Okasaki, T.; Bohidar, H.B.; Dubin, P.L. *Biomacromolecules*, **2000**, 1, 100.
- <sup>139</sup> de Vries, R. *Journal of Physical Chemistry*, **2004**, 120, 3475.
- <sup>140</sup> Mekhloufi, G.; Sanchez, C.; Renard, D.; Guillemin, S.; Hardy, J. *Langmuir*, **2005**, 21, 386.
- <sup>141</sup> Snowden, M.G.; Phillips, G.O.; Williams, P.A. *Food Hydrocolloids*, **1987**, 1, 291.



## Chapter II

# Thermodynamic characterization of interactions between $\beta$ -lactoglobulin and major molecular fractions of Acacia gum

### Abstract

The thermodynamic behavior of total Acacia gum (TAG) and its two major molecular fractions arabinogalactan-peptide (FI ~ 88 wt % of AG) and arabinogalactan-protein (FII ~ 10 wt % of AG) in interactions with  $\beta$ -lactoglobulin (BLG) was studied by Isothermal Titration Calorimetry (ITC) and optical density (O.D.) measurements. Thus, the ratio-induced macromolecules assembly (allowed by the titration) was investigated at pH 4.2 and 25 °C during titration of gum dispersion into BLG dispersion. The influence of the important physicochemical parameters that affect the binding parameters in such protein-polyelectrolyte system was studied, i.e. AG concentration, pH and temperature. BLG/TAG, BLG/FI and BLG/FII systems displayed similar binding curves but with different energy of interactions and stoichiometry of association. Compared to BLG/FI dispersion, the binding curve of BLG/FII revealed faster saturation of binding sites i.e. at lower charge ratio (lower stoichiometry) and stronger energy of interaction (higher values of  $\Delta H_{\text{obs}}$ ). These results were related to both higher accessibility of charges and higher charge density of FII molecular fraction. Thus, lower Pr:Pol charge ratios of structural transitions were defined in BLG/FII system as compared to BLG/FI dispersion, in agreement with more favorable complexation/coacervation. These ratios corresponded to:  $r_{\text{agg}}$ , the charge ratio of aggregation of complexes;  $r_{\text{isto}}$ , the charge ratio of initiation of stoichiometry;  $r_{\text{eq}}$ , the charge ratio of enthalpy/entropy equilibrium and  $r_{\text{sat}}$ , the charge ratio of saturation of binding sites. For overall Acacia gum molecules, electrostatic interactions mainly induced complexation with BLG. In addition, hydrogen bonding plays a significant role in the complex formation. The binding enthalpy decreases with increasing AG concentration and pH, in relation with the decrease of electrostatic binding strength with decreasing the initial Pr:Pol charge ratio and charge density of biopolymers. Increasing the temperature led to a decrease of the binding strength may be due to a heat-induced hydrogen bonds breakage. In addition, an increase of each parameter led to lower stoichiometry of interaction, in agreement with a lowering of the initial Pr:Pol charge ratio.

## II.1. Introduction

The stability of a blend, as assessed in the previous chapter, is governed by thermodynamics. For a blend to be stable, the change in Gibbs energy upon mixing ( $\Delta G_{\text{mix}}$ ) must be lower than zero. It is conceptually useful to express this energy of interaction in terms of the following contributions <sup>1</sup>:

$$\Delta G_{\text{mix}} = \Delta H - T\Delta S \quad \text{with } \Delta S = \Delta S_{\text{sol}} + \Delta S_{\text{conf}} + \Delta S_{\text{R, TR}} \quad \text{Eq. II.1}$$

Where  $\Delta S_{\text{sol}}$ ,  $\Delta S_{\text{conf}}$  and  $\Delta S_{\text{R, TR}}$  correspond respectively to the solvation, conformational and roto-translational entropies associated with the change in solvation, conformational space and configurational space of the binding molecules upon binding.  $\Delta H$  contains the energetic contribution of many individual interactions (electrostatic, hydrophobic, hydrogen bonding, van der Waals, etc.) between the two binding molecules, considering the solvent as a reference <sup>2,3</sup>. The expression of  $\Delta G_{\text{mix}}$  is evoked to indicate at the next the parameters that influence the thermodynamics of interactions between unlike-charged biopolymers.

Let us consider here the interactions in protein/polysaccharide systems (Pr/Pol). The knowledge is still lacking about the thermodynamics of complexation in these systems and contradictions exist between some studies <sup>17</sup>. A number of works showed that complexation in protein/polysaccharide mixtures is mainly driven by enthalpy changes, due to the decrease of the electrostatic free energy of system (Girard *et al.*, 2003). Some authors indicate that entropy is mainly driving complexation owing to the liberation of counterions and water molecules <sup>4</sup>.

Indeed, overall interactions between two biopolymers are made up from an average over the large number of different intermolecular forces arising between the various side-chains on the two macromolecules <sup>4,5</sup>. For protein/polysaccharide systems, a great number of works provided information about the main contribution of electrostatic interactions in the formation of complexes. However, much less is known about the importance of other type of interactions <sup>6,7,8,9</sup>. Using Isothermal Titration Calorimetry, Schmitt *et al.* (2006) and Girard *et al.* (2003) reported a major role of electrostatic interactions in the complexation of Pr/Pol

mixtures without explanation of other interaction contributions. Other works showed that the formation of complexes is extensively dependent on the balance of intermolecular forces (non-Coulombic and Coulombic interactions)<sup>10</sup>. In a recent study, Laneuville *et al.* (2006)<sup>11</sup> showed the importance of weak energy interactions (hydrophobic and hydrogen bonding) in the complexation mechanism of native  $\beta$ -lactoglobulin/xanthan gum mixtures.

As many protein/polysaccharide systems, the thermodynamics of complexation/coacervation between BLG and TAG is still ill-known. Recently, Schmitt *et al.* (2006) suggested, in a first thermodynamic study of interactions between BLG and TAG, that complex coacervation between the two biopolymers is driven by a decrease of enthalpy due to the formation of bonds during complexation and an increase of entropy due to the release of counter-ions<sup>12</sup>. Some works also showed that complexation of BLG/TAG system is enhanced by their polyelectrolyte nature, counter-ions increase the entropy of mixtures<sup>13</sup>.

It is well established that the nature (soluble/insoluble) and structure of Pr/Pol complexes are depending on many parameters, which include the energetic terms of interactions ( $\Delta H$  and  $\Delta S$ )<sup>14,15,16,17,18,19,20</sup>. Thus, the enthalpic factors influencing the nature of complexes can be the biopolymer charge density, the pH, the protein:polysaccharide ratio (Pr:Pol) and the ionic strength. The entropic factors are mainly the molecular weight and the structure (e.g. conformation, flexibility)<sup>21</sup>. At the molecular level, the Gibbs free energy for protein/polysaccharide results from the opposition of two main phenomena: the tendency of energy to decrease (formation of bonds, negative  $\Delta H$ ) and the tendency of the Brownian motion to disturb the binding characteristics (bond breakage, positive  $\Delta S$ )<sup>22</sup>. On this basis, it is expected that the difference in the molecular weight between AG fractions will affect  $\Delta S$ . Similarly, a change in biopolymer composition (e.g. protein-to-sugar ratio) will affect intermolecular interactions between the pair, and thus  $\Delta H$ .

In this chapter, a thermodynamic study of interactions between BLG and the two major molecular fractions of TAG was explored in order to give a better knowledge of interactions between BLG and AG, especially at the quantitative level. Since the intrinsic properties of macromolecules (e.g. molecular weight, size) and environmental parameters (e.g. pH, biopolymer concentration, Pr:Pol molar ratio, temperature) can influence largely the thermodynamic of complexation, the study of these factors was a mean to better understand

the complex coacervation process between BLG and AG.

Isothermal Titration Calorimetry (ITC) is widely used by biochemists and supramolecular chemists to characterize interacting systems. ITC was used to characterize the interactions between BLG and Acacia gum molecules. The procedure was to titrate an aqueous dispersion of BLG by aliquots of an aqueous dispersion of gum (TAG or its molecular fraction). ITC results were compared to optical density experiments made by spectrophotometry in the same physico-chemical conditions.



## II.2. Experimental Section

### II.2.1. Materials

*β-Lactoglobulin powder* (lot JE001-3-922) was purchased from Davisco Foods International Inc. (Lesueur, MN, USA). The powder was obtained using filtration and ion exchange chromatography. The powder composition was (g per 100 g): 93.6% protein (N x 6.38), 4.9% moisture and 1.5% ash (0.017% Ca<sup>2+</sup>, 0.003% Mg<sup>2+</sup>, 0.008% K<sup>+</sup>, 0.9 Na<sup>+</sup>, 0.03% Cl<sup>-</sup>). Before experiments, it was extensively dialysed against distilled water to remove salt ions and freeze-dried.

*Acacia gum powder* type from Acacia senegal trees (lot no 97 J 716) was a gift from CNI Company (Rouen, France). The powder composition was (g per 100 g): 90% polysaccharide, 6.6% moisture, 0.3% nitrogen and 3.1% ash (0.2% Mg<sup>2+</sup>, 0.61% Ca<sup>2+</sup>, 0.032% Na<sup>+</sup> and 0.9% K<sup>+</sup>). Before experiments, it was extensively dialyzed against distilled water to remove salt ions and freeze-dried.

*Arabinogalactan-peptide and Arabinogalactan-protein* powders. The two biopolymers were obtained by fractionation of the whole gum by hydrophobic interaction chromatography (HIC) in BIA laboratory (Unité de Recherches sur les Biopolymères, Interactions, Assemblages; Nantes, France). The appropriate fractions were pooled, extensively dialyzed against distilled water and freeze-dried for further analysis.

The isolated fractions are different in molecular weight and protein proportions. FI has a molecular weight of  $\sim 2.86 \cdot 10^5$  g/mol and it constitutes 88.5 wt % of the total gum. FII was identified with a molecular weight of  $1.86 \cdot 10^6$  g/mol and a percentage of 10.5 wt % in the total gum; it contains a proportion of protein of 8.7 wt %.

We show in Tab. II.1 the principal structural and chemical characteristic of FI and FII as determined by Renard *et al.* (2006)<sup>19</sup>.

*Glucono-δ-lactone*, GDL, (lot 052K0031, Calbochiem, Darmstadt, Germany) is an ester of gluconic acid obtained by oxidative fermentation of D-glucose (*Acetobacter suboxydans*).

*Sodium hydroxide and hydrochloric acid* were of analytical grade (Fischer Scientific SA,

Elancourt, France).

**Tab. II.1.** Number of negative charges and molecular parameters of TAG and its two major molecular fractions FI and FII. Adapted from Renard et al. (2006).

	<b>Total Acacia gum</b>	<b>Fraction I</b>	<b>Fraction II</b>
<b>Weight percentage</b>		88.5	10.5
<b>M<sub>w</sub> (g/mol)</b>	3.06 10 <sup>5</sup>	2.86 10 <sup>5</sup>	1.86 10 <sup>6</sup>
<b>M<sub>w</sub>/M<sub>n</sub></b>	1.25	1.28	1.33
<b>R<sub>G</sub> (nm)</b>	11.8	11.3	30
<b>R<sub>h</sub> (nm)</b>	10.7	13.2	34.4
<b>Number of negative charges</b>	368	225	1259

## II.2.2. Preparation of $\beta$ -Lactoglobulin (BLG) and Acacia gum (AG) stock dispersions

Stock dispersions of BLG, total Acacia gum (TAG), FI and FII were prepared by gradually adding the freeze-dried biopolymer to ultra pure deionized water under gentle stirring at  $20 \pm 1$  °C for at least 2 h at 0.6 wt % (for BLG) and 1.8 wt % (for AG) total biopolymer concentration. The pH of the BLG dispersion was adjusted to 5 (pH corresponding to the lowest BLG solubility) with 1 N HCl. Stock dispersions were stored at  $4 \pm 1$  °C during 18 h to allow good hydration of biopolymers. The stock solutions were then centrifuged during 40min at 10 000g to remove insoluble material and air bubbles. The concentration of BLG solution was checked by UV-Visible spectroscopy (Ultrospec 4000 UV/Visible, Pharmacia Biotech, England) using the specific extinction coefficient of 9.2 dl/cm.g at 278 nm, as determined experimentally. The absorbance at 278 nm was corrected for turbidity and the BLG dispersion concentration was finally adjusted to 0.1w%. The final pH was adjusted using 0.1 and 1N NaOH.

## II.2.3. Isothermal Titration Calorimetry

An isothermal titration calorimeter (VP-ITC, Microcal, Inc, Northampton, MA) was used to measure the enthalpic and entropic changes resulting from titration of BLG dispersion by Acacia gum dispersion (total or molecular fractions). The exchanged heat is measured in the  $\mu$ cal range at a constant fixed temperature. This parameter provides quantitative information about the interaction between BLG and AG (association constant, free energy, enthalpy and

entropy of association). The reference cell had an internal volume of 1.428 ml and it was filled with deionized water. Each injection lasted 20 sec and the experimental procedure was to inject a constant volume of 10  $\mu$ l of AG every 150 sec. A rotating 250  $\mu$ l Hamilton microsyringe ensuring constant stirring of the whole mixed dispersion at a speed of 260 rpm ensured the homogenization during injection. For most experiments, the temperature of the dispersion in the titration cell was 25 °C. Other experiments were made at various temperatures in the range 4-50 °C. Measurements were carried out in duplicate and were highly reproducible. The heat of dilution from the blank titration of deionized water into BLG dispersion and Acacia gum dispersion into deionized water were measured. The dilution heat of AG dispersion was subtracted from the raw data because of the binding process in such systems such as BLG/AG is frequently accompanied by changes in the conformation or oligomerization state of biopolymers.

#### II.2.4. Optical density

A spectrophotometer (Ultrospec 4000 UV/Visible, Pharmacia Biotech, England) was used to follow the optical density during the injection of AG into BLG in the same conditions as ITC experiments, at a wavelength of 633 nm. This experiment was made to elucidate the different structural transitions observed in the binding curves by comparing them with O.D. evolution upon titration of AG dispersion into BLG dispersion.

A separate experiment was made to measure the optical density of BLG/AG mixed dispersions during slow acidification by glucono- $\delta$ -lactone at  $\lambda$  of 633 nm. This experiment was done in order to compare the evolution of the strength of interaction and ratios of structural transitions with pH, measured by ITC, to those obtained by O.D. measurements.

Optical density (*O.D.*) values were determined from:

$$\text{O.D.} = \ln(I_0/I_t) / d \qquad \text{Eq.II.2}$$

where  $d$  is the thickness of the cell (1 mm),  $I_0$  the incident intensity and  $I_t$  the transmitted intensity.

## **II.3. Results and Discussion**

### **II.3.1. Thermodynamic characteristics of BLG/AG interactions**

Electrostatic interactions play a major role in determining the complexation/coacervation mechanism between BLG and AG. Thus, the high energetic contribution of electrostatic interactions may complicate the detection of other interaction forces that contribute to complexation in BLG/AG dispersions. Therefore, characterization of each biopolymer before measurement of interactions was necessary. This is to check the effect of some phenomena involving biopolymers under specific conditions of pH or temperature (e.g. dissociation-association, conformational changes), which can contribute to binding curves. Thus, the heats of dilution from the blank titration of the deionized water into BLG dispersion, and the AG dispersion into deionized water were measured.

Fig. II.1 shows the thermodynamic properties of BLG and TAG stock dispersions at pH 4.2 (the maximum of interaction in BLG/TAG system as determined by Sanchez *et al.*, 2006). Different thermodynamic characteristics between the titration curves of BLG and TAG dispersions were observed.

The dilution heat of TAG exhibits weak exothermic peaks for which the intensity decreased gradually with titration. The exothermic nature of peaks can be attributed to the disaggregation of AG oligomers. As titration proceeds, the injection of TAG dispersion into water may disturb its structure and lead to aggregation phenomena, which is an endothermic effect that can explain the decrease of peak intensity<sup>23</sup>.

The blank titration of BLG dispersion showed constant and weaker endothermic peaks as compared to TAG dispersion. Adding water into BLG dispersion can disturb its oligomerization state and affect also the affinity of oligomers to water molecules<sup>24</sup>, which promotes aggregation of BLG molecules and lead then to endothermic peaks. As titration proceeds, the magnitude of this disturbance was the same after each injection, since the peak intensity remains constant.

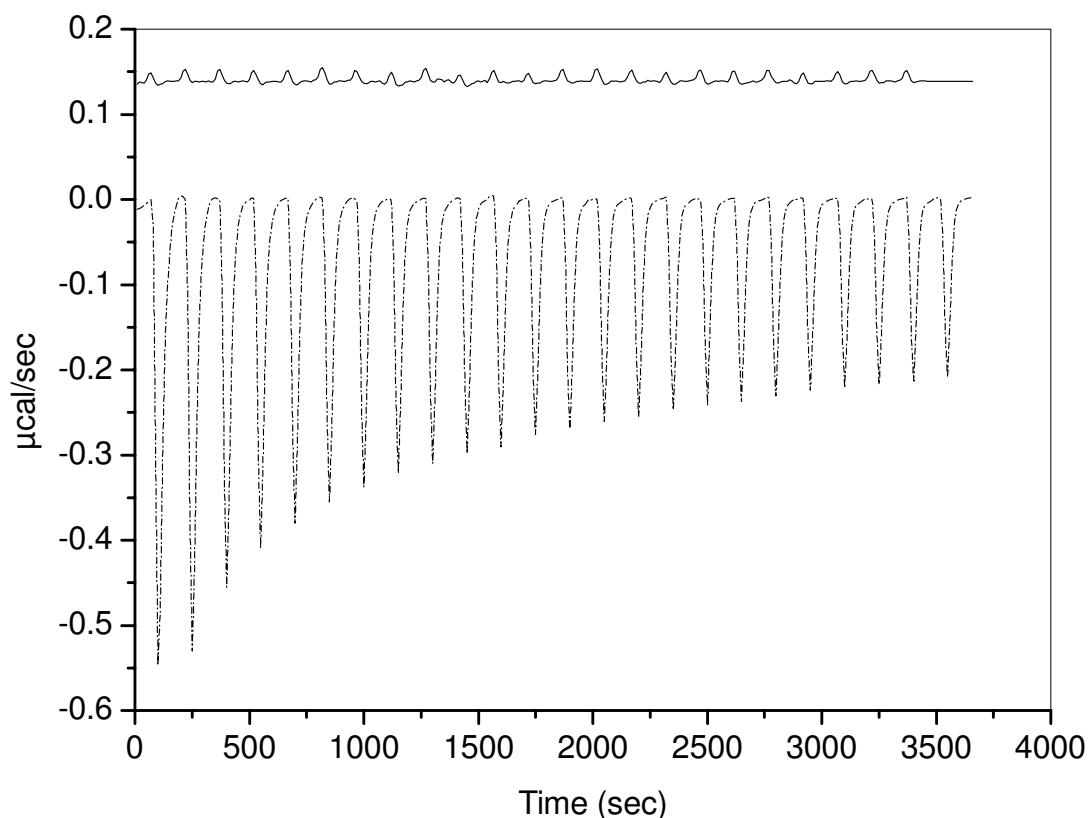


**Fig. II.1.** Microcalorimetric titration thermogram for the dilution of total Acacia gum (1.8 wt %) into water (...) and (—) water into  $\beta$ -lactoglobulin (0.6 wt %), at pH 4.2 and 25 °C. Each experiment was made in triplicate.

The dilution heat of the total Acacia gum was not affected by the increase of temperature (result not shown). However, heating BLG dispersion showed changes in its dilution heat. To better understand these thermodynamic properties of BLG, further experiments were made at temperatures of 25, 35, 40, 50 and 60 °C. Fig. II.2 shows a regular increase of the peak intensity with increasing temperature. The increase of temperature involves intra- and molecular changes of BLG<sup>25</sup>. This can lead to a transient and continuous aggregation of BLG. In addition, the number of BLG aggregates increases and then their affinity to water molecules decreases with increasing temperature. This feature is attributed to the formation of hydrophobic bonds, which is an endothermic phenomenon that can explain the increase of peak intensities.

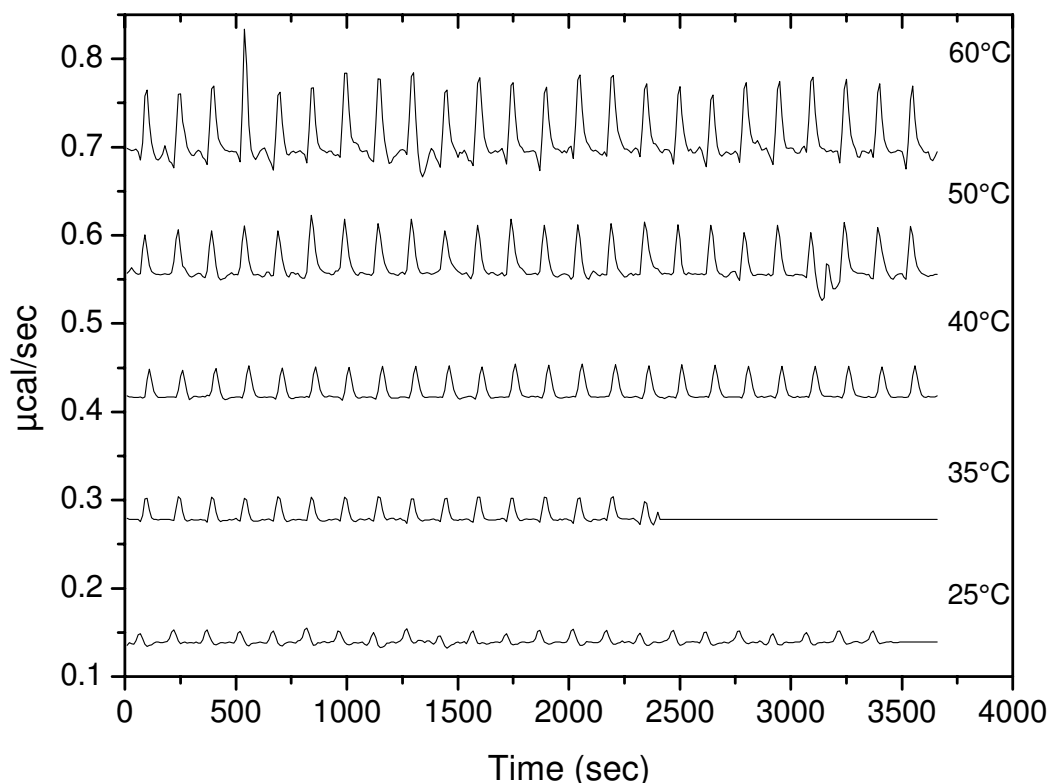


**Fig. II.2.** Thermograms corresponding to the titration of water into an aqueous dispersion  $\beta$ -lactoglobulin (0.6 wt %) at pH 4.2 and at different temperatures. Each experiment was made in duplicate.

Fig. II.3 shows the heat flow versus time and the corresponding binding isotherms resulting from injections of aliquots of TAG (BLG/TAG), FI (BLG/FI) or FII (BLG/FII) dispersion into BLG dispersion. Also, a mixture of FI and FII dispersions was made in order to reconstitute the total acacia gum, and it was similarly titrated into BLG (BLG/FI+FII mixture). The same titration curve as in the case of BLG/TAG was obtained (results not shown). For all curves, a sequence of relatively large exothermic peaks with constant released energy was initially observed. The constant energy may indicate that the binding sites occupied at each injection are similar and allow then the same released heat. Raw results show higher  $\mu\text{cal}$  range of the heat exchange as compared to raw results of BLG and TAG controls (Fig. II.1). As the titration proceeded, the released binding energy progressively decreased and then reversed. The high intensity of exothermic peaks can be attributed to binding of BLG to AG molecules. A second sequence of weaker endothermic peaks appeared (positive  $\Delta H$ ). The free energy once more reversed and a last sequence of weaker exothermic peaks reached the dilution heats of TAG in the absence of BLG (control), and tended to a state of thermodynamic stability toward the end of injections. In all cases, the titration curves

showed three inflection points. The first point (P1) was observed at the decrease of released energy, the second point (P2) appeared at the opposition of the reaction heat from exothermic to endothermic and the last one (P3) occurred at the onset of the curve stabilization.

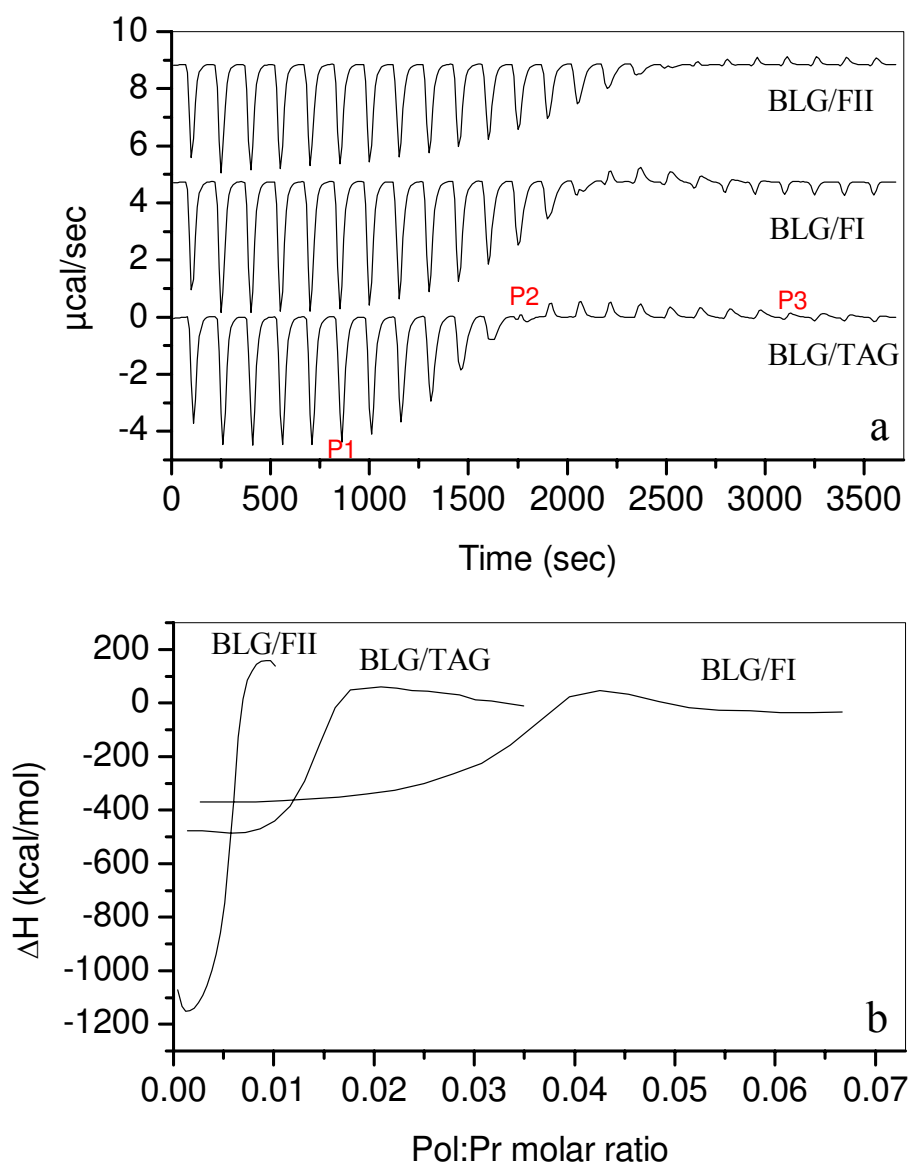


**Fig. II.3. (a)** Thermogram corresponding to the titration of an aqueous dispersion of total Acacia gum (1.8 wt %) or arabinogalactan-peptide fraction (FI) (1.8 wt %) or arabinogalactan-protein fraction (FII) (1.8 wt %) into an aqueous dispersion of  $\beta$ -lactoglobulin (0.6 wt %) at pH 4.2 and 25 °C. **(b)** Binding isotherm corresponding to the previous titration experiment. P1, P2 and P3 correspond to three transition points observed in binding isotherms. The experiments were made in duplicate.

Experiments indicate that complexation is mainly induced by enthalpy variations due to the major contribution of exothermic stage in the titration curves. de Kruif *et al.* (2001) reported that the decrease of Gibbs free energy during complex coacervation is accompanied by changes of either enthalpy or entropy or both. A release of counterions upon interaction

between unlike charged polymers increases the entropy of mixing, which can become the driving force for phase separation depending on the type of polymer<sup>26</sup>. Hence, the decrease of the released energy (at P1) could be attributed to the compensation of enthalpy by different entropic effects. Amongst these entropic contributions, there are the biopolymer structural changes, release of counterions and water molecules in the vicinity of binding sites<sup>27,28</sup>.

The associative phase separation process was studied in a number of systems such as polyelectrolyte/surfactant and biopolymer/surfactant systems. Studies have attributed the reversing of the binding heat (at P2) to changes in intermolecular forces of interactions, presence of a network of interpolymeric complexes, changes in conformation and aggregation of biopolymer<sup>24,29,31-43</sup>. From there, we suggest that the changes in enthalpy at the second endothermic stage of curves might be due to the aggregation of complexes or due to conformational changes of gum molecules and/ or BLG<sup>21,30</sup>. Mekhloufi *et al.* (2005) detected conformational changes of BLG during pH-induced complex coacervation of BLG and AG using circular dichroism (CD). Furthermore, it may be expected that condensation of aggregates arises at this stage, in parallel with liberation of water molecules from particles. This might produce hydrogen bonding breakage and lead to the appearance of endothermic peaks<sup>31,32</sup>.

Curve fitting of the binding isotherms of BLG/TAG, BLG/FI and BLG/FII systems with the Microcal Origin software was done to calculate the site binding model giving the best fit to the experimental data (minimization of  $\chi^2$ ) after subtraction of the heat of dilution. A non-linear least squares algorithm was used to provide the best fit values of the binding stoichiometry of complexes (N), the binding constant (K), the enthalpy, the entropy and the Gibbs free energy. Unfortunately, the shape of the binding curves precluded the fit of experimental data to any existing model, because of the exothermic-endothermic-exothermic alternative sequences occurring during titration of BLG by AG or FI or FII molecules<sup>33,34</sup>. Since the evolution of  $\Delta H_{\text{obs}}$  exhibits this unexpected behavior, only the association constant and binding parameters of the first exothermic contribution (first stage of the curve) were determined by fitting the binding isotherms of experiments with the one set of site ITC model. The fitting results are listed in Tab. II.2 and they will be analyzed in the next sections. We note that BLG/FI system exhibit both lower strength of interaction (lower enthalpy) and lower binding entropy than BLG/FII system. In addition, higher stoichiometry of association



between BLG and FI is shown.

**Tab. II.2.** Binding parameters of interaction between  $\beta$ -lactoglobulin and Acacia gum molecular fractions obtained from the titration of an aqueous dispersion of AG (1.8 wt %) into an aqueous dispersion of  $\beta$ -lactoglobulin (0.6 wt %) at 25 °C and pH 4.2. N: stoichiometry, K: binding constant,  $\Delta H_{\text{exo}}$ : binding enthalpy,  $\Delta S_{\text{exo}}$ : binding entropy and  $\Delta G_{\text{exo}}$ : free Gibbs energy of binding. exo: exothermic peaks. Parameters were calculated for the first exothermic stage in the titration curves.

pH	Mixture	N (Pol:Pr molar ratio)	N (Pr:Pol charge ratio)	K	$\Delta H_{\text{exo}}$ (kcal/mol)	$\Delta S_{\text{exo}}$ (kcal/mol.°K)	$\Delta G_{\text{exo}}$ (kcal/mol)
4.2	BLG/TAG	0.013	3.15	1.8E+05	-479.0	-1.5	-41.0
	BLG/FI	0.029	2.42	8.3E+04	-374.7	-1.1	-58.0
	BLG/FII	0.004	2.34	8.8E+05	-1246.1	-3.7	-155.4
	BLG/FI+FII	0.014	2.84	1.4E+05	-481.4	-1.4	-58.3

### II.3.2. Ratio-induced structural transitions during complexation between BLG and AG

Before reporting the role of TAG molecular fractions in the binding properties with BLG, we focus on a discussion on the structural transitions observed during titration. The protein:polysaccharide charge ratios (Pr:Pol) between BLG and AG at each injection were calculated using the corresponding value of the biopolymer charge at a given pH (Tab. II.3). The charge evolution of TAG, FI and FII with pH was taken from Renard *et al.* (2006). The authors determined the number of charges of AG from biochemical composition (glucuronic acid residues, GlcUA) and titration measurements (GlcUA + charged amino acids). The charge evolution of BLG was calculated from Cannan *et al.* (1941)<sup>35</sup> based on a three order polynomial equation. From these values, we calculated the Pr:Pol ratio and multiplied the result by the Pr:Pol molar ratio in order to determine the Pr:Pol charge ratio.

**Tab. II.3.** Number of charges in BLG, TAG, FI and FII dispersions at different pH values, determined by titration measurements (Renard *et al.*, 2006) or calculated (Cannan *et al.*, 1941).

pH	Number of charges			
	TAG	FI	FII	BLG
4.5	-292.8	-187.3	-1239.4	+7.5
4.2	-264.5	-161.6	-1220.4	+10.9
3.8	-204.7	-114.1	-1166.4	+15.7

From there, the titration curves were represented as a function of Pr:Pol charge ratio. The binding isotherms of mixtures (Fig. II.4) can be then divided into three zones based on the intersection point of two tangents to the curve and also on the inversion of the reaction heat.

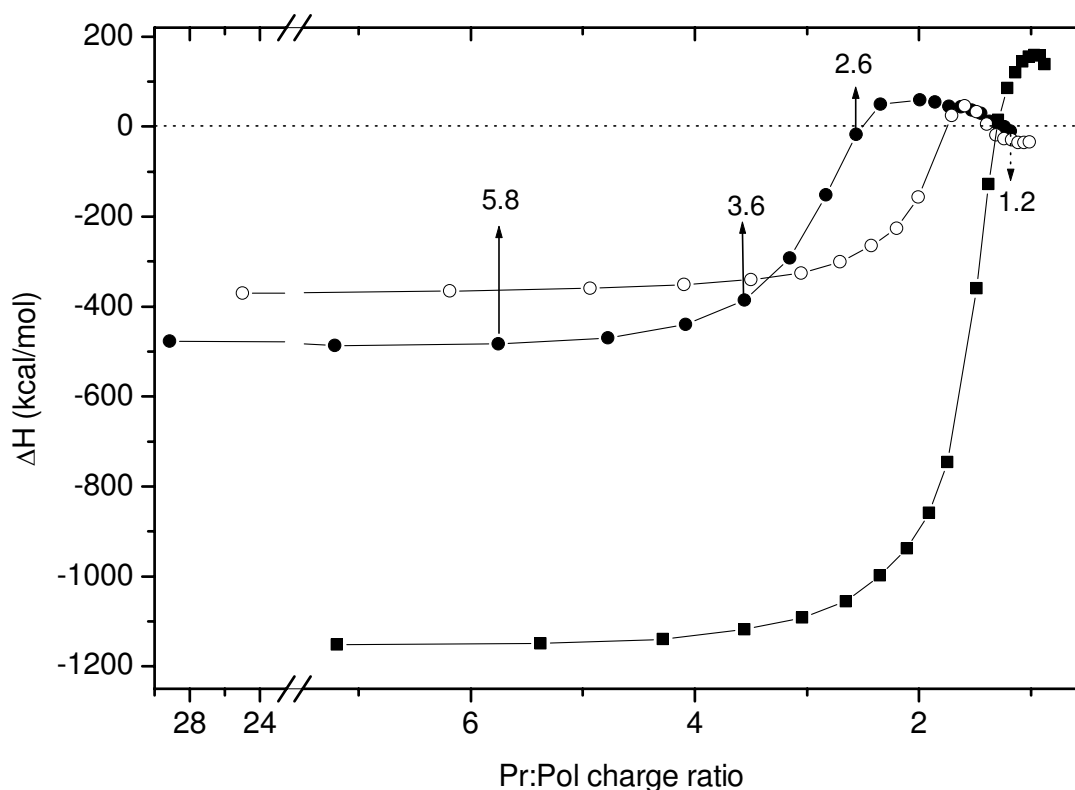


**Fig. II.4.** Binding isotherm derived from the titration of an aqueous dispersion of Acacia gum into an aqueous dispersion of  $\beta$ -lactoglobulin (0.6 wt %) at pH 4.2 and 25 °C. (●) titration of total Acacia gum (1.8 wt %) into  $\beta$ -lactoglobulin, (○) titration of FI fraction (1.8 wt %) into  $\beta$ -lactoglobulin and (■) titration of FII fraction (1.8 wt %) into  $\beta$ -lactoglobulin. Dotted line is guide for eyes. Each experiment was made in triplicate.

We first show the structural transitions in all binding isotherms and then discuss the shift of these zones by comparing the curves of all systems:

*Pr:Pol charge ratio  $\geq 5.0:1$* : the released energy remained constant until the Pr:Pol charge ratios of  $\sim 5.8:1$ ,  $5.0:1$  and  $5.4:1$  in BLG/TAG, BLG/FI and BLG/FII systems, respectively. This phase reflects strong complexation upon the first injection. It is mainly due to electrostatic interactions.

*Pr:Pol charge ratio comprised between  $5.0:1$  and  $3.0:1$* : at this stage, enthalpy slightly decreased until the Pr:Pol of  $3.6:1$ ,  $3.1:1$  and  $3.0:1$  in BLG/TAG, BLG/FI and BLG/FII systems, respectively.

*Pr:Pol charge ratio comprised between  $3.0:1$  and  $1.4:1$* : at this stage, enthalpy strongly

decreased until the Pr:Pol of 2.6:1, 2.0:1 and 1.4:1 in BLG/TAG, BLG/FI and BLG/FII systems, respectively. At these ratios, the sign of the released energy ( $\Delta H_{\text{exo}}$ ) is reserved from negative to positive (from exothermic to endothermic). It was expected that the decrease of  $\Delta H$  is due to enthalpy/entropy compensation at this ratio range. From there, we define these ratios as the onset of equilibrium between enthalpy and entropy changes ( $r_{\text{eq}}$ ).

*Pr:Pol charge ratio comprised between 1.4:1 and 0.9:1:*, the absorbed energy ( $\Delta H_{\text{endo}}$ ) decreased until reversing at 1.9:1 in BLG/TAG, 1.6:1 in BLG/FI and 1.0:1 in BLG/FII system. From these values, the enthalpy of reaction remained constant and became null at 1.2:1, 1.3:1 and 0.9:1 in BLG/TAG, BLG/FI and BLG/FII systems, respectively. These ratios of  $\sim 1:1$  reflect the existence of a stoichiometric electrical charge equivalence, where molecules carry equal but opposite charges and BLG-AG interactions are at their maximum. These ratios would correspond to the ratios of saturation of binding sites ( $r_{\text{sat}}$ ).

### **II.3.3. Thermodynamic contribution of individual molecular fraction of TAG in interactions with BLG**

All systems showed the same  $\Delta H_{\text{obs}}$  curve shape with Pr:Pol charge ratio. However, a shift of curves was observed, which characterizes the different thermodynamics of interaction of systems. Some differences in the area of peaks, magnitude of energy of interactions and structural transitions appeared between the binding curves corresponding to BLG/TAG, BLG/FI and BLG/FII systems. Fig. II.4 revealed lower Pr:Pol charge ratios of structural transitions and then lower stoichiometry of association (see Tab. II.2) in BLG/FII dispersions, with reflects favorable complexation. FII has higher number of charges as compared to TAG and FI. This implies higher number of binding sites, which requires higher amount of protein (i.e. higher Pr:Pol charge ratio) to be saturated. Nevertheless, the Pr:Pol ratios of structural transitions were shifted towards lower values in BLG/FII system. This feature might be due to the higher accessibility of charges of FII that is an entropic factor that favors complexation. This higher accessibility may result from the un-known structural properties of FII (e.g. flexibility, large specific surface, etc) and its charge density. Sanchez *et al.* (results not published) investigated the structure of FI and FII based on small angle neutron scattering (SANS) measurements. They showed that FI consists of a disk with a diameter of 20 nm and FII corresponds to an ellipsoid with 15 (a) and 50 (b) nm dimensions. We taken these values

and then estimated the surface charge densities of FI and FII at pH 4.2, which correspond to the amount of electric charge per unit surface. The total charge in a surface is then given by the following equation:

$$\sigma = Q/2S \quad \text{Eq. II.3}$$

Where  $\sigma$  is the surface charge density,  $Q$  is the charge number and  $S$  is the surface of the macromolecule. The 2 number is considering the two faces of the surface.  $S$  corresponds to  $\pi r^2$  for FI and  $\pi.a.b$  for FII. Generally,  $Q$  is the sum of charges and would correspond to the total charge value multiplied by the number of charges. The ill-known structures of AG molecules do not permit to calculate the real value of  $Q$ . Thus, we note that this calculus is simply an approximation to estimate the distribution of charges on the surface for each AG molecular fraction. We found 0.07 charges/nm<sup>2</sup> for FI and 0.26 charges/nm<sup>2</sup> for FII. This feature may indicate the presence of a higher charge density for FII, which favors complexation and explain then the lower stoichiometry of association.

Optical density measurements (O.D.) were made according to the titration procedure of ITC experiments, i.e. O.D. was followed during titration of BLG dispersion (in the spectrophotometer cell) by AG dispersion every 150 sec for 24 injections of 10  $\mu$ l. The goal of this experiment was to compare the profile of O.D. to the binding isotherm to give more information about the binding transition points. Fig. II.5 shows the O.D. evolution during complexation in BLG/TAG, BLG/FI and BLG/FII mixtures. All systems display a maximum of O.D. between two opposite ranges and a similar O.D. curve shape with pH. Firstly, O.D. increased suddenly until the Pr:Pol charge ratio of 5.8:1, 4.9:1 and 6.2:1 in BLG/TAG, BLG/FI and BLG/FII systems, respectively. From these ratios, O.D. becomes relatively constant. This range of constant O.D. values (at a constant optical index) can be explained in the following manner: *i*) the particle size increases and the volume fraction of objects remains constant, this fact is not very probable since the neutralization of binding sites proceeds at this range as shown in the binding curves; *ii*) the particle size increases and the volume fraction decreases, indicating a decrease in the concentration of objects in dispersion, in relation with particles dissociation; *iii*) the particle size decreases and the volume fraction of objects increases, which may indicate that certain objects disappear and others appear upon complexation. These hypotheses will be clarified in the next chapters. The ratio values of 5.8:1, 4.9:1 and 6.2:1 can be related to 5.8:1, 5.0:1 and 5.4:1 shown in ITC binding curves.

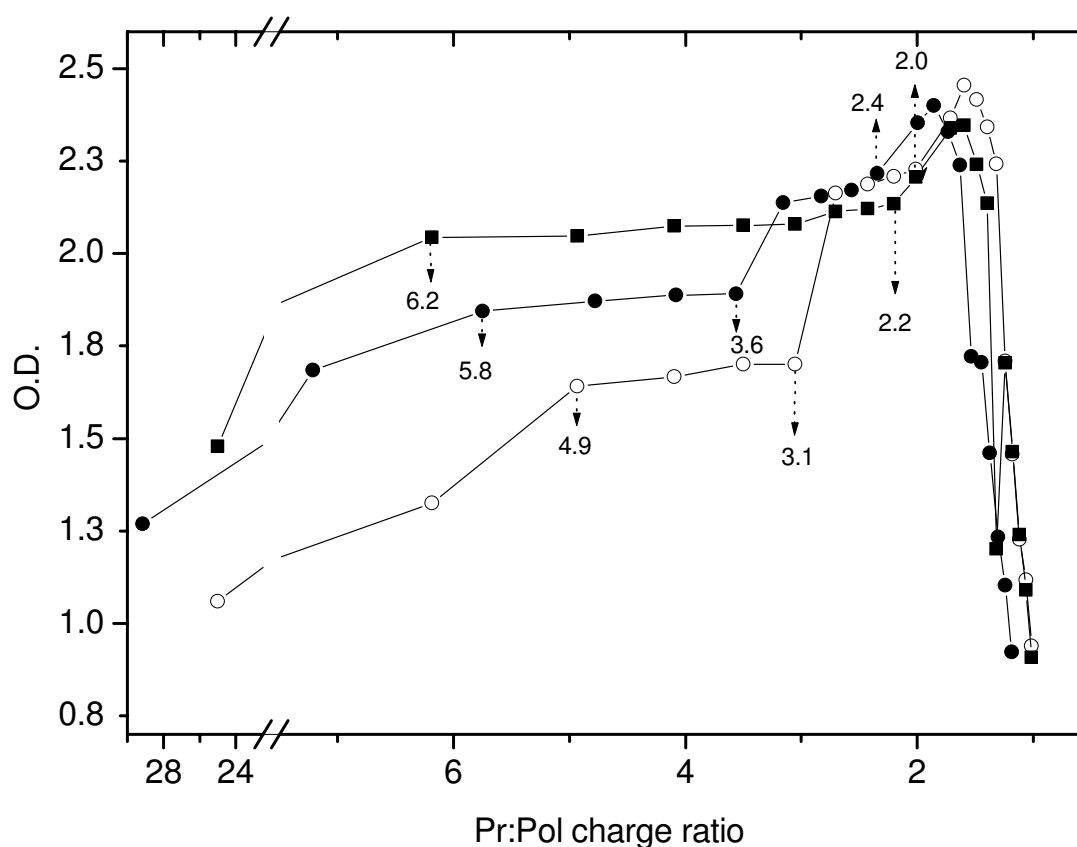


**Fig. II.5.** Evolution of the Optical Density (O.D.) as a function of Pr:Pol charge ratio during the titration of an aqueous dispersion of Acacia gum (1.8 wt %) into an aqueous dispersion of  $\beta$ -lactoglobulin (0.6 wt %) at pH 4.2 and 25 °C. (●) titration of total Acacia gum (1.8 wt %) into  $\beta$ -lactoglobulin, (○) titration of FI fraction (1.8 wt %) into  $\beta$ -lactoglobulin and (■) titration of FII fraction (1.8 wt %) into  $\beta$ -lactoglobulin. Dotted line is guide for eyes. Each experiment was made in triplicate.

On the basis of the last hypotheses and regarding the decrease of the binding strength from these ratio values, they may correspond to the aggregation of complexes ( $r_{agg}$ ). O.D. then increased markedly at a Pr:Pol charge ratio of 3.6:1 in BLG/TAG, 3.1 in BLG/FI and 2.2:1 in BLG/FII system. These ratios would correspond to the initiation of the stoichiometry of association in dispersions (stoichiometry: 3.15:1, 2.42:1 and 2.34:1 in Tab. II.2). From the Pr:Pol charge ratios of 2.4:1, 2.0:1 and 2.2:1 in BLG/TAG, BLG/FI and BLG/FII systems, O.D. increased strongly until reaching a maximum at 1.85:1 in BLG/TAG and 1.59:1 in BLG/FI and BLG/FII systems. These values agree with those shown by ITC where the  $\Delta H_{endo}$  decreased and they would correspond to a maximum number or size of particles present in dispersions, in agreement with a maximum of strength of interaction. Below the maximum, O.D. decreases strongly, which might be due to the decrease of size or volume fraction of particles. From there, four Pr:Pol charge ratios of structural transitions can be defined based on ITC and O.D. measurements:  $r_{agg}$ , the charge ratio of aggregation of complexes;  $r_{isto}$ , the

charge ratio of stoichiometry initiation;  $r_{eq}$ , the charge ratio of enthalpy/entropy equilibrium and  $r_{sat}$ , the charge ratio of maximum of interaction strength that would correspond to the ratio of saturation of binding sites determined from ITC binding curves.

Presumably, TAG has an intermediate thermodynamic role between FI and FII because it contains the two components. For each molecular fraction, we multiplied its weight percentage (88.5 wt% for FI and 10.5 wt% for FII) in the whole gum by its binding enthalpy shown in Tab.II.2. From there, the sum of these two values was calculated and compared to the binding enthalpy of BLG/TAG system determined in Tab. II.2. The same values were obtained at all pH conditions, which indicate that the binding parameters of BLG/TAG system are the sum of those of BLG/FI and BLG/FII systems. The different thermodynamic behaviors between FI and FII can be explained based on different studies. On the theoretical basis of the Flory-Huggins approximation for ternary systems (see chapter I), Katalin *et al.* (2004) showed that changes in the chemical structure cause changes in the value of segment-solvent pair interaction parameters, this lead to changes in interaction behaviors of mixtures<sup>36</sup>. This feature can be related to the different protein-to-sugar ratios in the AG molecular fractions. Velazquez *et al.* (2004) proved that small modifications in structure (e.g. chemical composition, molecular weight, conformational changes) of interacting macromolecules might generate significant changes in thermodynamic parameters. These effects correspond to the different charge densities, molecular weights and radius of gyration between the molecular fractions of TAG. Radius of gyration of TAG, FI and FII are respectively 11.8, 11.3 and 30 nm. Miura *et al.* (1999)<sup>37</sup> suggested that larger radius macromolecule might favor binding due to an entropy decrease, which can explain the faster complexation in BLG/FII system. Furthermore, FII has higher molecular weight than FI (Renard *et al.*, 2006). An increase of this intrinsic parameter lead to the decrease of mixing entropy and enhance then the ability of macromolecules to form a complex<sup>38</sup>. The highest binding strength determined in this case is due to the higher number of charged groups (uronic acids and charged amino acids residues) of FII that leads to a higher released energy.

#### **II.3.4. Parameters influencing the thermodynamic characteristics of the different BLG/AG systems**

In order to better define the binding characteristics of BLG and Acacia gum molecular

fractions, the influence of solution conditions such as pH, temperature, and biopolymer concentration was needed to understand the factors affecting the nature and strength of protein-polysaccharide interactions. The effect of these three parameters on the thermodynamic aspects of BLG/TAG, BLG/FI and BLG/FII interactions was studied.

### II.3.4.1. Initial concentration of AG

The effect of AG concentration was only studied in BLG/TAG system. For this, we show in the following solely results obtained for BLG/TAG system. In a first sequence of experiments, we changed the initial concentration of TAG between experiments in order to better understand what happened in the endothermic stage of the binding isotherms. This is because of the increase of TAG concentration can lead to earlier saturation of binding sites and then to a gain in the number of endothermic peaks against the exothermic ones. Four experiments were made with a number of ratios of concentration in the syringe to concentration in the measuring cell (ratio =  $[AG]_{\text{initial}} / [BLG]_{\text{initial}}$ , initial: before injections): 3, 4, 5 and 10. Fig. II.6 shows the effect of the initial concentration of Acacia gum on the binding isotherm with BLG at pH 4.2.

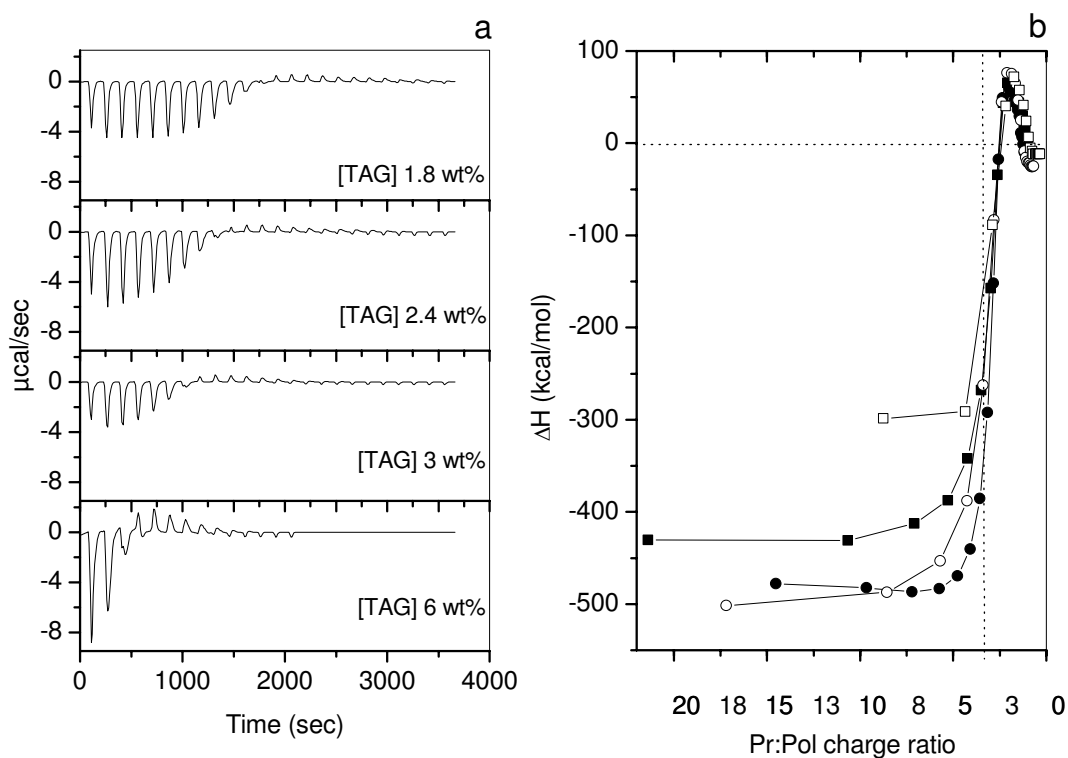


**Fig. II.6.** (a) Thermograms corresponding to the titration of an aqueous dispersion of Acacia gum into an aqueous dispersion of  $\beta$ -lactoglobulin (0.6 wt %) at different concentrations for Acacia gum at pH 4.2 and 25 °C. (b) Binding isotherm corresponding to the previous titration experiments. (●) 1.8 wt %, (○) 2.4 wt %, (■) 3 wt % and (□) 6 wt %. Dotted line is guide for eyes. Each experiment was made in duplicate.

An increase of AG concentration led to a continuous decrease of the number of first exothermic peaks, and to an increase of the number of endothermic ones. Thus, a shift in the structural transitions towards lower time values was observed. This result reveals faster saturation of binding sites due to the increase of AG amounts at each injection. It was also shown an increase of the intensity of endothermic peaks with increasing the AG concentration. It must be noticed that the Pr:Pol charge ratio of 3.7:1 can divide the binding curves into two zones at all concentration conditions. In the first zone, enthalpy of association and stoichiometry change with the Pr:Pol charge ratio; whereas, in the second one binding curves are approximately the same and then binding parameters remained constant. It was suggested that the neutralization of binding sites arises at a Pr:Pol charge ratio of ~1:1. Generally, complex coacervation in BLG/AG dispersion requires neutrality to occur. Therefore, it may be expected that complex coacervation in all BL/AG systems takes place at the Pr:Pol charge ratio of 1:1. Regarding the two zones of  $\Delta H$  evolution with AG concentration, we suggest that the initial concentration of AG and then the initial Pr:Pol ratio affect the complexation between biopolymers and not the phase separation.

The influence of the biopolymer concentration on phase separation is not extensively reported in the literature, and it depends on the polyelectrolyte. Indeed, above a critical amount of biopolymers, the efficiency of coacervation decreases and may be suppressed. As increasing AG concentration modify the total biopolymer concentration and Pr:Pol mixing ratio at each injection, its influence is considered as a mass action effect<sup>4,39</sup>. The increase of polysaccharide concentration is likely to induce steric hindrance, which might favor the self association of biopolymers (i.e. at lower stoichiometry), in relation with an entropy decrease<sup>40</sup>. These steric effects can also decrease the Brownian motion of particles and favors thus weak interactions than electrostatic, which can be the reason of the decrease of binding strength<sup>41</sup>.

#### **II.3.4.2. pH**

The strength of complexation in protein-polysaccharide mixtures is largely influenced by the net electrical charge on individual biopolymer that is directly depending on the pH of dispersion. Therefore, in order to better understand the binding characteristics of the different BLG/AG blends, the effect of pH was investigated.



Since all systems displayed similar evolution of thermodynamic parameters as a function of pH, we show solely the binding curves for BLG/TAG and then we discuss differences between systems. The ability of interactions of BLG and TAG with changing pH is illustrated in Fig. II.7. At all pH values, two main series of peaks appeared: a large sequence of sharp exothermic peaks and a second sequence of relatively weaker endothermic-exothermic peaks. From the beginning of titration until the sixth injection, the exothermic sequence displayed constant peak intensities at pH 4.2. However, from the third injection, the peak intensity markedly decreased at the other pH values. Thus, a gain in the number of endothermic peaks against the exothermic ones was observed with increasing pH. It must be noticed that this decrease in intensity revealed more remarkable at pH 4.5. Changes in the strength of interactions were observed. The electrostatic binding enthalpy ( $\Delta H_{\text{exo}}$ ) decreased with increasing pH and displayed a maximum value at pH 4.2. The increase of pH led to the shift of all structural transitions to lower time values, in agreement with a complexation at lower stoichiometry of association. The charge densities of BLG and AG decrease with increasing the pH, which allow lower initial Pr:Pol charge ratio. Therefore, the saturation of binding sites of TAG bears lower amount of BLG charges to occur i.e. lower stoichiometry of association.

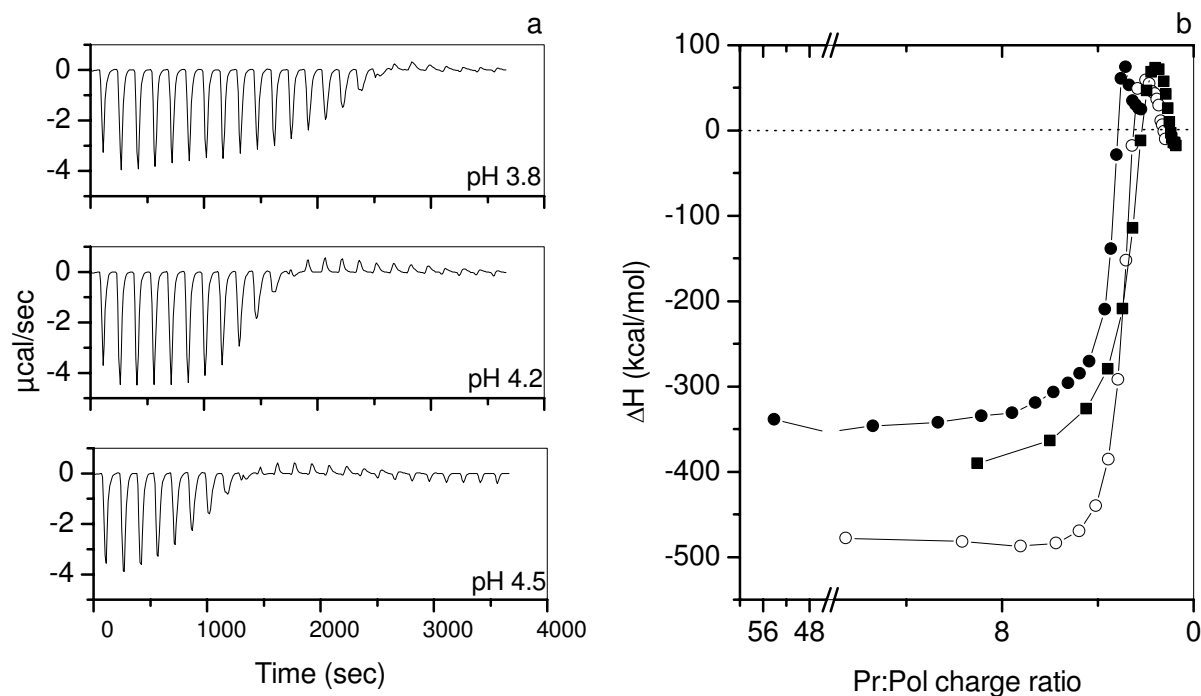


**Fig. II.7.** (a) Thermograms corresponding to the titration of an aqueous dispersion of Acacia gum (1.8 wt %) into an aqueous dispersion of  $\beta$ -lactoglobulin (0.6 wt %) at 25 °C and different pH. (b) Binding isotherm corresponding to the previous titration experiments. (●) pH 3.8, (○) pH 4.2 and (■) pH 4.5. Dotted line is guide for eyes. Each experiment was made in duplicate.

Tab. II.4 shows the thermodynamic binding parameters of systems studied at different pH, calculated for the first exothermic sequence of the binding isotherms with the one set of binding sites model. All dispersions showed the same evolution of parameters with pH. Thus, increasing pH allows complexation with lower stoichiometry. At all pH values, higher enthalpy of association was determined in BLG/FII system, indicating stronger interaction between BLG and FII. This could result from the higher number of charges of FII that would release higher energy upon association.

**Tab. II.4.** Binding parameters of interaction between  $\beta$ -lactoglobulin and Acacia gum molecular fractions obtained from the titration of an aqueous dispersion of AG (1.8 wt %) into an aqueous dispersion of  $\beta$ -lactoglobulin (0.6 wt %) at 25 °C. N: stoichiometry, K: binding constant,  $\Delta H_{\text{exo}}$ : binding enthalpy,  $\Delta S_{\text{exo}}$ : binding entropy and  $\Delta G_{\text{exo}}$ : free Gibbs energy of binding. exo: exothermic peaks. Parameters were calculated for the first exothermic stage in the titration curves.

pH	Mixture	N (Pol:Pr molar ratio)	N (Pr:Pol charge ratio)	K	$\Delta H_{\text{exo}}$ (kcal/mol)	$\Delta S_{\text{exo}}$ (kcal/mol.°K)	$\Delta G_{\text{exo}}$ (kcal/mol)
3.8	BLG/TAG	0.020	3.70	1.2E+05	-357.5	-1.1	-20.7
	BLG/FI	0.036	3.47	4.4E+04	-237.1	-0.7	-20.9
	BLG/FII	0.008	2.71	7.2E+05	-1128.3	-3.3	-149.4
4.2	BLG/TAG	0.013	3.15	1.8E+05	-479.0	-1.5	-41.0
	BLG/FI	0.029	2.42	8.3E+04	-374.7	-1.1	-58.0
	BLG/FII	0.004	2.34	8.8E+05	-1246.1	-3.7	-155.4
	BLG/FI+FII	0.014	2.84	1.4E+05	-481.4	-1.4	-58.3
4.5	BLG/TAG	0.009	2.97	1.2E+05	-393.4	-1.1	-50.7
	BLG/FI	0.014	2.93	5.6E+04	-351.6	-0.8	-99.8
	BLG/FII	0.003	2.05	8.3E+05	-959.0	-2.9	-82.9

Furthermore, lower stoichiometry of association between BLG and FII was determined at all pH conditions, in agreement with the higher accessibility of FII charges for interaction as assessed above. The binding entropy in BLG/FII was higher as compared to BLG/FI system at all pH conditions. This result can be attributed to the higher chain flexibility of FII. Sanchez (results not published) determined a persistence length of 3 nm for FII, which can allow high flexibility of its macromolecular chain.

A separate experiment was made by addition of Glucono- $\delta$ -Lactone into a mixed dispersion of BLG and AG, at a fixed Pr:Pol weight ratio of 2:1 in order to slow-acidify mixtures and to study the pH-induced structural transitions in mixtures. The experiment was done in order to correlate the effect of pH on the strength of interaction and structural transitions shown by

ITC to O.D. measurements. Fig. II.8 shows the evolution of O.D. as a function of pH. The curve shows the presence of a maximum at pH of 4.23, 4.22 and 4.18 in BLG/TAG, BLG/FI and BLG/FII systems, respectively. These pH are equivalent to the Pr:Pol charge ratios of 1.15:1, 1.0:1 and 0.9:1 for BLG/TAG, BLG/FI and BLG/FII dispersions, respectively. These ratios are in agreement with the ratios of saturation of binding sites ( $r_{\text{sat}}$ ) determined from the binding isotherms (Fig. II.4) and indicate the presence of a maximum number or size of particles in dispersions.

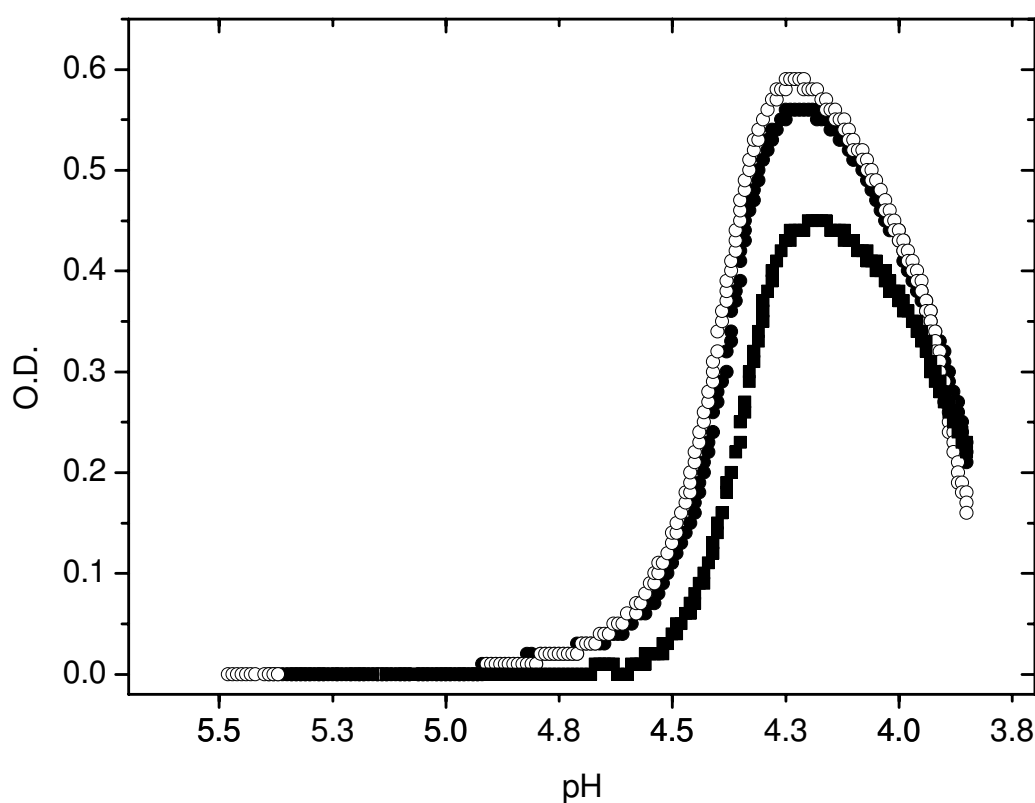


**Fig. II.8.** Evolution of the Optical Density (O.D.) at 633 nm as a function of pH for the Pr/Pol mixed dispersions at 0.1 wt % total biopolymer concentration and Pr:Pol weight ratio of 2:1. (●) BLG/TAG, (○) BLG/FI, (■) BLG/FII. Each curve is the average of three independent experiments.

The formation of protein/polysaccharide complexes is a consequence of different factors such as the flexibility and charge density of polysaccharide, the surface charge heterogeneity of the protein and the ease of unfolding of its native structure<sup>42,43,44,45,46</sup>. Complex coacervation of protein-polysaccharide mixtures is generally occurring in a pH window where the two biopolymers are oppositely charged ( $pI_{\text{Pol}} < \text{pH} < pI_{\text{Pr}}$ ). Using SALS, Mekhloufi *et al.* (2005)<sup>4</sup> and Sanchez *et al.* (2002)<sup>15</sup> showed that the maximum of interactions in BLG/AG system is occurring at pH 4.2, in agreement with ITC and O.D. results. The contribution of a protein in interactions with a polysaccharide depends largely on the solution pH that must be far from its

$pI$ . Near to  $pI_{Pr}$ , the complexation is weak and more favorably occurred than coacervation. Increasing pH reflects a decrease in the net charge on BLG and then weak interactions occur, which is in accordance with the decrease of binding strength at pH 4.5<sup>47</sup>.

### II.3.4.3. Temperature

Generally, increasing temperature generates changes in the conformation and aggregation of biopolymer and may lead to appreciable change in their functional attributes and surface activity<sup>7,22</sup>. Thermal treatment of protein-polysaccharide systems is an important factor influencing formation and stability of complexes during food processing. In the present experiment, we have studied the effect of temperature on interactions in BLG/AG systems. One of the major objectives was to check whether other weak energy interactions (e.g. hydrophobic interactions and hydrogen bonding) played a significant role in complexation between BLG and AG.

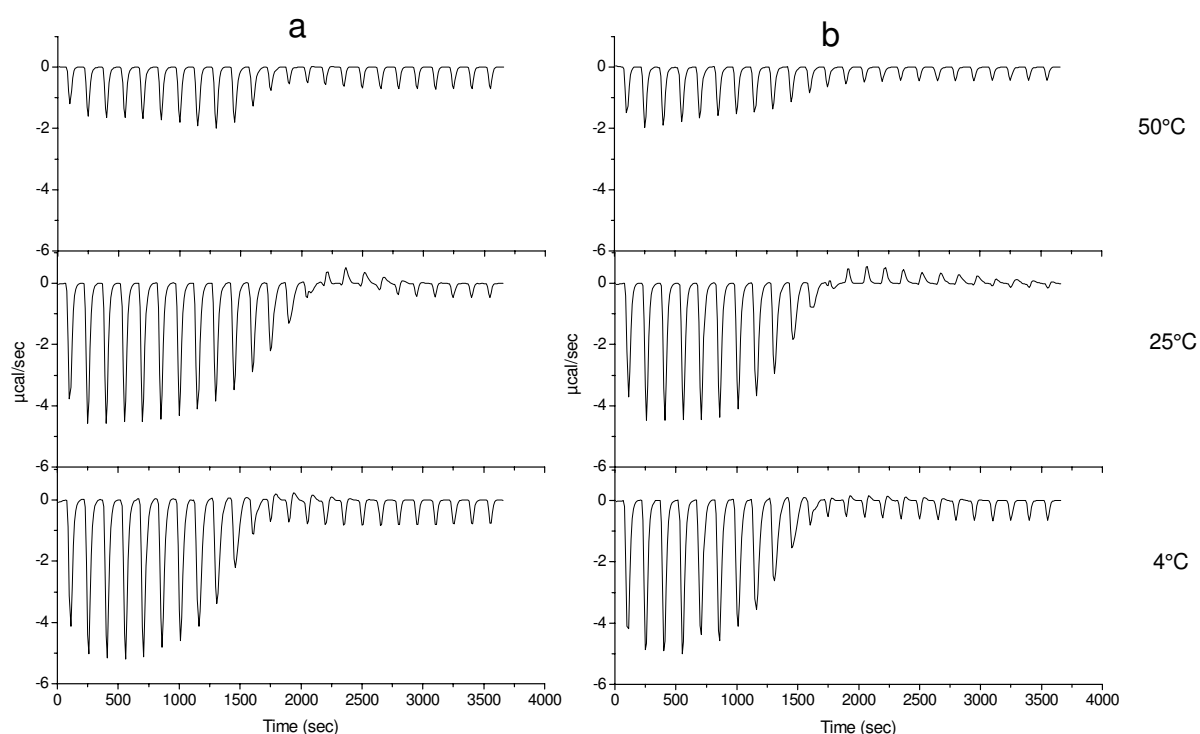


**Fig. II.9.** Thermograms corresponding to the titration of an aqueous dispersion of Acacia gum (1.8 wt %) into an aqueous dispersion of  $\beta$ -lactoglobulin (0.6 wt %) at pH 4.2 and different temperatures. (a) titration of total Acacia gum (1.8 wt %) into  $\beta$ -lactoglobulin, (b) titration of FI fraction (1.8 wt %) into  $\beta$ -lactoglobulin. Each experiment was made in duplicate.

All systems were studied at three different temperatures 4, 25 and 50°C. Similar effects of the

temperature were observed in all systems as shown in Fig. II.9 for BLG/TAG and BLG/FI dispersions. At 4 and 50°C, the titration curves reveal two zones of exothermic peaks with different intensities. On the other hand, a sequence of sharp exothermic peaks and another series of weaker endothermic-exothermic peaks appeared at 25°C.

It can be observed in Fig. II.9 and Fig. II.10 that heating BLG and TAG at pH 4.2 induced a clear decrease of the intensity of exothermic peaks. Consequently, the apparent binding enthalpy decreased, in agreement with lower strength of interaction between BLG and AG. In parallel, the endothermic peak disappeared at the temperature of 4°C and with increasing temperature from 35°C. The disappearance of the second endothermic step from binding curves may be due to the decrease of binding strength, in relation with less complexation extent.

Some works suggested that many types of interaction such as hydrogen bonding and van der Waals interactions could be associated (included) to the negative values of enthalpy and entropy of binding<sup>48</sup>. On this basis, we suggest that the exothermic step in the binding curve contains, in addition to the electrostatic interactions, the contribution of hydrogen bonding. Thus, the decrease of strength of interaction and the disappearance of endothermic peaks can be attributed to hydrogen bonds breakage. This feature can be present in our systems because the electrostatic interactions are significant and their energetic contribution is likely to mask the other interaction forces. From these results, it is likely that hydrogen bonding, enhanced at low temperatures, play a role in the complexation between BLG and AG. On the other hand, hydrophobic interactions, enhanced at high temperature, seem not to have significant contribution in the complexation.

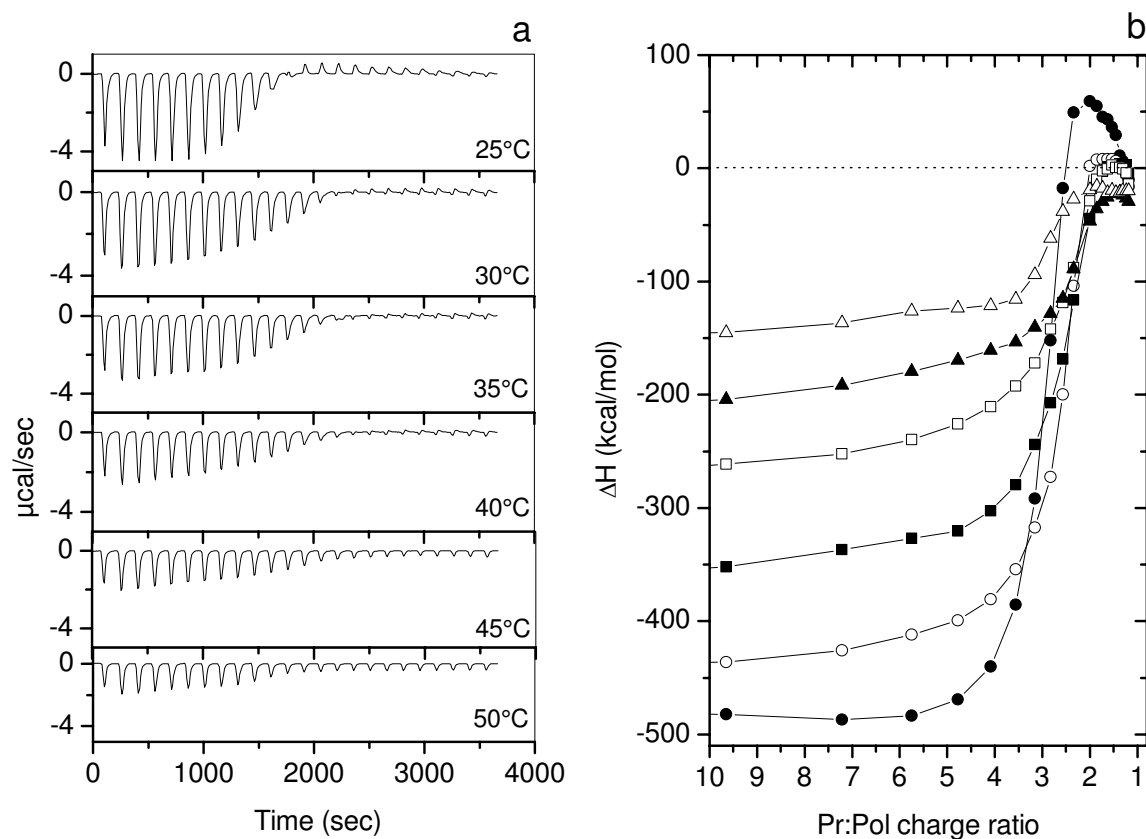


**Fig. II.10.** (a) Thermograms corresponding to the titration of an aqueous dispersion of Acacia gum (1.8 wt %) into an aqueous dispersion of  $\beta$ -lactoglobulin (0.6 wt %) at pH 4.2 and different temperatures. (b) Binding isotherm corresponding to the previous titration experiments. (●) 25°C, (○) 30 °C, (■) 35 °C, (□) 40 °C, (▲) 45 °C and (△) 50 °C. Dotted line is guide for eyes. Each experiment was made in duplicate.

Furthermore, the first constant exothermic sequence of binding curves gradually disappeared with increasing temperature. To better highlight the effect of temperature on the binding isotherms, we plotted in Fig. II.11 the evolution of the first transition point ( $r_{\text{agg}}$ ), from which the released energy was not constant, as a function of temperature for BLG/TAG system. The trend of evolution shows an increase of this ratio until the temperature of 35°C. From this temperature, the ratio of aggregation remained constant. Results reveal then the complexation with a lower number of injections, i.e. at lower stoichiometry, in agreement with the formation of protein aggregates during heating, which favors complexation<sup>4,23</sup>. Moreover, the temperature seems to not affect the stoichiometry of association; whereas, it influence the binding strength.

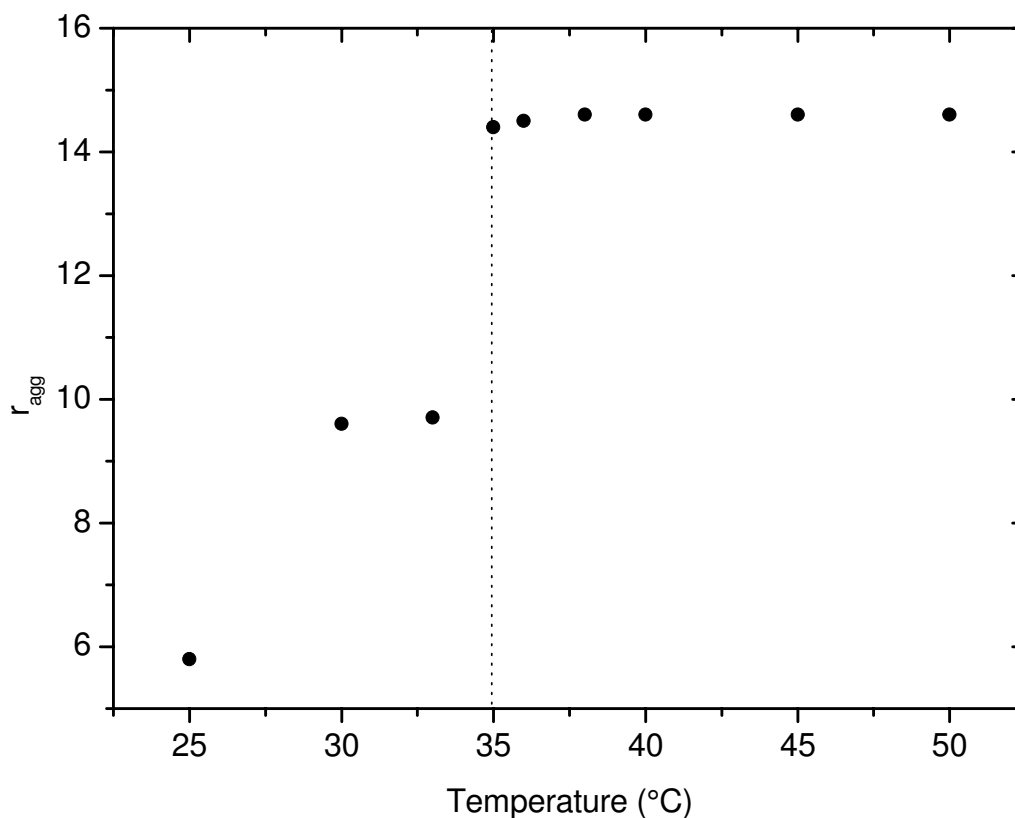


**Fig. II.11.** Evolution of the ratio of complex aggregation ( $r_{agg}$ ) as a function of temperature during the titration of an aqueous dispersion of total Acacia gum (1.8 wt %) into an aqueous dispersion of  $\beta$ -lactoglobulin (0.6 wt %) at pH 4.2 and different temperatures. Dotted line is guide for eyes. Each experiment was made in duplicate.

The heat capacity changes ( $\Delta C_p$ ) is a key thermal parameter allowing the determination of all relevant thermodynamic parameters (as shown in Eq.II.3 and Eq.II.4). Its effect is remarkable in a system comprising multiple, weak, intermolecular forces<sup>49</sup>. It is generally attributed to the peculiar properties of solvent water. For this, it is determined in order to better understand the influence of temperature on the thermodynamics of interactions.

$$\Delta H = \int_0^T \Delta C_p \cdot dT \quad \text{Eq. II.4}$$

$$\Delta S = \int_0^T (\Delta C_p / T) \cdot dT \quad \text{Eq. II.5}$$

Fig. II.12 shows a linear decrease of  $|\Delta H_{exo}|$  with increasing temperature. A  $\Delta C_p$  of 13.51 kcal.mol<sup>-1</sup>.°C<sup>-1</sup> was determined. This high positive value of  $\Delta C_p$  indicates that complex formation is accompanied by the disappearance of hydrophilic groups, exposed to the solvent with increasing temperature<sup>50</sup>. This feature may indicate a breakage of hydrogen bonds with

heating and neglect the role of hydrophobic interactions.

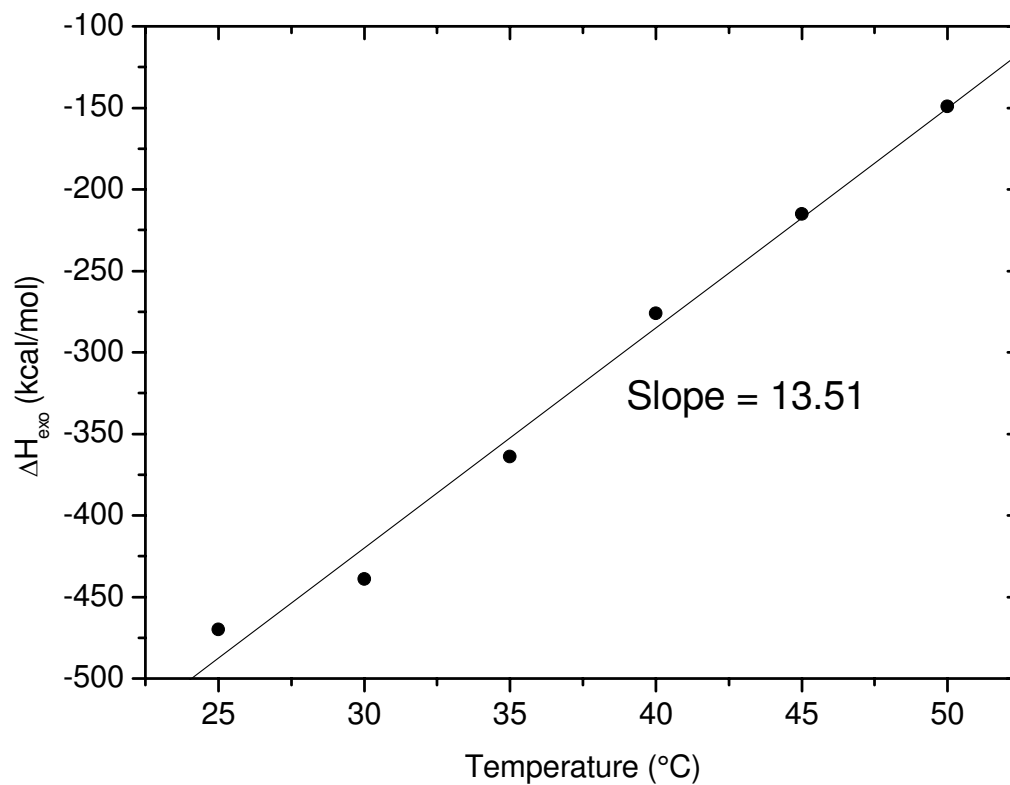


**Fig. II.12.** Evolution of  $\Delta H_{\text{exo}}$  with temperature during the titration of an aqueous dispersion of total Acacia gum (1.8 wt %) into an aqueous dispersion of  $\beta$ -lactoglobulin (0.6 wt %) at pH 4.2. Line corresponds to a linear fit of data. Each experiment was made in duplicate.



## II.4. Conclusions

Complexation between BLG and major molecular fractions of Acacia gum has been studied by varying physicochemical parameters affecting interactions in any protein-polyelectrolyte system such as biopolymer concentration, pH and temperature, using Isothermal Titration Calorimetry (ITC). The shape of titration curves of BLG by total Acacia gum and their two major fractions FI and FII were similar. However, the thermodynamic behavior of FII was different from that of FI. Favorable complexation (lower stoichiometry) and stronger energy of interactions (higher values of  $\Delta H_{\text{obs}}$ ) characterized the titration of BLG by FII. For both Acacia gum fractions, the binding curves with BLG consisted of a large sequence of sharp exothermic peaks and a sequence of weaker endothermic peaks. This tendency indicated that electrostatic interactions mainly induced complexation. ITC experiments have been performed at pH 4.2 and the general binding isotherm was studied in term of structural transitions. Four ratios of structural transitions were identified and compared to those obtained by optical density measurements:  $r_{\text{agg}}$ , the charge ratio of aggregation of complexes;  $r_{\text{isto}}$ , the initiated stoichiometric charge ratio;  $r_{\text{eq}}$ , the charge ratio of enthalpy/entropy equilibrium and  $r_{\text{sat}}$ , the charge ratio of saturation of binding sites. These ratios were lower in BLG/FII system, in agreement with lower stoichiometry of association and favorable complexation. However, the saturation of binding sites occurred at the Pr:Pol charge ratio of  $\sim 1:1$  in all systems, indicating that phase separation took place at a stoichiometric electrical charge equivalence. Effects of initial concentration of AG, pH and temperature on interactions were studied. An increase of AG all parameters led to lower stoichiometry of association of BLG to AG. The binding strength decreases with increasing temperature and gum concentration, and it reached a maximum at a pH of 4.2, in agreement with optical density measurements done in the same conditions. The increase of temperature allowed to determine a high positive value ( $13.51 \text{ kcal}\cdot\text{mol}^{-1}\cdot\text{C}^{-1}$ ) of the heat capacity ( $\Delta C_p$ ), which indicated a role of the hydrogen bonding in complexation/coacervation between BLG and AG and a disappearance of hydrophilic groups during interactions.

For macromolecular systems as BLG/AG, the effect of biopolymer concentration affects the influence of pH and temperature, e.g. increasing the total biopolymer concentration reduces the influence of pH on complex coacervation. Therefore, further ITC experiments are needed

to better understand the binding curve of BLG and Acacia gum molecular fractions. New information about the structural parameters of AG fractions is necessary to determine their charge densities, which can be fruitful for analyzing more precisely the ITC results as well as the role of each fraction on the complex coacervation process.

## II.5. References

- 
- <sup>1</sup> Luque, I.; Freire, E. *Methods in Enzymology*, **1998**, 295, 100.
  - <sup>2</sup> Luque, I.; Freire, E. *Proteins*, **2002**, 49, 181.
  - <sup>3</sup> Hallberg R.K. ; Dubin, P.L. *Journal of Physical Chemistry B*, **1998**, 102, 8629
  - <sup>4</sup> Weinbreck, F.; de Vries, R.; Schrooyen, P.; de Kruif, C.G. *Biomacromolecules*, **2003**, 4, 293.
  - <sup>5</sup> Mekhloufi, G., Sanchez, C.; Renard, D.; Guillemin, S.; Hardy, J. *Langmuir*, **2005**, 21, 386.
  - <sup>6</sup> Turgeon, S.L.; Beaulieu, M.; Schmitt, C.; Sanchez, C. *Current Opinion in Colloid and Interface Sciences*, **2003**, 8, 401.
  - <sup>7</sup> Schmitt, C.; Sanchez, C.; Despond, S.; Renard, D.; Thomas, F.; Hardy, J. *Food Hydrocolloids*, **2000**, 14, 403.
  - <sup>8</sup> Doublier, J.-L.; Garnier, C.; Renard, D.; Sanchez, C. *Current Opinion in Colloid and Interface Sciences*, **2000**, 5, 202.
  - <sup>9</sup> Sanchez, C.; Mekhloufi, G.; Renard, D. *Journal of Colloid and Interface Science*, **2006**, 299, 867.
  - <sup>10</sup> Velazquez-Campoy, A.; Todd, M.J.; Freire E. *Biochemistry*, **2000**, 39, 2201.
  - <sup>11</sup> Laneuville, S. ; Turgeon, S.L. ; Sanchez, C. ; Paquin, P. *Langmuir*, **2006**, 22, 7531.
  - <sup>12</sup> Schmitt, C.; da Silva, T.P.; Bovay, C.; Rami-Shojaei, S.; Frossard, P.; Kolodziejczyk, E.; Leser, M.E. *Langmuir*, **2005**, 21, 7786.
  - <sup>13</sup> Tolstoguzov, V.B. *Food Hydrocolloids*, **2001**, 17, 1.
  - <sup>14</sup> Thongngam, M.; McClements, D.J. *Langmuir*, **2004**, 21, 79.
  - <sup>15</sup> Sanchez, C.; Mekhloufi, G.; Schmitt, C. ;Renard, D.; Robert, P.; Lehr, C.-M; Lamprecht, A.; Hardy, J. *Langmuir*, **2002**, 18 , 10323.
  - <sup>16</sup> Antonov, Y.A.; Wolf, B.A. *Biomacromolecules*, **2005**, 6, 2980.
  - <sup>17</sup> Schmitt, C.; Sanchez, C.; Desobry-Banon, S.; Hardy, J. *Critical Reviews in Food Science and Nutrition*, **1998**, 38, 689.
  - <sup>18</sup> Randall, R.C.; Phillips, G.O.; Williams, P.A. *Food Hydrocolloids*, **1989**, 3, 65.
  - <sup>19</sup> Renard, D.; Lavenant-Gourgeon, L.; Ralet, M.; Sanchez, C. *Biomacromolecules*, **2006**, 7, 2637.
  - <sup>20</sup> Ibanoglu, E. *Journal of Food Engineering*, **2001**, 52, 273.
  - <sup>21</sup> Girard, M.; Turgeon, S.L.; Gauthier, S.F. *Journal of Agricultural and Food Chemistry*, **2003**, 51, 4450.

- <sup>22</sup> Cooper, A. *Current Opinion in Chemical Biology*, **1999**, 3, 557.
- <sup>23</sup> Thongngam, M.; McClements, D.J. *Journal of Agricultural and Food Chemistry*, **2004**, 52, 987.
- <sup>24</sup> Rutten, A.A.C.M.; Bouwman, W.G.; van der Leeden, M.C. *Colloids and Surfaces A*, **2002**, 210, 243.
- <sup>25</sup> Unterhaslberger, C.; Schmitt, C.; Sanchez, C.; Appolonia-Nouzille, C.; Raemy, A. *Food Hydrocolloids*, **2006**, 20, 1006.
- <sup>26</sup> de Kruif, C.G.; Tuinier, R. *Food Hydrocolloids*, **2001**, 15, 555.
- <sup>27</sup> Guzey, D.; McClements, D.J. *Food Hydrocolloids*, **2006**, 20, 124.
- <sup>28</sup> Velazquez-Campoy, A.; Todd, M.J.; Freire, E. *Biochemistry*, **2000**, 39, 2201.
- <sup>29</sup> Bai, G.; Nichifor, M.; Lopes, A.; Bastos, M. *Journal of Physical Chemistry B*, **2004**, 109, 518.
- <sup>30</sup> Lu, C.; Pelton, R.; Valliant, J.; Bothwell, S.; Stephenson, K. *Langmuir*, **2002**, 18, 4536.
- <sup>31</sup> Schmitt, C. INPL thesis, Institut National Polytechnique de Lorraine, France, **2000**.
- <sup>32</sup> Wanksakan, A.; Chinachoti, P.; McClements, D.J. *Journal of Agricultural and Food Chemistry*, **2003**, 51, 7810.
- <sup>33</sup> Nigen, M.; Croguennec, T.; Renard, D.; Bouhallab, S. *Biochemistry*, **2007**, 46, 1248.
- <sup>34</sup> Bai, G.; Santos, L.M.B.F.; Nichifor, M.; Lopes, A.; Bastos, M. *Journal of Physical Chemistry B*, **2004**, 108, 405.
- <sup>35</sup> Cannan, R.K.; Kibrick, A.L.; Palmer, A.H. *Annals of the New York Academy of Sciences*, **1941**, 16, 243.
- <sup>36</sup> Katalin, F.C., Miklós, N.; Ferenc, C. *Journal of Prosthetic Dentistry*, **2003**, 8, 45.
- <sup>37</sup> Miura, N.; Dubin, P.L.; Moorefield, C.N.; Newkome, G.R. *Langmuir*, **1999**, 15, 4245.
- <sup>38</sup> Fredheim, G.E. *Biomacromolecules*, **2003**, 4, 232.
- <sup>39</sup> Zhang, G.; Foegending, E.A. *Food Hydrocolloids*, **2003**, 17, 785.
- <sup>40</sup> Morris, E.R. *Polysaccharide Rheology and in-mouth Perception*. In A.M. Stephen (Ed.), *Food Polysaccharides and their Applications*. New York: Marcel Dekker, **1995**, p 517.
- <sup>41</sup> Gao, J.Y.; Dubin, P.L. *Biopolymers*, **1999**, 49, 185.
- <sup>42</sup> Ball, V.; Winterhalter, M.; Schwinte, P.; Lavalley, Ph.; Voegel, J.-C.; Schaal, P. *Journal of Physical Chemistry B*, **2002**, 106, 2357.
- <sup>43</sup> Csaki, K.F.; Nagy, M.; Csemesz, F. *Langmuir*, **2004**, 21, 761.
- <sup>44</sup> Gao, J.Y.; Dubin, P.L.; Muhoberac, B.B. *Analytical Chemistry*, **1997**, 69, 2945.

- 
- <sup>45</sup> Timasheff, S.N.; Mescanti, L.; Basch, J.J.; Towned, R. *Journal of Biological Chemistry*, **1966**, 241, 2496.
- <sup>46</sup> Kavanagh, G.M.; Clark, A.H.; Ross-Murphy, S.B. *International Journal of Biological Macromolecules*, **2000**, 28, 41.
- <sup>47</sup> Casal, H.L.; Kohler, U.; Mantsch, H.H. *Biochemica and Biophysica Acta*, **1988**, 957, 11.
- <sup>48</sup> Barratt, E.; Bingham, R.J.; Warner, D.J.; Laughton, C.A.; Phillips, S.E.V.; Homans, S.W. *Journal of American Chemical Society*, **2005**, 127, 11827.
- <sup>49</sup> Dunitz, J.D. *Journal of Biological Chemistry*, **1995**, 2, 709.
- <sup>50</sup> Record, M.T.; Anderson, C.F.; Lohman, T.M. *Quarterly Review of Biophysics II*, **1978**, 2, 103.



## Chapter III

# Influence of Acacia gum molecular polydispersity on the complex coacervation with $\beta$ -lactoglobulin

### Abstract

pH-induced complexation/coacervation between  $\beta$ -Lactoglobulin (BLG) and Acacia gum (AG) was studied by following static light scattering, electrophoretic mobility and particles diameter as determined using dynamic light scattering during slow *in situ* acidification of BLG/AG mixed dispersions. Three mixtures were studied: BLG/TAG, BLG/FI and BLG/FII at a protein to polysaccharide weight ratio of 2:1 and a total biopolymer concentration of 0.1wt %. For all mixtures, the scattering profiles  $I(q)$  vs  $q$  showed the presence of a correlation peak in a specific pH range (4.4-3.9) during acidification. The peak first shifted to higher  $q$  values then shifted toward smaller  $q$  values with decreasing pH. As a consequence, a similar mechanism of Nucleation and Growth characterizes phase separation in the three systems. However, mixed dispersions displayed some differences. Faster rate of phase separation was observed in BLG/FII system as compared to BLG/FI mixture, in relation with the complexation of FII at lower charge density of BLG. Smaller particles were also shown in this case. Moreover, the scattering profiles,  $I(q)$  vs  $q^{-\gamma}$ , for BLG/FII system displayed lower exponent  $\gamma$  values at the last stage of phase separation, in agreement with more heterogeneous interfaces than that of BLG/FI mixture. These results are mainly attributed to the higher accessibility of charges of FII that favors complexation. Five pH of structural transitions were determined in all mixtures:  $pH_{sc}$ , pH of formation of soluble complexes;  $pH_{ca}$ , pH of complex aggregation;  $pH_{ps}$ , pH of phase separation;  $pH_{coa}$ , pH of coacervate formation (coacervation) and  $pH_{neut}$ , pH of charges neutralization. From the  $pH_{ps}$ , the pH of structural transitions were shifted to lower values in BLG/FII system. This result may indicate that the first phase of complexation in the three systems displays the same transitions pH. However, from the phase separation onset the pH of structural transitions are different.





### III.1. Introduction

The structural transitions during complexation/coacervation were investigated in a great number of polyelectrolyte-polyelectrolyte dispersions<sup>1,2,3,4,5,6,7,8,9,10,11,12</sup>. Polyions with opposite charge stick together and form in time soluble complexes (intrapolymeric complexes) and later insoluble complexes (interpolymeric complexes). The formed aggregates slowly rearrange to form droplets called coacervate<sup>13</sup>. As time proceeds, coacervates coarsen and sediment to form the so-called coacervated phase<sup>14,15</sup>. pH-induced phase separation allowed to investigate the structural transitions in polymer and biopolymer systems. In the abundant literature, two characteristic pH-delimited structural and morphological changes were identified,  $pH_c$  and  $pH_\phi$ <sup>16,17,18,19</sup>.  $pH_c$ , the critical pH, reflects a phase transition on the molecular scale and it corresponds then to the formation of intrapolymeric complexes.  $pH_\phi$  is considered as a transition on the microscopic level at which phase separation begins.

Regarding the coacervation mechanism in most protein-polysaccharide systems studied, dynamic features of complexation and phase separation phenomena have not yet elucidated<sup>19,20,21,22</sup>. On the other hand, more than two pH induced structural transitions were identified in  $\beta$ -lactoglobulin (BLG) /Acacia gum (AG) mixed dispersions<sup>23</sup>. Six structural transitions occurring during slow acidification of the dispersions were identified<sup>23</sup>. These transitions were described as corresponding to (i) the formation of soluble complexes,  $pH_{sc}$  (ii) conformational change of the protein induced by complexation,  $pH_{pct}$  (iii) aggregation of complexes,  $pH_{ca}$  (iv) initiation of phase separation,  $pH_{psi}$  (v) phase separation,  $pH_{ps}$  and (vi) first appearance of coacervates,  $pH_{coa}$ . On the same system, Sanchez *et al.*<sup>24</sup> showed that complex coacervation could be described as a Nucleation and Growth process.

It is well established that TAG is a complex hetero-polysaccharide with a high molecular weight polydispersity<sup>25</sup>. As a consequence, the most significant difficulty to understand complex coacervation mechanism between BLG and TAG at the molecular level is the TAG molecular weight polydispersity and the presence of different molecular fractions in the whole gum. Most of the chemical studies in literature have shown that TAG consists of three principal fractions i.e. an arabinogalactan-peptide fraction denoted FI (85-90wt%), an

arabinogalactan-protein fraction denoted FII (10-12wt%) and a glycoprotein fraction (2wt%)<sup>25</sup>. More recently, Renard *et al.*<sup>26</sup> defined TAG as a continuum of molecular species differing both by their sugar to protein ratio, molecular weight and charge. Despite the wealth of information describing the chemical structure of TAG, little is currently known about the conformation and physico-chemical properties of individual fractions and about their specific role in complexation process<sup>1,27,28,29,30,31,32,33,34,35</sup>. Therefore, structural studies should take into account this heterogeneity by fractionating TAG before performing measurements<sup>36,37</sup>. The effect of TAG polydispersity on its binding with other macromolecules has not been studied.

From this perspective, the present work aimed to the determination of the phase separation mechanism and structural transitions occurring at different observation scales in BLG mixed with the two main molecular fractions of TAG, FI and FII. Slow acidification of the mixtures was obtained as a function of time by hydrolysis of glucono- $\delta$ -lactone in order to induce complexation and phase separation. Time-resolved small angle static light scattering (SALS), dynamic light scattering (DLS) and electrophoretic mobility ( $\mu_E$ ) measurements were performed during slow acidification of the three mixed dispersions BLG/TAG, BLG/FI and BLG/FII in order to study *in situ* pH-induced structural and phase transitions.

## III.2. Experimental section

### III.2.1. Materials

*β-Lactoglobulin (BLG)* powder (lot JE001-3-922) was provided by Davisco Foods International Inc. (Lesueur, MN, USA). The powder composition was (g per 100 g): 93.6% protein (N x 6.38), 4.9% moisture and 1.5% ash (0.017% Ca<sup>2+</sup>, 0.003% Mg<sup>2+</sup>, 0.008% K<sup>+</sup>, 0.9 Na<sup>+</sup>, 0.03% Cl<sup>-</sup>). The powder was extensively dialyzed against distilled water then freeze-dried.

*Acacia gum (TAG)* powder type from Acacia Senegal trees (lot n° 97 J 716) was a gift from CNI Company (Rouen, France). The powder composition was (g per 100 g): 90% polysaccharide, 6.6% moisture, 0.3% nitrogen and 3.1% ash (0.2% Mg<sup>2+</sup>, 0.61% Ca<sup>2+</sup>, 0.032% Na<sup>+</sup> and 0.9% K<sup>+</sup>). The powder was extensively dialyzed against distilled water then freeze-dried. TAG powder dialysed and freeze-dried was fractionated using hydrophobic interaction chromatography (HIC) (Renard *et al*, 2006). The two purified main molecular fractions, in weight, arabinogalactan-peptide fraction (FI) (88.5wt%) and arabinogalactan-protein fraction (FII) (10.5wt%), respectively, were further dialyzed against distilled water then freeze-dried for further analysis. The isolated FI and FII molecular fractions were both different in molecular weight and protein content. FI has a molecular weight of 2.86.10<sup>5</sup> g/mol and a protein content of 1.1wt%. FII has a molecular weight of 1.86.10<sup>6</sup> g/mol and a protein content of 9wt%.

*Glucono-δ-lactone (GDL)* (lot 052K0031, Calbochiem, Darmstadt, Germany) is an ester of gluconic acid obtained by oxidative fermentation of D-glucose (*Acetobacter suboxydans*).

*Sodium hydroxide and hydrochloric acid* were of analytical grade (Fischer Scientific SA, Elancourt, France).

## **III.2.2. Samples preparation**

### **III.2.2.1. Stock solutions of $\beta$ -lactoglobulin (BLG) and Acacia Gum (AG)**

Before preparing BLG/TAG, BLG/FI and BLG/FII mixed dispersions, aqueous stock BLG and AG solutions at 0.12 wt% total biopolymer concentration were prepared by dissolving powders in ultra pure deionized water (resistivity: 18 m $\Omega$ ) (Purite, Fischer Scientific, England) under gentle stirring at  $20 \pm 1$  °C for at least 2h. pH of BLG solution was adjusted to 5.00 (pH corresponding to the lowest BLG solubility) using 1N HCl. 170  $\mu$ l of 0.1N NaOH were added to AG solution in order to reach a pH value of  $\sim 7.00$ . The solutions were stored at  $4 \pm 1$  °C during 18h to allow good hydration of biopolymers. The stock solutions were then centrifuged during 40min at 10 000g to remove insoluble material and air bubbles. The concentration of BLG solution was checked by UV-Visible spectroscopy (Ultrospec 4000 UV/Visible, Pharmacia Biotech, England) using the specific extinction coefficient of 9.2 dl/cm.g at 278 nm, as determined experimentally. The absorbance at 278 nm was corrected for turbidity and the BLG dispersion concentration was finally adjusted to 0.1wt%, and pH 7.30 using 0.1 and 1N NaOH.

### **III.2.2.2. Mixed dispersions**

Most BLG/TAG, BLG/FI and BLG/FII mixed dispersions were prepared by adding AG to BLG solution at a protein (Pr): polysaccharide (Pol) weight ratio of 2:1, ratio corresponding to the maximum strength of interactions between BLG and AG, as shown in the previous chapter and in ref [23]. The blend was gently stirred for 30min at room temperature. The pH of the blend was at 7.30 at the end of the stirring period. Mixed dispersions were filtered through 0.22 $\mu$ m syringe filter (Millipore, Bedford, USA). 0.11wt% of GDL was then added to the mixed dispersion and dissolved under stirring for 5 min. In aqueous medium, GDL is hydrolyzed until equilibrium is reached between gluconic acid and GDL. Gluconic acid releases protons and gluconate in the medium. This proton release leads to a slow medium acidification. The following mixed dispersions were also prepared:

- 1) BLG/FI 88% at a Pr:Pol weight ratio of 2.3:1; in this case, FI solution contained 88wt% of FI and 12wt% of water.
- 2) BLG/FII12% at a Pr:Pol weight ratio of 16.7:1; in this case, FII solution was composed of 12wt% of FII and 88wt% of water.

3) BLG/(FI+FII) at a Pr:Pol weight ratio of 2:1, where TAG solution was replaced in this case by a mixed solution of FI and FII (88wt% of FI and 12wt% of FII).

### III.2.3. Dynamic light scattering

A Nanosizer ZS (HPPS 5001, Malvern Instrument, England) was used to follow the evolution of the size of particles in BLG/TAG, BLG/FI and BLG/FII mixed dispersions during acidification. The apparatus is equipped with a 4 mW He-Ne laser (633 nm), a measurement cell, a photomultiplier and a correlator. Samples were placed in vertical cylindrical cuvettes (10 mm-diameter).

Measurements were performed at a scattering angle of  $173^\circ$  relative to the source using an avalanche photodiode detector, at room temperature ( $23 \pm 2^\circ\text{C}$ ). The pattern allows considerable reduction of the signal due to multiple scattering events and enables measurements in slightly turbid media (NIBS technology). Intensity fluctuations were recorded every 10 s during 60 min, then the corresponding autocorrelation functions  $g_2(t)$  were analyzed by the Cumulant method (integrated in the Malvern Zetasizer software) in order to determine the distribution of translational diffusion coefficients,  $D_T$ . The  $D_T$  parameter is related to the hydrodynamic radius ( $R_h$ ) of particles through the Stokes-Einstein relationship:

$$D_T = \frac{k_B T}{6\pi\eta R_h} \quad \text{Eq. III.1}$$

where  $\eta$  is the solvent viscosity and  $k_B T$  the thermal energy.

Results from the Cumulant method allows the determination of both  $R_h$  distribution and respective amplitude of each population. In the present study, we calculated the hydrodynamic diameter (“z-averaged” diameter) of the biopolymers and complexes, which is simply  $2xR_h$  by suggesting that particles correspond to spheres.

### III.2.4. Electrophoretic mobility measurements ( $\mu_E$ )

Electrophoretic mobility measurements ( $\mu_E$ ) were performed on the same apparatus than in the section III.2.3 by means of laser Doppler electrophoresis. The sample was put in a

standard capillary electrophoresis cell equipped with gold electrodes. Measurements were recorded every 10 s during 60 min. Measurements on control AG dispersions were performed at 1 wt% to ensure a good signal to noise ratio. Measurements on control dispersions (BLG) were performed at 0.066 wt% (BLG concentration in the blend). For the purposes of clarity, electrophoretic mobility units ( $\mu\text{m}\cdot\text{cm}\cdot\text{s}^{-1}\cdot\text{V}^{-1}$ ) will be referred to e.m.u. in the following.

### **III.2.5. Small Angle Static Light Scattering (SALS)**

The pH-induced structural and phase transitions of mixtures were followed during 2 h with a measurement step of 10 sec using SALS. Light scattering experiments were carried out using a Mastersizer S long bench (Malvern Ltd., U.K.). A He-Ne laser light ( $\lambda = 632.8$  nm) was passed through a 0.5-mm-width measurement cell (Malvern Ltd) in which the mixed dispersions were injected using a syringe. The beam was converged by a reverse Fourier 300-mm focusing lens. A series of 37 detectors covering the scattering wave vector  $q$  range  $2.1 \times 10^{-2} - 10.414 \mu\text{m}^{-1}$  collected the scattered light. The resulting scattered intensity was corrected for turbidity according to the relationship:

$$I_c(\tau) = I_m(\theta) \exp(\tau d / \cos \theta) [\tau d (\cos^{-1} \theta - 1)] \{ \exp[\tau d (\cos^{-1} \theta - 1)] - 1 \}^{-1} - 1 \quad \text{Eq. III.2}$$

with  $\tau d = -\ln T(t)$

where  $I_c$  and  $I_m$  are respectively the corrected and measured scattered intensity distributions,  $\theta$  the scattering angle,  $d$  the sample thickness,  $\tau$  the turbidity and  $T(t)$  the transmittance of the sample at a given time  $t$ . The corrected scattered intensity  $I_c$  will be described as  $I(q)$  hereafter with  $I_{46}$  corresponding to the intensity recorded at the highest  $q$  value ( $q = 10.414 \mu\text{m}^{-1}$ ). This highest  $q$  value corresponds to a scattering angle  $\theta$  of  $46^\circ$  at which smaller structural entities can be detected by the spectrometer. Scattering profiles,  $I(q)$  vs  $q$ , were fitted with polynomial functions using Origin 7.5 software (OriginLab co., Northampton, MA, USA) and xlx-trfun freeware (Advanced Systems Design and Development, Red Lion, PA, USA), in order to extract relevant structural parameters (the intensity and corresponding wave vector at which a scattering maximum appeared,  $I_{\text{max}}$  and  $q_{\text{max}}$ ).

### III.3. Results and Discussion

SALS, DLS and  $\mu_E$  measurements are complementary methods to analyze phase ordering kinetics in BLG/AG mixed dispersions. Scattered light intensity is a physical parameter depending on the shape, size, number and optical properties of particles.  $\mu_E$  provides the measurement of the net charge of complexes based on the migration rate of particles, as a function of their size and charge density. FII has the highest charge, molecular weight and hydrodynamic radius as compared to FI. These intrinsic molecular characteristics can modify the extent of complexation and phase separation, inducing changes in the measured physical parameters<sup>38</sup>. The effect of TAG polydispersity in complexation/coacervation with BLG was investigated for BLG/AG mixtures differing in the type of molecular fraction purified from TAG. Different parameters (size, hydrodynamic diameter, scattered light intensity and its derivative, wave vector at which a correlation peak appeared ( $q_{\max}$ ) and exponent of the scattering profiles  $I(q) \sim q^{-\gamma}$ ) were collected from dynamic/static light scattering and electrophoretic mobility measurements in order to characterize phase and structural transitions occurring during slow acidification of mixtures.

#### III.3.1. Dynamic light scattering (DLS)

Dynamic light scattering allowed the determination of the pH-induced evolution of particles size in BLG/TAG, BLG/FI and BLG/FII dispersions during the complex coacervation process. Fig. III.1 shows the evolution of particles hydrodynamic diameter ( $d$ ) in all systems as a function of pH. The evolution of  $d$  during acidification exhibits the same trend in all mixtures and can be divided into five zones based on the intersection point of two tangents to curves.

*From pH 5.3 to pH ~5.0:*  $d$  was almost constant at ~ 29 nm and 26 nm until pH 5.11 in BLG/TAG and BLG/FI mixtures, whereas  $d$  remained constant at 52 nm until pH 5.0 in BLG/FII system. For each mixture, these values corresponded to the size of AG (e.g. TAG or FI or FII) obtained for stock dispersions (Fig. III.2). It must be noticed that these size values are about equivalent to the double of  $R_h$  noticed in chapter II, which reveals a good agreement. The average BLG diameter is too small (~ 2 nm) to be detected. The discontinuity of  $d$  in this stage would correspond to the initiation of interaction.

*From pH 5.0 to pH ~4.45:* From pH ~5.0, a slight increase of  $d$  was observed. From pH ~4.6 and ~4.5,  $d$  of BLG/TAG and BLG/FI mixtures markedly increased from ~29 and 26 nm to ~50 and ~70 nm. However for BLG/FII mixture, when the pH ranged from ~5.0 to pH ~4.45,  $d$  increased and reached respectively the value of ~84 nm at pH 4.47. It must be then noticed that FI produced smaller size of complexes as compared to FII.

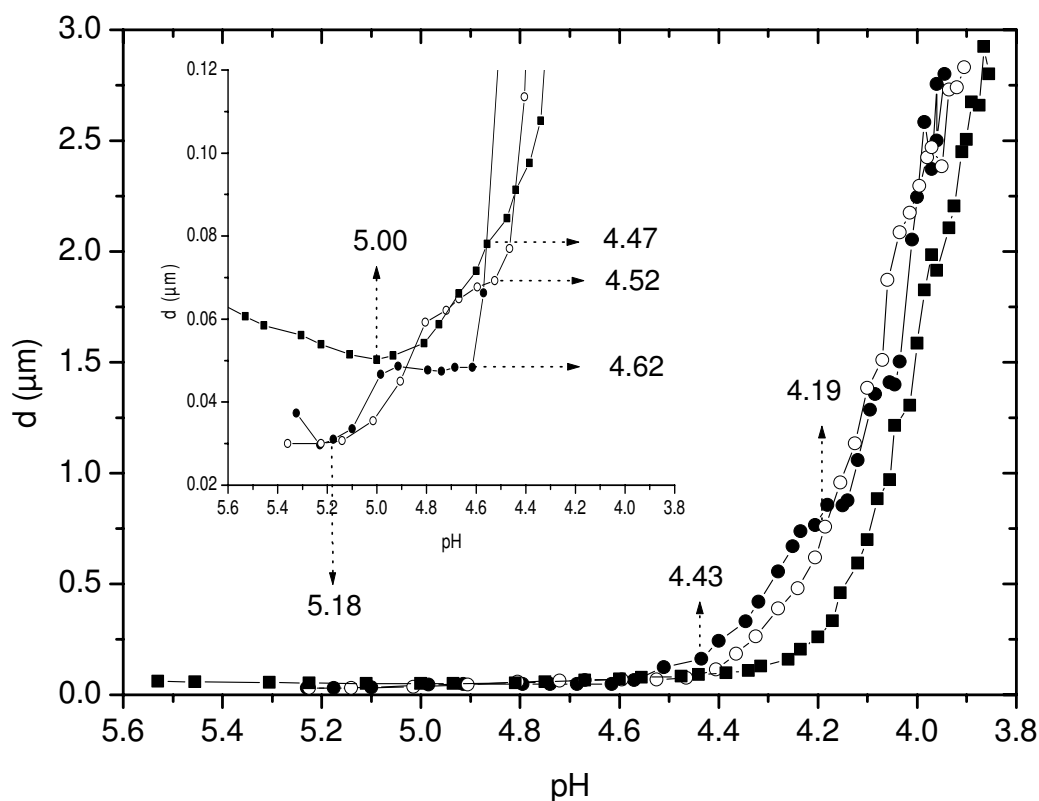


**Fig. III.1.** Evolution of the diameter of particles as a function of pH for  $\beta$ -lactoglobulin (BLG) / Acacia Gum (TAG) or Arabinogalactan-peptide (FI) or Arabinogalactan-protein (FII) mixed dispersions at 0.1wt% total biopolymer concentration and Pr:Pol weight ratio of 2:1. (●) BLG/TAG, (○) BLG/FI, (■) BLG/FII. Each experiment was made in triplicate. Inset: a zoomed region of the same curve.

*From pH 4.45 to pH 4.20:* in this pH range,  $d$  continued to increase steadily until pH 4.51, 4.40 and 4.25 in BLG/TAG, BLG/FI and BLG/FII dispersions. Structural entities were then larger, their  $d$  increased up to ~765 nm in BLG/TAG against 618 nm in BLG/FI and ~260 nm in BLG/FII mixtures at pH 4.2. Phase separation would occur in this pH range.

*Below pH 4.20:* In this pH range, structures grew in size due to the coalescence of particles<sup>23</sup>. The increase of  $d$  considerably accelerated from pH ~4.2 with still larger particles in BLG/TAG and BLG/FI systems. At this stage, although size differences between mixtures



were present, the tendency of evolution of  $d$  with pH was the same in all mixtures. At pH 4.00,  $d$  reached 2.17  $\mu\text{m}$  in BLG/FI, 2.05  $\mu\text{m}$  in BLG/TAG and 1.30  $\mu\text{m}$  in BLG/FII mixture. This system displayed the smallest size of particles and BLG/TAG had intermediate particle size between BLG/FI and BLG/FII mixtures.

To summarize, FI led to the formation of larger size of particles except at the highest pH values. It was complexed with less positively charged BLG (i.e. at higher pH values) as compared to FII.

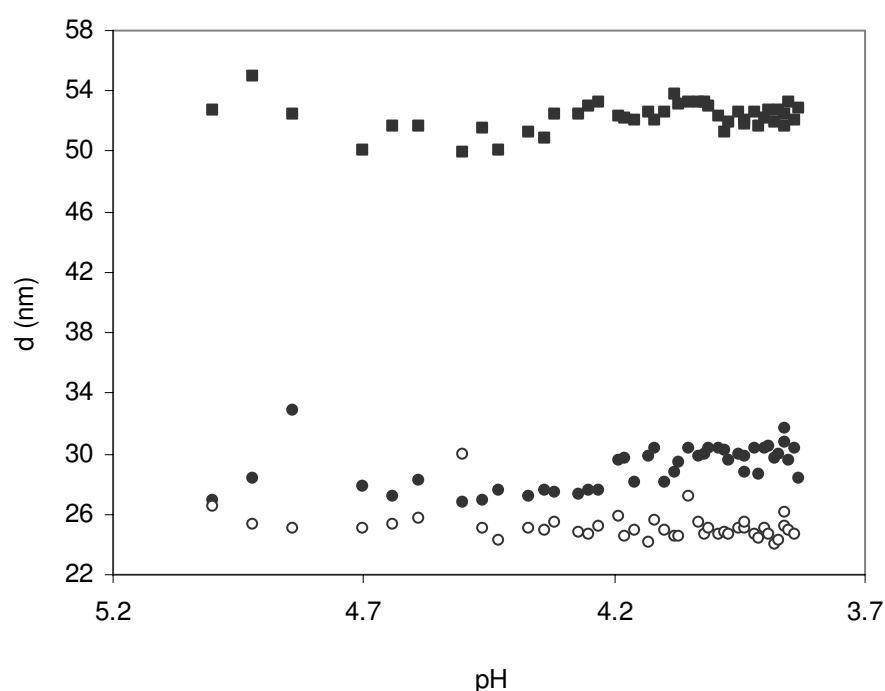


**Fig. III.2.** Evolution of the particles diameter ( $d$ ) (nm) as a function of pH for Acacia Gum (TAG) or Arabinogalactan-peptide (FI) or Arabinogalactan-protein (FII) stock dispersions at 0.1wt% total biopolymer concentration and Pr:Pol weight ratio of 2:1. (●) TAG, (○) FI, (■) FII. Each experiment was made in duplicate.

### III.3.2. Electrophoretic mobility ( $\mu_E$ )

Since complex coacervation between BLG and AG is mainly controlled by electrostatic interactions, electrophoretic mobility ( $\mu_E$ ) measurements were used to give information about the total surface charges of BLG, TAG, FI, FII and complexed BLG/TAG, BLG/FI and BLG/FII systems. Fig. III.3 represents the pH-induced  $\mu_E$  changes for biopolymers alone or complexed. The BLG  $\mu_E$  changed from  $-0.28$  e.m.u. at pH 5.45 to  $+2.28$  e.m.u. at pH 3.75,

depending on the charge balance between the amino and the carboxylic groups carried by the protein. The zero  $\mu_E$  value of the BLG was reached at pH 5.22 and, as expected, closely corresponded to the lowest BLG solubility, which is determined by spectrophotometry (see the materials and methods section). This value is also close to the theoretical isoelectric pH of BLG. The  $\mu_E$  of TAG, FI and FII were negative in the pH range considered in the present study (from 5.90 to 3.72), due to the presence of glucuronic acid residues in the gum ( $pK_a < 3.6$ ).

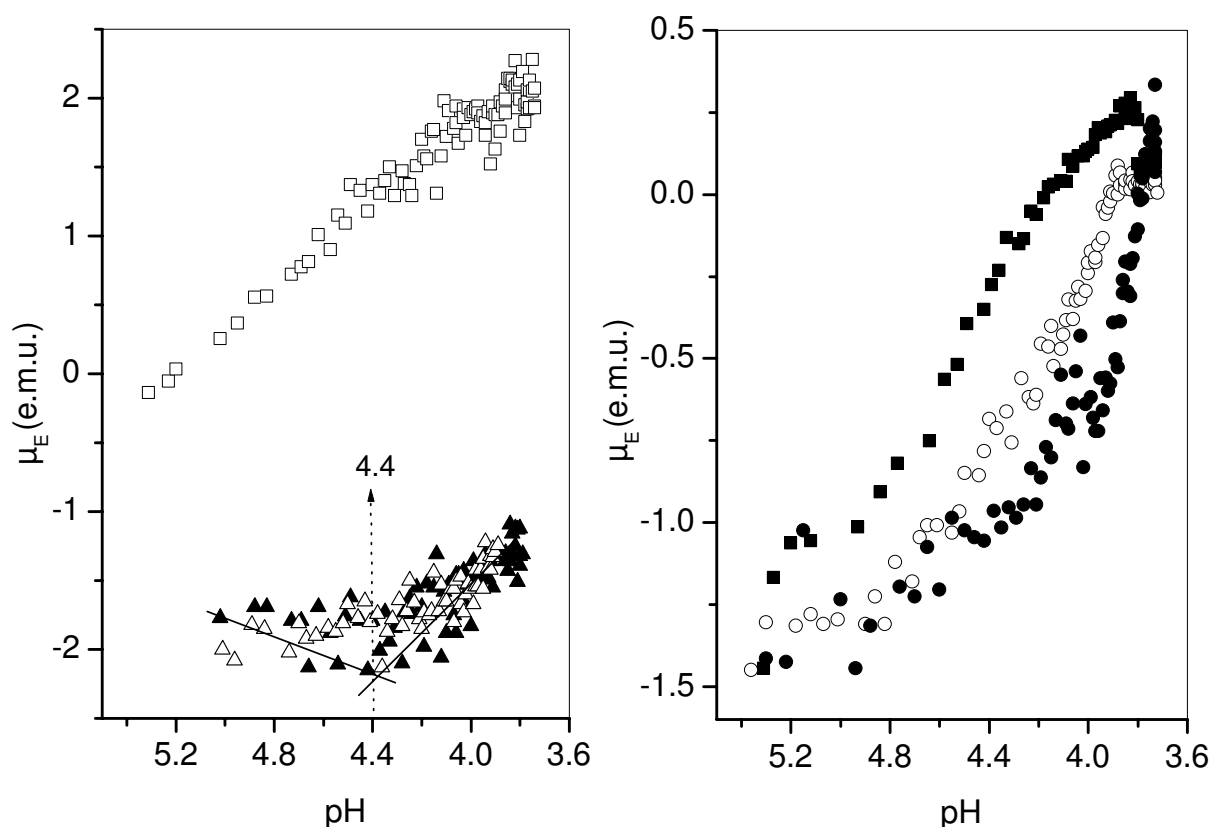


**Fig. III.3.** Evolution of the electrophoretic mobility ( $\mu_E$ ) (e.m.u.) as a function of pH at 0.1wt% total biopolymer concentration and Pr:Pol weight ratio of 2:1 for  $\beta$ -lactoglobulin (BLG) / Acacia Gum (TAG) or Arabinogalactan-peptide (FI) or Arabinogalactan-protein (FII) mixed dispersions and for  $\beta$ -lactoglobulin (BLG) or Acacia Gum (AG) stock dispersions. (●) BLG/TAG, (○) BLG/FI, (■) BLG/FII, (□) BLG, (▲) TAG and (Δ) FII. Dotted line is guide for the eye. Each experiment was made in duplicate.

The total surface charges of TAG and its molecular fractions show a minimal  $\mu_E$  at pH  $\sim$ 4.4 (only results for TAG and FII dispersions are shown because the reliability of measurements was unsatisfactory for FI). From this pH, all AG molecules became less negatively charged. In all mixed dispersions studied,  $\mu_E$  was also negative in the 5.9 – 4.4 pH range and displayed a similar whole evolution than that of Acacia gum (or FI or FII) alone. This highlighted the main contribution of AG molecules to the  $\mu_E$  evolution of the mixed dispersions as shown

previously (Mekhloufi *et al.*, 2005).

For all mixtures,  $\mu_E$  slowly decreased between pH  $\sim 5.4$  and pH  $4.9 \pm 0.05$ . In the 4.9 - 4.4 pH range,  $\mu_E$  evolution becomes faster until reaching zero at pH 3.8, 3.9 and 4.2 in BLG/TAG, BLG/FI and BLG/FII mixtures, respectively. Moreover, BLG/FII dispersion shows lower absolute  $\mu_E$  than BLG/TAG and BLG/FI dispersions whatever the pH. At the pH values at which neutral complexes (zero mobility) were present, the Pr:Pol charge ratios were 2.5:1, 1.8:1 and 0.9:1 in BLG/TAG, BLG/FI and BLG/FII systems, respectively. By comparing these values to the charge ratios of enthalpy/entropy equilibrium ( $r_{eq}$ ) determined in chapter II, we find 2.6:1, 2.0:1 and 1.4:1 in ITC measurements. The values show a good agreement between ITC and  $\mu_E$  experiments. Thus, the same tendency was observed i.e. lower stoichiometric charge ratio was obtained for BLG/FII system. This feature would indicate that FII induces favorable complexation/coacervation with BLG. The explanation may be the chemical and structural features of FII that allow a stronger binding to BLG, i.e. in pH conditions where the BLG charge density is lower. A decrease in the number of negative charges was observed in the mixed dispersions between pH 5.9 and pH 5.20. This is due to the neutralization of charges that leads to a decrease of BLG negative charge, since in the same pH range, BLG  $\mu_E$  was less negative and tended to electroneutrality close to 5.22.

The migration rate of particles (or the  $\mu_E$ ) is highly dependent on its charge-to-mass ratio ( $C/M_w$ )<sup>39</sup>. Therefore, it was determined in order to better understand the differences in  $\mu_E$  evolution between mixtures. The evolution of this parameter as a function of pH displays similar curve shape for all AG dispersions (Fig. III.4). In all cases, two phases can be observed. A first region of constant values appeared until pH  $\sim 5.20$ , 5.41 and 4.55 for TAG, FI and FII dispersions, respectively. A second region displays a gradual decrease of  $C/M_w$  with decreasing pH. The intersection point between these two regions was reached at 4.49, 4.58 and 4.24 in TAG, FI and FII dispersions, respectively. These pH values correspond to those (4.51, 4.40 and 4.25) shown for the  $d$  evolution at the third stage (4.45-4.2). This feature may indicate that complexation/coacervation is controlled by both the number of charges and molecular weight of AG. It must be noticed that TAG displayed the lowest values of  $C/M_w$  whatever the pH. These values were the highest for FII below pH 4.55. These higher values of  $C/M_w$  may be the reason for the favorable complexation between BLG and FII. On the other hand, the  $\mu_E$  that would be proportional to  $C/M_w$  shows an unexpected behavior in BLG/TAG

and BLG/FII dispersions, i.e. disproportional values to  $C/M_w$ . Since FI and FII have different number of charges, this result can be attributed to the formation of smaller size of BLG/FII complexes that allow lower  $\mu_E$  values.

We have suggested above that phase separation is carried out in this pH range (4.45-4.2) because the size of complexes ( $d$ ) started to increase markedly from pH  $\sim$ 4.4. Furthermore from pH  $\sim$ 4.4, the absolute  $\mu_E$  of TAG decreased gradually. According to Mekhloufi *et al.* (2005), the lowering of the number of TAG negative charges promotes more efficient charge neutralization of aggregated complexes and then provides the initiation of phase separation at pH  $\sim$ 4.4. This is in spite of the fact that  $\mu_E$  do not reached the zero at this pH. The occurrence of phase separation for complexes with a negative total charge in protein-polyanionic polymers was also found by Xia *et al.* (1993)<sup>14</sup>.

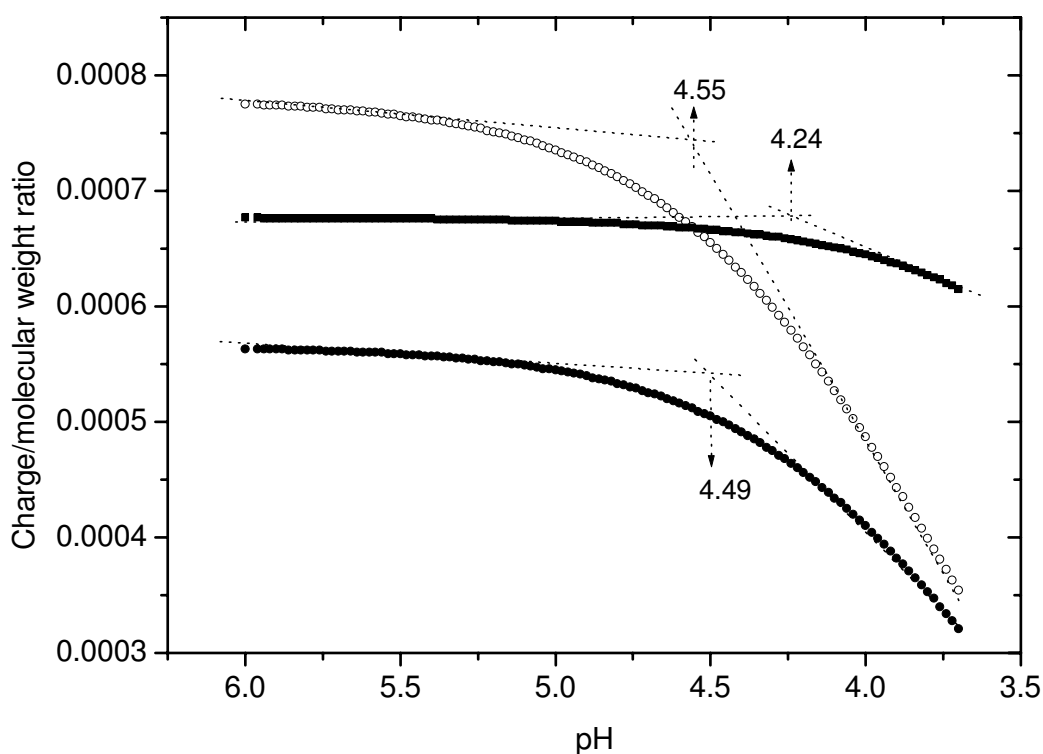


**Fig. III.4.** Evolution of the charge-to-molecular weight ratio ( $C/M_w$ ) with pH for TAG, FI and FII stock dispersions. (●) TAG, (○) FI, (■) FII. The charge values of all biopolymers were determined by titration measurements (Renard *et al.*, 2006).

### III.3.3. Small angle static light scattering (SALS)

In addition to the previous method of light scattering, small angle static light scattering was used to better understand the phase ordering kinetics in all mixtures. Fig. III.5 represents the

scattered light intensity at  $46^\circ$  scattering angle ( $I_{46}$ ) as a function of pH for BLG/TAG, BLG/FI, BLG/FII, and BLG/(FI+FII) mixtures. In a first stage,  $I_{46}$  remained steady until a critical pH value was reached. The scattering intensity then upturned reflecting the growth of inhomogeneities due to complexes formation.

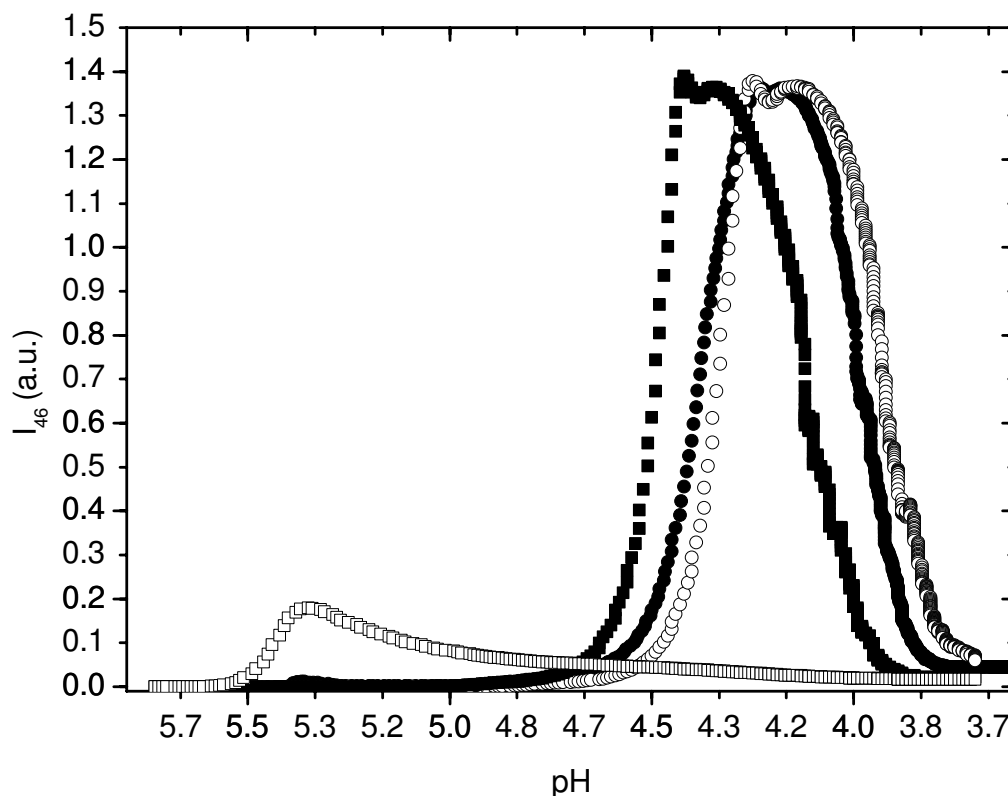


**Fig. III.5.** Evolution of the scattered light intensity at a scattering angle of  $46^\circ$  ( $I_{46}$ ) (arbitrary units) as a function of pH for  $\beta$ -lactoglobulin (BLG) / Acacia Gum (TAG) or Arabinogalactan-peptide (FI) or Arabinogalactan-protein (FII) mixed dispersions at 0.1wt% total biopolymer concentration. ( $\bullet$ ) BLG/TAG 2:1 weight ratio, ( $\circ$ ) BLG/(FI+FII) 2:1, ( $\blacksquare$ ) BLG/FI 2.3:1, ( $\square$ ) BLG/FII 17:1. Each experiment was made in triplicate.

The evolution of  $I_{46}$  with pH then displayed a maximum whatever the mixture. The pH at which a maximum of intensity was reached corresponded to the maximum of interaction strength ( $\text{pH}_{\text{mis}}$ ) between unlike charged biopolymers. A second increase of  $I_{46}$  then appeared after  $\text{pH}_{\text{mis}}$  (for BLG/TAG and BLG/FI systems) was reached followed by a decrease of  $I_{46}$  indicating a decrease of the number or concentration of particles in all mixtures. In addition, it was observed that BLG/TAG and BLG/(FI+FII) mixtures displayed the same scattering profile indicating the same phase separation mechanism. BLG/FI (weight ratio 2.3:1) mixtures displayed a profile that was shifted towards higher pH values traducing the occurrence of a faster phase separation. This feature indicates that the formation of BLG/FI complexes and their coarsening rate arise at lower positive charge density of BLG because of

the increase of BLG amount in dispersion. On the other hand, BLG/FII (weight ratio 17:1) mixtures showed a scattered light intensity considerably reduced with a profile that was shifted towards the highest pH values. The Pr:Pol weight ratios of 2:1, 2.3:1 and 17:1 are equivalent to 1.3:1, 1.5:1 and 11:1 charge ratios for BLG/TAG mixed dispersions. The lower value of the maximum of intensity in BLG/FII mixtures can be attributed to a decrease of the strength of interactions between BLG and FII due to a large excess of BLG charges. This large excess also can explain the shifting of the scattering profiles towards higher pH <sup>40</sup>.

In order to better evaluate these first results and, in particular, to discriminate between the effect of charge ratio differences and the strength of interactions between biopolymers, experiments were made to compare BLG/TAG, BLG/FI and BLG/FII dispersions at two different weight ratios, 2:1 and 40:1. As reported in Fig. III.5, Fig. III.6 shows approximately the same profiles for  $I_{46}$  as a function of pH at all ratios.

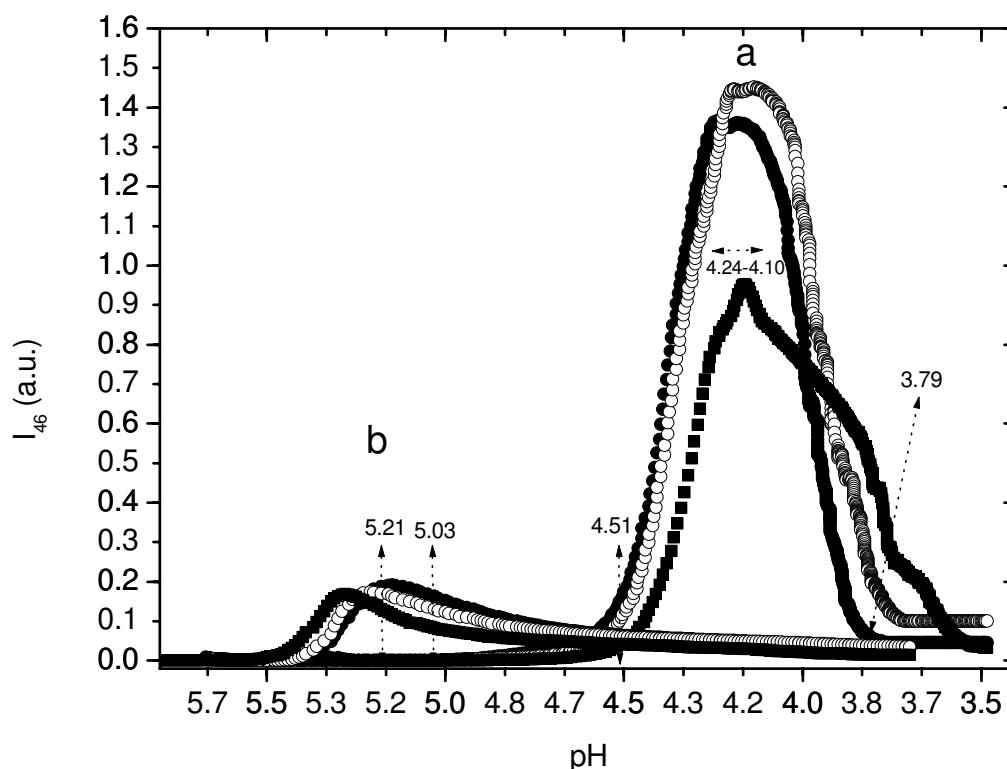


**Fig. III.6.** Evolution of the scattered light intensity at a scattering angle of  $46^\circ$  ( $I_{46}$ ) (arbitrary units) as a function of pH for  $\beta$ -lactoglobulin (BLG) / Acacia Gum (TAG) or Arabinogalactan-peptide (FI) or Arabinogalactan-protein (FII) mixed dispersions at 0.1wt% total biopolymer concentration and protein:polysaccharide (Pr:Pol) weight ratio of 2:1 (a) and 40:1 (b). (●) BLG/TAG, (○) BLG/FI, (■) BLG/FII. Each experiment was made in triplicate.

At a Pr:Pol weight ratio of 2:1, a constant evolution of  $I_{46}$  appeared for all mixtures until pH 5.03 ( $\pm 0.05$ ) was reached. Between pH 5.03 and pH 4.51 ( $\pm 0.05$ ),  $I_{46}$  slightly increased. At

pH 4.51 ( $\pm 0.05$ ),  $I_{46}$  increased remarkably revealing the phase separation initiation. The maximum of intensity at  $\text{pH}_{\text{mis}}$  was reached at pH 4.25, 4.20 and 4.16 in BLG/TAG, BLG/FI and BLG/FII mixtures, respectively. Below pH  $\sim 4.20$ , a second maximum of intensity appeared then  $I_{46}$  decreased strongly, except for BLG/FII mixtures where, between pH 4.20 and 3.93 ( $\pm 0.07$ ), a constant decrease of the scattering intensity values was observed. In addition, the lower scattering intensity values together with a lower  $I_{46}$  maximum at pH  $\sim 4.20$  could be attributed to the presence of smaller particles in BLG/FII mixtures based on the size results (Fig. III.1).  $I_{46}$  finally becomes constant below pH  $\sim 3.79$ . At a given pH, FII has a higher negative charge value than FI (Tab. II.3). Therefore, complexation between BLG and FII would occur with higher amounts of BLG.

In order to get new insights into the complexation/phase separation kinetics, we determined the Pr:Pol charge ratio as a function of pH (see chapter II). Whatever the pH, BLG/FII dispersion has lower Pr:Pol charge ratios due to the higher number of charges and molecular weight of FII, since we multiply the ratio of number of charges by the molar ratio to obtain the charge ratio. At the  $\text{pH}_{\text{mis}}$  for example (4.25, 4.20 and 4.16 for the three dispersions), the Pr:Pol charge ratios were  $\sim 1.26:1$ ,  $1.08:1$  and  $0.97:1$  for BLG/TAG, BLG/FI and BLG/FII mixtures. This feature reveals that BLG/AG system exhibit a maximum of interaction strength at a Pr:Pol charge ratio of  $\sim 1:1$ . This Pr:Pol charge ratio is comparable with the ratio of saturation of binding sites ( $r_{\text{sat}}$ ) determined in the previous chapter, which corresponds to a stoichiometric charge ratio where a neutralization of charges in dispersions arises.

As noticed in the previous chapter, the higher number of charges of FII bears higher number of opposite BLG charges to be neutralized, which would lead to higher Pr:Pol charge ratio of complexation/phase separation in BLG/FII system. However, results showed that the maximum of interaction was reached at the same charge ratio in all systems, revealing faster coarsening rate of particles in BLG/FII dispersion. This is might be due to the chemical, molecular and structural properties of FII, i.e. the higher molecular weight and accessibility of charges. By titration measurements and in order to determine the number of charges of TAG and its molecular fractions, Renard *et al.* (2006) revealed that 91.3% and 8.7% of charges came from polysaccharide moieties (i.e. glucuronic acids) and polypeptidic backbone (i.e. protein compounds) for FII. However, 100% of charges came from polysaccharide moieties for FI. In addition, it was predicted the presence of secondary (e.g.  $\beta$ -sheet) and random coil structures for FII, whereas no secondary structure was detected for FI. Therefore, we suggest

that steric hindrance and conformational changes of FII may result from the protein backbone and favor association with BLG. This is in addition to the expected higher charge density of FII that promotes favorable complexation, as shown in the previous chapter.

The scattering profiles obtained for the 2:1 Pr:Pol weight ratio were shifted to lower pH and showed higher peak heights of intensity as compared to the 40:1 Pr:Pol weight ratio. Increasing the Pr:Pol ratio leads to an increase of number of BLG positive charges in dispersions, which favors electrostatic interactions and provides complexation with AG at higher pH values where BLG has lower charge density<sup>41</sup>.

In Fig. III.7, the derivative of  $I_{46}$  ( $dI_{46}/dt$ ) was plotted as a function of pH for the three mixtures in order to get more information about the phase ordering kinetics.

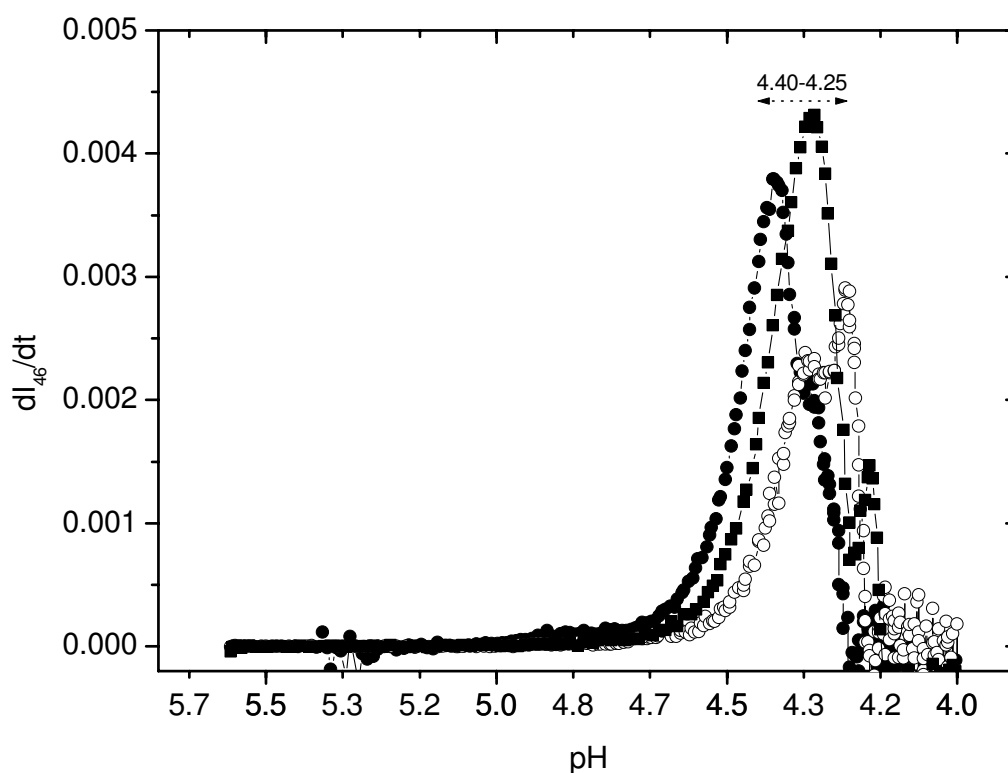


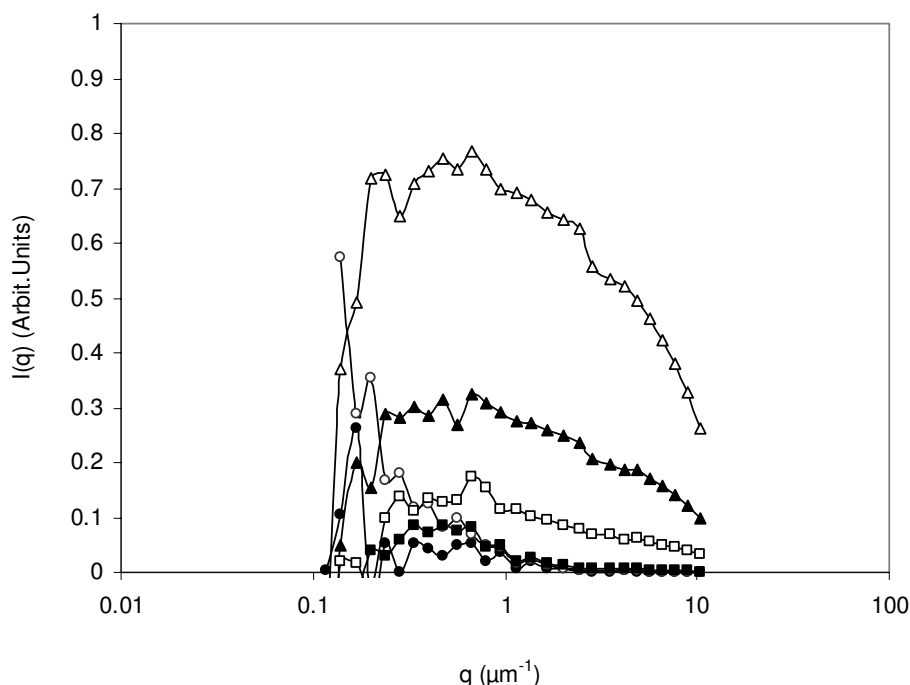
**Fig. III.7.** Evolution of the derivative of the scattered light intensity at  $46^\circ$  scattering angle  $dI_{46}/dt$  (arbitrary units) as a function of pH for  $\beta$ -lactoglobulin (BLG) / Acacia Gum (TAG) or Arabinogalactan-peptide (FI) or Arabinogalactan-protein (FII) mixed dispersions at 0.1wt% total biopolymer concentration and Pr:Pol weight ratio of 2:1. (●) BLG/TAG, (○) BLG/FI, (■) BLG/FII. Each curve is the average of three independent experiments.

The pH value for which a maximum rate in intensity change appeared was observed at 4.40, 4.25 and 4.31 for BLG/TAG, BLG/FI and BLG/FII dispersions, respectively. These pH



values would correspond to the phase separation onset. This indicates different phase ordering kinetics between mixtures. BLG/FI system exhibits both lower maximum of  $dI_{46}/dt$  and transitions pH, in agreement with a slower coarsening rate of particles as compared to BLG/FII mixture.

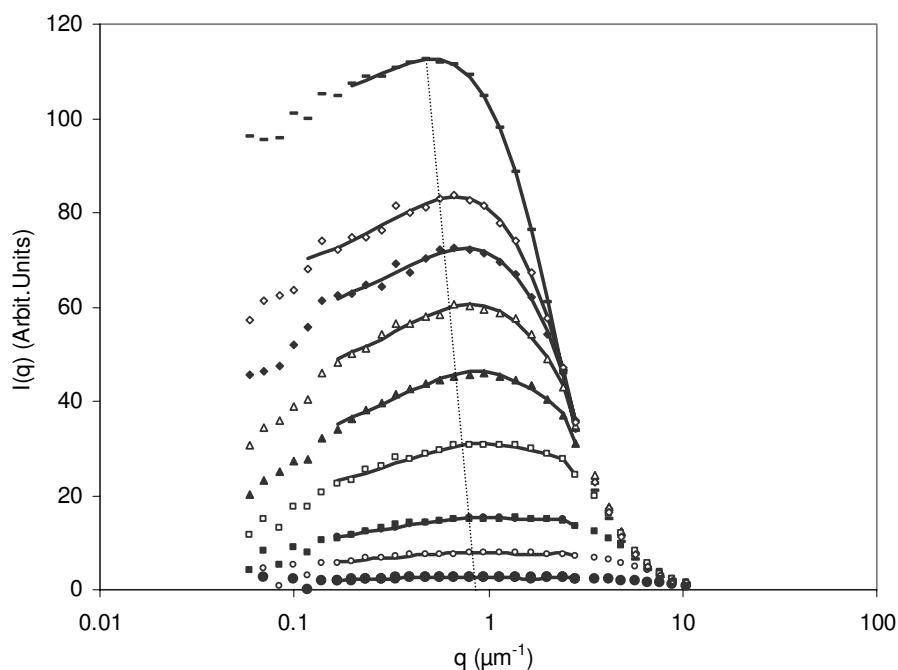
The scattering profiles  $I(q)$  vs  $q$  were used to define the phase separation mechanism driving complex coacervation in BLG/AG systems. It was noticed three steps in the shape of the scattering profiles as a function of acidification time. Firstly, no peak correlation was detected with increasing scattering angle from the beginning of acidification until pH  $\sim 4.6$  (Fig. III.8).



**Fig. III.8.** Scattering profiles  $I(q)$  (arbitrary units) as a function of  $q$  ( $\mu\text{m}^{-1}$ ) recorded during slow acidification of BLG/TAG mixed dispersion at 0.1wt% total biopolymer concentration and Pr:Pol weight ratio of 2:1 in a pH range where a correlation peak does not appear. (●) pH 5.4, (○) pH 5.2, (■) pH 5.0, (□) pH 4.8, (▲) pH 4.6 and (Δ) pH 4.5. Each experiment was made in triplicate.

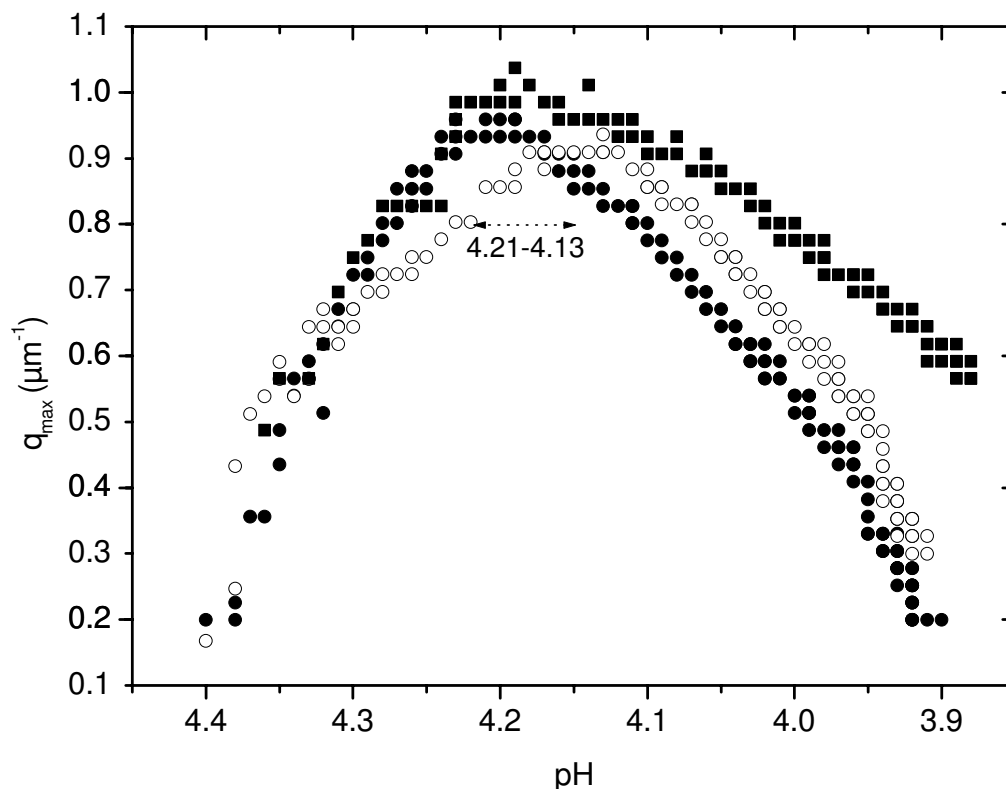
Secondly, a correlation peak appeared as acidification proceeded (Fig. III.9). In order to determine the maximum scattered intensity  $I_{\text{max}}$  and the corresponding wave vector  $q_{\text{max}}$ , the plots were fitted to a polynomial function (three or four order depending on the pH range). Two phases of evolution of the maximum wave vector  $q_{\text{max}}$  were observed in the pH range where a maximum was present. During the first phase occurring between pH  $\sim 4.6$  and 4.2,  $q_{\text{max}}$  shifted towards higher  $q$  values, suggesting an increase in the number of particles. During the second phase below pH  $\sim 4.2$ , the peak shifted to smaller  $q$  values, which may be due to

coarsening of particles. According to Sanchez *et al.* (2006), the shape of the scattering profiles and the temporal evolution of  $q_{\max}$  allowed to define the phase separation as a Nucleation and Growth mechanism (NG). The same behavior of the correlation peak was observed whatever the mixture, BLG/TAG, BLG/FI and BLG/FII (Fig. III.10). Therefore, phase separation in the three mixtures was driven by a NG mechanism.



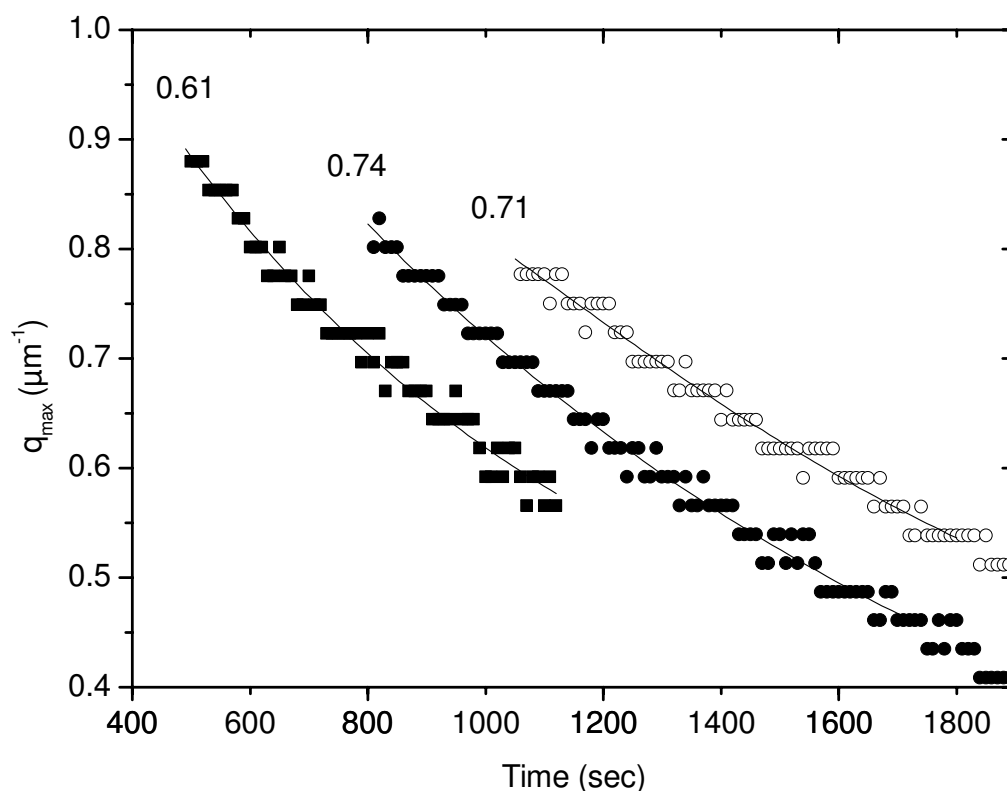
**Fig. III.9.** Scattering profiles  $I(q)$  (arbitrary units) as a function of  $q$  ( $\mu\text{m}^{-1}$ ) recorded during slow acidification of BLG/TAG mixed dispersion at 0.1wt% total biopolymer concentration and Pr:Pol weight ratio of 2:1 in a pH range where a correlation peak appeared. (●) pH 4.33, (○) pH 4.25, (■) pH 4.2, (□) pH 4.18, (▲) pH 4.12, (△) pH 4.10, (◆) pH 4.04, (◇) pH 4.00 and (-) pH 3.95. Continuous lines correspond to weighted curve fits with three or fourth-order polynomial function. Dot line highlights the shift of the scattering maximum towards smaller  $q$  values. Each experiment was made in triplicate.

Fig. III.10 shows the evolution of the maximum wave vector  $q_{\max}$  with pH,  $q_{\max}$  being obtained by fitting the scattering profiles in a time window where a peak was present.  $q_{\max}$  increased until a maximum close to pH 4.2 ( $\pm 0.1$ ) was reached; between pH  $\sim 4.2$  and pH 3.9 ( $\pm 0.05$ ),  $q_{\max}$  decreased with acidification time with a power law evolution  $q_{\max} \sim t^{-\alpha}$ . The increase of  $q_{\max}$  lead to the decrease of the distance  $R$  between particles ( $R = 2\pi/q_{\max}$ ), which indicates an increase of the number of particles. Therefore, the first pH range (from pH 4.6 to 4.2) in Fig. III.10 seems to correspond to a nucleation phase. The second pH range (from pH 4.2 to 3.9) at which  $q_{\max}$  decreased corresponds to a growth of particles. In this pH range, BLG/FII mixture has higher  $q_{\max}$  values as compared to BLG/FI system. This feature is in agreement with a lower size of BL/FII particles.



**Fig. III.10.** Evolution of the maximum wave vector  $q_{\max}$  ( $\mu\text{m}^{-1}$ ) as a function of pH for  $\beta$ -lactoglobulin (BLG) / Acacia Gum (TAG) or Arabinogalactan-peptide (FI) or Arabinogalactan-protein (FII) mixed dispersions at 0.1wt% total biopolymer concentration and Pr:Pol weight ratio of 2:1. (●) BLG/TAG, (○) BLG/FI, (■) BLG/FII. Each experiment was made in triplicate.

As stated above,  $q_{\max}$  decreases with a power law  $q_{\max} \sim t^{-\alpha}$  below  $\text{pH} \sim 4.2$  (Fig. III.11). Interestingly, the evolution of  $q_{\max}$  with time for BLG/FII mixture allowed to observe a scattering maximum at lower time values than with the two other blends. Therefore, faster complexation/phase separation rate may occur in BLG/FII mixture, in agreement with the rate intensity change ( $dI_{46}/dt$ ). A lower power law exponent of  $0.61 (\pm 0.05)$  was obtained as compared to  $\sim 0.7 (\pm 0.04)$  for BLG/FI mixture. These exponent values indicate that phase separation is driven by both hydrodynamic and diffusion phenomena, in relation with particles velocity fluctuations and coalescence<sup>23</sup>. Regarding the shift of BLG/FII curves to lower time values, the lower  $\alpha$  value can not reflect a slower coarsening rate of particles. The difference in power law exponents may result from the different time range where a maximum was observed, which affects the exponent value.



**Fig. III.11.** Evolution of the maximum wave vector  $q_{\max}$  ( $\mu\text{m}^{-1}$ ) as a function of time for  $\beta$ -lactoglobulin (BLG) / Acacia Gum (TAG) or Arabinogalactan-peptide (FI) or Arabinogalactan-protein (FII) mixed dispersions at 0.1wt% total biopolymer concentration and Pr:Pol weight ratio of 2:1. ( $\bullet$ ) BLG/TAG, ( $\circ$ ) BLG/FI, ( $\blacksquare$ ) BLG/FII. Continues lines correspond to weighted curve fits using a power law function. Each experiment was made in triplicate.

The parameter  $\gamma$  corresponds to the compacity of aggregates, which is related to the scattered light intensity by the following relationship:

$$I(q) = K \theta^\gamma \quad \text{Eq. III.3}$$

where  $K$  is a constant and  $\theta$  the scattering angle. In the particular case of a rough phase-separated interface and for slope values between  $\sim 3$  and  $4$ , the scattered light intensity is related to the exponent  $\gamma$  by the following relationship:

$$I(q) \sim q^{(6-\gamma)} \quad \text{Eq. III.4}$$

The morphology of the phase separated interfaces was analyzed by determining the exponent  $\gamma$  of the power law  $I(q) \sim q^{-\gamma}$  at high  $q$  values. Fig. III.12 illustrates the  $\gamma$  dependence vs pH.

This curve was also used to determine the different structural transitions<sup>23</sup>. The three mixtures showed the same curve shape of  $\gamma$  vs pH and nearly the same transition pH values. Five transition pH were identified from the evolution of  $\gamma$  with pH for BLG/AG systems.

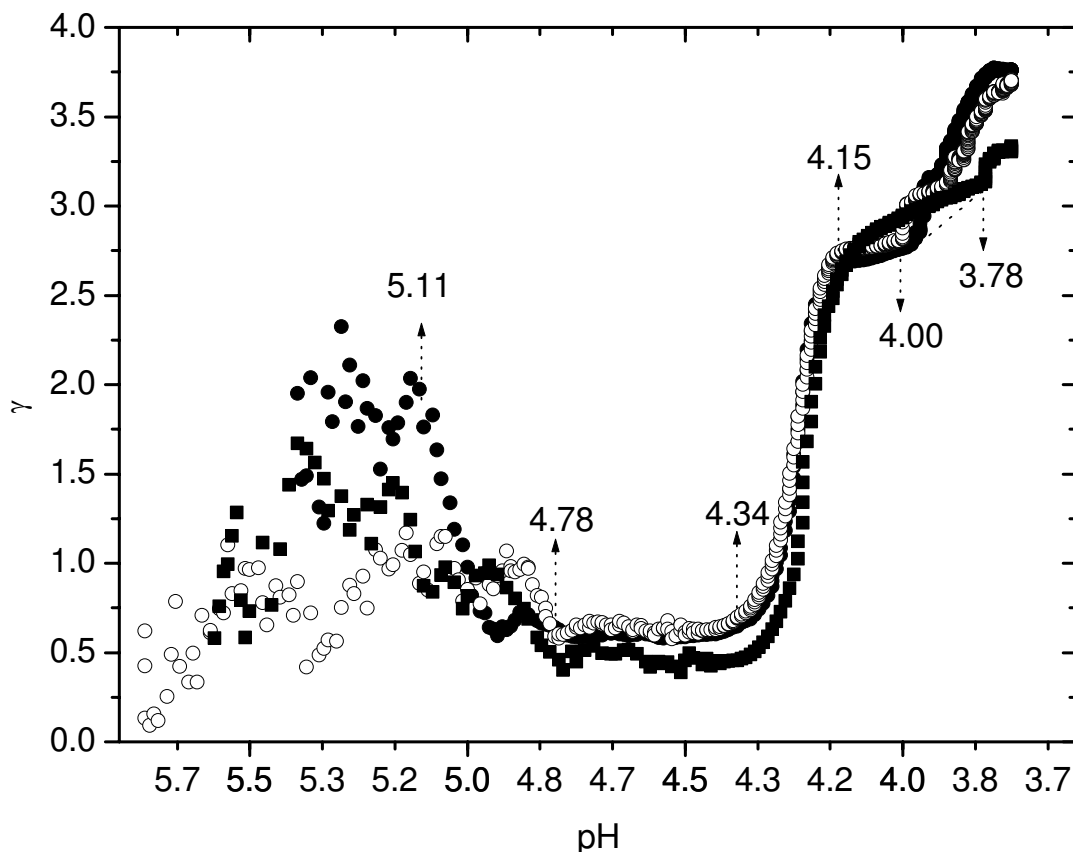


**Fig. III.12.** Evolution of the exponent  $\gamma$  obtained from the scattering profiles  $I(q) \sim q^{-\gamma}$  ( $3.546 < q < 10.414 \mu\text{m}^{-1}$ ) of the  $\beta$ -lactoglobulin (BLG) / Acacia Gum (TAG) or Arabinogalactan-peptide (FI) or Arabinogalactan-protein (FII) mixed dispersions at 0.1wt% total biopolymer concentration and Pr:Pol weight ratio of 2:1. (●) BLG/TAG, (○) BLG/FI, (■) BLG/FII. Each experiment was made in triplicate.

After a relatively constant evolution of  $\gamma$  to reach  $\sim 2$ , 1.2 and  $\sim 1$  in BLG/TAG, BLG/FI and BLG/FII mixtures, the first transition was observed at pH 5.11 ( $\pm 0.04$ ). With decreasing pH,  $\gamma$  decreased gradually to reach 0.6 ( $\pm 0.02$ ) until the second transition at pH 4.78 ( $\pm 0.03$ ) occurred.  $\gamma$  values then remained constant at 0.75 ( $\pm 0.02$ ) until the appearance of the third transition at pH 4.34 ( $\pm 0.02$ ). Below pH 4.3,  $\gamma$  abruptly increased to reach 2.5 ( $\pm 0.05$ ) at pH 4.15 ( $\pm 0.05$ ), which corresponds to the fourth transition. At this pH, the exponent values reveal the presence of compact aggregates in all dispersions. Below pH 4.0,  $\gamma$  then suddenly increased to reach the values of  $\sim 2.76$ , 2.82 and  $\sim 3.00$  in BLG/TAG, BLG/FI and BLG/FII mixtures. As shown above in size curve that coacervation occurs at pH  $\sim 4.2$ , these values can

be attributed to the appearance of spherical particles the so-called coacervates. The higher  $\gamma$  values for BLG/FII mixture in the 4.13-4.0 pH range, indicates the appearance of higher compacity of particles and can be due to a faster coarsening rate of complexes or different structures present. The last transition pH 3.78 ( $\pm$  0.03) was only observed in BLG/FII mixture, in agreement with this determined at pH 3.8 by  $I_{46}$  and by Sanchez *et al.* (2006). However, BLG/FII displayed relatively lower  $\gamma$  values below pH  $\sim$ 4.0. For example, at pH 3.75, we determined the surface dimensions of 2.7 for BLG/FII, 2.3 for BLG/TAG and 2.4 for BLG/FI mixtures. This feature reflects the presence of more heterogeneous interfaces in BLG/FII mixture than in BLG/FI and BLG/TAG systems where they were smoother.

Six pH-delimited phase transitions in all BLG/AG mixtures were identified from light scattering and electrophoretic mobility measurements (Tab. III.1). For each method, the pH values were determined graphically as the intersection point of two tangents to the curve. Each pH corresponds to the average of three independent values with a standard deviation less than 1%. The physical meanings of these pH-delimited phase transitions are explained below in relation with Mekhloufi *et al.* (2005):

(i) *from pH 5.8 to pH 5.2*: constant values of all static light scattering parameters (e.g.  $I_{46}$ ,  $dI_{46}/dt$ ) mean that biopolymers coexisted without interaction.

(ii) *from pH 5.2 to pH 4.9*: beyond pH 5.2,  $I_{46}$ ,  $dI_{46}/dt$ , and  $d$  slowly increased. Hence, local structural inhomogeneities appeared in mixed dispersions. pH 5.2 ( $\pm$  0.5) would correspond to the initial pH of intrapolymeric (soluble: as  $\mu_E$  is negative in this pH range) complex formation (**pH<sub>sc</sub>**).

(iii) *from pH 4.9 to pH 4.4*:  $I_{46}$  and  $dI_{46}/dt$  monotonically increased until pH 4.8 ( $\pm$  0.1), in agreement with the growth of structural entities present in the mixtures.  $\mu_E$  gradually decreased as expected from the increasing charge neutralization until pH  $\sim$ 4.4. In the soluble complex region, a decrease in pH leads to an increase in the concentration of intrapolymer complexes, followed by formation of interpolymer complexes. pH  $\sim$ 4.8 would correspond to the pH of aggregation of complexes (**pH<sub>ca</sub>**). pH  $\sim$ 4.4 (in BLG/TAG and BLG/FI mixtures) and pH  $\sim$ 4.24 (in BLG/FII mixture) would correspond to the onset of phase separation (**pH<sub>ps</sub>**) when interpolymeric complexes were formed and a maximum of scatterer particles in the mixtures were present.

**Tab. III.1.** Characteristic pH of structural transitions in BLG/TAG, BLG/FI and BLG/FII mixed dispersions at a total biopolymer concentration of 0.1wt% and a protein:polysaccharide (Pr:Pol) weight ratio of 2:1, determined by different parameters derived from light scattering and electrophoretic mobility measurements. Each value is the average of three independent experiments.

		pH <sub>sc</sub>	pH <sub>ca</sub>	pH <sub>ps</sub>	pH <sub>coa</sub>	pH <sub>neut</sub>
<b>BLG/TAG</b>	<b>d</b>	5.18		4.43	4.19	
	<b>μ<sub>E</sub></b>			4.41		3.80
	<b>I<sub>46</sub></b>	5.06		4.53	4.24	
	<b>dI<sub>46</sub>/dt</b>	5.06	4.71	4.40		
	<b>γ</b>	5.11	4.78	4.34	4.20	
	<b>averaged pH</b>	<b>5.10</b>	<b>4.75</b>	<b>4.42</b>	<b>4.21</b>	<b>3.80</b>
<b>BLG/FI</b>	<b>d</b>	5.18		4.41	4.18	
	<b>μ<sub>E</sub></b>			4.45		3.90
	<b>I<sub>46</sub></b>	5.05		4.52	4.20	
	<b>dI<sub>46</sub>/dt</b>	5.03	4.73	4.45	4.24	
	<b>γ</b>	5.09	4.78	4.34	4.22	
	<b>averaged pH</b>	<b>5.09</b>	<b>4.76</b>	<b>4.43</b>	<b>4.21</b>	<b>3.90</b>
<b>BLG/FII</b>	<b>d</b>	5.00		4.25	4.00	
	<b>μ<sub>E</sub></b>			4.20		4.20
	<b>I<sub>46</sub></b>	4.92		4.16		
	<b>dI<sub>46</sub>/dt</b>	4.95	4.69	4.31		
	<b>γ</b>	4.96	4.77	4.28	4.10	
	<b>averaged pH</b>	<b>4.96</b>	<b>4.73</b>	<b>4.24</b>	<b>4.05</b>	<b>4.20</b>
<b>Averaged pH</b>		<b>5.05</b>	<b>4.74</b>	<b>4.37</b>	<b>4.17</b>	<b>3.96</b>

d: particles hydrodynamic diameter determined from DLS; μ<sub>E</sub>: electrophoretic mobility (e.m.u., μm·cm·s<sup>-1</sup>·V<sup>-1</sup>); I<sub>46</sub>: scattered light intensity at 46° scattering angle; dI<sub>46</sub>/dt: I<sub>46</sub> first derivative; γ: exponent derived from the scattering profile I(q) vs q<sup>-γ</sup> at high q range (3.546 < q < 10.414 μm<sup>-1</sup>). pH<sub>sc</sub>: pH of formation of soluble complexes, pH<sub>ca</sub>: pH of complex aggregation, pH<sub>ps</sub>: pH of phase separation, pH<sub>coa</sub>: pH of coacervate formation (coacervation), pH<sub>neut</sub>: pH of charges neutralization.

(iv) from pH 4.4 to pH 4.2: in this pH range, I<sub>46</sub> and dI<sub>46</sub>/dt strongly increased, involving the acceleration of complexation. In addition, a maximum in the evolution of these parameters was observed at pH 4.2 (± 0.05). Regarding the size of particles in this pH range (> 500 nm, see Fig. III.1) and based on a number of studies about complex coacervation in BLG/TAG system<sup>17,23,24,28,31</sup>, pH ~4.2 (for BLG/TAG) would correspond to the onset of complex coacervation (pH<sub>coa</sub>) where coacervates are formed following the structuring of strongly aggregated complexes.

(v) from pH 4.2 to pH 4: within this pH range, I<sub>46</sub> and dI<sub>46</sub>/dt slightly decreased. Soluble complexes seemed still present in BLG/TAG and BLG/FI systems in this pH range, since μ<sub>E</sub> was negative. However, from pH ~4.19 μ<sub>E</sub> approaches zero in BLG/FII dispersion, which indicates the presence of neutral and insoluble complexes in this case. This difference

between mixtures could be due to the favorable structural properties of FII for complexation (accessibility of charges, radius of gyration, molecular weight, number of charges).

(vi) *from pH 4 to pH 3.7*:  $I_{46}$  and  $dI_{46}/dt$  gradually decreased, in relation with a decrease of particles size and number in the dispersions. It must be noticed that BLG/FII dispersion shows an additional transitional point at pH  $\sim 3.8$ , from which  $I_{46}$  decreased strongly. pH  $\sim 3.8$  and  $\sim 3.9$  would correspond to the pH of neutralization of charges ( $pH_{neut}$ ) in BLG/TAG and BLG/FI mixtures. Further decrease in pH redissolves the coacervate.

The present work allowed us to identify five remarkable pH of structural transitions ( $pH_{sc}$ ,  $pH_{ca}$ ,  $pH_{ps}$ ,  $pH_{coa}$  and  $pH_{neut}$ ). Results showed lower pH values for BLG/FII dispersion from  $pH_{ps}$ , as compared to BLG/FI system. Whereas, similar structural transitions in all systems were determined during the complexation. It may be expected that the decrease of strength of interaction below the  $pH_{ps}$  promoted to detect the role of the different intrinsic properties of AG, i.e. its larger radius of gyration that would allow to the formation of larger particles. Our pH values agree to those determined by Mekhloufi *et al.* (2005). However, these authors identified one additional pH for BLG/TAG system using complementary methods,  $pH_{pct}$  at 4.77 which corresponds to a pH where conformational changes of BLG were observed using circular dichroism. A +0.2 shift of our pH values compared to those of Mekhloufi *et al.*, was observed. This difference is due to the dialysis of BLG and AG that removes salt ions, which are able to screen interactions.



### III.4. Conclusions

Effects of Acacia gum molecular polydispersity on complex coacervation with BLG were investigated. Slow acidification using glucono-delta-lactone of three mixed dispersions, BLG/TAG, BLG/FI and BLG/FII, was performed at a Pr:Pol mixing weight ratio of 2:1 in order to follow *in situ* phase ordering transitions during complexation/coacervation using static, dynamic light scattering and electrophoretic mobility methods. Nucleation and growth (NG) was the mechanism of phase separation in all mixtures. In the three mixed dispersions, five pH-delimited structural transitions were determined:  $pH_{sc}$ : pH of formation of soluble complexes,  $pH_{ca}$ : pH of complex aggregation,  $pH_{ps}$ : pH of phase separation,  $pH_{coa}$ : pH of coacervate formation (coacervation) and  $pH_{neut}$ : pH of charges neutralization. In the  $pH_{sc}$ - $pH_{ps}$  range, all systems exhibited similar transition points. From  $pH_{ps}$ , BLG/FII system exhibited lower pH of structural transitions as compared to BLG/FI dispersion, may be due to the decrease of strength of interaction between biopolymers, which highlight the effect of AG characteristics. All the pH of structural transitions were carried out at the approximately same Pr:Pol charge ratios in the three systems. Regarding the higher number of charges of FII, it was concluded that it induced faster rate of phase separation than FI. In addition, FII led to the formation of smaller particles, which exhibit more heterogeneous interfaces upon the occurrence of phase separation. The present work probed the effect of TAG polydispersity on the pH-induced complexation/coacervation mechanism with BLG. The use of complementary methods such as spectroscopic techniques would be necessary to better explain the structural transitions at different scale. An extensive study of the protein-to-polysaccharide ratio could be an approach to better understand both the structural role of AG molecules and the transition occurring between complexation and coacervation. Regarding the favorable structural features of FII (higher molecular weight and number of charges); it may be expected to induce faster phase separation kinetics than FI, at the same mixing charge ratio. Thus, as a prospect, mixed dispersions at the same Pr:Pol charge ratio must be prepared for a better comparison between mixtures.

### III.5. References

- <sup>1</sup> Schmitt, C.; Sanchez, C.; Despond, S.; Renard, D.; Thomas, F.; Hardy, J. *Food Hydrocolloids*, **2000**, 14, 403.
- <sup>2</sup> Tribet, C.; Porcar, I.; Bonnefont, P.A.; Audebert, R. *Journal of Physical Chemistry B*, **1998** 102, 1327.
- <sup>3</sup> Tsuchida, E. *Journal of Molecular Science – Pure Applied Chemistry*, **1994**, A31, 1.
- <sup>4</sup> Kaibara, K.; Watanabe, T.; Miyakawa, K. *Biopolymers*, **2000**, 53, 369.
- <sup>5</sup> Burgess, D.J. In *Macromolecular Complexes in Chemistry and Biology*; Dubin, P.L., Bock, J., Davis, R., Schulz, D.N., Thies, C., Eds.; Springer Verlag: Berlin, **1994**, 281.
- <sup>6</sup> Sterge, M.A.; Dubin, P.L.; West, J.S.; Flinta, C.D. In *Protein purification: from molecular mechanisms to large scale processes*; Ladisch, M., Wilson, R.C., Painton, C.C., Builder, S.E., Eds.; ACS Symposium Series: Washington DC, **1990**; Vol. 427, p 66.
- <sup>7</sup> Weinbreck, F.; Nieuwenhuijse, H.; Robijn, G.W.; de Kruif, C.G. *Langmuir*, **2003**, 19, 9404.
- <sup>8</sup> Zancong, S.; Mitragotri, S. *Pharmaceutical Research*, **2002**, 19, 391.
- <sup>9</sup> Prokop, A.; Kozlov, E.; Newman, G.W.; Newman, M. *Journal of Biotechnology and Bioengineering*, **2002**, 78, 459.
- <sup>10</sup> Kabanov, V.A.; Evdakov, V.P.; Mustafaev, M.I.; Antipina, A.D. *Journal of Molecular Biology*, **1977**, 11, 582.
- <sup>11</sup> Sanchez, C.; Paquin, P. In *Food Proteins and Their Applications*; Damodaran, S.; Paraf, A.; Dekker Marcel; Eds.; Inc.: New York, **1997**, p 503.
- <sup>12</sup> Tolstoguzov, V.B. *International Review of Cytology*, 2000, 192, 3.
- <sup>13</sup> Veis, A.; Aranyi, C. *Journal of Physical Chemistry*, **1960**, 64, 1203.
- <sup>14</sup> Xia, J.; Dubin, P.L.; Kim, Y.; Muhoberac, B.B.; Klimkowski, V.J. *Journal of Physical Chemistry*, **1993**, 97 4528.
- <sup>15</sup> Mattisson, K.W.; Wang, Y.; Grymonpré, K.; Dubin, P.L. *Macromolecules symposium*, **1999**, 140, 53.
- <sup>16</sup> Dubin, P.L.; Murell, J.M. *Macromolecules*, **1998**, 21, 2291.
- <sup>17</sup> Park, J.M.; Muhoberac, B.B.; Dubin, P.L.; Xia, J. *Macromolecules*, **1992**, 25, 290.
- <sup>18</sup> Mattison, K.W.; Brittain, I.J.; Dubin, P.L. *Biotechnology Progress*, **1995**, 11, 632.
- <sup>19</sup> Ibanoglu, E. *Journal of Food Engineering*, **2001**, 52, 273.
- <sup>20</sup> Weinbreck, F.; de Vries, R.; Schrooyen, P.; de Kruif, C.G. *Biomacromolecules*, **2003**, 4,

---

293.

- <sup>21</sup> Girard, M.; Turgeon, S.L.; Gauthier, S.F. *Food Hydrocolloids*, **2002**, 16, 585.
- <sup>22</sup> Girard, M.; Turgeon, S.L.; Gauthier, S.F. *Journal of Agricultural and Food Chemistry*, **2003**, 51, 4450.
- <sup>23</sup> Mekhloufi, G.; Sanchez, C.; Renard, D.; Guillemin, S.; Hardy, J. *Langmuir*, **2005**, 21, 386.
- <sup>24</sup> Sanchez, C.; Mekhloufi, G.; Renard, D. *Journal of Colloid and Interface Science*, **2006**, 299, 867.
- <sup>25</sup> Snowden, M.G.; Phillips, G.O.; Williams, P.A. *Food Hydrocolloids*, **1987**, 1, 291.
- <sup>26</sup> Renard, D.; Lavenant-Gourgeon, L.; Ralet, M.; Sanchez, C. *Biomacromolecules*, **2006**, 7, 2637.
- <sup>27</sup> Bungenberg de Jong, H.G. *In Colloid Science; H.G. Kruyt; Eds.; Elsevier: Amsterdam, Vol. 2, 1949*, p 232.
- <sup>28</sup> Schmitt, C.; Sanchez, C.; Thomas F.; Hardy, J. *Food Hydrocolloids*. **1999**, 13, 483.
- <sup>29</sup> Dickinson, E. *Royal Society of Chemistry*, **1992**, p 77.
- <sup>30</sup> Xia, J.; Dubin, P.L. *In: Macromolecular Complexes in Chemistry and Biology, Springer Verlag: Berlin, 1994*, p 247.
- <sup>31</sup> Idris, O.H.M.; Williams, P.A.; Phillips, G.O. *Food Hydrocolloids*, **1998**, 12, 379.
- <sup>32</sup> Picton, L.; Battaille, I.; Muller, G. *Carbohydrate Polymers*, **2000**, 42, 23.
- <sup>33</sup> Leon de Pinto, G.; Martinez, M.; Sanabria, L. *Food Hydrocolloids*, **2001**, 15, 461.
- <sup>34</sup> Redgwell, R.J.; Schmitt, C.; Beaulieu, M.; Curti, D. *Food Hydrocolloids*, **2004**, 19, 1005.
- <sup>35</sup> Randall, R.C.; Phillips, G.O.; Williams, P.A. *Food Hydrocolloids*, **1989**, 3, 65.
- <sup>36</sup> Osman, M.E.; Menzies, A.R.; Martin, B.A.; Williams, P.A.; Phillips, G.O.; Baldwin, T.C. *Phytochemistry*, **1995**, 38, 409.
- <sup>37</sup> Fenyo, J. C.; Vandavelde, M. C. *Gums and Stabilizers for the Food Industry 5, Royal Society of Chemistry*, **1989**, p 17.
- <sup>38</sup> Tromp, R.H. Jones, R.A.L. *Macromolecules*, **2006**, 29, 8109.
- <sup>39</sup> Skinner, E.R.; Kertesz, Z.I. *Journal of Polymer Science*, **2003**, 149, 99.
- <sup>40</sup> Miura, N; Dubin, P.L. Moorefield, C.N.; Newkome G.R. *Langmuir*, **1999**, 15, 4245.
- <sup>41</sup> Girard, M.; Sanchez, C.; Laneuville, S.I.; Turgeon, S.L.; Gauthier, S.F. *Colloids and Surfaces B: Biointerfaces*, **2004**, 35, 15.



## Chapter IV

# Control of the strength of interactions between $\beta$ -lactoglobulin and Acacia gum molecular fractions

### Abstract

The complexation/coacervation mechanism between  $\beta$ -lactoglobulin (BLG) and Acacia gum (TAG) or its two major molecular fractions, FI and FII, was investigated by changing the binding strength through the protein:polysaccharide weight ratio (Pr:Pol) and total biopolymer concentration (Cp) using Small Angle static Light Scattering (SALS) and Dynamic Light Scattering (DLS), Granulo-Polarimetry and optical microscopy. All techniques showed a strong and complex dependence on Pr:Pol and Cp of the phase separation mechanism. SALS and DLS patterns showed that increasing the Pr:Pol ratio favors interactions and lead to a rapid complexation or phase separation. Moreover, it was emphasized that the increase of (Pr:Pol) ratio (until a certain value) allowed to observe different particles size in the three mixtures. At 2:1 mixing weight ratio, BLG/FII system displayed smaller particles as compared to BLG/FI dispersion. Above the mixing weight ratio of 2:1, the complexation resulted in the association of large aggregates in BLG/FII system as compared to BLG/FI system. This feature may indicate that increasing the strength of interaction (at 2:1) masked the specific role of FII that in theory would lead to the formation of larger particles. BLG/FII mixed dispersions exhibited favorable complexation whatever the ratio due to both the higher charge density and higher accessibility of charges of FII as compared to FI. SALS patterns revealed also that at a given (Pr:Pol) ratio (above 2:1) and pH, BLG/FII complexes had higher compacity as compared to BLG/FI ones. A gradual increase of the exponent  $\gamma$ , in the scattering profiles  $I(q) \sim q^{-\gamma}$  at high  $q$  range, until reaching the Porod regime ( $\gamma = 4$ ) was observed with increasing ratio in BLG/FII system. This indicates a gain in the interfaces homogeneity. By the contrary,  $\gamma$  in BLG/FI mixture decreases above a Pr:Pol ratio of 16:1, in agreement with lower particles compacity and more heterogonous interface. This result shows that decreasing the binding strength can highlight the structural role of each AG fraction. Granulo-Polarimetry, in concentrated medium, showed the appearance of smaller BLG/FII particles with lower concentration in dispersions as compared to BLG/FI particles, in agreement with DLS results. Before the onset of coacervation ( $\text{pH}_{\text{mis}}$ ), the particle size remained constant in BLG/TAG and BLG/FII systems. Moreover, the scatterer volume fraction showed a maximum of evolution at  $\text{pH}_{\text{mis}}$  between two zones with decreasing the pH. This feature revealed that the coacervation in mixtures may follow simultaneously the growth and dissociation of particles. By optical microscopy, it was also observed larger BLG/FI particles and that increasing the total amount of biopolymers in dispersions did not affect the phase separation mechanism, since the structural transitions remained constant.



## IV.1. Introduction

The influence of various parameters on the electrostatic interactions and self-association in protein-polyelectrolyte mixtures was largely investigated<sup>1,2,3,4,5,6,7,8,9,10,11,12,13</sup>. Among overall parameters, it is now well known that charge density, pH, ionic strength and polymer flexibility are the main that can regulate the strength of electrostatic interactions<sup>14,15,16,17,18,19,20</sup>. At very low charge densities, coacervation is suppressed<sup>21</sup> and at very high charge densities, precipitation may occur<sup>22</sup>. The representative molecular parameters are primarily the weight average molecular weight ( $M_w$ ), the radius of gyration ( $R_G$ ) or the hydrodynamic radius ( $R_h$ ) and the second virial coefficient,  $A_2$ , which is the second coefficient in the expansion of the chemical potentials of both solvent and biopolymer on a biopolymer concentration<sup>23</sup>. The sign and the magnitude of  $A_2$  provide the information on an initial deviation of a macromolecular solution from the ideal state and reflect the nature and the intensity of the intermolecular pair interactions (biopolymer-biopolymer and biopolymer-solvent) in solutions (see chapter I)<sup>24</sup>.

The structural transitions depend on the listed several parameters, but do not depend – or very little - on total biopolymer concentration<sup>25</sup>. Mattison *et al.* demonstrated that the biopolymer concentration ( $C_p$ ) only influences the amount of complexes formed and that  $pH_c$  and  $pH_\phi$  values are independent of concentration for a system of BSA-PDADMAC. Nevertheless, the total biopolymer concentration seems to affect the kinetics of complexation between macromolecules and the number of particles formed (Weinbreck *et al.*, 2003). Thus, the effect of  $C_p$  on the strength of electrostatic interactions might appear in a definite  $C_p$  range<sup>26,27</sup>. For the BLG/TAG system, Schmitt *et al.* (2000)<sup>28</sup> found that increasing biopolymer concentration reduces the influence of pH on complex coacervation. Increasing  $C_p$  leads to the formation of more particles due to the increase of the number of ionic pairs between reacting biopolymers<sup>16</sup>.

In the previous chapter, we have focused on the role of TAG molecular fractions in the complexation/coacervation mechanism with BLG. Indeed, little differences were observed between systems studied. This is because the high strength of interaction at which the mixed dispersions were studied (Pr:Pol mixing ratio of 2:1) may hide the influence of the chemical and structural parameters (e.g. pH and  $M_w$ ). From there, the protein:polysaccharide weight

(Pr:Pol) ratio and total biopolymer concentration ( $C_p$ ) were selected to modulate the interaction strength between BLG and AG. Investigations of complexation/coacervation in BLG/TAG, BLG/FI and BLG/FII mixtures were carried out by time-resolved dynamic and static light scattering, electrophoretic mobility and epi-fluorescence optical microscopy. Slow acidification of the mixtures was obtained as a function of time by the hydrolysis of glucono- $\delta$ -lactone in order to induce associative phase separation in diluted (0.1wt %) and concentrated medium (4wt %). By LS and  $\mu_E$ , the turbidity, size and surface charge in mixtures was collected as a function of pH for many Pr:Pol weight ratios: 2:1, 3:1, 4:1, 8:1, 16:1 and 40:1 in order to characterize the pH-induced structural changes in all mixed dispersions at 0.1wt %. The Granulo-Polarimetry method was used to follow structural transitions and size changes during acidification at 2:1 Pr:Pol weight ratio and 4wt% total biopolymer concentration. Experiments were only made at this concentration because the technique is adapted to dense media and limits then the measurement at lower amount of biopolymers. Epi-fluorescence optical microscopy allowed to follow the microstructural changes in mixtures as a function of pH at Pr:Pol mixing ratio of 2:1, and 0.1 and 4wt % total biopolymer concentrations.



## IV.2. Experimental section

### IV.2.1. Materials

*β-Lactoglobulin powder* (lot JE001-3-922) was purchased from Davisco Foods International Inc. (Lesueur, MN, USA). The powder composition was (g per 100 g): 93.6% protein (N x 6.38), 4.9% moisture and 1.5% ash (0.017% Ca<sup>2+</sup>, 0.003% Mg<sup>2+</sup>, 0.008% K<sup>+</sup>, 0.9 Na<sup>+</sup>, 0.03% Cl<sup>-</sup>). *Acacia gum powder* from Acacia Senegal trees (lot no 97 J 716) was a gift from CNI Company (Rouen, France). The powder composition was (g per 100 g): 90% polysaccharide, 6.6% moisture, 0.3% nitrogen and 3.1% ash (0.2% Mg<sup>2+</sup>, 0.61% Ca<sup>2+</sup>, 0.032% Na<sup>+</sup> and 0.9% K<sup>+</sup>). TAG powder was extensively dialyzed against distilled water and freeze-dried.

*TAG molecular fractions*. The total Acacia gum powder was fractionated using hydrophobic interaction chromatography (HIC) (Renard *et al.*, 2006). The appropriate fractions were pooled, extensively dialyzed against distilled water and freeze-dried for further analysis. In the present study, the two major molecular fractions in weight i.e. *Arabinogalactan-peptide* (FI) and *Arabinogalactan-protein* (FII) molecular fractions were used. FI represented 88.5wt% of TAG with a molecular weight of  $2.86 \cdot 10^5$  g/mol while FII represented 10.5wt% of TAG with a molecular weight of  $1.86 \cdot 10^6$  g/mol.

*Glucono-δ-lactone*, GDL, (lot 052K0031, Calbochiem, Darmstadt, Germany) is an ester of gluconic acid obtained by oxidative fermentation of D-glucose. *Sodium hydroxide and hydrochloric acid* were of analytical grade (Fischer Scientific SA, Elancourt, France).

### IV.2.2. Preparation of β-Lactoglobulin (BLG), Acacia gum (AG) stock dispersions and BLG/AG mixed dispersions

Aqueous stock dispersions of BLG and AG at 0.12 and 4.6wt% total biopolymer concentration were prepared by dissolving biopolymer powders in ultra pure deionized water (resistivity: 18 mΩ) (Purite, Fischer Scientific, England) under gentle stirring at 20±1 °C for at least 2 h. The pH of the BLG dispersion was adjusted to 5 (pH corresponding to the lowest

BLG solubility) with 1N HCl. 170  $\mu$ l of 0.1N NaOH were added to AG solution in order to reach a pH value of  $\sim$  7.00. The dispersions were stored at  $4\pm 1$  °C during 18h to allow good hydration of biopolymers. The stock dispersions were centrifuged during 40min at 10 000g to remove insoluble matter and air bubbles. The concentration of BLG dispersion was checked by measuring absorbance at 278 nm (Ultrospec 4000 UV/Visible, Pharmacia Biotech, England), using the specific extinction coefficient of  $9.2 \text{ dl.cm}^{-1}.\text{g}^{-1}$  determined experimentally. The absorbance at 278 nm was corrected for turbidity and the BLG dispersion concentration was finally adjusted to 0.1wt%. The pH of the BLG dispersion was then adjusted to 7.30 using 0.1 and 1N NaOH.

BLG/TAG, BLG/FI and BLG/FII mixed dispersions were prepared by adding gum dispersion to BLG dispersion at protein to polysaccharide (Pr:Pol) weight ratios of 2:1, 3:1, 4:1, 8:1, 16:1 and 40:1 (see the following figures). The blends were gently stirred for 30min at room temperature. pH of the blends was of 7.30 at the end of the stirring period. Mixed dispersions were filtered through 0.22 $\mu$ m syringe filter (Millipore, Bedford, USA). 0.11 wt% (at Cp of 0.1wt%) and 2 wt% (at Cp of 4wt%) of glucono-delta-lactone (GDL) was then added to the blends and mixed for 5min. In aqueous medium, GDL is hydrolyzed until an equilibrium is reached between gluconic acid and GDL. Gluconic acid releases protons and gluconate in the medium. This proton release leads to a slow acidification of the dispersions.

### **IV.2.3. Dynamic light scattering**

A Nanosizer ZS (HPPS 5001, Malvern Instrument, England) was used to follow the evolution of the size of particles in BLG/TAG, BLG/FI and BLG/FII mixed dispersions during acidification at Cp of 0.1wt%. The apparatus is equipped with a 4 mW He-Ne laser (633 nm), a measurement cell, a photomultiplier and a correlator. Samples were placed in vertical cylindrical cuvettes (10 mm-diameter).

Measurements were performed at a scattering angle of  $173^\circ$  relative to the source using an avalanche photodiode detector, at room temperature ( $23 \pm 2^\circ\text{C}$ ). The pattern allows considerable reduction of the signal due to multiple scattering events and enables measurements in slightly turbid media (NIBS technology). Intensity fluctuations were recorded every 10 s during 60 min, then the corresponding autocorrelation functions  $g_2(t)$  were analyzed by the Cumulant method (integrated in the Malvern Zetasizer software) in order to

determine the distribution of translational diffusion coefficients,  $D_T$ . The  $D_T$  parameter is related to the hydrodynamic radius ( $R_h$ ) of particles through the Stokes-Einstein relationship:

$$D_T = \frac{k_B T}{6\pi\eta R_h} \quad \text{Eq. IV.1}$$

where  $\eta$  is the solvent viscosity and  $k_B T$  the thermal energy.

Results from the Cumulant method allows the determination of both  $R_h$  distribution and respective amplitude of each population. In the present study, we calculated the hydrodynamic diameter (“z-averaged” diameter) of the biopolymers and complexes. The objects were considered as spheres and then the hydrodynamic diameter corresponds simply to  $2xR_h$ .

#### IV.2.4. Electrophoretic mobility measurements ( $\mu_E$ )

Electrophoretic mobility measurements ( $\mu_E$ ) were performed on the same apparatus than in the section III.2.3 by means of laser Doppler electrophoresis. The sample with a Cp of 0.1wt% was put in a standard capillary electrophoresis cell equipped with gold electrodes. Measurements were recorded every 10 s during 60 min. Measurements on control AG dispersions were performed at 1 wt% to ensure a good signal to noise ratio. Measurements on control dispersions (BLG) were performed at 0.066, 0.075, 0.08, 0.088, 0.094 and 0.098 wt% (BLG concentration in the blend) for the Pr:Pol weight ratios of 2:1, 3:1, 4:1, 8:1, 16:1 and 40:1, respectively. For the purposes of clarity, electrophoretic mobility units ( $\mu\text{m.cm.s}^{-1}.\text{V}^{-1}$ ) will be referred to e.m.u. in the following.

#### IV.2.5. Small Angle Static Light Scattering (SALS)

The pH-induced structural and phase transitions of mixtures at Cp of 0.1wt% were followed during 2 h with a measurement step of 10 sec using SALS. Light scattering experiments were carried out using a Mastersizer S long bench (Malvern Ltd., U.K.). A He-Ne laser light ( $\lambda = 632.8$  nm) was passed through a 0.5-mm-width measurement cell (Malvern Ltd) in which the mixed dispersions were injected using a syringe. The beam was converged by a reverse Fourier 300-mm focusing lens. A series of 37 detectors covering the scattering wave vector  $q$

range  $2.1 \times 10^{-2}$  -  $10.414 \mu\text{m}^{-1}$  collected the scattered light. The resulting scattered intensity was corrected for turbidity according to the relationship:

$$I_c(\tau) = I_m(\theta) \exp(\tau d / \cos \theta) [\tau d (\cos^{-1} \theta - 1)] \{ \exp[\tau d (\cos^{-1} \theta - 1)] - 1 \} - 1 \quad \text{Eq. IV.2}$$

with  $\tau d = -\ln T(t)$

where  $I_c$  and  $I_m$  are respectively the corrected and measured scattered intensity distributions,  $\theta$  the scattering angle,  $d$  the sample thickness,  $\tau$  the turbidity and  $T(t)$  the transmittance of the sample at a given time  $t$ . The corrected scattered intensity  $I_c$  will be described as  $I(q)$  hereafter with  $I_{46}$  corresponding to the intensity recorded at the highest  $q$  value ( $q = 10.414 \mu\text{m}^{-1}$ ). This highest  $q$  value corresponds to a scattering angle  $\theta$  of  $46^\circ$  at which smaller structural entities can be detected by the spectrometer. Scattering profiles,  $I(q)$  vs  $q$ , were fitted with polynomial functions using Origin 7.5 software (OriginLab co., Northampton, MA, USA) and xlx-trfun freeware (Advanced Systems Design and Development, Red Lion, PA, USA), in order to extract relevant structural parameters (the intensity and corresponding wave vector at which a scattering maximum appeared,  $I_{\text{max}}$  and  $q_{\text{max}}$ ).

#### IV.2.6. Granulo-Polarimetry

pH-induced complexation/coacervation of BLG/TAG, BLG/FI and BLG/FII mixtures, at biopolymer concentration of 4wt% (high concentrated dispersion is required by the apparatus), was followed using Granulo-Polarimetry stationary measurements under and without shear. The apparatus was performed on home built equipment at the LEMTA laboratory (INPL, France). The description of the apparatus is reported in reference [29]. An optical measuring path integrated into a commercial rheometer (AR2000 TA) was used for dynamic measurements. The experimental setup consists of a laser (632.8 nm) focalized on sample. A system of anti-reflecting blade and mirrors allows to study the backscattered spot by the sample. This system guides the laser light, and collimates it into the sample. The acquisition is carried out by a numerical camera (1024x1024 pixels 12bits). Images are acquired by a digital image acquisition system (Imasys) controlled by a PC computer, and with a size very large compared to the size of scatterers objects. Ten images are acquired at each acquisition. The image acquisition was carried out every 10 sec during 45 min in a pH range of 4.8-3.8 where the turbidity of mixtures was sufficient to allow measurements ( $I^*$

<5mm). A linear combination between these images gives the characteristic Muller matrices of the medium and allows to determine the photon transport length,  $l^*$ . A method of calculation based on the theory of the propagation of light in turbid media is used to calculate the transport length in the medium. In addition to the determination of the scattered light intensity, the polarization of light is characterized. The polarization of light allows then to determine the size of scatterer objects. To be able to calculate the volume fraction of these objects ( $\phi$ ) based on the measured  $l^*$ , we assumed that the optical properties of complexes are known, i.e.  $m \cong 1.2$ , where  $m$  is the ratio between both refractive index values of BLG and AG. The experiments were made under and without shearing (shear rate was 200 rpm). Shearing was used to prevent the sedimentation of particles that can contribute in the results and limit measurements of  $l^*$  in a narrow pH range. No influence of the shearing on complex coacervation mechanism was observed. Thus, results obtained without shearing will be shown.

#### **IV.2.7. Epi-fluorescence Microscopy**

An epi-fluorescence microscope (Leica DMRB, Wetzlar, Germany) was used to monitor the pH-induced structural changes in BLG/TAG, BLG/FI and BLG/FII mixed dispersions. A 10- $\mu$ l sample was taken from dispersions (at 4wt% total biopolymer concentration) during acidification with GDL and put between glass slides. Pictures were taken by an image processor (Kappa ImageBase 2.5) at x40 magnification. The contrast and the brightness of pictures were processed by the ImageJ freeware (version Beta 1.36) in order to better visualize light fluctuations.

## **IV.3. Results and Discussion**

The objective of this work was to get new insights into the complexation/coacervation mechanism in BLG/AG systems by varying the strength of interactions through the mixing ratio of dispersions. Experiments were done in a range of ratios covering weak and strong interaction forces in order to highlight the role of each Acacia gum molecular fractions in complexation with BLG.

### **IV.3.1. Effect of the Pr:Pol ratio on complexation/coacervation mechanism**

#### **IV.3.1.1. Dynamic light scattering**

Insights into the structure of complexes and coacervates may be obtained from DLS and  $\mu_E$  measurements. The pH dependence of the particles diameter ( $d$ ) for BLG/TAG, BLG/FI and BLG/FII mixed dispersions at different Pr:Pol weight ratios is shown in Fig. IV.1. An increase of  $d$  as a function of decreasing pH is observed whatever the ratio. At a given pH, the size of complexes was higher as a function of the Pr:Pol mixing ratio in all mixtures. We have shown in the previous chapter that  $d$  curves upturned at pH 4.43, 4.41 and 4.25 in BLG/TAG, BLG/FI and BLG/FII mixtures at a Pr:Pol of 2:1. These pH were identified as the onset of phase separation ( $pH_{ps}$ ). With increasing the Pr:Pol weight ratio,  $d$  curves shifted to higher pH, in agreement with the complexation at lower positive charge density of BLG. This is due to the increase of number of positive BLG charges in dispersions.

In order to better evaluate the effect of ratio on the pH-induced size changes in systems, we show in Tab. IV.1 the evolution of  $pH_{ps}$  and the corresponding particle diameter, as a function of the Pr:Pol mixing weight ratio. In all systems, the  $pH_{ps}$  increases as a function of the mixing ratio, except for BLG/FI system at 16:1. At the  $pH_{ps}$ , all systems showed approximately similar size of particles. BLG/FII system displayed lower  $pH_{ps}$  whatever the ratio, in agreement with results obtained in the previous chapter. Overall results shown in Tab. IV.2 will be completely analyzed next.

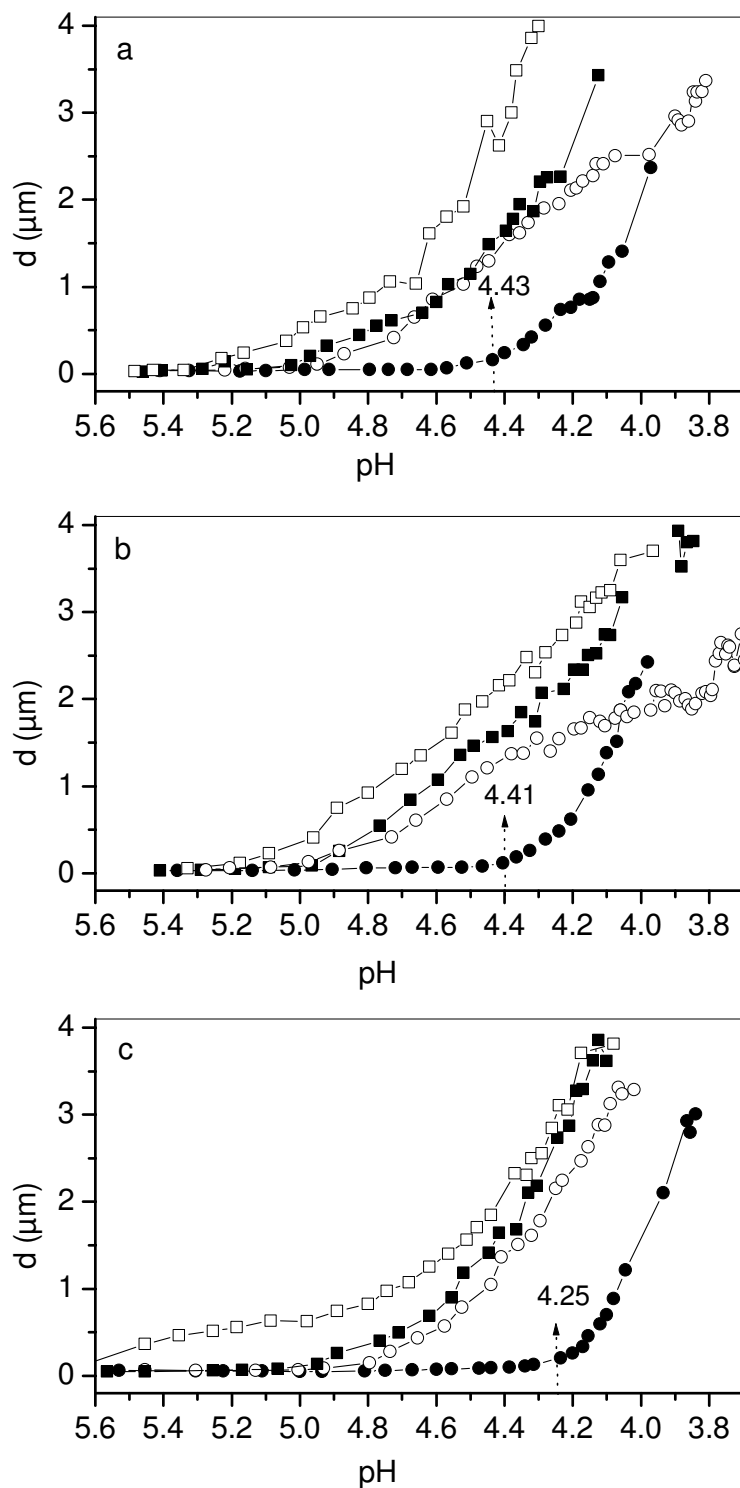


**Fig. IV.1.** Evolution of the particle diameter  $d$  ( $\mu\text{m}$ ) as a function of pH for the BLG/TAG (a), BLG/FI (b) and BLG/FII (c) mixed dispersions at 0.1 wt % total biopolymer concentration and different Pr:Pol weight ratios. (●) 2:1, (○) 4:1, (■) 8:1 and (□) 16:1. Each experiment was made in duplicate.

**Tab. IV.1.** Size of particles,  $d$  ( $\mu\text{m}$ ), determined at both the pH of phase separation ( $\text{pH}_{\text{ps}}$ ) and pH of neutralization ( $\text{pH}_{\text{neut}}$ ) (where  $\mu_{\text{E}}$  is zero e.m.u.) as a function of the Pr:Pol mixing weight ratio.  $r_{\text{neut}}$ : the Pr:Pol charge ratio of neutralization determined at  $\mu_{\text{E}}$  is zero e.m.u.

Pr:Pol weight ratio		$\text{pH}_{\text{ps}}$	$d$ ( $\mu\text{m}$ ) at $\text{pH}_{\text{ps}}$	$\text{pH}_{\text{neut}}$	$d$ ( $\mu\text{m}$ ) at $\text{pH}_{\text{neut}}$	$r_{\text{neut}}$
2:1	BLG/TAG	4.43	0.16	3.80	2.37	2.5:1
	BLG/FI	4.41	0.14	3.90	2.43	1.8 :1
	BLG/FII	4.25	0.13	4.20	0.26	0.9:1
4:1	BLG/TAG	4.95	0.11	4.30	1.74	2.2:1
	BLG/FI	4.97	0.13	4.34	1.38	1.7:1
	BLG/FII	4.79	0.14	4.15	2.63	1.9:1
8:1	BLG/TAG	5.02	0.10	4.42	1.64	3.7:1
	BLG/FI	4.97	0.09	4.35	1.85	3.3:1
	BLG/FII	4.98	0.08	4.27	2.85	3.3:1
16:1	BLG/TAG	5.23	0.18	4.48	1.92	6.7:1
	BLG/FI	5.17	0.11	4.70	0.84	3.3:1
	BLG/FII	5.45	0.13	4.41	2.33	5.8:1

Fig. IV.2 shows the increase of  $d$  in BLG dispersions with the increase of its amount in water. Above a ratio of 2:1, a gradual aggregation of BLG as a function of pH is observed until  $\text{pH} \sim 4.8$ . Below this pH, the size of aggregates remained relatively constant.

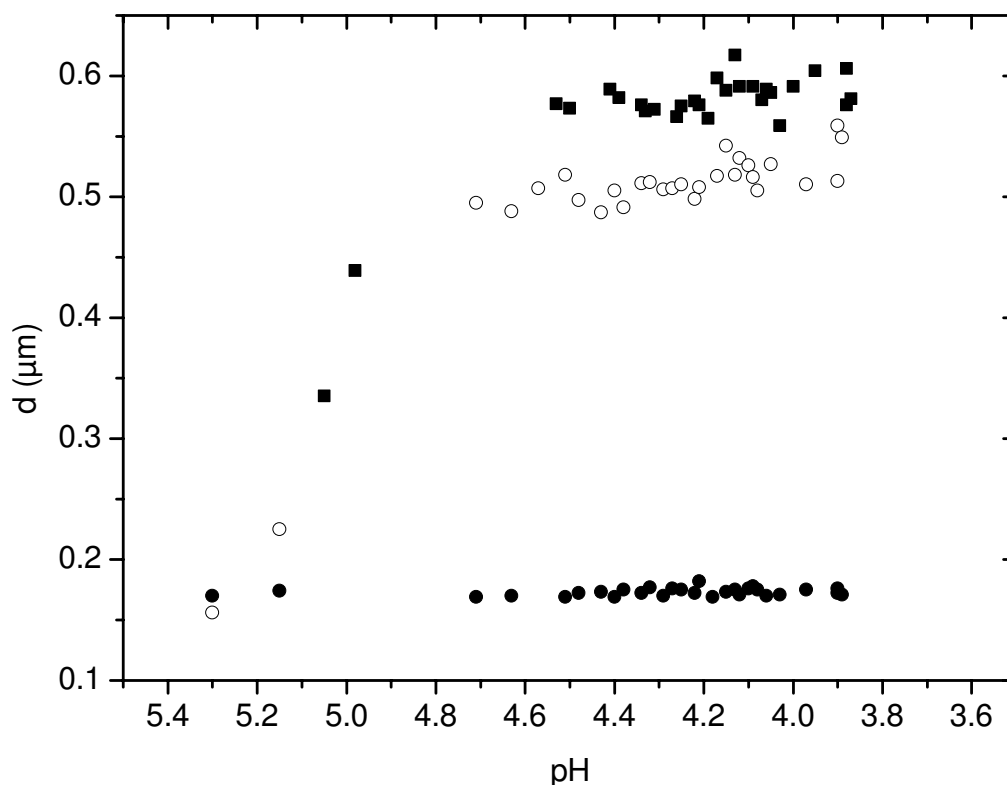


**Fig. IV.2.** Evolution of the particle diameter  $d$  ( $\mu\text{m}$ ) as a function of pH for the BLG stock dispersion at 0.066, 0.08 and 0.088 wt % total biopolymer concentration and BLG to water ratio of (●) 2:1, (○) 4:1 and (■) 8:1, respectively. Each experiment was made in duplicate.



This highlights the aggregation of BLG molecules, which can increase the particle size of complexes with ratio. At pH  $\sim 5.0$  that corresponds to the initiation of interaction, BLG aggregates show higher size as compared to the complexes (Fig. IV.1). This feature indicates that the complexation decreases the level of aggregation of BLG. Schmitt *et al.* (2000)<sup>30</sup> demonstrated that the presence of BLG aggregates in dispersion favor complex coacervation with TAG. This is in agreement with our results where increasing the amount of BLG allows faster (higher pH values) complexation or phase separation depending on the strength of interactions between biopolymers.

### IV.3.1.2. Electrophoretic mobility

Fig. IV.3 shows the evolution of  $\mu_E$  with the Pr:Pol ratio in all dispersions. At all Pr:Pol ratios (except the 4:1 for BLG/FI dispersions), the absolute  $\mu_E$  decreased as a function of pH in all mixtures, indicating the complex formation. The gradual decrease of  $\mu_E$  can be attributed to the increase of the amount of positive charges of BLG in dispersions. In addition, the increase of the mixing ratio led to more positively charged particles below the pH of electroneutrality (zero  $\mu_E$ ). This feature may indicate the formation of more stable systems with increasing the Pr:Pol mixing ratio. The electroneutrality of complexes was carried out at pH 3.8, 3.9 and 4.2 in BLG/TAG, BLG/FI and BLG/FII mixtures at a Pr:Pol weight ratio of 2:1.

We showed in Tab. IV.1 the gradual increase of these pH as a function of the mixing ratio. The particle sizes were determined at these pH. BLG/TAG and BLG/FI showed gradual decrease of particle size with increasing the mixing ratio until the ratio of 4:1. Above this ratio, the two systems exhibited a certain size polydispersity. In BLG/FII, the particle size increased as a function of ratio except at the ratio of 4:1. This result may indicate that the lowering of the strength of interaction with increasing the mixing ratio highlighted the role of FII properties. Thus, the higher radius of gyration of FII led to the formation of larger particles in BLG/FII system at low binding strength. The Pr:Pol charge ratios that correspond to an neutrality occurrence in mixtures ( $r_{\text{neut}}$ ) gradually increased with increasing the ratio in BLG/FII system. On the other hand, BLG/TAG and BLG/FI dispersions displayed relatively constant ratio of neutralization below the weight ratio of 16:1. From this mixing ratio, the  $r_{\text{neut}}$  gradually increased in BLG/TAG system; whereas, it increased until the ratio of 8:1 and then remained constant in BLG/FI dispersion.

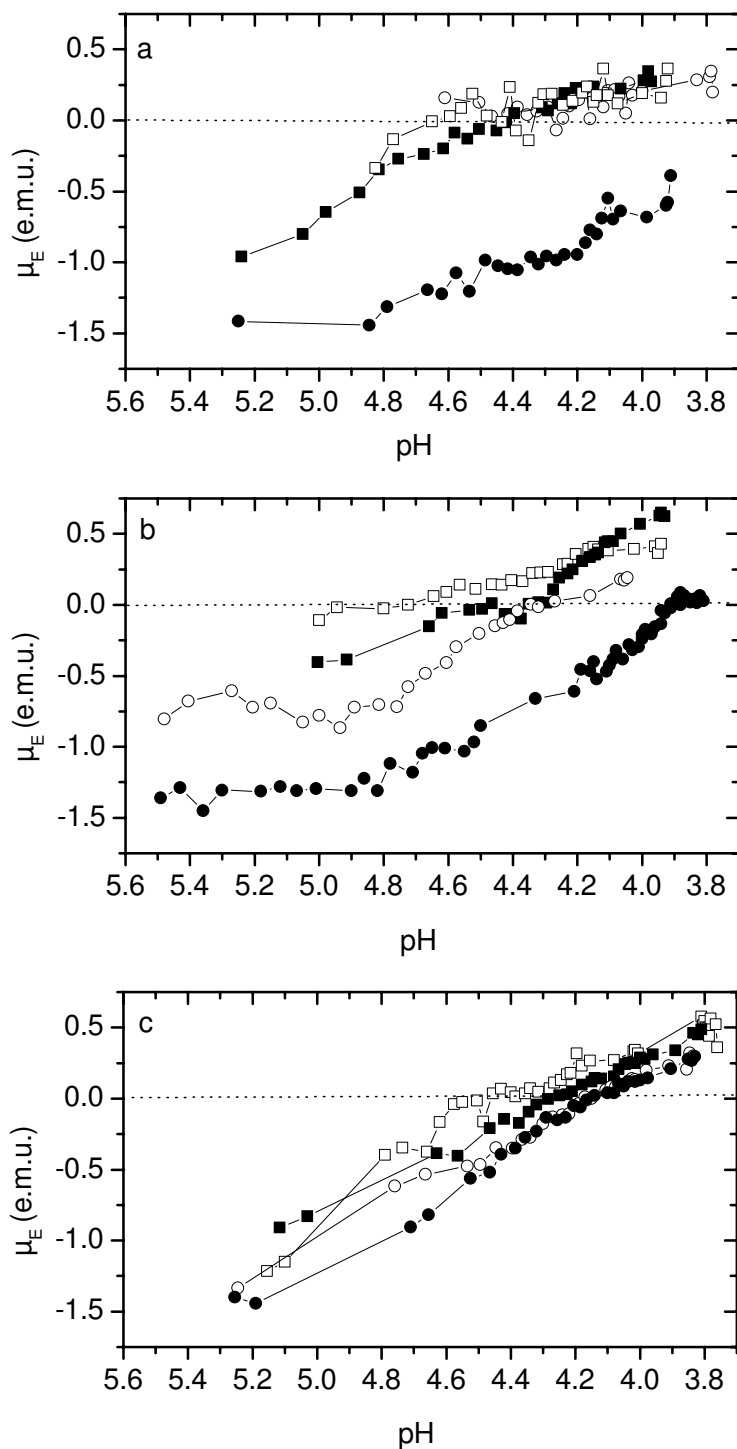


**Fig. IV.3.** Evolution of the electrophoretic mobility  $\mu_E$  (e.m.u.) as a function of pH for the BLG/TAG (a), BLG/FI (b) and BLG/FII (c) mixed dispersions at 0.1 wt % total biopolymer concentration and different Pr:Pol weight ratios. (●) 2:1, (○) 4:1, (■) 8:1 and (□) 16:1. Each experiment was made in duplicate.

$\mu_E$  results reveal that the complexation/coacervation of AG arises at lower positive charge

density of BLG if we increase the Pr:Pol weight ratio. Furthermore, above a Pr:Pol ratio of 2:1, BLG/TAG and BLG/FI systems show remarkable changes of  $\mu_E$  (Fig. IV.3). However, the effect of ratio was not significant in  $\mu_E$  curves of BLG/FII mixture as compared to BLG/FI mixture. This feature may be due to the higher strength of interactions between BLG and FII (see chapter II).

### IV.3.1.3. Small angle static light scattering

Fig. IV.4 shows the (Pr:Pol) ratio dependence of the scattered light intensity at 46° scattering angle for BLG/TAG, BLG/FI and BLG/FII mixed dispersions as a function of pH. The peak height of the scattered intensity reached a maximal value at Pr:Pol weight of 2:1 and pH ~4.2 (pH of coacervation in BLG/TAG system). With increasing the Pr:Pol ratio,  $pH_{coa}$  shifted toward higher pH values (Tab. IV.2), which indicates that complex coacervation of AG occurred at lower positive charge density of BLG. The binding of polyelectrolyte (e.g. TAG) and oppositely charged particles depends on the amount of charges of each polymer in dispersion<sup>32</sup>. Thus, the increase of the mixing ratio induces a mass action effect that favor the complexation<sup>31</sup>.

On the other hand, the peak height of the scattered intensity decreased. This result is due to the decrease of particles size and/or strength of interaction. The particle size in BLG/TAG and BLG/FI systems decreased in the 2:1-8:1 Pr:Pol ratio range, as shown in Tab. IV.2 .

**Tab. IV.2.** Size of particles,  $d$  ( $\mu\text{m}$ ), determined at the pH of complex coacervation ( $pH_{coa}$ ) as a function of the Pr:Pol mixing weight ratio.

Pr:Pol weight ratio		$pH_{coa}$	$d$ ( $\mu\text{m}$ ) at $pH_{coa}$
2:1	BLG/TAG	4.25	0.74
	BLG/FI	4.20	0.62
	BLG/FII	4.16	0.36
4:1	BLG/TAG	4.77	0.55
	BLG/FI	4.90	0.26
	BLG/FII	4.79	0.36
8:1	BLG/TAG	4.90	0.32
	BLG/FI	4.91	0.25
	BLG/FII	4.99	0.46
16:1	BLG/TAG	4.94	0.66
	BLG/FI	5.02	0.23
	BLG/FII	5.09	0.63

However, above the ratio of 8:1, the particles size increased in BLG/TAG system and remained approximately constant in BLG/FI system. At 2:1, the particle size in BLG/FII dispersion was lower as compared to BLG/FI system. However, with increasing the ratio, the particle size in BLG/FII system gradually increased and became higher as compared to BLG/FI mixtures.

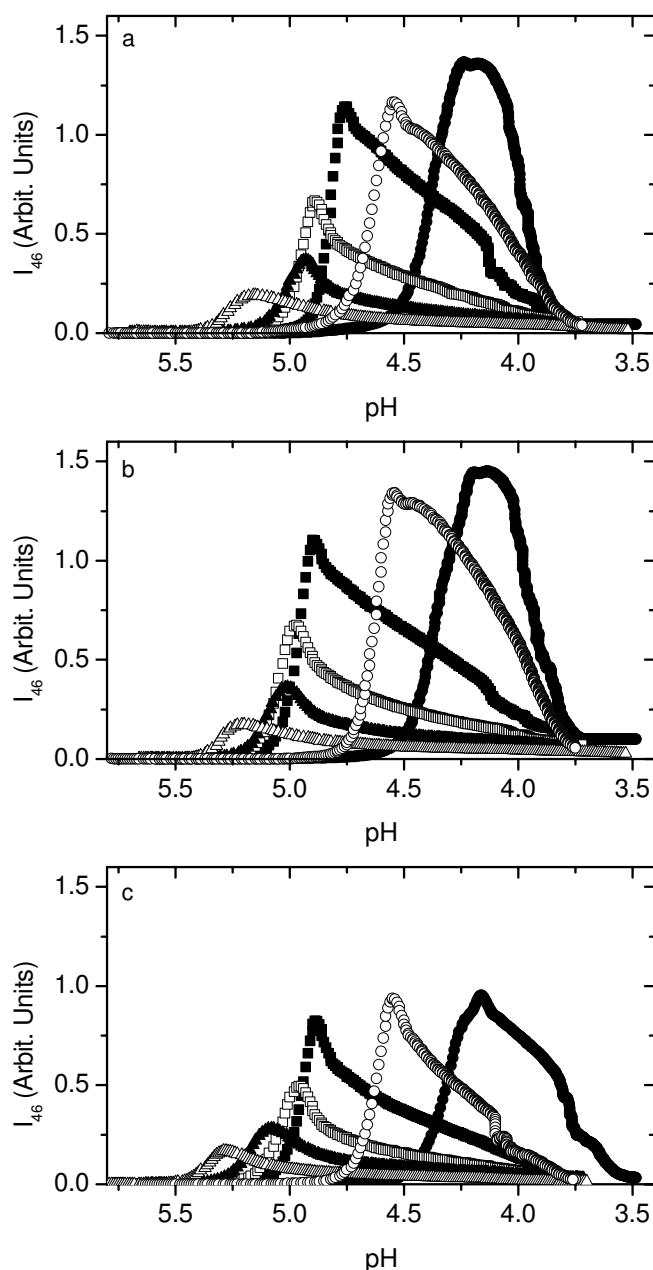


**Fig. IV.4.** Evolution of the scattered light intensity  $I_{46}$  (Arbitrary Units) at  $46^\circ$  scattering angle as a function of pH for the BLG/TAG (a), BLG/FI (b) and BLG/FII (c) mixed dispersions at 0.1 wt % total biopolymer concentration and different Pr:Pol weight ratio. (●) 2:1, (○) 3:1, (■) 4:1, (□) 8:1, (▲) 16:1 and (△) 40:1. Each experiment was made in duplicate.

At all mixing ratios, the maximum of the scattered intensity for BLG/FII mixture was lower as compared to BLG/TAG and BLG/FI mixtures except at a Pr:Pol ratio of 40:1. This feature may indicate the presence of lower number of particles in BLG/FII mixture. It is important to note that increasing the amount of charges by increasing the protein concentration may shift the coacervation in a mixed dispersion toward complexation (charged complexes) or co-solubility<sup>32</sup>. Thus, an increase of the Pr:Pol ratio can lead to a sharp transition from complex coacervation to complexation that arises from the coalescence of large size particles due to the presence of Pr-Pr cluster aggregates<sup>33</sup>. Moreover, Li *et al.* (1994)<sup>34</sup> indicated that the variation of mixing ratio results in change in the level of complexes aggregation.

Since at any given mixing weight ratio the Pr:Pol charge ratio is different between mixtures, all Pr:Pol weight ratios were converted into Pr:Pol charge ratios in order to better evaluate the contribution of TAG molecular fractions and to complete the previous results. Tab. IV.3 shows the Pr:Pol charge ratios at pH 4.2 for the three mixed dispersions studied. At any given Pr:Pol weight ratio, the Pr:Pol charge ratio for BLG/FII is the lowest compared to both BLG/TAG and BLG/FI mixed dispersions. This indicates that more of negative charges are present in BLG/FII mixtures. Nevertheless, the charge ratio is stoichiometric in BLG/FI mixture, in agreement with the higher maximum of scattered light intensity in this case. Thus, results reveal that FII was complexed with lower number of charges of BLG. This is despite its higher number of charges that requires higher amount of BLG to allow complexation/phase separation as compared to FI may be because its higher charge density.

**Tab. IV.3.** Calculated Pr:Pol charge ratios for BLG/TAG, BLG/FI and BLG/FII mixed dispersions at pH 4.2.

Pr:Pol weight ratio	Pr:Pol charge ratio		
	BLG:TAG	BLG:FI	BLG:FII
2 :1	1.15	1.05	0.90
3 :1	1.95	1.58	1.36
4 :1	2.60	2.10	1.81
8 :1	5.21	4.20	3.62
16 :1	10.41	8.40	7.23
40 :1	26.03	21.01	18.09

Fig. IV.5 shows the effect of the mixing ratio on turbidity during interactions at two Pr:Pol mixing ratios 2:1 and 16:1. For all mixtures, the curves were shifted to higher pH values at 16:1. Furthermore, a lower maximum of turbidity, extending over a higher pH range, was observed at 16:1. The decrease of turbidity values for the ratio of 16:1 can be explained by the

decrease of the (Tab. IV.2) number of particles and/or strength of interactions between macromolecules.

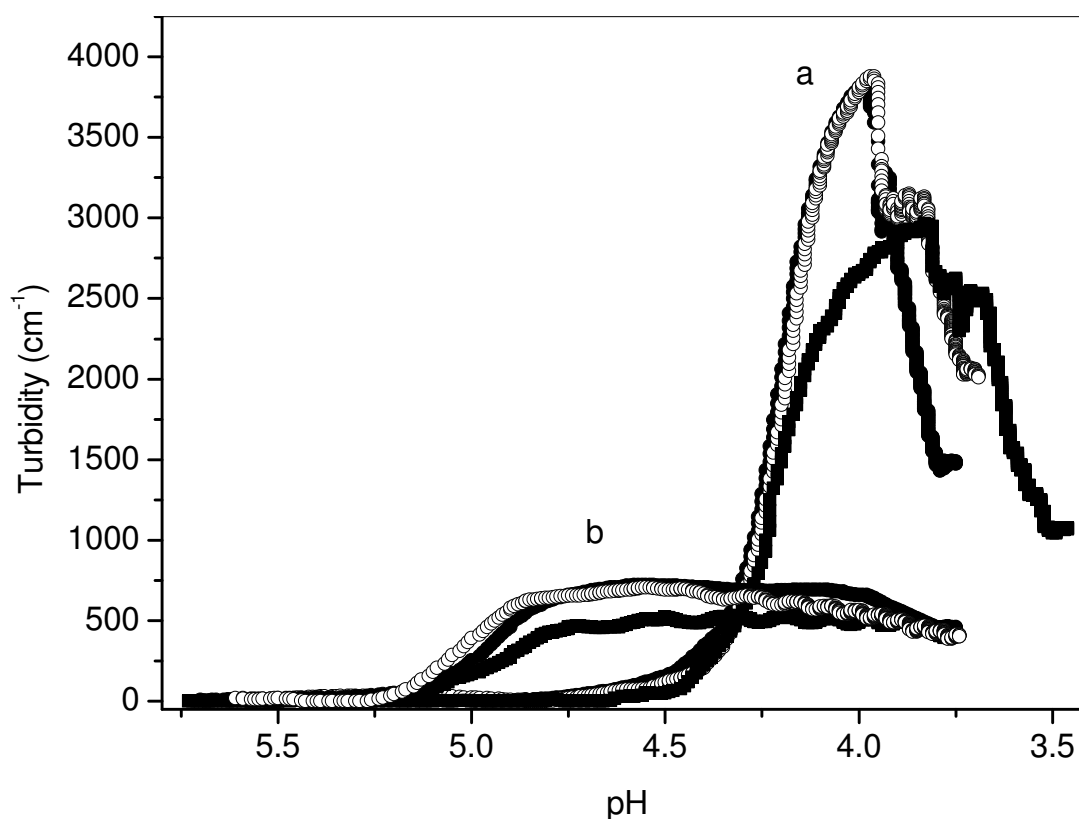


**Fig. IV.5.** Evolution of the turbidity  $\tau$  ( $\text{cm}^{-1}$ ) as a function of pH for mixed dispersions at 0.1 wt % total biopolymer concentration and Pr:Pol weight ratio of 2:1 (a) and 16:1 (b). (●) BLG/TAG, (○) BLG/Fl and (■) BLG/FII. Each experiment was made in duplicate.

When complex coacervation arises in dispersion, the maximum of turbidity corresponds to a peak where a maximum number of particles is formed. From this maximum, the turbidity decreases corresponding to a decrease in the number of particles and increase in their size. BLG/FII system displayed lower maximum of turbidity at the two mixing ratios, in agreement with lower number of objects.

The scattering profiles  $I(q) \sim q$  that allow to define the complex coacervation mechanism were represented in Fig. IV.6 for BLG/TAG system at a Pr:Pol weight ratio of 16:1. From the beginning of acidification until  $\text{pH} \sim 4.94$ , no correlation peak was observed. From this pH, a scattering maximum appeared at  $q \sim 1$ . This maximum firstly shifted to higher  $q$  values and then toward lower  $q$  values. As assessed in the previous chapter, this tendency corresponds to

a Nucleation and Growth mechanism, which reveals the occurrence of a similar mechanism with increasing the Pr:Pol ratio. However, it was possible to observe a scattering maximum at higher pH values, in agreement with a faster complexation/phase rate.

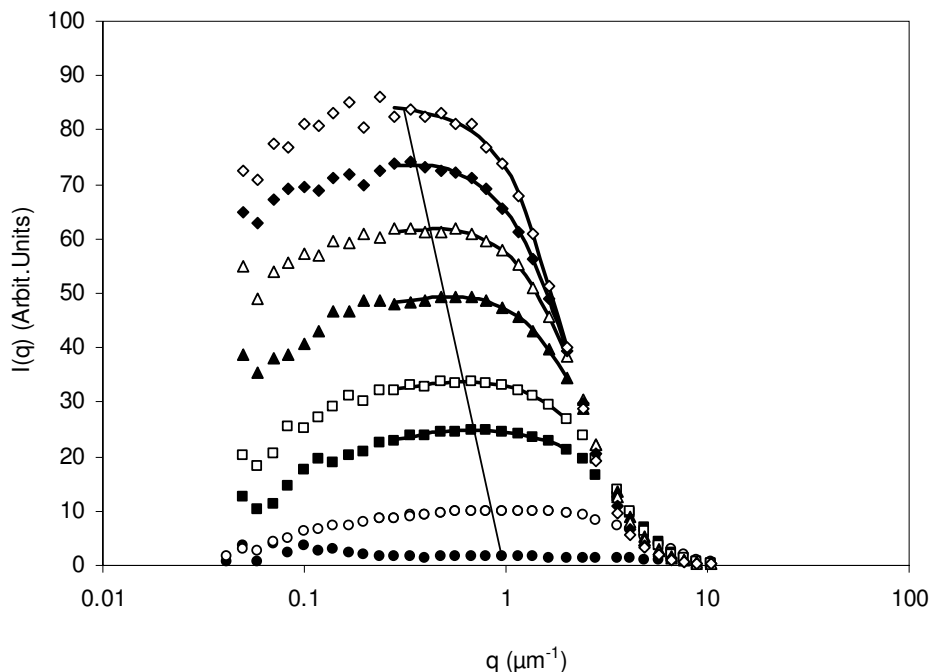


**Fig. IV.6.** Scattering profiles  $I(q)$  (arbitrary units) as a function of  $q$  ( $\mu\text{m}^{-1}$ ) recorded during slow acidification of BLG/TAG mixed dispersions at 0.1wt% total biopolymer concentration and Pr:Pol weight ratio of 16:1 in a pH range where a correlation peak appeared. ( $\bullet$ ) pH 4.94, ( $\circ$ ) pH 4.83, ( $\blacksquare$ ) pH 4.73, ( $\square$ ) pH 4.65, ( $\blacktriangle$ ) pH 4.51, ( $\triangle$ ) pH 4.40, ( $\blacklozenge$ ) pH 4.29 and ( $\diamond$ ) pH 4.20. Continuous lines correspond to weighted curve fits with three or fourth-order polynomial function. Dot line highlights the shift of the scattering maximum towards smaller  $q$  values. Each experiment was made in triplicate.

From the scattering profiles, we have determined  $q_{\text{max}}$  in the pH range where a peak was present. Plots of  $q_{\text{max}}$  versus time were built and fitted with a power law (Fig. IV.7). It must be noticed that fitting data above a Pr:Pol ratio of 16:1 was difficult because of the weakness of signal. The power law exponent  $\alpha$  remained constant from Pr:Pol of 2:1 until 16:1, taking into account the error of measurement and fit. On the other hand, large differences in the temporal evolution of  $q_{\text{max}}$  were observed in conditions of high (Pr:Pol ratio of 2:1) and low (Pr:Pol ratio of 16:1) ratio. All curves were shifted to lower time values with increasing ratio. The exponent values at any ratio were smaller than 1 ( $\sim 0.8 \pm 0.1$ ). The exponent values indicate that diffusion and convection phenomena drive phase separation in all mixtures.

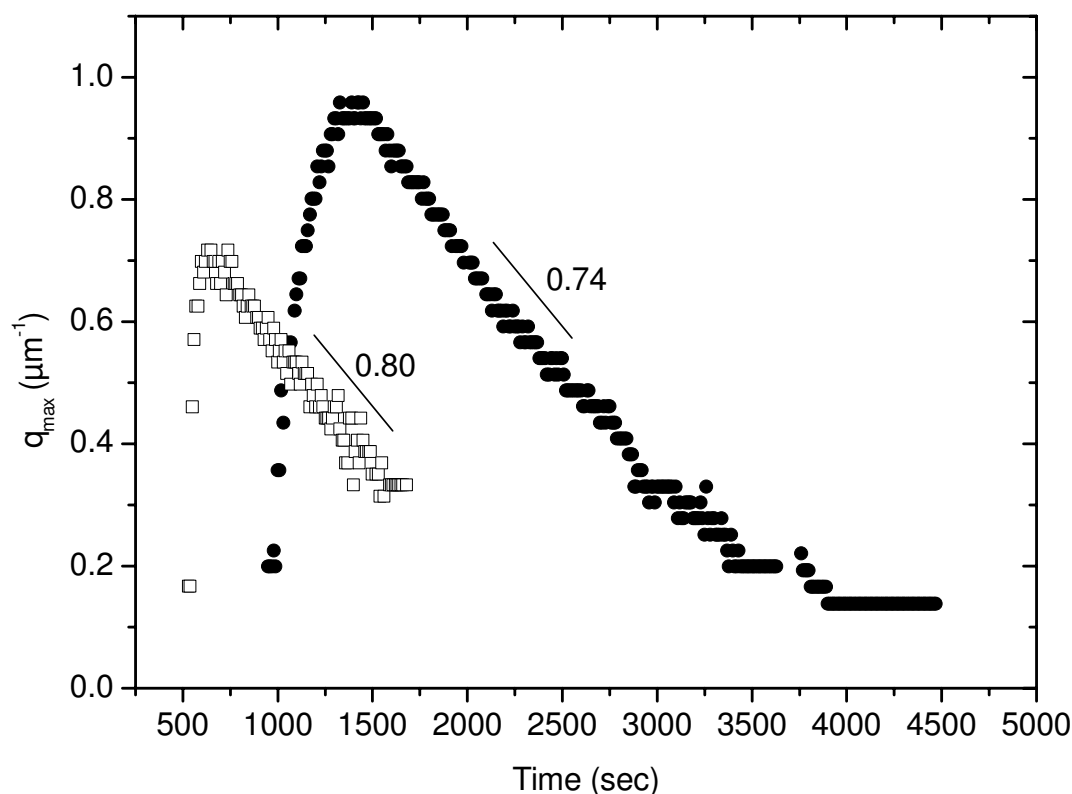


**Fig. IV.7.** Evolution of the maximum wave vector  $q_{\max}$  ( $\mu\text{m}^{-1}$ ) as a function of time for the BLG/TAG mixed dispersions at 0.1 wt % total biopolymer concentration and two Pr:Pol weight ratios. (●) 2:1, (○) 16:1. Each experiment was made in duplicate.

Fig. IV.8 shows the slope  $\gamma$  of the log-log plots  $I(q) \sim q^{-\gamma}$  in the high  $q$  region for all samples at four different mixing ratios. The  $\gamma$  plots shifted toward higher pH values with increasing ratio due to a mass effect. On the other hand, the number of transition points decreased with increasing ratio. Interestingly, the 4.8 - 4.4 pH range, observed at a ratio of 2:1, becomes increasingly narrow with ratio. The disappearance of certain transition points from the log-log plots reflects a more rapid coarsening rate of complexes. Similar plots in all mixtures were obtained at a Pr:Pol ratio of 2:1. However, lower exponent values were observed in BLG/FII mixture at this ratio, especially below pH  $\sim$  4.2. It is important to note that BLG/TAG and BLG/FI mixtures exhibit similar  $\gamma$  curves until the ratio of 16:1, and then the same structuring kinetics of particles. It is important to note that BLG/FII particles showed higher exponent values at the beginning of acidification above the Pr:Pol ratio of 4:1. These values decreased as acidification proceeded, which might be due to the presence of large aggregates that disaggregate upon complexation. The large aggregates may result from the large size of BLG at high ratios (Fig. IV.2) or the larger radius of gyration of FII.



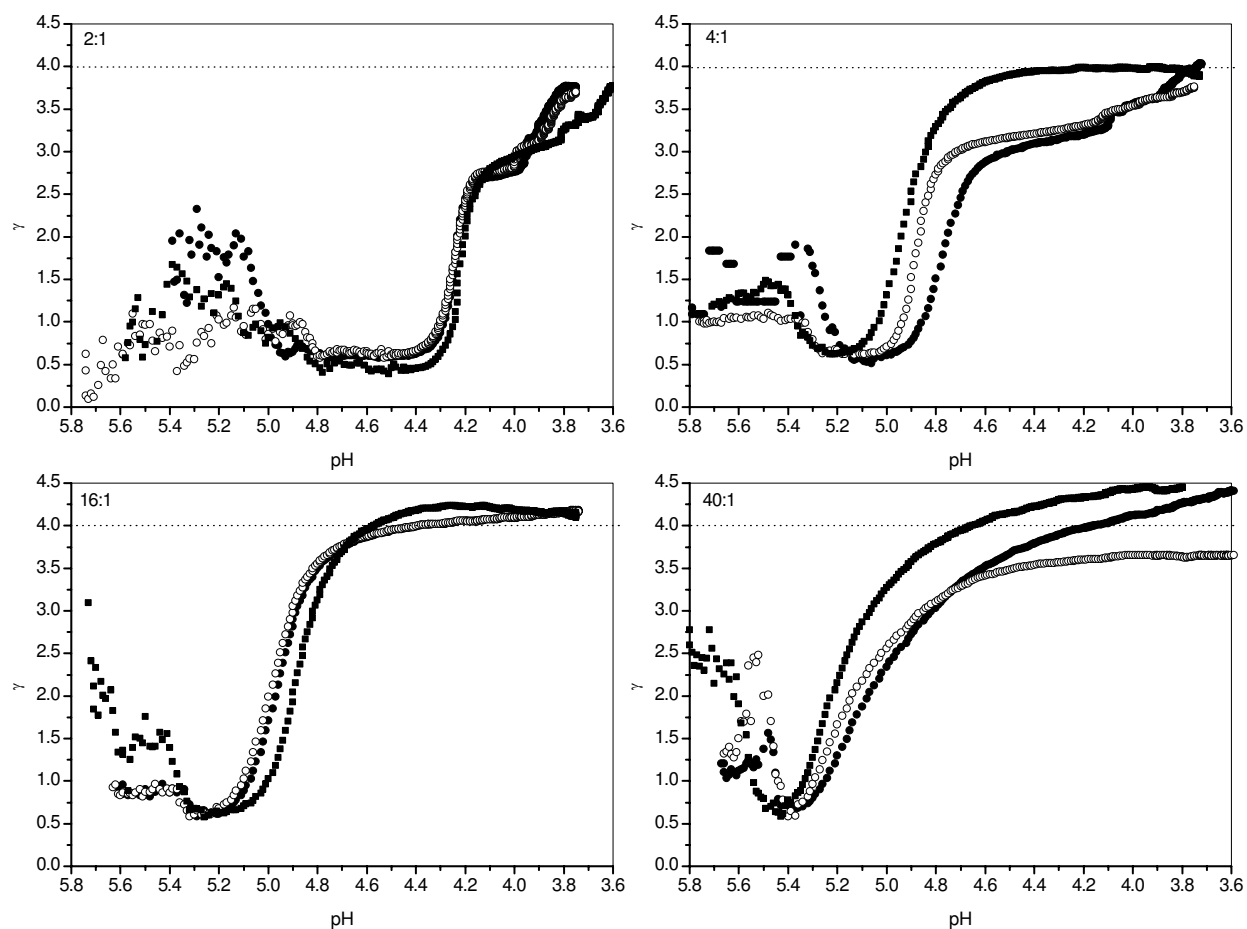


**Fig. IV.8.** Evolution of the slope value  $\gamma$  of  $\log I$  vs  $\log q$  ( $3.546 < q < 10.414 \mu\text{m}^{-1}$ ) with pH for BLG/AG mixed dispersions at 0.1 wt % total biopolymer concentration and different Pr:Pol weight ratios. (●) BLG/TAG, (○) BLG/FI and (■) BLG/FII. Dotted lines are guide for eyes. Each experiment was made in duplicate.

At a Pr:Pol ratio of 4:1, the  $\gamma$  values in BLG/FII mixture increased and rapidly reached the value of 4 as compared to BLG/FI system. This feature highlights the appearance of more homogeneous surface in BLG/FII droplets. Between the Pr:Pol ratios of 4:1 and 16:1, the differences in  $\gamma$  between mixtures were not significant. From 16:1, BLG/FII system displays higher values than BLG/FI dispersion, in relation with higher compacity of particles. At the ratio of 40:1, BLG/FI mixture shows a constant evolution of  $\gamma$  below pH~4.6, with values that did not reach 4. This indicates a decrease in the interface homogeneity of BLG/FI system above a certain Pr:Pol mixing ratio.

To better show the formation of different morphology of the phase-separated interfaces in all samples as a function of the mixing ratio, we have extracted at a pH 3.8 (the last structural transition determined in the previous chapter) the exponent  $\gamma$  of scattering profiles  $I(q) \sim q^{-\gamma}$

and we have plotted  $\gamma$  values versus the Pr:Pol weight ratio (Fig. IV.9).

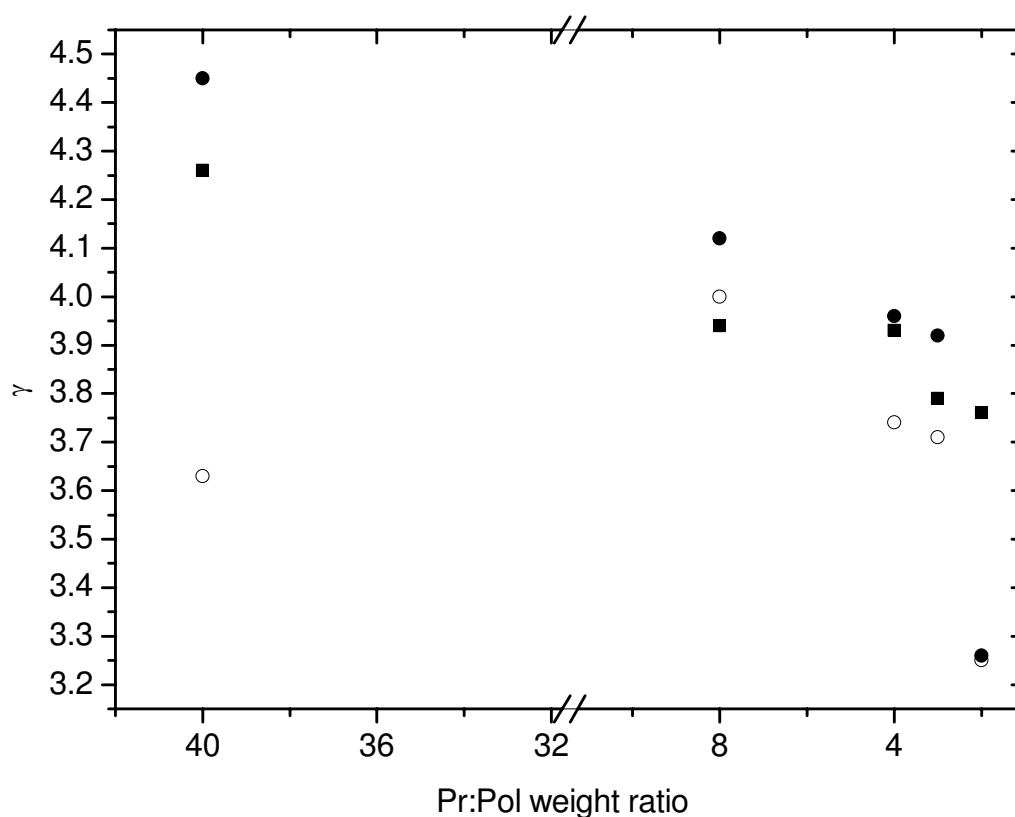


**Fig. IV.9.** Evolution of the slope value  $\gamma$  as a function of Pr:Pol weight ratio at pH 3.8. (●) BLG/TAG, (○) BLG/FI and (■) BLG/FII. Each experiment was made in duplicate.

The curve can be divided into two regions. Below 16:1,  $\gamma$  strongly increased with increasing ratio for all samples. From 16:1,  $\gamma$  increased slower with ratio and then reached the Porod value of 4 except for BLG/FI mixture. As  $\gamma$  exceeds the Porod value close to a Pr:Pol ratio of 8:1, the formation of an interfacial layer is expected at ratios  $\geq 8:1$  in BLG/FII and BLG/TAG mixtures. This feature was not observed in BLG/FI mixture and can reflect its slower phase separation rate as compared to BLG/FII system. Presumably, systems showed different structures of particles with increasing the mixing ratio. From there, we suggest that the role of the molecular and structural features of AG on the structure of complexes can be highlighted by decreasing the strength of interaction in mixtures based on a variation of the mixing ratio.

### IV.3.2. Effect of the total biopolymer concentration ( $C_p$ )

The effect of  $C_p$  was studied for many reasons:

- i)* to give more information about the structural transitions during pH-induced complexation/coacervation in all mixtures
- ii)* to observe the structure and size of particles for concentrated (4wt%) dispersions in order to better understand the complexation/coacervation mechanism

#### IV.3.2.1. Granulo-Polarimetry

The Granulo-Polarimetry method is a meaningful tool for the quantitative study of random media. It allows to characterize a dense system by measuring the light transport length ( $l^*$ ) under varying external conditions (e.g. shearing).  $l^*$ , that is the mean free path of light in a medium, corresponds to the only parameter necessary to quantify the scattering of light. The employment of usual optical techniques has some limitations (diffusive wave spectroscopy, DWS) or cannot be used (SALS and DLS) in dense media and needs generally a number of approximations on the speckles of the light such as suggesting that the optical index is constant in dispersions during interaction. Indeed, the complexity (e.g. complex structure of gum, heterogeneity of both biopolymers, and diversity of types of interaction) of our mixture has not permitted to determine the optical properties of complexes as well as their size using different usual optical techniques in diluted medium. Therefore, the present apparatus can be of great interest to get more information about the structure of particles.

Fig. IV.10 shows the evolution of the transport length during pH-induced structuring in all mixtures studied. Regarding the curve shape, all mixtures show similar evolution of  $l^*$  as a function of pH. Thus, a minimum was reached between two opposite pH ranges. In the first range,  $l^*$  decreased from pH  $\sim 4.8$  to pH 4.12, 4.21 and 4.24 in BLG/TAG, BLG/FI and BLG/FII mixtures, indicating the increase of turbidity in mixtures. At these pH,  $l^*$  reached minimum values of 1.4, 2.3 and 0.8 mm. An increase of  $l^*$  then appeared indicating a decrease of turbidity. The minimum of  $l^*$  corresponds to a maximum of turbidity in dispersions.

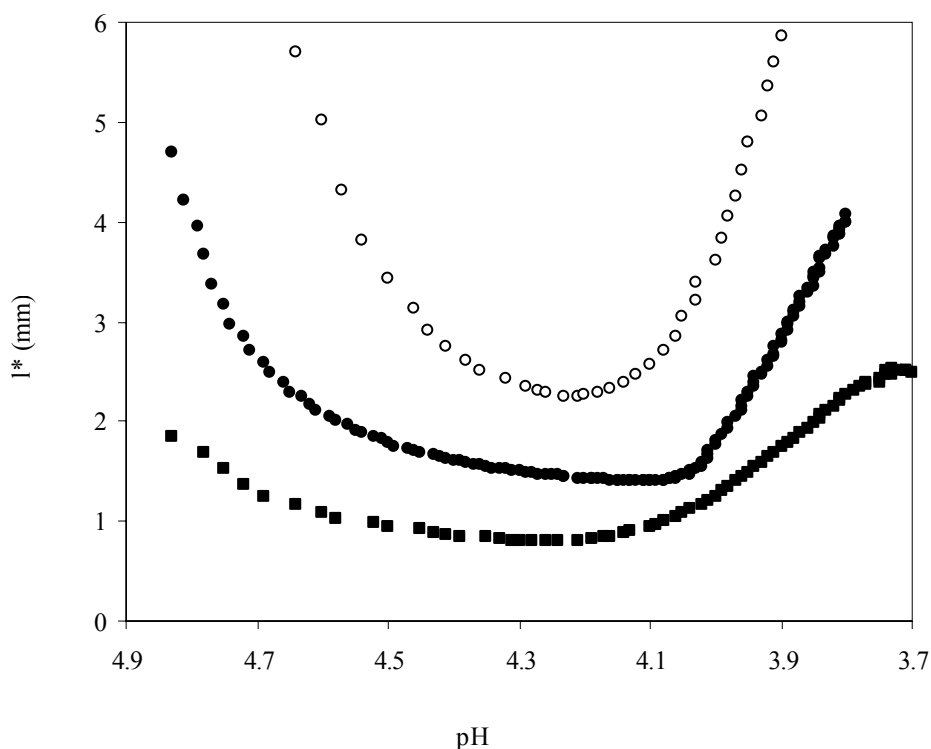


**Fig. IV.10.** Evolution of the transport length ( $l^*$ ) (mm) as a function of pH for  $\beta$ -lactoglobulin (BLG) / Acacia Gum (TAG) or Arabinogalactan-peptide (FI) or Arabinogalactan-protein (FII) mixed dispersions at 4wt% total biopolymer concentration and Pr:Pol weight ratio of 2:1. (●) BLG/TAG, (○) BLG/FI, (■) BLG/FII. Each experiment was made in duplicate.

Generally, a decrease of  $l^*$  can be due to an increase of the scatterer volume fraction and/or decrease in the size of scatterer objects. SALS results showed that phase separation follows nucleation and growth with a transition point at  $\text{pH} \sim 4.2$ . From there, the minimum of  $l^*$  can be attributed to the maximum of interaction strength ( $\text{pH}_{\text{mis}}$ ) between biopolymers. The increase of  $l^*$  below  $\text{pH}_{\text{mis}}$  can be due to a decrease of the number of particles. At a given pH, BLG/FII system exhibits lower  $l^*$  than BLG/FI mixture, in agreement with higher turbidity in dispersion due to a higher strength of interactions between FII and BLG, as shown in chapter II.

The transport of light polarization was used in order to measure the particle size independently of the volume fraction. The measurement of size was obtained from the amplitude of the effects of linear polarization. An inversion in size was made by Monte Carlo simulations corresponding to an index parameter  $m$  of 1.2. From the polarization amplitude, an averaged size of objects was deduced. Fig. IV.11 shows the evolution of particle size as a function of pH in all systems. Two opposite phases of evolution can be observed in all

systems. Firstly,  $d$  decreases until a minimum of  $\sim 598$  nm is reached at pH 4.23 in BLG/FI mixture. The decrease of size in BLG/FI dispersions can be attributed to the dissociation of particles and/or the increase of the volume fraction of objects.

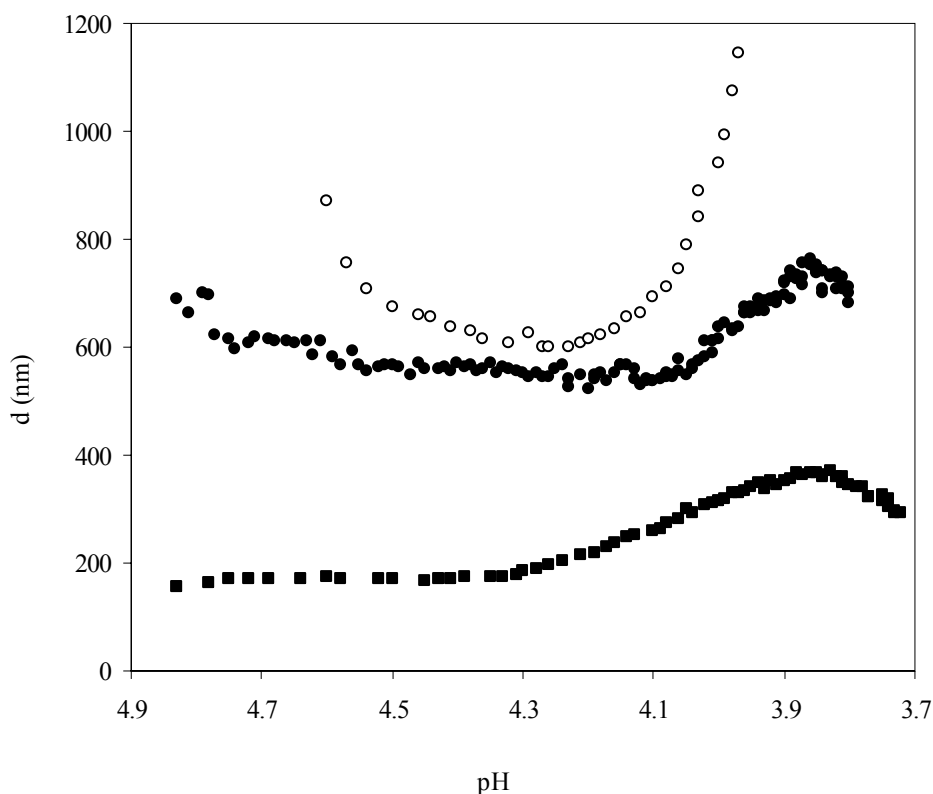


**Fig. IV.11.** Evolution of the diameter of scatterers particles  $d$  (nm) as a function of pH for  $\beta$ -lactoglobulin (BLG) / Acacia Gum (TAG) or Arabinogalactan-peptide (FI) or Arabinogalactan-protein (FII) mixed dispersions at 4wt% total biopolymer concentration and Pr:Pol weight ratio of 2:1. (●) BLG/TAG, (○) BLG/FI, (■) BLG/FII. Each experiment was made in duplicate.

On the other hand, a relatively constant evolution of size appeared in BLG/TAG and BLG/FII mixtures until pH 4.12 ( $\sim 539$  nm) and 4.35 ( $\sim 172$  nm), respectively. In the second phase, the size increases in all mixtures. It seems that BLG/TAG particles have an intermediate size between those of the other blends. Whatever the pH, smaller size of particles is observed in BLG/FII system as compared to BLG/FI mixture, in agreement with DLS results. From there, it is important to note that BLG/FI and BLG/FII exhibited different trends of evolution of  $d$  at high  $C_p$  value. BLG/TAG and BLG/FII mixtures showed similar shape of curves. Thus,  $d$  results showed different size in the three systems at high total biopolymer concentration. It must be noticed that the high strength of interaction in BLG/FII dispersion as compared to BLG/FI dispersion may mask the role of its structural properties and lead then to a constant evolution of size in the first pH range (4.8-4.35) during acidification.

Knowing either the size and optical properties ( $m = 1.2$ ), the use of Mie theory (described in ref 35) allows the calculation of the volume fraction of the scatterer objects,  $\phi$ . Raw data in Fig. IV.12 shows that  $\phi$  vs pH curve displays the same kinetics as compared to  $I^*$  in all systems.

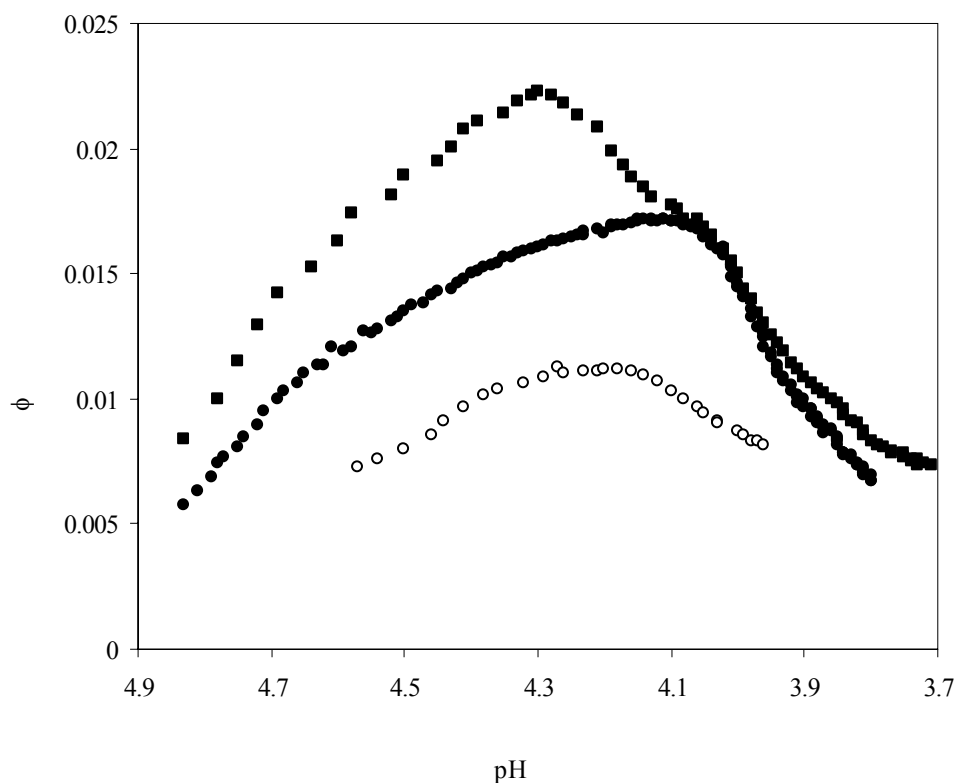


**Fig. IV.12.** Evolution of the fraction of photons internally scattered ( $\phi$ ) as a function of pH for  $\beta$ -lactoglobulin (BLG) / Acacia Gum (TAG) or Arabinogalactan-peptide (FI) or Arabinogalactan-protein (FII) mixed dispersions at 4wt% total biopolymer concentration and Pr:Pol weight ratio of 2:1. (●) BLG/TAG, (○) BLG/FI, (■) BLG/FII. Each experiment was made in duplicate.

A maximum of  $\phi$  was reached at pH 4.13, 4.21 and 4.31 in BLG/TAG, BLG/FI and BLG/FII mixtures. Between pH 4.8 and these pH, the volume fraction increases revealing an increase in the number of particles (Fig. IV.11). Below these pH, the concentration of objects decreases, which corresponds to a decrease in the number of particles due to their coalescence and growth. BLG/FII system displays the highest values of  $\phi$  whatever the pH, indicating the presence of a higher number of particles in dispersion.

In chapter II, it was suggested that the volume fraction can remain constant or decrease, above the  $pH_{mis}$ , during acidification (Fig. II.5). However, the present results obtained in concentrated medium show an increase of the scatterer volume fraction from the beginning of acidification until  $pH_{mis}$ . Moreover, the particle size remained constant in BLG/TAG and

BLG/FII systems above  $pH_{mis}$ . Therefore, we suggest that certain particles disappear and simultaneously others appear upon the complexation. Thus, a dissociation of particles arises during the nucleation phase of complex coacervation mechanism.

To summarize about the Granulo-Polarimetry study, BLG/FI and BLG/FII mixtures displayed different behaviors during pH-induced complexation/coacervation with BLG in concentrated medium. BLG/FI system had higher  $l^*$  and lower scatterer volume fraction values, in relation with larger size and lower number of particles, as compared to BLG/FII mixture. Although the larger size of FII (higher  $R_G$ ) would lead in theory to higher size of particles, the inverse was observed. Since an excess of negative charges is present in BLG/FII (see Tab. IV. 4), we suggest that both electrostatic and steric repulsive interactions may exist between the early neutralized BLG/FII particles that do not favor the coalescence of complexes as compared to BLG/FI ones. The steric repulsion may result from the higher number of BLG/FII particles present in dispersions as shown in the volume fraction results.

#### **IV.3.2.2. Optical microscopy**

In order to get more information about the size evolution in dispersions, optical microscopy was used in parallel to follow the pH-induced microstructural changes in concentrated medium as for Granulo-Polarimetry measurements. We show the results for BLG/TAG mixture (Fig. IV.13). Two phases of size evolution with pH appeared. From the beginning of acidification until  $pH \sim 4.14$ , a gradual increase in the number of structural entities was observed with constant size. At  $pH \sim 4.14$ , a maximum number of particles was observed. Below  $pH \sim 4.14$ , particles grew in size but their number is reduced. This feature can be attributed to the coalescence of coacervates or Ostwald ripening, and also probably to sedimentation of the largest particles. The trend of evolution of  $d$  is in agreement with the size evolution obtained by SALS and Granulo-Polarimetry measurements. It can be inferred that coacervation occurred in the 4.25-3.9 pH range, since spherical droplets of  $2\mu m$  diameter were detected in this pH range.

We show in Fig. IV.14 the micrographs of the three mixtures at pH 4.25 and 3.88 in order to highlight the size differences between systems. It was observed smallest structures in BLG/FII mixture as compared to BLG/FI mixture at each the pH values. BLG/TAG system

displays particles with an intermediate size between those of BLG/FI and BLG/FII mixtures. It must be noticed that Granulo-Polarimetry showed a maximum size of  $\sim 1.18 \mu\text{m}$  in BLG/FI system: whereas, in the optical micrographs, the particles size reached an averaged value of  $4.5 \mu\text{m}$  at pH 3.7. This size difference between the two techniques can be attributed to the fact that Granulo-Polarimetry allowed to determine an averaged size and also to the approximation done (constant scatterer volume fraction during interaction) in the calculus method.

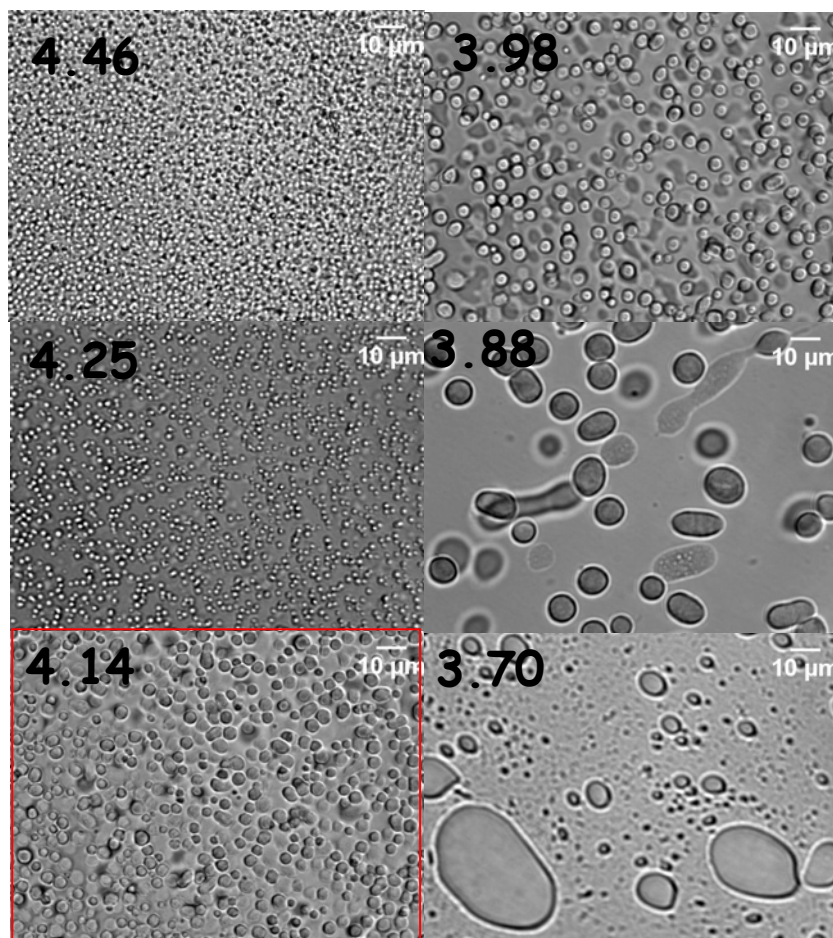


**Fig. IV.13.** Epi-fluorescence micrographs taken during the pH-induced complex coacervation for the BLG/TAG mixed dispersions at 4wt% total biopolymer concentration and Pr:Pol weight ratio of 2:1. Bar represents  $10\mu\text{m}$ . Contrast and brightness of micrograph were treated by the ImageJ freeware (version Beta 1.36).

Granulo-Polarimetry and optical microscopy results showed similar pH of structural transitions in concentrated medium as compared to transitions pH obtained in diluted medium in the previous chapters. Thus, an increase of the total biopolymer concentration (40 times) has altered neither the phase behavior nor the kinetics of phase separation. This result is in agreement with Mattison *et al.* (1995) that indicated that  $\text{pH}_c$  and  $\text{pH}_\phi$  remained constant with increasing  $C_p$ . The main reason is that the charge balance between BLG and AG molecules is



not modified by increasing  $C_p$ . Thus, the phase boundaries will occur at the same transitions pH. The microstructural changes during pH-induced phase separation of BLG and TAG at  $C_p$  of 0.1wt% were investigated by Mekhloufi *et al.* (2005)<sup>36</sup>. The first detection of structures was at pH 4.20. However, in our micrographs it was possible to observe small light fluctuations on the monitor screen at pH 4.90, which indicates an earlier occurrence of phase separation in our systems as compared to these authors. One possible reason is the purification of our biopolymers that remove the screening of ions and accelerate then the interactions.

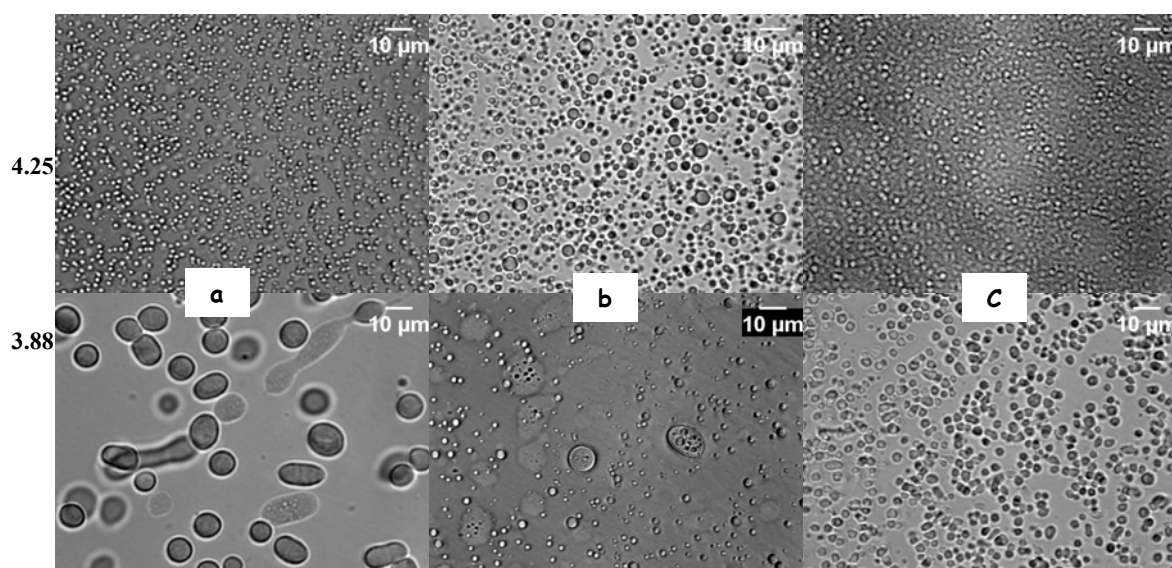


**Fig. IV.14.** Epi-fluorescence micrographs at pH 4.25 and 3.88 ( $\pm 0.02$ ) for the BLG/AG mixed dispersions at 4wt% total biopolymer concentration and Pr:Pol weight ratio of 2:1. (a) BLG/TAG, (b) BLG/FI and (c) BLG/FII. Bar represents 10 $\mu$ m. Contrast and brightness of micrograph were treated by the ImageJ freeware (version Beta 1.36).

The evolution of number and size of particles with acidification, in diluted and concentrated medium, is in good agreement with the nucleation and growth mechanism discussed in chapter III, which indicates that the phase separation mechanism is not modified with increasing  $C_p$ . Then, the phase separation mechanism of BLG/AG systems is independent on the total amount of biopolymers, but it depends on the pH, mixing ratio and intrinsic properties of macromolecules. However, structures of higher number and larger size were formed at high  $C_p$  at all pH values. This is due to the higher amounts of AG and BLG at high  $C_p$ . We note that the high strength of interaction at high  $C_p$  revealed the differences between systems. However, the low strength of interaction at low mixing ratio permitted to observe the different behaviors of the three systems

To summarize about the effect of TAG polydispersity, FI and FII showed different phase ordering kinetics during complexation/coacervation with BLG. The different behaviors observed in mixtures are due to differences in the structural and molecular features (charge density, molecular weight, radius of gyration, number of charges) of AG molecules. In general, polymers with high molecular weight have a strong tendency to induce phase separation because of their high exclusion volume and steric effects, as denoted in chapter I (see the depletion model of phase separation)<sup>37</sup>. This is due to the restriction of degree of freedom that reduces the mixture entropy and allows easier phase separation. Indeed, when molecular weight and flexibility (persistence length of FII  $\sim$ 3 nm, Sanchez *et al.*, results not published) of a molecule increase, the number of sites able to interact with another molecule increases, in agreement with the faster coarsening rate of phase separation in BLG/FII mixture<sup>38,39</sup>.

It must be noticed that Granulo-Polarimetry and optical density has no show major differences between mixtures despite the different intrinsic properties of AG molecules. This could be due to the high strength of electrostatic interactions at 2:1 Pr:Pol weight ratio, which can mask the effect of TAG molecular and structural properties<sup>40</sup>. From there, study of the effects of Pr:Pol mixing ratio and total biopolymer concentration in a wide range on complexation/coacervation between BLG and TAG molecular fractions could be an alternative approach to better elucidate their structural behaviors.

## IV.4. Conclusions

Time-resolved dynamic and static light scattering (DLS and SALS), electrophoretic mobility ( $\mu_E$ ), Granulo-Polarimetry and optical microscopy measurements have permitted to characterize the complexation/coacervation between  $\beta$ -lactoglobulin and major molecular fractions of TAG, FI and FII. In conditions of strong and weak interactions, the effect of the mixing ratio and total biopolymer concentration on characteristics of complexes was investigated. Increasing the Pr:Pol weight ratio allowed complexation/or phase separation to occur at higher pH values i.e. at lower positive charge density of BLG in all systems. BLG/FII system showed lower particle size at the mixing ratio of 2:1, as compared to BLG/FI system. However, above this ratio, the size of BLG/FII particles increased and was higher than that of BLG/FI particles. This feature may be due to the higher strength of interaction at 2:1 that masked the role of the structural characteristics of FII. By DLS, it was found that favorable complexation occurred between FII and BLG as compared to FI, in relation with the possible higher charge density of FII. Smaller BLG/FII complexes were observed, which can be attributed to repulsive interactions between the like-charged particles due to an excess of negative charges in BLG/FII dispersions. At high ratios (above 8:1), the  $\gamma$  exponent of the log-log plots ( $I(q)$  vs  $q$ ) increased and then reached the Porod value  $\geq 4$ , which reveals the appearance of an interfacial layer in dispersions. The morphology of the interface was more homogeneous for BLG/FII mixtures at high ratios, as compared to BLGFI system. According to DLS results, Granulo-Polarimetry measurements in concentrated medium showed the formation of larger particles with a lower number in BLG/FI mixture. The total biopolymer concentration ( $C_p$ ) of mixtures has not affect the dynamics and kinetics of complex coacervation in all mixtures. The similar mechanism of nucleation and growth drives phase separation; it was also established that nucleation can be accompanied by dissociation of particles. In addition, the pH of structural transitions remained constant with increasing  $C_p$ . Nevertheless, at high  $C_p$ , the coacervates formed are larger and more numerous as shown by optical density measurements.



## IV.5. References

- 
- <sup>1</sup> Wang, Y.; Kimura, K.; Huang, Q.; Dubin, P.L. *Macromolecules*, **1999**, 32, 7128.
  - <sup>2</sup> Tsuboi, A.; Izumi, T.; Hirata, M.; Xia, J.; Dubin, P.L.; Kokufuta, E. *Langmuir*, **1996**, 12, 6295.
  - <sup>3</sup> Dubin, P.L.; Gao, J.; Mattison, K. *Separation and Purification Methods*, **1994**, 23, 1.
  - <sup>4</sup> Sanchez, C.; Mekhloufi, G.; Schmitt, C.; Renard, D.; Robert, P.; Lehr, C.-M.; Lamprecht, A.; Hardy, J. *Langmuir*, **2002**, 18, 10323.
  - <sup>5</sup> Frugier, D. Thesis, Université de Pierre et Marie Curie, France, **1988**.
  - <sup>6</sup> Cooper, C.L.; Dubin, P.L.; Kayitmazer, A.B.; Turksen, S. *Current Opinion in Colloid and Interface Sciences*, **2005**, 10, 52.
  - <sup>7</sup> Girard, M.; Turgeon, S.L.; Gauthier, S.F. *Journal of Food Agricultural and Chemistry*, **2003**, 51, 4450.
  - <sup>8</sup> Girard, M.; Sanchez, C.; Laneuville, S.I.; Turgeon, S.L.; Gauthier, S.F. *Colloids and Surfaces B: Biointerfaces*, **2004**, 35, 15.
  - <sup>9</sup> Weinbreck, F.; Nieuwenhuijse, H.; Robin, G.W.; de Kruif, C.G. *Journal of Food Agricultural and Chemistry*, **2004**, 52, 3550.
  - <sup>10</sup> Mekhloufi, G.; Sanchez, C.; Renard, D.; Guillemin S.; Hardy, J. *Langmuir*, **2005**, 21, 386.
  - <sup>11</sup> Maarten Biesheuvel, P.; Cohen Stuart, M. A. *Langmuir*, **2004**, 20, 2785-2791.
  - <sup>12</sup> Tolstoguzov, V.B. *Food Hydrocolloids*, **2001**, 17, 1.
  - <sup>13</sup> Schmitt, C.; da Silva, T.P.; Bovay, C.; Rami-Shojaei, S.; Frossard, P.; Kolodziejczyk, E.; Leser, M. E. *Langmuir*, **2005**, 21, 7786.
  - <sup>14</sup> Wen, Y-P.; Dubin, P.L. *Macromolecules*, **1997**, 30, 7856.
  - <sup>15</sup> Mattison, K.W.; Dubin, P.L.; Brittain, I.J. *Journal of Physical Chemistry B*, **1998**, 102, 3830.
  - <sup>16</sup> Weinbreck, F.; de Vries, R.; Schrooyen, P.; de Kruif, C.G. *Biomacromolecules*, **2002**, 4, 293.
  - <sup>17</sup> Sanchez, C.; Mekhloufi, G.; Renard, D. *Journal of Colloid and Interface Science*, **2006**, 299, 867.
  - <sup>18</sup> Piculell, L.; Lindman, B. *Advances in Colloid and Interface Sciences*, **1992**, 41, 149.

- 
- <sup>19</sup> Lindman, B.; Thalberg, K. *In Interaction of Surfactants with Polymers and Proteins; Goddard, E. D., Ananthapadmanabhan, K. P., Eds.; CRC Press: Boca Raton, FL, 1993*, Chapter 5.
- <sup>20</sup> Thongngam, M.; McClements, D.J. *Langmuir*, **2004**, 21, 79.
- <sup>21</sup> Burgess, D.J. *Journal of Colloid and Interface Science*, **1990**, 140, 227.
- <sup>22</sup> Goddard, E. D.; Hannan, R. B. *Journal of Colloid and Interface Science*, **1976**, 55, 73
- <sup>23</sup> Tanford, C. *Physical Chemistry of Macromolecules*. New York: Wiley, **1961**.
- <sup>24</sup> Schmitt, C.; Sanchez, C; Desobry-Banon, S.; Hardy, J. *Critical Reviews in Food Science and Nutrition*, **1998**, 38 689.
- <sup>25</sup> Mattison, K.W.; Brittain, I.J.; Dubin, P.L. *Biotechnology Progress*, **1995**, 11, 632.
- <sup>26</sup> Eliçabe, G. E.; Larrondo, H.A.; Williams, R.J.J. *Macromolecules*, **1997**, 30, 6550.
- <sup>27</sup> Eliçabe, G.E.; Larrondo H.A.; Williams R.J.J. *Macromolecules*, **1998**, 31, 8173.
- <sup>28</sup> Schmitt, C. Thesis, Institut National Polytechnique de Lorraine, France, **2002**.
- <sup>29</sup> Baravian, C.; Caton, F.; Dillet, J.; Mouge, J. *Physical Review E*, **2005**, 71, 066603.
- <sup>30</sup> Schmitt, C.; Sanchez, C.; Despond, D.; Renard, D.; Thomas, F.; Hardy, J. *Food Hydrocolloids*, **2000**, 14, 403.
- <sup>31</sup> Kruyt, H.R. *Colloid Science; Elsevier Publication Company: New York, 1949*, Vol. II, p 335.
- <sup>32</sup> Wang, Y.; Kimura, K.; Huang, Q.; Dubin, P.L. *Macromolecules*, **1999**, 32, 7128.
- <sup>33</sup> Tromp, R.H.; Jones, R.A.L. *Macromolecules*, **2006**, 29, 8109.
- <sup>34</sup> Li, Y.; Xia, J.; Dubin, P.L. *Macromolecules*, **1994**, 27, 7049.
- <sup>35</sup> Bohren, C.; Huffman, D. *Absorption and Scattering of Light by Small Particles, Wiley, New York, 1983*.
- <sup>36</sup> Mekhloufi, G.; Sanchez, C.; Renard, D.; Guillemain, S.; Hardy, J. *Langmuir*, **2005**, 21, 386.
- <sup>37</sup> Laneuville, S. Thesis, Laval University, Quebec, Canada, **2004**.
- <sup>38</sup> Gao, J.Y.; Dubin, P.L., *Biopolymers*, **1999**, 49, 185.
- <sup>39</sup> Girard, M. Thesis, Laval University, Quebec, Canada, **2003**.
- <sup>40</sup> Kim, A.Y.; Berg, J.C. *Langmuir*, **2000**, 16, 2101.

## Summary

This thesis aimed at the study of interactions and dynamics in mixed dispersions of  $\beta$ -lactoglobulin (BLG) and Acacia gum (AG). The effect of the molecular polydispersity of Acacia gum was studied in order to better understand the specific contributions of the major gum molecular fractions in interaction with  $\beta$ -lactoglobulin. The objective was to get new information into the resulting complex coacervation mechanism between  $\beta$ -lactoglobulin and Acacia gum.

In chapter I, an introduction into the interactions and demixing mechanisms in macromolecular dispersions is given. The DLVO (electrostatic, van der Waals) non-DLVO interactions (hydrophobic, steric effects) were described in order to understand their role in the stability of macromolecular blends. Emphasis is put on the complex coacervation demixing mechanism in particular. Complex coacervation is a liquid-liquid phase separation arising from the formation of a coacervate layer composed of highly concentrated protein/polysaccharide complexes. We focused on complex coacervation in BLG/AG system where the problematic is the ill-know structure of AG that limit the understanding of interactions and phase separation mechanism. We introduced the characteristics of BLG, AG, BLG/AG mixtures and the present knowledge about complex coacervation in BLG/AG system.

In chapter II, BLG/AG thermodynamic properties were studied by Isothermal Titration Calorimetry method and optical density (O.D.) measurements. The strength of interactions was monitored by varying the environmental conditions such as pH, biopolymer concentration and temperature in order to elucidate the nature of interactions and complex formation. The measurements considered the titration of a dispersion of the total Acacia gum (TAG) or its two major molecular fractions (FI or FII) into BLG dispersion. A comparison between the behaviors of all AG molecules in complexation with BLG was reported. Generally, the three systems studied showed similar titration curves. However, Favorable complexation (lower stoichiometry) and stronger energy of interactions (higher values of  $\Delta H_{\text{obs}}$ ) characterized the titration of BLG by FII. For both Acacia gum fractions, the binding curves with BLG consisted of a large sequence of sharp exothermic peaks and a sequence of

weaker endothermic peaks. This tendency indicated that electrostatic interactions mainly induced complexation. ITC experiments have been performed at pH 4.2 and the general binding isotherm was studied in term of structural transitions. Four ratios of structural transitions were identified and compared to those obtained by optical density measurements:  $r_{agg}$ , the ratio of aggregation of complexes;  $r_{isto}$ , the initiated stoichiometric charge ratio;  $r_{eq}$ , the ratio of enthalpy/entropy equilibrium and  $r_{sat}$ , the ratio of saturation of binding sites. These ratios were lower in BLG/FII system, in agreement with lower stoichiometry of association and favorable complexation. However, the saturation of binding sites occurred at the Pr:Pol charge ratio of  $\sim 1:1$  in all systems, indicating that phase separation AG took place at a stoichiometric electrical charge equivalence. Effects of initial concentration of AG, pH and temperature on interactions were studied. An increase of all parameters led to lower stoichiometry of association of BLG to AG. The binding strength decreases with increasing temperature and gum concentration, and it reached a maximum at a pH of 4.2, in agreement with optical density measurements done in the same conditions. The increase of temperature allowed to determine a high positive value ( $13.51 \text{ kcal.mol}^{-1}.\text{°C}^{-1}$ ) of the heat capacity ( $\Delta C_p$ ), which indicated a role of the hydrogen bonding in complexation/coacervation between BLG and AG and a disappearance of hydrophilic groups during interactions.

For macromolecular systems as BLG/AG, the effect of biopolymer concentration affects the influence of pH and temperature, e.g. increasing the total biopolymer concentration reduces the influence of pH on complex coacervation. Therefore, further ITC experiments are needed to better understand the binding curve of BLG and Acacia gum molecular fractions. New information about the structural parameters of AG fractions is necessary to determine their charge densities, which can be fruitful for analyzing more precisely the ITC results as well as the role of each fraction on the complex coacervation process.

The work presented in chapter III deals with effects of the molecular polydispersity of TAG on its pH-induced complex coacervation with BLG. Slow acidification using glucono-delta-lactone of three mixed dispersions, BLG/TAG, BLG/FI and BLG/FII, was performed in order to follow *in situ* phase ordering transitions during interaction using static and dynamic light scattering (SALS and DLS) and electrophoretic mobility measurements. In all mixtures, the complexation/coacervation followed a Nucleation and growth (NG) mechanism. In the three mixed dispersions, five pH-delimited structural transitions were determined:  $pH_{sc}$ : pH of formation of soluble complexes,  $pH_{ca}$ : pH of complex aggregation,  $pH_{ps}$ : pH of phase



separation,  $\text{pH}_{\text{coa}}$ : pH of coacervate formation (coacervation) and  $\text{pH}_{\text{neut}}$ : pH of charges neutralization. In the  $\text{pH}_{\text{sc}}\text{-pH}_{\text{ps}}$  range, all systems exhibited similar transition points. From  $\text{pH}_{\text{ps}}$ , BLG/FII system exhibited lower pH of structural transitions as compared to BLG/FI dispersion, may be due to the decrease of strength of interaction between biopolymers, which highlight the effect of AG characteristics. All the pH of structural transitions were carried out at the approximately same Pr:Pol charge ratios in the three systems. Regarding the higher number of charges of FII, it was concluded that it induced faster rate of phase separation than FI. In addition, FII led to the formation of smaller particles, which exhibit more heterogeneous interfaces upon the occurrence of phase separation. The present work probed the effect of TAG polydispersity on the pH-induced complexation/coacervation mechanism with BLG. The use of complementary methods such as spectroscopic techniques would be necessary to better explain the structural transitions at different scale. An extensive study of the protein-to-polysaccharide ratio could be an approach to better understand both the structural role of AG molecules and the transition occurring between complexation and coacervation. Regarding the favorable structural features of FII (higher molecular weight and number of charges); it may be expected to induce faster phase separation kinetics than FI, at the same mixing charge ratio. Thus, as a prospect, mixed dispersions at the same Pr:Pol charge ratio must be prepared for a better comparison between mixtures.

Chapter IV provides a more general view on the complex coacervation mechanism of BLG/AG system based on the variation of the interaction strength by changing the mixing ratio (Pr:Pol) and total amounts of biopolymers ( $C_p$ ). SALS, DLS and electrophoretic mobility measurements (at low  $C_p$ ), Granulo-Polarimetry and optical microscopy (at high  $C_p$ ) were complementary methods to investigate the influence of these parameters on complexation/coacervation between BLG and AG. Increasing the Pr:Pol weight ratio allowed complexation/or phase separation to occur at higher pH values i.e. at lower positive charge density of BLG in all systems. BLG/FII system showed lower particle size at the mixing ratio of 2:1, as compared to BLG/FI system. However, above this ratio, the size of BLG/FII particles increased and was higher than that of BLG/FI particles. This feature may be due to the higher strength of interaction at 2:1 that masked the role of the structural characteristics of FII. By DLS, it was found that favorable complexation occurred between FII and BLG as compared to FI, in relation with the possible higher charge density of FII. Smaller BLG/FII complexes were observed, which can be attributed to repulsive interactions between the like-

charged particles due to an excess of negative charges in BLG/FII dispersions. At high ratios (above 8:1), the  $\gamma$  exponent of the log-log plots ( $I(q)$  vs  $q$ ) increased and then reached the Porod value  $\geq 4$ , which reveals the appearance of an interfacial layer in dispersions. The morphology of the interface was more homogeneous for BLG/FII mixtures at high ratios, as compared to BLGFI system. According to DLS results, Granulo-Polarimetry measurements in concentrated medium showed the formation of larger particles with a lower number in BLG/FI mixture. The total biopolymer concentration ( $C_p$ ) of mixtures has not affect the dynamics and kinetics of complex coacervation in all mixtures. The similar mechanism of nucleation and growth drives phase separation; it was also established that nucleation can be accompanied by dissociation of particles. In addition, the pH of structural transitions remained constant with increasing  $C_p$ . Nevertheless, at high  $C_p$ , the coacervates formed are larger and more numerous as shown by optical density measurements.

All studies showed complementary and coherent results that can be summarized in the following manner: The two major molecular fractions of Acacia gum interact differently with BLG during pH-induced complex coacervation in the same solution conditions. Complexation/coacervation between BLG and FII displayed faster kinetics and stronger binding. One possible reason is that the structural features of this molecular fraction (e.g. higher charge density, molecular weight and number of charges, and larger radius of gyration) allow favorable complexation with BLG.

It must be noticed that the three mixed dispersions were prepared at the same mixing weight ratio but different mixing charge ratios. Therefore, future works would study the three systems at the same Pr:Pol mixing charge ratio to better highlight the characteristic behavior of FI and FII.

Although it was difficult to attribute a binding model for ITC curves, it was a fruitful method to study complex coacervation at the molecular level and then reveal the effect of the polydispersity of TAG. Other approaches can be used to better understand the thermodynamic properties obtained by ITC such as the investigation of the effect of ionic strength. Moreover, the influence of a given solution condition on the effect of another one may elucidate the low energy interactions, since ITC showed that complex coacervation of BLG/AG is not even arising from electrostatic interactions. Studying the effects of ionic strength, biopolymer concentration and temperature by light scattering and other methods can be also a great mean

to get new information about ITC results and to give a better knowledge of the role of TAG fractions in complex coacervation with BLG. Size measurements at different Pr:Pol charge ratios are envisaged to better evaluate the evolution of size with mixing ratio and to complete the DLS results.

The use of a molecular fraction instead of another fraction can be suggested to allow certain suitable properties of complex coacervation or coacervates depending on the requirement of studies. For example, FII can be used to promote higher binding strength, faster phase separation and smaller coacervates at high strength of interaction with BLG. For some experiments such as ITC that needs lower polydispersity and purity of the material, FI can replace TAG since it exhibits similar behavior. It is also important to note that our approach “the effect of the molecular polydispersity of AG”, which reflects its structural impact on interaction, can offer the opportunity to better understand the complex structure of AG in the future.

## Acknowledgments

During all my thesis years at the Laboratoire de Science et Génie Alimentaires (LSGA), I developed a passion for complex coacervation, I learned a lot in the field of macromolecule assemblies and I owe it to a lot of people. This work couldn't be achieved without the help and support of a great amount of people to whom I wish to express my sincere gratitude:

- ✓ Pr. Christian Sanchez, my supervisor, for giving me the opportunity to do a challenging PhD research, for his guidance, his perpetual enthusiasm and his trust during these years. I consider myself very lucky to have worked with so motivated people as him. Christian, avec toi c'était toujours agréable de discuter mais aussi d'aboutir. Je pense qu'avec ton aide j'ai beaucoup mûri scientifiquement.
- ✓ The director of LSGA laboratory Pr. Stéphane Desobry and Pr. Joel Hardy for giving me the opportunity to make this PhD.
- ✓ Dr. Saïd Bouhallab, research director at the INRA-Rennes for his participation to the jury of examination of my thesis.
- ✓ Pr. Frank Boury (Professor at the INSERM-Angers) and Dr. Luc Picton (lecturer at the university of Rouen) for their examination of the PhD as reporters of jury.
- ✓ Special thanks to Dr. Denis Renard, for his participation to the examination of the thesis, his trust and support. Thanks for your comments about the publications and for your friendly scientific discussions when I was at Nantes, and sometimes by e-mail.
- ✓ All my colleagues of the LSGA for the good time I had during my PhD. In particular, I would like to thank Reine, Ghozlène and Kassem. It was very fruitful to have regular meetings among each other to discuss science and life. A lot of people helped me to arrive at this stage in my PhD especially: Mrs. Marie-Noelle Maucourt and Carole.
- ✓ My other LSGA colleagues and especially: Elmira, Sandrine, Ali, Atmane, Virginie, Claire and Angélica.
- ✓ The Laboratoire de maturation d'ARN et d'enzymologie moléculaire (MAEM) for providing me the Isothermal Titration Calorimetry; Alexandre Kriznic for his help and interest to my experiments.
- ✓ My family, especially my parents. Thanks for your perpetual support and request that is my arm for the life

And most of all my fiancé Safi Jradi. We were together day-by-day during my thesis and I would like to thank you for the interest you have always shown in my PhD, original ideas about my work, and above all, for your love.

## **Curriculum Vitae**

Suzanna Akil was born on the 08<sup>nd</sup> September 1980 in Berlin, Germany. She finished her high school in June 1998, and in September 1998 she started her 4-year Chemistry study at the Lebanese University, faculty of sciences (section I) in Lebanon. In June 2002 she obtained her degree in Chemistry. In October 2002 she started her 1-year Physical-Chemistry Master at the Université de Hautes Alsaces (UHA) in France. In July 2003 she obtained her master degree in Physical-Chemistry. In October 2003 she started her 3-year PhD thesis at the Institut National des Polytechniques de Lorraine (INPL). The subject of the research regarded the understanding of the complex coacervation in protein-polysaccharide mixtures. The PhD project was supervised by Dr. Christian Sanchez, Professor at the laboratoire de science et génie alimentaires of the Ecole Nationale Supérieure d'Agronomies et d' Industries Alimentaires, INPL, France.

AUTORISATION DE SOUTENANCE DE THESE  
DU DOCTORAT DE L'INSTITUT NATIONAL  
POLYTECHNIQUE DE LORRAINE

oOo

VU LES RAPPORTS ETABLIS PAR :

Monsieur Luc PICTON, Maître de Conférences, Université de Rouen, UFR Sciences et Techniques,  
Mont Saint-Aignan

Monsieur Franck BOURY, Professeur, INSERM, Angers

Le Président de l'Institut National Polytechnique de Lorraine, autorise :

**Madame AKIL Suzanna**

NANCY BRABOIS  
2, AVENUE DE LA  
FORET-DE-HAYE  
BOITE POSTALE 3  
F - 54501  
VANDŒUVRE CEDEX

à soutenir devant un jury de l'INSTITUT NATIONAL POLYTECHNIQUE DE LORRAINE,  
une thèse intitulée :

"Etude du mécanisme de conservation complexe entre les fractions principales de la  
gomme d'Acacia et la B-lactoglobuline - Comparaison avec la gomme d'Acacia non  
fractionnée"

en vue de l'obtention du titre de :

DOCTEUR DE L'INSTITUT NATIONAL POLYTECHNIQUE DE LORRAINE

Spécialité : « Procédés biotechnologiques et alimentaires »

Fait à Vandœuvre, le 04 avril 2007

Le Président de l'INPL,

F. LAURÉNT

